Diverse Primitive Basalts from an Extensional Back-arc Setting: Fort Rock Volcanic Field, Oregon

by

Frank Michael Popoli, Honours. B.Sc.

Brock University

Submitted

in partial fulfillment of the requirements

for the degree

Master of Science in Earth Sciences

Faculty of Mathematics and Science, Brock University

St. Catharines, Ontario

Master of Science (2016) Brock University

(Earth Sciences) St. Catharines, ON, Canada

TITLE: Diverse Primitive Basalts from an Extensional Back-arc Setting: Fort Rock Volcanic Field, Oregon

AUTHOR: Frank Michael Popoli, Honours B.Sc.

(McMaster University, Hamilton, Ontario, Canada, 2010)

SUPERVISOR: Professor, Dr. Mariek E. Schmidt

NUMBER OF PAGES: 186

ABSTRACT

The Fort Rock Volcanic Field study area (FRVF) is situated in a highly complex volcanic and tectonic extensional back arc setting, influenced by multiple episodes involving the subduction of the Juan de Fuca Plate under the North American Plate, eruptions from the Western and High Cascades, High Lava Plains (HLPs), Newberry, and extension from the Basin & Range continental rift zone. Hydrovolcanic eruptions created tuff rings/cones and maars, while conventional eruptions created cinder cones, and lava fields in the FRVF area. These landforms contain a diverse array of primitive basalts, with an Mg# (xMgO / (xMgO + xFeO) * 100) > 60 (molar %), deducing information of mantle source regions and melting processes through geochemical analyses of major and trace elements to achieve a greater understanding of the complex tectonic framework and eruptive history of the FRVF. Geochemical data was acquired through X-ray fluorescence (XRF) and Inductively Coupled Plasma Mass Spectrometry (ICP-MS) for 75 mafic basaltic samples. FRVF basalts analyzed four diverse primitive magma types; low-K tholeiites (LKTs), calc-alkaline basalts (CABs), high Mg# basaltic andesites (BAs), and ocean island basalts (OIBs). These magma types are further separated into western/central and eastern sections of the FRVF based on their major and trace element variations. These variations suggest the subduction enrichment, mantle fertility, and the depth and degree of partial melting trends of their primary mantle sources depend on their distribution across the FRVF.

Key words: Fort Rock Volcanic Field; back arc; primitive; basalts; geochemistry; petrography; major and trace element compositions

ACKNOWLEDGEMENTS

First and foremost, I extend my greatest praise towards my supervisor Dr. Mariek Schmidt. I am extremely grateful for the opportunity to take on this project as Mariek's master student, being trusted to work independently and productively throughout the past few years to comprise an acceptable thesis paper. Thank you for encouraging and believing that I could achieve much more adequate structuring of my thesis throughout the many revisions throughout each of my chapters. Funding for the research was provided by graduate research and fellowship scholarships through Dr. Mariek Schmidt.

I would also like to thank Dr. Nigel Blamey and Dr. Gregory Finn for being on my committee, and for making suggestions to improve this document. Much thanks to Dr. Frank Fueten for the special topics course that providing me much knowledge and information on the overwhelming complexity of the tectonics in my study area.

A special thanks goes to microprobe technician Yanan Liu at the University of Toronto. She provided me with much needed user training on the electron microprobe such as machine calibrating, routine setup, and data evaluation for acquiring useful compositional analyses of plagioclase, olivine, and spinel crystal phases in my chosen basaltic samples. She was very helpful and easy to talk to, allowing me additional machine scheduling dates when I needed to.

Thank you Matthew Nikitczuk, Jeff Berger, and Rebekka Lee for assisting in the collection of samples and field observations in Fort Rock, Oregon. Also thanks to the lab technicians at Washington State GeoAnalytical Laboratory for their X-ray Fluorescence and Inductively Coupled Plasma Mass Spectrometry analyses of all my basaltic samples collected around my study area.

Last but not least, I would like to add one more note of appreciation to my mother Patricia Popoli for encouraging and supporting my efforts throughout these past few years.

TABLE OF CONTENTS

LIST OF FIGURES

Chapter 1

Chapter 2

Chapter 3

Chapter 4

LIST OF TABLES

Chapter 1

Chapter 2

Chapter 3

Chapter 4

LIST OF ABBREVIATIONS AND SYMBOLS

An……anorthite

BA…… basaltic andesite

BABB……back-arc basin basalts

BFZ……Brothers Fault Zone

CAB……....calc-alkaline basalt

cpx……....clinopyroxene

Cr#.....chromium number

EIB……...enriched island basalts

Fo……forsterite

FRVF…….Fort Rock Volcanic Field

hbl……hornblende

gt…… garnet

HFSE…….High Field Strength Element

HKCAB……. high-K calc-alkaline basalt

HLP…….High Lava Plains

HREE…….Heavy Rare Earth Element

ICP-MS…… Inductively Coupled Plasma Mass Spectrometry

JDFP……..Juan de Fuca Plate

KM ……. Klamath Mountains

LILE…….Large Ion Lithophile Element

LKT……... low-K tholeiite

LOD…… limit of detection

LREE……..Light Rare Earth Element

mag……magnetite

mc……magnesiochromite

mf……magnesioferrite

Mg#.....magnesium number

MORB……...mid-ocean ridge basalt

NAP……North American Plate

n.d……not detected

N-MORB…….normalized mid-ocean ridge basalt

OIB…….ocean island basalt

ol……olivine

PL……..plagioclase

sp……spinel

Tmt……titanomagnetite

ves……..vesicle

XRF…… X-ray fluorescence

CHAPTER 1: Introduction

The Fort Rock volcanic field (FRVF), an extensional back-arc basin, contains a diversity of geological landforms derived through multiple volcanic and tectonic influences. This unique area includes an ancient pluvial lake system that existed from late Pliocene through late Pleistocene time, numerous hydrovolcanic features including tuff rings/cones and maars, and lava fields along with cinder pits associated with conventional eruptions. A long history of volcanism, faulting, deformation, and extension created the Western and High Cascades, the High Lava Plains (HLPs), and the northwestern Basin & Range continental rift zone area in southeast Oregon. Basaltic eruptions in the back-arc are subjected to multiple influences from the subduction of the Juan de Fuca oceanic plate under the North American continental plate, High Lava Plain eruptions, Newberry volcanic eruptions, and northwest-southeast trending faults associated with the extensional Basin & Range province.

Previous studies of the Mariana, east Scotia, Lau, and Manus back-arc basin spreading centers analyzed major and trace element compositions of back-arc basin basalts (BABBs) to deduce the complexity of their mantle sources (Hart et al. 1972; Pearce & Cann, 1973; Hawkins, 1976; Gill, 1976; Tarney et al. 1977; Saunders & Tarney, 1979; Hart, 1985; Hawkins & Melchior, 1985; Sinton & Fryer, 1987; Stopler & Newman, 1994; Hawkesworth et al. 1995; Taylor & Martinez, 2003; Pearce et al. 2006; Wiens et al. 2006; Bézos et al. 2009). The compositions of BABBs can be very complex, containing major and trace element concentrations that are similar to mid-ocean ridge basalts (MORBs), calc-alkaline basalts (CABs), and ocean island basalts (OIBs), and also concentrations that are intermediate between MORBs and OIBs containing higher concentrations of large ion lithophile elements (LILEs) than MORBs, and lower concentrations high field strength elements (HFSEs) than OIBs. Pearce et al. (2005) suggest that these compositional differences are extensively a result of variable enrichment of a subduction component to their mantle sources.

Primitive basalt geochemical studies aid in unraveling the complexity of the tectonic influences on mantle melting beneath this back-arc basin. Primitive magmas are the least modified magmas during ascent, with minimal fractionation and assimilation

affecting their “near” primary mantle source compositions (Bacon, 1990; Conrey et. al, 1997). Trace element compositions of primitive basalts are useful in determining the possible depth/degree of partial melting, subduction enrichment, and mantle fertility trends of their primary end-member mantle sources (Pearce et al. 2006). HFSEs reside in the mantle wedge and are relatively unaffected by subduction process, and therefore their concentrations in primitive basalts are useful for determining the fertility and extent of melting of their primary mantle sources (Pearce et al. 2006). HFSE enriched primitive basalts may have originated from an intraplate OIB primary mantle source domain. LILEs are controlled by varying degrees of subduction enrichment, and therefore their increased concentrations in primitive basalts may represent a greater contribution of a subduction component to their primary mantle source domain (Pearce et al. 2006).

A total of 75 FRVF basaltic samples were collected along the outcrops of vents, large lava flows, cinder cones, and hydrovolcanic bombs in altered tuff rings. Among those samples, 31 primitive basalts contain high Mg relative to Fe contents, yielding an Mg# ((xMgO/ (xMgO+xFeO)*100) (molar %) that have a value greater than or equal to 60. The most primitive FRVF basalt analyzed for an Mg# of 68, which is still not considered a very high value for most primitive basalts in previous geochemical studies. For the purposes of this study, FRVF primitive rocks represent an Mg# $\geq$ 60, the closest analyzed samples to primary magma compositions.

This study focuses on determining information of mantle source regions and melting processes through geochemical analyses of major and trace elements of FRVF back-arc primitive end-members to achieve a greater understanding the complex tectonic framework and eruptive history of the Oregon Cascades and back-arc region.

1.1 Geological/ Tectonic Setting

The Pliocene to Pleistocene FRVF is situated in a back-arc extensional setting approximately 65 km east of the Central Oregon High Cascades (Figure 1-1). FRVF is located underneath the Brothers Fault Zone (BFZ) and HLPs just southeast of the Newberry caldera within the Basin & Range area (Figure 1-1). The Brothers fault zone cuts obliquely across the HLPs, a province of westward younging silicic volcanism. The Oregon Cascade range resides in western North America along the coast of the Pacific Ocean (Figure 1-1). The arc consists of a series of Quaternary age stratovolcanoes generated throughout subduction related volcanism, resulting from the convergence of the Juan de Fuca oceanic plate beneath the North American continental plate (Figure 1-1). The Juan de Fuca plate is subducting approximately 40-45 mm/year, dipping beneath the Coast Range at approximately 13-16 degrees (Riddihough, 1984; Wang et al. 2003). Many of the volcanic vents in the High Cascades region are localized along north-northwest oriented graben and normal fault structures (Wells et al. 1999) (Figure 1-1).

1.1.1 FRVF Back-arc

The Fort Rock pluvial lake basin existed from the late Pliocene to the end of the Pleistocene era (Figure 1-2). The basin is approximately 64 km long and 40 km wide, and can be separated into 3 sub-basins that include Fort Rock, Silver Lake, and Christmas Valley (Bevis, 2013) (Figure 1-2). Newberry volcanic flows impinge on the FRVF, as well as the HLPs, the BFZ, and the north-western Basin & Range area (Figure 1-2). Eruptions of HLP, Basin & Range, and Newberry basaltic magmas occurred along northwest trending normal faults that cut across the basin and adjacent highland, influencing the formation of tuff rings, maars, cinder cones, and lava fields within and around the FRVF pluvial lake margins (Bevis, 2013) (Figure 1-2). Small, isolated tuff rings are located at Table Mountain, Flat Top, and Green Mountain SW & S along the pluvial lake basin margins. Larger maars that represent explosion craters are located at Big Hole and Hole-in-the-Ground (Figure 1-2). Tuff rings and complexes include Fort Rock, Table Rock, the Black Hills and St. Patrick's Mountain (Figure 1-2).

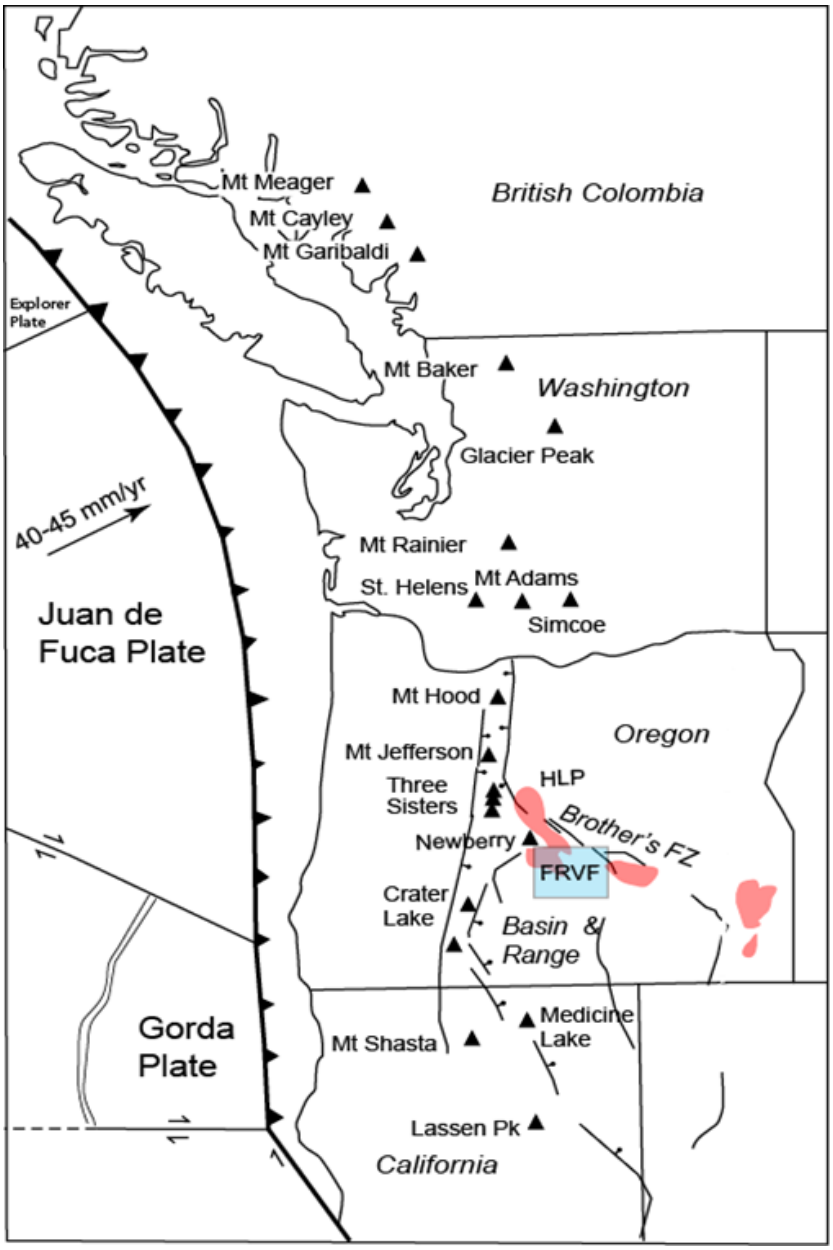

Figure 1-1. Tectonic map of the Cascadia subduction zone, modified after Schmidt et al. (2008). Major volcanic centers (black triangles) located along the High Cascades. Blue box indicates Fort Rock Volcanic Field (FRVF) study area. Red blotches are the High Lava Plains (HLP) basaltic eruptions coinciding along the northwest-southeast trending faults of the Brothers Fault Zone (BFZ). Basin & Range extension located in the southeastern section of Oregon.

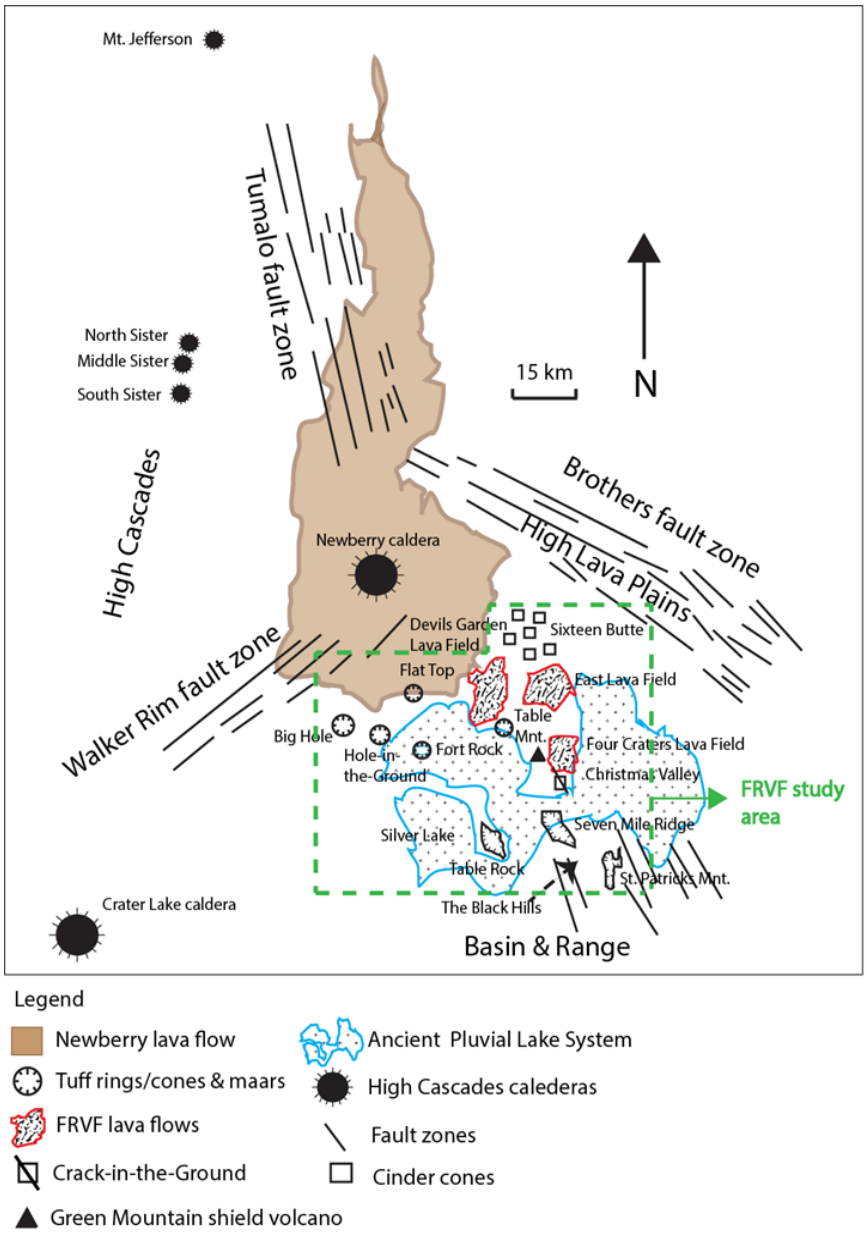

Figure 1-2. Geological features associated with the FRVF study area (green dashed box). Newberry caldera is situated at the apex of the Walker Rim fault zone, Tumalo fault zone, and the BFZ. Eruptions of the HLPs, the north-western Basin & Range, and Newberry impinge on the FRVF back-arc basin, aligning themselves along the northwest southeast trending faults of the BFZ. FRVF geological features are influenced by the HLP and Newberry eruptions, as well as the extension through accommodation of the Basin & Range province. Modified after (Heiken 1971; Jordan et al. 2002; Jensen et al. 2009; and Meigs et al. 2009), extracted from Overview of the High Lava Plains PDF file [www.wou.edu/las/physci/taylor/eisi/orr_orr1.PDF] Western Oregon University.

1.1.2 FRVF Lava Fields

Large lava fields are found east of Fort Rock, consisting of the Four Craters Lava Field, East Lava Field, and the Devils Garden Lava Field (Figure 1-2). The Devils Garden contains basaltic bombs, pahoehoe lava flows, rubble, and lava tube caves. Four Craters and East Lava Field are 'a'a basaltic lava flows (Figure 1-3). These lava fields are suggested to have originated from northwest-trending fissures associated with the HLPs, BFZ, and the Basin & Range rift zone (Jordan et al. 2002; Brand & Heiken, 2009; Jensen et al. 2009; Meigs et al. 2009).

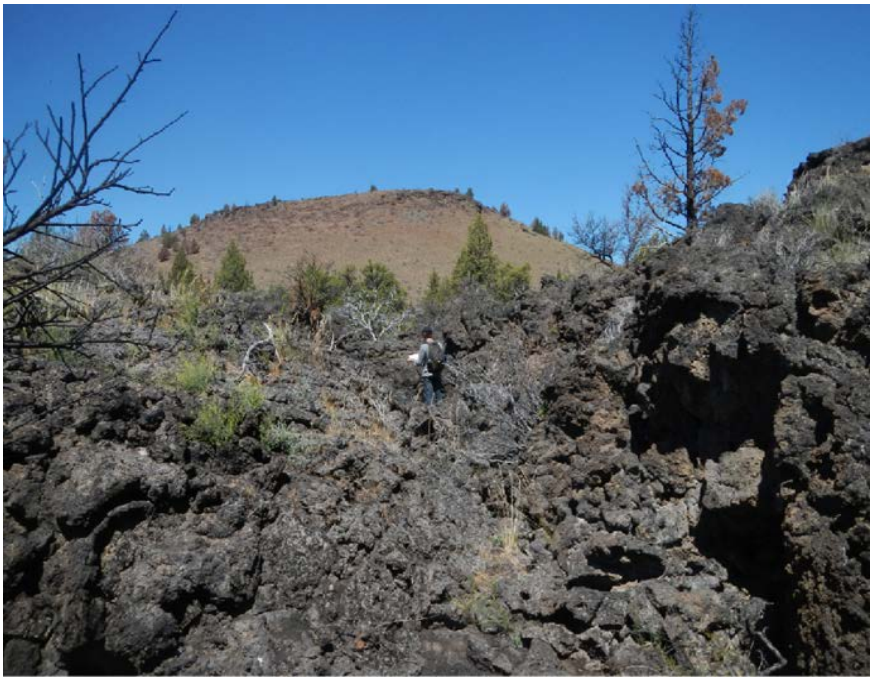

Figure 1-3. Photograph of the author standing on the basaltic 'a'a flows of the East Lava Field.

Green Mountain is a scoriaceous summit cone of a small, older Pleistocene shield volcano located near the Four Craters lava field, erupted approximately 740 ka (Jordan et al. 2002; Bevis, 2013) (Figure 1-2). This area contains Crack-in-the-Ground, and is approximately a 5 km long trending rift fracture created by early Holocene pahoehoe basaltic lava flows from the Green Mountain shield volcano (Figure 1-2). (Bevis, 2013). Pezzopane & Weldon (1993) suggest the Crack-in-the-Ground fracture aligns with the normal northwest fault patterns displayed in the Basin & Range province, and that the

Four Craters lava contains cracked flows that indicate Holocene extensional displacement (Figure 1-2) (Meigs et al. 2009).

Studies from Mackey et al. (2014) use cosmogenic ^{3}He exposure dating of basalt lava flows from the Four Craters lava field to quantify the timing of the northwest fault zones, and the age of the lava fields. These results suggest that FRVF lava fields are approximately 14,000 years old (Figure 1-4). This age coincides with the exposure age of the adjacent Crack in the Ground normal fault, indicating that the timing of volcanic activity coincides with the timing of extensional faulting in these areas (Figure 1-4; Mackey et al. 2014).

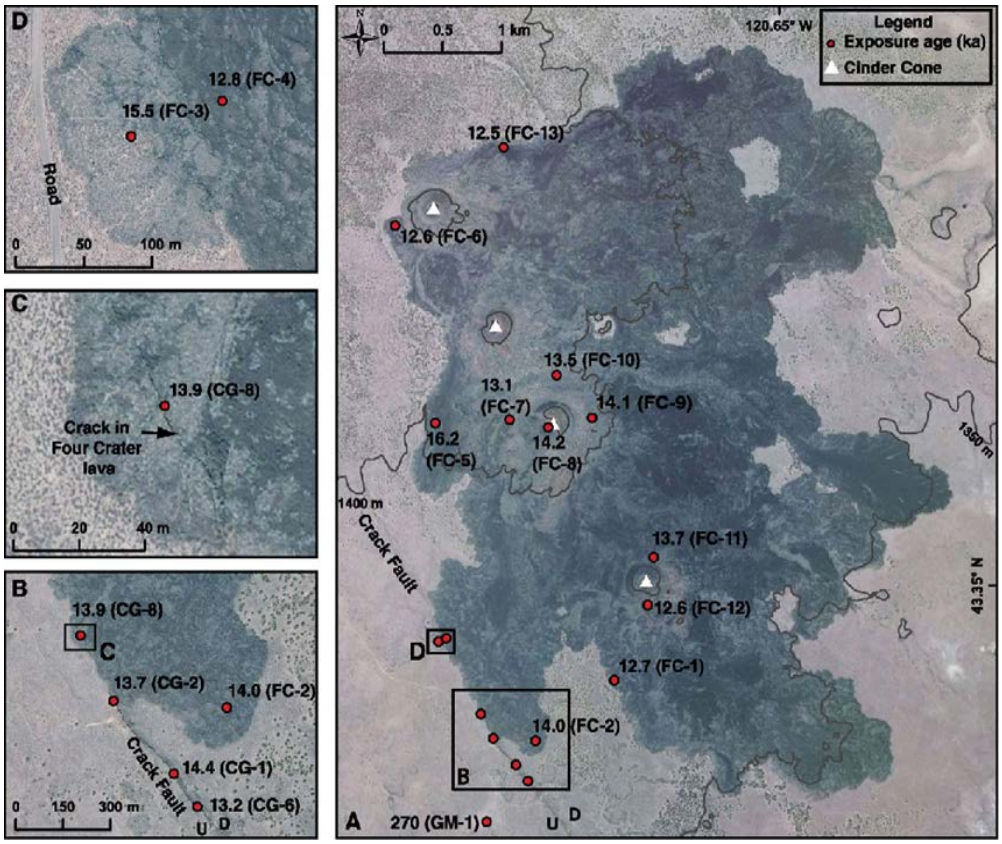

Figure 1-4. Aerial photograph of Four Craters Lava Field and Crack-in-the Ground with basaltic sample locations and ages. Red dots mark the location and exposure ages of basaltic samples; FC- Four Craters; CG- Crack-in-the-Ground; and GM- Green Mountain. Image extracted from Mackey et al. 2014.

1.1.3 FRVF Tuff Rings/Cones & Maars

Tuff rings, tuff cones, and maars are a result of hydrovolcanic eruptions. Hydrovolcanic eruptions occur when intruding magma violently fragments after contact and mixing with shallow surface water or groundwater (Heiken, 1971, Morrisey et al. 2000, Gonnermann & Manga, 2003; Parfitt, 2004; Clarke et al. 2005; Mason et al. 2006; Brand & Heiken, 2009; Traglia et al. 2009; Poili et al. 2009). Mild eruptions generated basaltic tuff rings and cones, such as Fort Rock and Table Mountain, while more energetic steam eruptions created explosion craters such as Big Hole and Hole-in-the-Ground (Bevis, 2013) (Figure 1-5).

The occurrence of maar volcanoes in the FRVF displays evidence for an extensive period of occupation by water once contained in the ancient pluvial lake system (Heiken, 1971; Bevis, 2013). Maars form when rising magma comes into contact with subsurface water, and succeeding phreatic explosions excavate a hole in the country rock, leaving craters in the ground (Heiken, 1971; Brand & Heiken, 2009) (Figure 1-5A). These explosion craters eruption craters are often found associated with lacustrine deposits, which suggests that these eruptions occurred containing saturated sediments (Heiken, 1971; Bevis, 2013). Hole-in-the-Ground is a maar formed when Newberry magmas entered the water-saturated sediment of the Fort Rock Basin possibly as early as 50,000 years ago (Meigs et al. 2009) (Figure 1-5A).

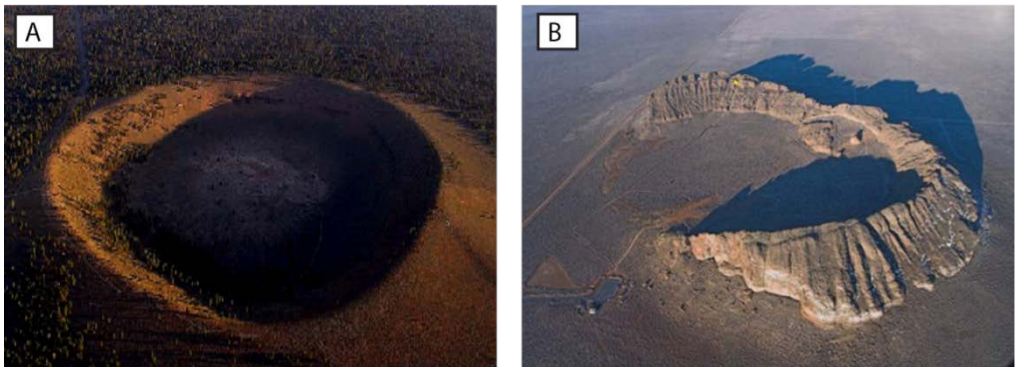

Figure 1-5. Aerial photographs of; A) Hole-in-the-Ground maar, and B) Fort Rock tuff ring. Extracted from the Bend Hiking Group [http://www.meetup.com/TheBendHikingGroup/events/53850902/].

The Table Rock maar complex contains a tuff cone, along with two tuff rings, and up to six smaller tuff rings and eroded vents (Brand & Heiken, 2009) (Figure 1-2).This complex divides the Fort Rock-Christmas Valley sub-basin from the Silver Lake sub-basin (Figure 1-2). Fort Rock is a volcanic near circular ring of lapilli tuff that is the result of a Surtseyan eruption that occurred approximately 50-100 ka (thousand years ago) (Brand & Heiken, 2009) (Figure 1-5B). St. Patrick's Mountain contains tuff cones and rings that are intruded by a northwest-southeast trending dike through accommodation of the extension in the Basin & Range province (Figure 1-2). The Black Hills mountain region contains multiple tuff rings and cones.

1.1.4 FRVF Cinder Cones

The Sixteen Butte area is highly concentrated in scoria and cinder cones derived from Strombolian eruptions. These relatively mild explosions occur from the accumulation of gas beneath the cooled upper surface of a magma column (Clarke et al. 2005, Poili et al. 2009). The magma then reaches the surface and the difference in air pressure causes the gas bubbles to burst into an explosive eruption (Parfitt, 2004; Clarke, 2005; Brand & Heiken, 2009; Traglia et al. 2009). These eruptions generally build cinder cones from the accumulation of small volcanic bomb and lapilli fragments, forming scoria and basaltic spatter samples along north-western fissures (Clarke, 2005).

1.2 Volcanic & Tectonic History of Oregon

Oregon includes an extensive history of subduction, volcanism, and formation of sediments and mountains from 400 Ma to present day (Table 1-1). Oregon's oldest rocks are exotic terranes that formed volcanic island arcs in the Pacific Ocean between 400-100 Ma. These rocks are covered by volcanic and sedimentary rocks as old as 60 million to 2 million years old, which include an ancient arc buried by several large volcanoes (Madin, 2009). A creation of a varied suite of rocks such as limestone, serpentinite, basalt, and large areas of crushed and broken mélange rocks constitute Oregon's basement rock assemblage (Madin, 2009). The Siletz terrane compressed itself into the subduction zone near the North American continent approximately 60 Ma (Wells et al. 1999) (Table 1-1). The terrane wedged onto the edge of the continent creating a basement assemblage for the Coast Range.

Table 1-1. Summary of Oregon's Geological Episodes

Geological timeline (Ma)	Geological Episode
400- 100 Ma.	Oregon's oldest rocks formed as volcanic islands. Sedimentary rocks deposited.
130-50 Ma.	Siletz terrane migrated towards the subduction zone.
60-48 Ma.	Ancestral Western Cascade arc volcanism. Early High Cascade volcanism.
~ 45-6 Ma.	High Cascade volcanism continued. HLP eruptions began (~10 Ma).
6 Ma – 220 years ago.	Late High Cascade volcanism, forming major volcanic centers, HLP eruptions continued.
~ 7,700 years ago	High Cascade volcano Mount Mazama erupted.

Cascadia subduction in the Pacific Northwest dates back to approximately 35–40 Ma, which is comprised of older (~ 45–10 Ma) Western Cascade volcanism, and younger (<10 Ma) High Cascade volcanism (du Bray & John, 2011) (Table 1-1; Figure 1-7). HLP bimodal volcanism began approximately 10 Ma (Lawrence, 1976, Eager et al. 2011) (Table 1-1; Figure 1-7). Mount Mazama erupted approximately 7,700 years ago to form the Crater Lake caldera in the southern Oregon Cascades (Madin, 2009) (Table 1-1).

1.2.1 Fore-arc Migration and Motion in the Cascades

The Oregon Cascadia fore-arc is divided into Washington, Oregon Coastal, and Sierra Nevada blocks which contain Quaternary Cascade arc and major volcanoes. The subduction of the Juan de Fuca plate (JDFP) from the west under the North American Plate (NAP) triggered Neogene deformation, paleomagnetic rotations, and seismic activity that ultimately causes fore-arc migration of these blocks northward approximately 9 mm/yr. along the western coast of North America (Wells et al. 1998) (Figure 1-6).

Located north of Sierra Nevada block is the thick, accreted seamount crustal block called the Oregon Coastal block. The block is located in a central extensional arc where it is not seismically active, has high extrusion rates of volcanic material, and a large fore-arc rotation. This block is separated from the Basin and Range extensional arc, which is characterized by having higher heat flow and higher volcanic eruption rates (Wells et al. 1998) (Figure 1-6)

North of the Oregon Coastal block is the Washington block, which is found in a northern compressional arc area where it is seismically active with low extrusion rates of volcanic material. There is lower heat flow in the Washington area resulting in smaller fore-arc rotations (Wells et al. 1998) (Figure 1-6).

The motion of the Sierra Nevada block west-northwest towards southwest Oregon occurs by rotating about an Euler pole in the Klamath Mountains (KM) (Wells et. al, 1998) (Figure 1-6). This clockwise rotation of the Oregon fore-arc block creates an extensional arc along the trailing edge of the Oregon Coastal block. The southern edge of the Oregon block absorbs the Sierra Nevada displacement to the southern-west Oregon

subduction zone. The northward moving Oregon Coastal block causes the Washington fore-arc to break up into smaller blocks causing the blocks to become smaller and shorten. Deformation caused by the Oregon block creates north-south compression, uplift, thrust faulting and earthquakes (Wells et al. 1998) (Figure 1-6). In the back-arc setting of the Basin and Range area, Quaternary extension decreases northward due to the rotating Oregon Coastal block. The Siletzia accreted basalt basement resides under the Oregon coastal block.

Overall, the subduction of the JDFP-NAP created a complex and seismically active convergent zone containing volcanic arcs in the fore-arc and back-arc settings. The convergence of these two plate boundaries caused arc-parallel migration of the fore-arc, and motions of the large block bodies (Wells et al. 1998).

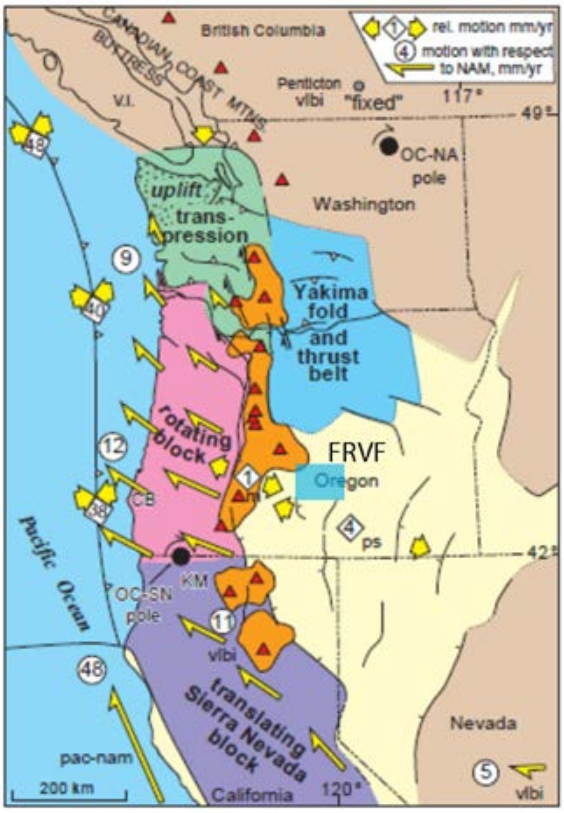

Figure 1-6. Pink Oregon block is rotating and linked to the purple Sierra Nevada block by an Euler pole (OC-SN) in the Klamath Mountains (KM). Green Washington block deformed by Oregon block migration northward. FRVF represented by blue box. Thin yellow arrows depict the relative motion of the blocks with respect to the North American Plate motion; Extracted from Wells et al. (1998).

1.2.2 Ancestral Western & High Cascades Volcanism

Ancestral arc volcanism began approximately 45 Ma and continued for ~ 40 million years (Figure 1-7). Early ancestral arc basalts contain tholeiitic to calc-alkaline compositions (du Bray & John, 2011). The majority of the younger ancestral arc basalts contain calc-alkaline characteristics. This transition from tholeiitic to calc-alkaline basaltic compositions suggests that tholeiitic basalts erupted during the time where the crust was thin and immature (du Bray & John, 2011). The interaction with thicker and more evolved crust, as well as more conventional subduction-related magmatic processes allowed for calc-alkaline characteristics to dominate (du Bray & John, 2011). The predominance of tholeiitic mafic compositions of the early ancestral arc basalts possibly reflects the extensional tectonics that occurred during these earlier periods of ancestral Western arc volcanism (du Bray & John, 2011).

The modern day High Cascade rocks (~ 6 Ma to present) contain a diverse suite of basaltic magma types that dominate the central Oregon Cascade arc (Figure 1-7). Calc-alkaline basalts (CABs) are the most abundant basalt type in the High Cascades, due to enrichment of LILEs through the addition of the subducting component to the mantle wedge. The early High Cascade basalts, which erupted in the late Miocene to early Pliocene era, contain basalts that displayed depleted light rare earth element (LREE) and LILE abundances that correspond to MORB LREE and LILE concentrations. Extensional related mafic volcanic production increased due to a decrease in the convergence rate of the Juan de Fuca oceanic plate and North American plate, erupting MORB-like basalts. Late High Cascade basalts erupted during the late Miocene and early Pliocene era contain HFSE concentrations that resemble OIBs (Bacon, 1990; Hughes, 1990; Bacon et al. 1997; Conrey et al. 1997; Jordan et al. 2002; Schmidt et al. 2008; Rowe et al. 2009; Schmidt & Grunder, 2011; du Bray & John, 2011). Hughes (1990) argues that an oceanic mantle source beneath the central Cascades is due to the existence of the Columbia embayment in which a part of the oceanic lithosphere was compressed and thickened, and possibly results in the central High Cascade OIBs (Figure 1-7).

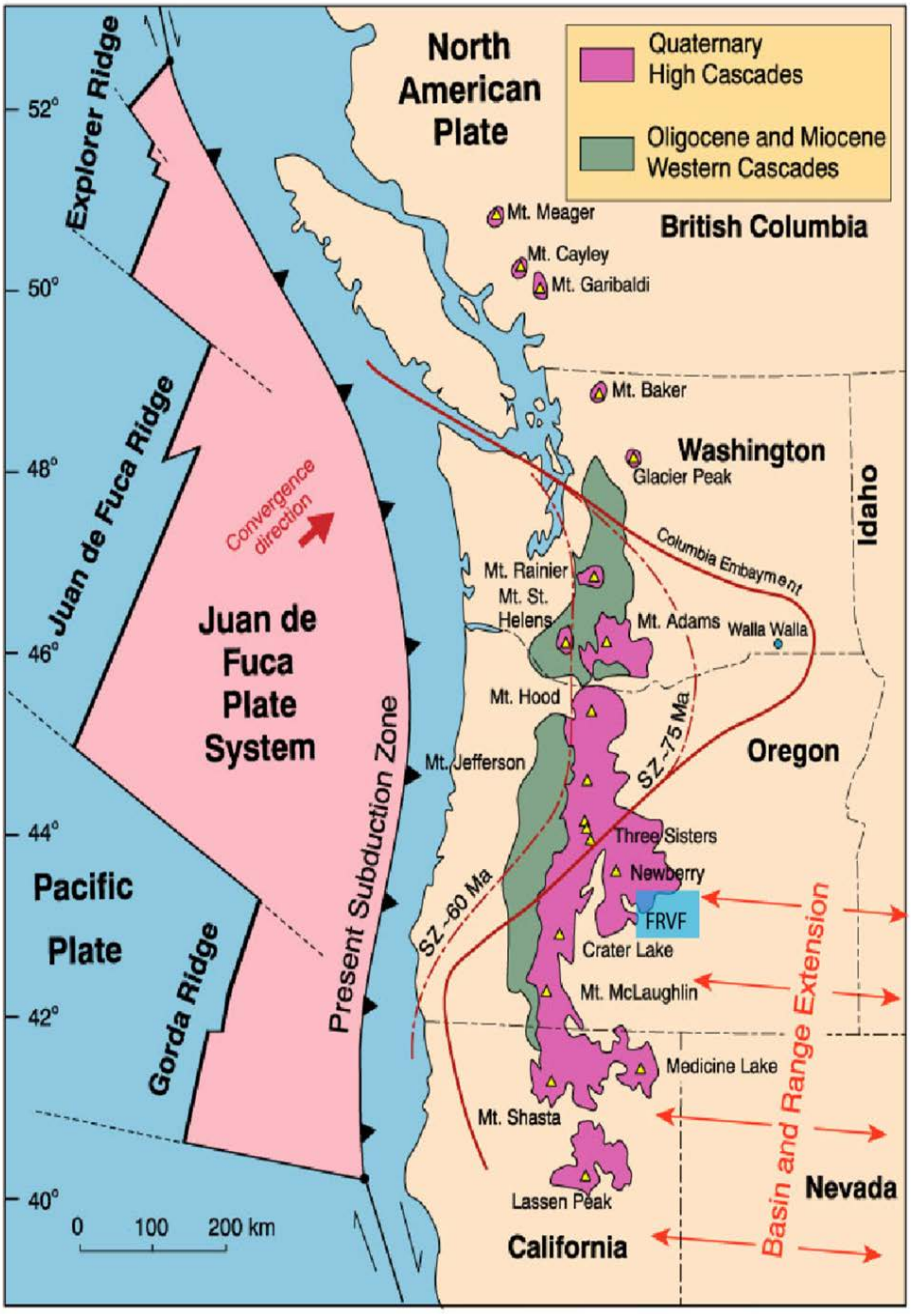

Figure 1-7. Geological map depicting continental arc magmatism of the older ancestral Western Cascades (~ 45-10 Ma) and younger High Cascades (~ < 10 Ma). Yellow triangles represent major volcanic centers associated with the High Cascades. Red line depicts the western margin of the Columbia Embayment (pre-Tertiary continental rocks); red dashed lines depict approximate locations of the subduction zone (SZ) at ~ 75 Ma and 60 Ma to its present day location through westward migration, extracted from Hughes (1990). Modified from McBirney & White (1982), and Winter (2001).

1.2.3 Bimodal Volcanism of the HLPs

HLP eruptions aligned themselves in a broad belt overlapping the Brothers Fault Zone ~10 Ma, characterized by small, northwest-trending normal faults (Lawrence, 1976, Eager et al. 2011) (Figure 1-1; Figure 1-2; Figure 1-8). The Brothers strike-slip faults have been interpreted as the surface expression of the boundary between the thinner crust of the Basin & Range, and thicker crust of the Blue Mountains (Eager et al. 2011) (Figure 1-8). The Brothers fault zone was generated by the same tectonic forces that warped Oregon in a clockwise rotation through the Cenozoic era (Eager et al. 2011). A distinctive suite of abundant basalts and rhyolites express a pattern of bimodal volcanism (Eager et al. 2011; Streck & Grunder, 2012) (Figure 1-8). The rhyolites display a uniform decrease in age from east to west, where Newberry crater in the west lavas extruded less than 1 Ma (Walker, 1974; McKee et al. 1976; MacLeod et al. 1975; Jordan & Grunder, 2004; Meigs et al. 2009; Eager et al. 2011) (Figure 1-8). Unlike the rhyolites, the basalts display no spatial correlation with age (Meigs et al. 2009) (Figure 1-8). This Quaternary bimodal volcanism occupies a complex tectonic setting affected by Cascadia subduction, extension associated with the Basin & Range province, and the Yellowstone plume (Meigs et al. 2009, Ford et. al, 2013).

Past research suggests that this bimodal volcanism is related to the impingement of the Yellowstone mantle plume on the underlying lithospheric plate beginning approximately 15-16 million years ago (Kistler & Peterman, 1978; Draper, 1991; Christiansen et al., 2002; Glen & Ponce, 2002; Hooper et al. 2002; Camp & Ross, 2004; Jordan et al. 2004; Bevis, 2013). More recent studies from Ford et al. (2013) propose that the volcanism in the HLP and Basin & Range does not require a mantle plume system, only a Cascadia slab plate-driven asthenospheric flow to produce this type of mantle flow. Volcanism in the HLPs and the northwest Basin & Range area is driven by this flow, due to slab rollback, steepening, and back-arc extension (Ford et al. 2013).

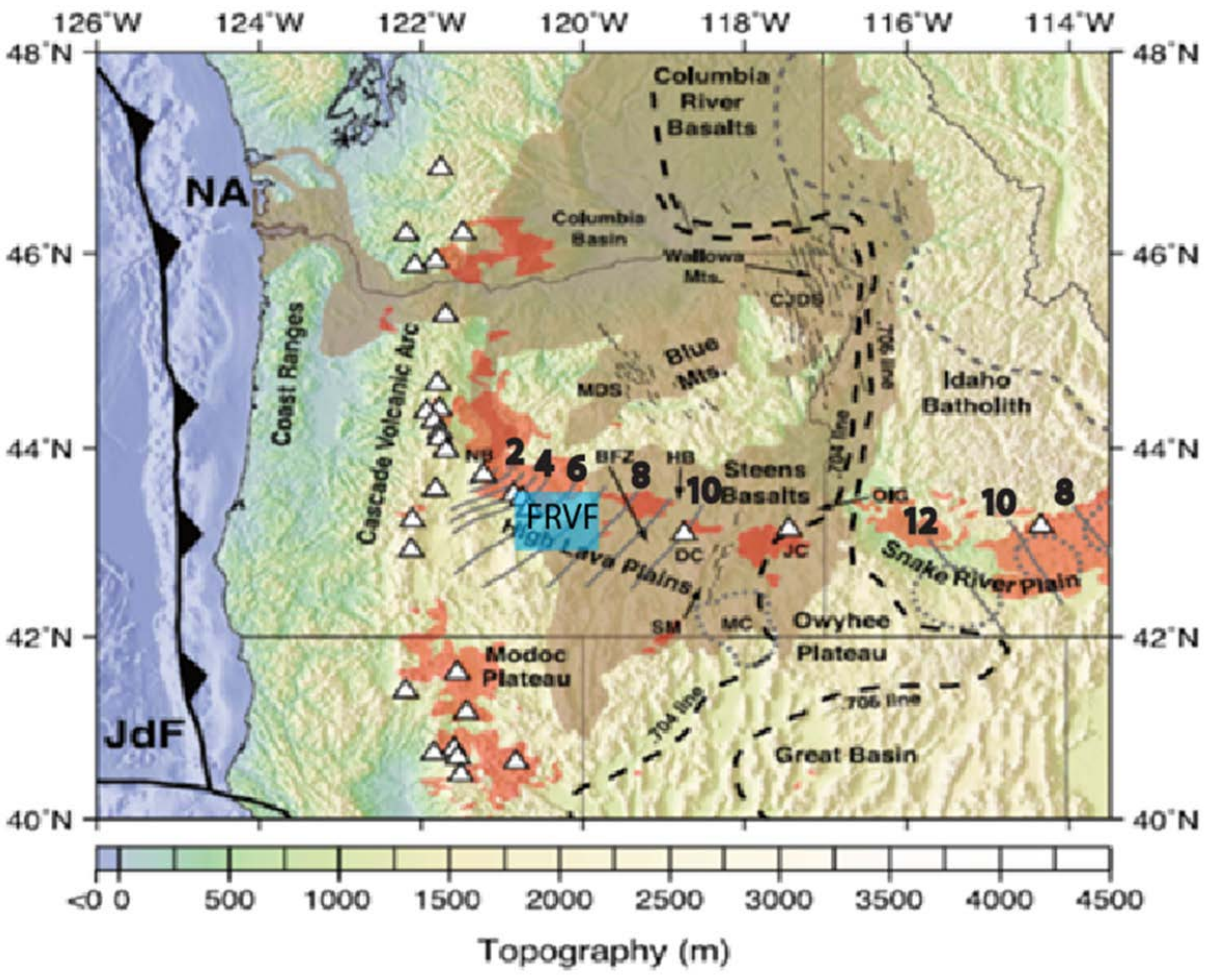

Figure 1-8. Geologic and tectonic map of the Pacific Northwest, United States, modified from Eager et al. (2011). The Juan de Fuca plate (JdF), North American plate (NA), Newberry Volcano (NB), Harney Basin (HB), Brothers Fault Zone (BFZ), dike swarms and other geologic provinces are labeled. Mid-Miocene Steens and Columbia River flood basalt are the light brown shaded regions with overlain associated dike swarms (after Camp & Ross, 2004). Areas of Quaternary basalt (red blotches) indicate High Lava Plains (HLP) lava erupted along the BFZ. Locations of Holocene volcanism are denoted by white triangles. Isochrones of rhyolitic volcanism (grey lines with ages recorded in Ma); eruptive centers (gray dotted outlines) are displayed across the High Lava Plains (Pierce & Morgan, 1992; Jordan et al. 2004). Blue box= FRVF.

1.2.4 Newberry Volcanism

Newberry is the largest shield volcano in the High Cascades volcanic arc, situated at the apex of the three converging fault zones. The Tumalo Fault Zone disrupts lavas on the volcano's northwestern slopes, the west-northwest trending Brothers Fault Zone extends toward Newberry Volcano's northeast flank, and the Walker Fault Zone trends northeast onto Newberry's southwestern slopes (Figure 1-2) (Higgins, 1973; Bevis, 2013). The Newberry caldera is a compound collapse structure formed of several walls and ring-fractures developed during two major periods of explosive volcanism that erupted silicic and intermediate magmas representing younger volcanic material (Bevis, 2013). The north-south trending oval shape of the Newberry volcano is related to the distribution of its more voluminous basalt, basaltic andesite and andesite vents and lava flows, whereas its dacitic to rhyolitic volcanism has been more confined to the central summit and eastern slopes (Bevis, 2013). The longer northern and southern flanks of the volcano are covered with a thick accumulation of basalt and basaltic andesite lava flows. The eruption of Mount Mazama that formed Crater Lake covered Newberry with ash on the volcano's southern flank (Higgins, 1973; Meigs et al. 2009; Bevis, 2013).

A fissure located on the eastern rim of the Newberry caldera erupted basaltic cinders, spatter, scoria, and lava flows which occurred approximately 10,000 years ago. Basaltic andesitic lavas erupted from fissure vents on the northwestern and southern flanks, as well as multiple spatter, cinder, and lava flows which occurred approximately 7,000 years ago (Higgins, 1973; Bevis, 2013; Meigs et al. 2009).

1.3 Petrogenesis of Oregon's Primitive Basalts

Geochemical and petrological studies of primitive basalts in central Oregon, the western/ central HLPs, the northwestern Basin & Range province, and Newberry studies are important in understanding the tectonic complexity surrounding the vicinity of the FRVF back-arc. These are four distinct primitive basaltic end-members based largely on major and trace element compositions, which includes: low K- tholeiites (LKTs), CABs, basaltic andesites (BAs), and OIBs (Bacon, 1990; Hughes, 1990; Bacon et al. 1997; Conrey et al. 1997; Jordan et al. 2002; Schmidt et al. 2008; Rowe et al. 2009; Schmidt & Grunder, 2011; du Bray & John, 2011).

These primitive magmas originated by partial melting in response to adiabatic upwelling within the mantle wedge. Tectonic extension associated with the northwestern Basin & Range contributes to the mantle upwelling, and facilitates the eruptions of these primitive magmas. Three mantle components contribute to the eruptions of the primitive LKT, CAB/BA, and OIB magma types. A depleted mantle source similar to MORBs generates the LKTs; a mantle enriched by a modern, hydrous subduction component generates LILE enriched CABs; and a HFSE-enriched source like intraplate mantle domain generates OIBs. Primitive LKTs widely suggested a result of high degrees of melting of a shallower, depleted mantle source, while primitive CABs, BAs, and OIBs result from low degrees of melting of a deeper, more enriched mantle source (Bacon, 1990; Hughes, 1990; Conrey et al. 1997; Rowe et al. 2009).

1.3.1 Central Cascades Primitive Basalts

Primitive basalts are abundant around the central Oregon High Cascades arc area due to intra-arc rifting of the thin mafic crust (Meigs et al. 2009). Primitive basalts in this area display LKTs, CABs, high Mg# BAs, and OIBs. Primitive basalts at Crater Lake include LKTs and CABs. LKTs generally contain high Al contents (> 17 wt % Al_2O_3), high Ca contents (most are >11 wt % CaO), low Na (~ 2.5 wt % to ≥ 3 wt % Na_2O), and K_2O contents as low as 0.09 wt %. These samples are generally low viscosity lava flows with phenocryst-poor to aphyric magmas, containing diktytaxitic textures with a subophitic groundmass containing augite (Bacon, 1990; Conrey et al. 1997).

CABs contain SiO_2 contents (≤ 52 wt %), while BAs contain (> 52 wt % SiO_2). These primitive basalts contain higher LILE, SiO_2, and K_2O contents than LKTs and display a depletion of HFSEs and heavy rare earth elements (HREEs). LILE characterized enrichment relative to HFSEs and HREEs defines these basalts. CABs and BAs do not reach as high Al_2O_3, CaO and MgO contents as LKTs. These basalts generally contain more abundant olivine and plagioclase phenocrysts than LKTs, where flows are thicker and more oxidized (Bacon, 1990; Conrey et al. 1997). OIBs display HFSE enrichment trends, especially in Nb. These basalts contain intermediate phenocryst and groundmass textures between LKTs and CABs/BAs (Rowe et al. 2009).

1.3.2 HLP Primitive Basalts

The Majority of the HLPs primitive basalts are LKTs, along with some CABs and BAs. Primitive LKTs contain compositional similarities to MORBs. Primitive LKTs contain diktytaxitic textures with some degree of subophitic groundmass textures. Primitive CABs and BAs are generally aphyric to sparsely porphyritic, containing olivine and plagioclase as the dominant phenocryst phases, with clinopyroxene in a few samples (Jordan et al. 2002). Roth et al. (2008) investigated surface expression of recent HLP volcanism that produced these primitive LKTs using seismic tomography. Results depicted a region of low seismic velocity beneath these LKTs that extent to shallow depth of approximately 100-150 km, indicating a shallow origin of these primitive LKTs (Roth et al. 2008).

1.3.3 Newberry Primitive Basalts

Newberry primitive basaltic eruptions contain geochemical characteristics that include LKTs and CABs. The primitive LKTs are characterized by containing lower SiO_2 and K_2O concentrations, higher FeO and TiO_2 concentrations, and lower enrichment of LILEs relative to the primitive CABs. Primitive CABs also display strong deficiencies in HFSEs. Primitive LKTs are aphyric, equigranular basalts containing intersertal textures, and are highly diktytaxitic and vesicular (Meigs et al. 2009).

1.4 Layout of Thesis

Diverse geological landforms of tuff rings and maars, cinder cones, and lava fields situated within an ancient pluvial lake system created a unique back-arc area within the FRVF study area. The tectonic and petrological complexity of FRVF appear to be influenced by the subduction of the Juan de Fuca plate under the North American plate, eruptions from the central High Cascades, Newberry, and the HLPs, as well as extension of the Basin & Range province through accommodation of the Brothers Fault Zone.

Chapter 2 discusses FRVF major element concentrations through X-ray Fluorescence (XRF) data for 75 mafic bulk lava samples through whole rock variation diagram plots to classify these diverse back-arc magma types. These samples are divided into primitive (Mg# $\geq$ 60) and non-primitive samples useful for determining primary mantle source compositions by analyzing trace element data.

Chapter 3 discusses eruptive styles of the lava, scoria/spatter, and juvenile bombs in tuff rings and maars across the FRVF, indicative of their variations in groundmass crystallinity content, groundmass grain sizes, and vesicularity. The geochemistry of plagioclase and olivine phenocrysts, as well as spinel grain inclusions in olivine investigate possible mantle melting and crystallization processes.

Chapter 4 analyzes compatible and incompatible trace element data of primitive FRVF basalts to determine differences in mantle source compositions between magma types. Differences in subduction input, mantle fertility, and depth/degree of partial melting of primitive magma sources for each magma type, and same magma types found in different areas (western/central vs. eastern basalts) utilizing trace element diagrams is the main focus of this chapter.

Chapter 5 combines the results of the previous chapters into conclusive evidence of variable mantle melting processes beneath the FRVF back-arc. Geochemical variations of the diverse primitive basalts based on their distribution across the FRVF are the key result towards deducing differences in primary mantle sources.

CHAPTER 2: Fort Rock Volcanic Field Major Element Geochemistry: Analyses of a Diverse Suite of Basalts

2.1 Introduction

The Pliocene to Pleistocene Fort Rock Volcanic Field (FRVF) is a complex extensional back-arc setting influenced by multiple tectonic and volcanic events. A series of hydrovolcanic and conventional basaltic eruptions built a foundation of tuff rings, tuff cones, maars, cinder and spatter cones, and lava fields around the FRVF back-arc in which an ancient pluvial lake system once resided. Eruptions of these landforms deposited a diverse array of basaltic magmas with fluctuating major and trace element concentrations. These differences in geochemistry are best described through investigations of back-arc basin systematics.

Previous studies of the Mariana, east Scotia, Lau, and Manus back-arc basin spreading centers analyzed major and trace element compositions of back-arc basin basalts (BABBs) (Hart et al. 1972; Pearce & Cann, 1973; Hawkins, 1976; Gill, 1976; Tarney et al. 1977; Saunders & Tarney, 1979; Hawkins & Melchior, 1985; Sinton & Fryer, 1987; Stopler & Newman, 1994; Taylor & Martinez, 2003; Pearce et al. 2005; Wiens et al. 2006; Bézos et al. 2009). The compositions of BABBs can be very complex, and it is not entirely evident whether BABBs are simply transitional between mid-ocean ridge basalts (MORBs) and calc-alkaline basalts (CABs), or even truly their own distinct magma type (Pearce et al. 2005). These variations in basaltic compositions are widely considered to be a result of mantle melting of three separate primary mantle sources; a large ion lithophile element (LILE) enriched mantle source through addition of a subduction component, a fertile, high field strength element enriched (HFSE) intraplate mantle source, and a chemically depleted mid-ocean ridge basalt (MORB)- like mantle source (Pearce et al. 2005).

This chapter analyzes major and trace element data through X-ray Fluorescence (XRF) from 75 mafic bulk lava samples in an attempt to classify the different FRVF basalts into their most closely resembled magma type. Classifying basalts into primitive

samples Mg# ((xMgO / (xMgO + xFeO) * 100) of at least greater than 60 (molar) can aid in determining mantle characteristics and melting processes beneath the FRVF back-arc.

2.2 Methods

A total of 75 fresh basaltic rock samples were collected around the FRVF study area. A Garmin Oregon GPS device was used to record accurate sample coordinates located on 28 adjoining 7.5' quadrangles (Appendix A) (Figure 2-1). Brief hand sample descriptions were recorded (Appendix A).

All collected samples were chipped with an alumina jaw crusher, chipping approximately 20-50 gram rock chips per sample, and sent to the GeoAnalytical Laboratory at Washington State University (WSU) for X-ray fluorescence (XRF) analysis for 29 major and trace elements (Appendix B). Major elements concentrations are expressed as oxide weight percentages each > 0.1 % that include; SiO_2, TiO_2, Al_2O_3, FeO*, MnO, MgO, CaO, Na_2O, K_2O, and P_2O_5. Trace elements are reported in parts per million (ppm) with concentrations < 0.1 % that include; Ni, Cr, Sc, V, Ba, Rb, Sr, Zr, Y, Nb, Ga, Cu, Zn, Pb, La, Ce, Th, Nd, and U (Appendix B). The XRF technique uses a single low dilution fusion (2:1 ratio) of Li-tetraborate fused bead for both major and trace elements to provide maximum efficiency without loss of accuracy for data values (Johnson et al. 1999). The oxidation state of iron and volatile content of the rock are ignored, so that the original major element values can be normalized to 100% volatile-free concentrations (Johnson et al. 1999). All iron is expressed as FeO*, assuming all iron is Fe^{2+}.

2.3 Field Observations & Basalt Descriptions

A total of 81 magmatic rock samples (75 basaltic samples; 6 rhyolite samples) were collected from the FRVF area, extending as far west as Big Hole and Wickiup Spring quadrants, and as far east as Fandango Canyon (Appendix A, Figure 2-1). Volcanic features in the area included spatter cones, scoria cones, maar volcanoes, massive basaltic lava flows, flow banded rhyolites, lava tubes, shield volcanoes, and pyroclastic deposits (Appendix A, Figure 2-1). FRVF basaltic rock samples were collected along outcrops of vents, large lava flows, cinder cones, and as juvenile bombs and lapillis in altered tuff rings (Appendix A, Figure 2-1).

Large lava fields are found east of the Fort Rock basin at the Four Craters Lava Field near Crack-in-the Ground, East Lava Field in Jack's Place quadrant, and lava surrounding Cougar Mountain and the Devils Garden areas where multiple samples were collected. (Appendix A, Figure 2-1). Four Craters Lava flows aligned along a NW-SE trending fault trace, where six basaltic samples were collected, including Reed Rock samples (Appendix A, Figure 2-1). Green Mountain is the northern scoriaceous summit cone of a small, older Pleistocene shield volcano, where four basaltic samples were collected (Appendix A, Figure 2-1). The Devils Garden Lava Flow is bordered by low spatter ramparts, located in the Sixteen Butte quadrant north of the Fort Rock Basin. This area contained outcrops of oxidized red scoria (highly vesicular, altered weathered basalt) from cinder cones, and also lighter felsic volcanic rhyolites (Appendix A, Figure 2-1). Six basaltic samples were obtained from the Oatman Flat area south of the Fort Rock Basin. Tuff rings of the Black Hills contained some juvenile lapillis (small fresh basaltic fragments ~ 2 mm to 64 mm in diameter). Connley Hills contained rhyolite samples with shaly, devitrified glassy textures (Appendix A, Figure 2-1).

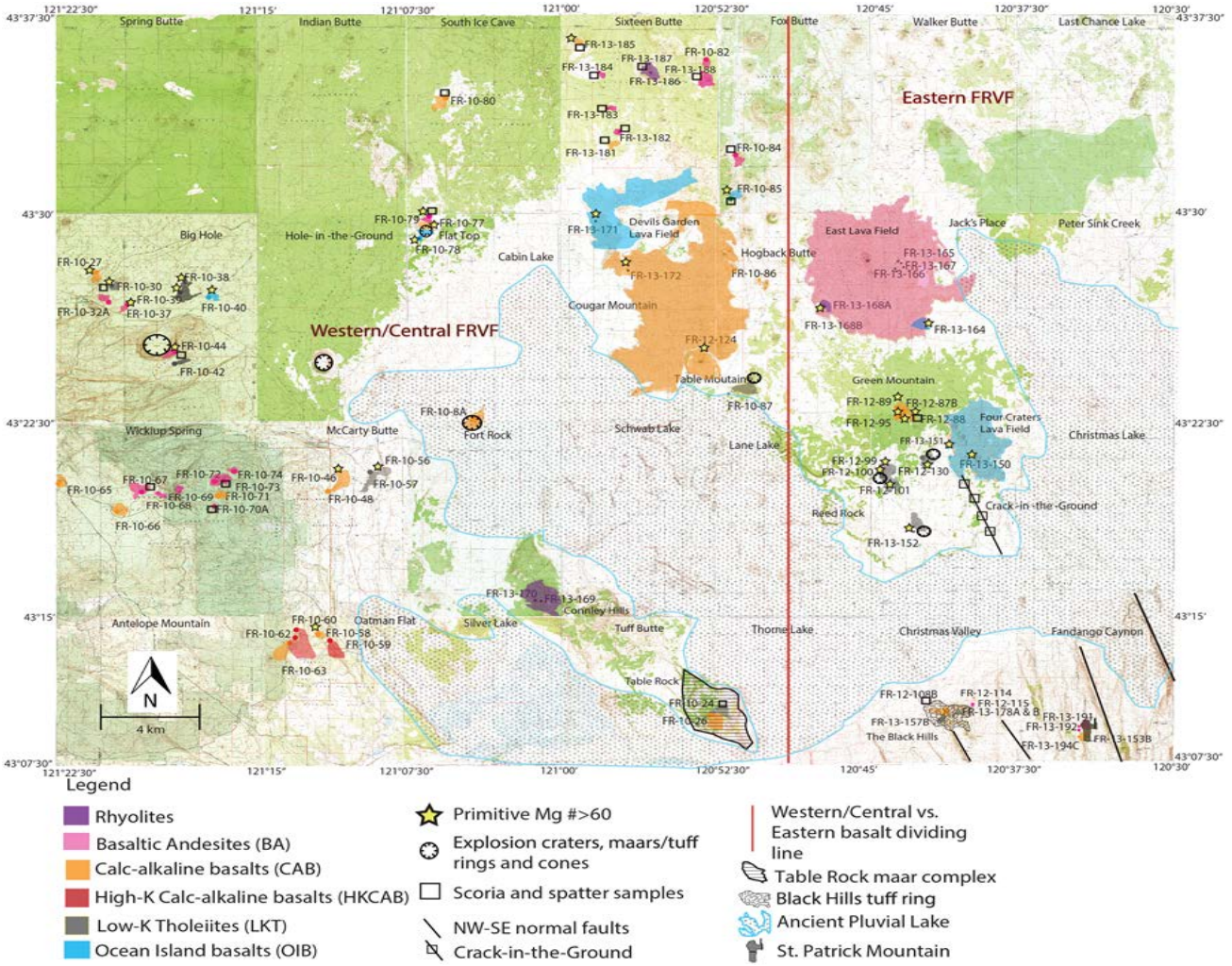

Figure 2-1. Petrographic map of FRVF study area. Distribution of maars, tuff rings and cones, scoria and spatter samples from cinder cones, and lava fields to the ancient pluvial lake system.

Multiple hydrovolcanic basaltic samples were collected around the vicinity of the Big Hole, Hole-in-the-Ground, Flat Top, Fort Rock, Table Rock, Table Mountain, the Black Hills, and St. Patrick's Mountain tuff rings/cones and maars (Appendix A, Figure 2-1). These areas also contained lava samples concentrated around the McCarty Butte and Oatman Flat areas (Appendix A, Figure 2-1).

Phenocrysts of olivine and plagioclase occur in the majority of basaltic samples as translucent green fractured crystals and milky white crystal laths with cleavage, respectively. Phenocrysts of plagioclase tend to be more abundant than olivine phenocrysts in most basaltic samples (Appendix A).

2.4 XRF Results:

2.4.1 Classification of FRVF Magma Types

XRF analysis of major element compositions of 75 basaltic FRVF samples fall within the general major element compositional ranges typical of basalts (Appendix B). FRVF basalts contain 48.11-56.34 wt % SiO_2, 1.92-8.89 wt % MgO, 2.89-5.83 wt % total alkalis (Na_2O+K_2O), 0.917-1.940 wt % TiO_2, 7.77-11.97 wt % FeO, 15.10-20.87 wt % Al_2O_3, 7.37-11.87 wt % CaO, and 0.123-0.544 wt % P_2O_5 (Appendix B). A total of 6 samples contained SiO_2 contents that were > 68 wt % SiO_2 and were classified as rhyolitic samples (Appendix B).

Alkali-metal abundances (Na_2O+K_2O) with increasing SiO_2 in FRVF whole rock concentrations confirm that the majority of the samples are classified as basalts and basaltic andesites (BAs) (Figure 2-2). Samples with <52 wt % SiO_2 and Na_2O+K_2O < 5 wt % are classified as basalts, while magmas with >52 wt % SiO_2 are classified as BAs (Figure 2-2). One sample FR-12-115 plots within the basaltic trachy-andesitic area, reaching the highest N_2O+K_2O value of 5.83 wt % at a SiO_2 value of 52.7 wt % (Figure 2-2). There is an overall positive correlation of increasing incompatible elements Na_2O+K_2O as SiO_2 increases with increasing fractional crystallization and assimilation (Figure 2-2). All samples plot into the subalkaline field, except for the basalt trachy-andesitic sample FR-12-115.

FRVF basaltic samples can further be classified as primitive (Mg# > 60) or more evolved non-primitive samples (Mg# < 60) (Figure 2-3). A total of 31 out of 75 samples are considered primitive basalts in this study. The highest Mg# basalt (68) is sample FR-13-152 located south of Reed Rock near the Crack-in-the-Ground quadrant of FRVF (Figure 2-2). An unusually low Mg# 28 sample was analyzed in a BA containing 52.7 wt % SiO_2 (Figure 2-2).

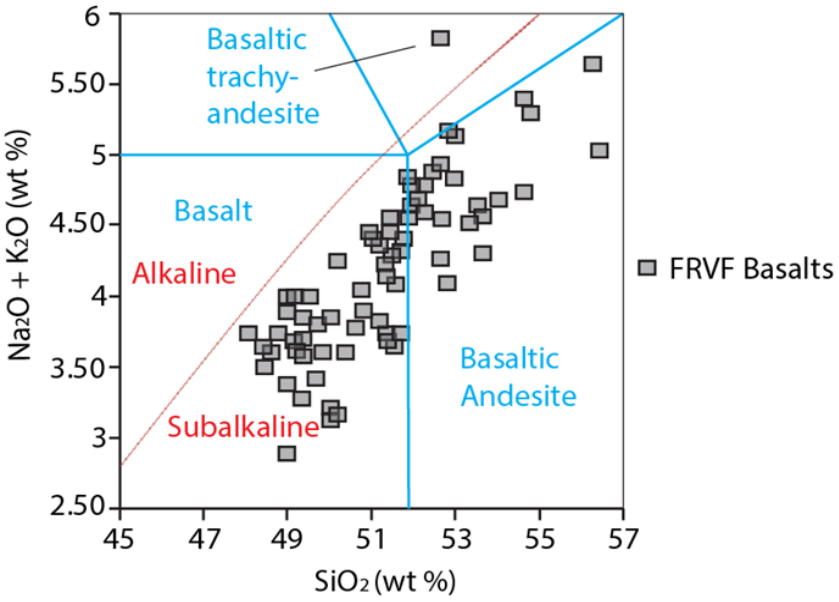

Figure 2-2. Total alkali content $Na_2O + K_2O$ vs. SiO_2 (wt %). Blue solid lines represent division of basalt types. Red curved line divides alkaline vs. subalkaline basalts (extracted from MacDonald & Katsura (1964). FRVF basalts are subalkaline basalts and BAs. BA sample FR-12-115 is an alkaline basaltic trachy-andesite. Values represented as wt % oxides.

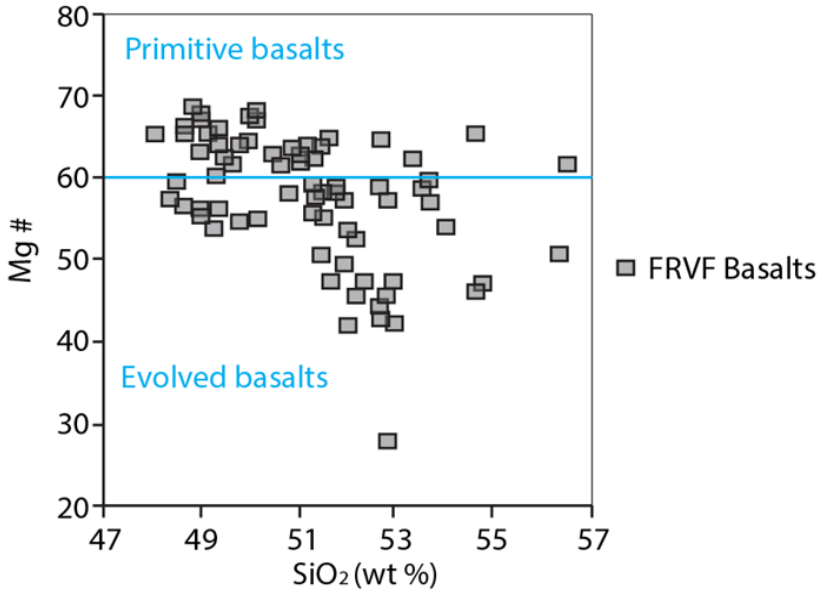

Figure 2-3. Mg# (xMgO/(xMgO+xFeO)*100) (molar %) vs. SiO_2 (wt %). Blue solid line represents division of primitive basalts (Mg# > 60) from evolved basalts (Mg# < 60). Values represented as wt % oxides.

Whole rock geochemistry of major and trace element compositions of these FRVF basalts analyzed for five diverse magma types. They include LKTs, CABs, high-K calc-alkaline basalts (HKCABs), BAs, and OIBs.

FRVF LKTs contain lower K_2O values (0.22-0.44 wt %) and reach lower Ba/Nb ratios than the other magma types (Tables 2-1 & 2-2). Primitive LKT samples display the lowest alkali abundances (2.89-3.67 wt % Na_2O+K_2O) and do not reach as high SiO_2 values as the CABs, HKCABs and primitive OIBs (Tables 2-1 & 2-2). CABs tend to be enriched in Ba relative to Nb (high Ba/Nb ratios) than other magmas containing $\leq$52 wt % SiO_2, and do not reach as high CaO, and as low Na_2O/K_2O values as the LKTs (Tables 2-1 & 2-2). HKCABs are similar to CABs except they reach higher K_2O values (up to 1.11 wt %) and higher P_2O_5 values (0.441-0.449 wt %) (Tables 2 & 3). BAs contain >52 wt % SiO_2 and reach high Ba/Nb ratios (Tables 2-1 & 2-2). OIBs contain high Nb concentrations $\geq$12.1 ppm, and do not reach as high Ba concentrations as CABs and BAs, and contain higher TiO_2 concentrations than the other primitive magma types (Tables 2-1 & 2-2). FRVF CAB and BA magmas are the most abundant and chemically variable basalt group in the FRVF back-arc.

Table 2-1. Representative Analyses of FRVF Magma Types

Sample	FR-10-39	FR-13-152	FR-10-27	FR-12-89	FR-10-44	FR-10-85	FR-10-62
Quad.	Big Hole	Reed Rock	Big Hole	Green Mnt.	Big Hole	Blowouts	Oatman Flat
Type	LKT	LKT	CAB	CAB	BA	OIB	HKCAB
SiO_2	49.18	48.92	50.85	51.29	54.56	48.11	51.77
TiO_2	1.49	0.92	1.32	1.21	1.08	1.64	1.32
Al_2O_3	17.19	17.56	17.48	17.23	16.45	16.65	17.59
FeO*	9.75	8.66	9.33	8.72	7.91	10.21	9.38
MnO	0.16	0.16	0.16	0.16	0.14	0.17	0.16
MgO	8.89	8.89	7.62	6.95	7.15	9.11	6.21
CaO	9.48	11.87	9.08	10.38	7.70	10.02	8.71
Na_2O	3.24	2.67	3.31	2.95	3.56	3.13	3.30
K_2O	0.41	0.22	0.60	0.80	1.19	0.61	1.11
P_2O_5	0.22	0.12	0.26	0.30	0.26	0.35	0.44
Na_2O+K_2O	3.64	2.89	3.91	3.76	4.75	3.73	4.41
Ni	187	145	143	69	155	180	101
Cr	298	253	165	171	272	296	123
Sc	29	41	27	38	24	32	25
V	217	209	208	226	157	207	211
Ba	161	71	235	424	408	153	570
Rb	6	3	8	16	28	9	16
Sr	355	190	431	482	345	305	643
Zr	113	73	110	117	158	155	146
Y	26	24	25	27	26	29	29
Nb	6	3	7	7	7	19	8
Ga	17	13	18	17	17	15	18
Cu	74	88	67	59	54	74	93
Zn	80	61	79	74	74	75	89
Pb	1	1	2	3	5	1	6
La	8	1	7	16	9	14	18
Ce	23	12	25	35	28	30	47
Th	0	0	1	3	2	0	2
Nd	15	8	16	20	17	19	26
U	1	0	1	1	1		1
Mg#	66	68	63	63	65	65	58

Total Fe represented as FeO*. Samples analyzed by XRF. XRF major element analyses were normalized to 100%. Whole-rock powders were analyzed at the Washington State GeoAnalytical Laboratory.

Table 2-2. Summary of Compositional Ranges of FRVF Magma Types

All Magmas	SiO_2 (wt %)	MgO (wt %)	Mg#	Al_2O_3 (wt %)	FeO* (wt%)	CaO (wt%)	K_2O (wt%)	P_2O_5 (wt%)	Ba (ppm)	Nb (ppm)
<52% SiO_2										
LKT	48.40-50.08	6.52-8.89	55-68	16.64-18.67	8.36-11.85	9.48-11.87	0.22-0.44	0.123-0.347	71-309	3-7
CAB	49.24-51.97	3.60-8.21	42-65	16.79-20.87	8.43-11.97	7.91-10.61	0.45-0.90	0.196-0.357	170-431	3-10
OIB	48.11-51.15	7.05-9.23	62-67	16.56-17.62	8.86-10.21	9.20-10.02	0.52-0.93	0.298-0.375	153-302	12-19
HKCAB	51.41-51.89	5.96-6.24	57-58	17.50-17.59	9.38-9.48	8.71-8.82	1.05-1.11	0.441-0.459	570-606	8-9
>52% SiO_2										
BA	52.13-56.34	1.92-7.15	28-65	15.10-19.30	7.77-11.86	7.37-9.21	0.63-1.69	0.178-0.544	268-709	3-13

Primitive	SiO_2 (wt%)	MgO (wt%)	Mg#	Al_2O_3 (wt%)	FeO* (wt%)	CaO (wt%)	K_2O (wt%)	P_2O_5 (wt%)	Ba (ppm)	Nb (ppm)
<52% SiO_2										
LKT	48.92-50.08	7.67-8.89	61-68	17.19-18.67	8.36-9.94	9.48-11.87	0.22-0.44	0.12-0.28	71-250	3-7
CAB	49.28-51.61	6.95-8.21	60-65	17.09-17.52	8.43-10.65	9.08-10.61	0.45-0.82	0.24-0.35	170-426	5-10
OIB	48.11-51.15	7.05-9.23	62-67	16.56-17.62	8.86-10.21	9.20-10.02	0.52-0.93	0.30-0.38	153-302	12-19
>52% SiO_2										
High Mg# BA	52.70-56.34	5.62-7.15	61-65	16.45-17.28	7.56-8.21	7.70-9.13	0.85-1.41	0.236-0.325	268-501	7-12

Division of primitive (Mg# > 60) and all FRVF basalt compositional ranges represented in wt% oxides and ppm. All Fe represented as FeO*. Mg#= (xMgO/(xMgO+xFeO)*100)

2.4.2 Major Element Concentrations

Major element whole rock variation diagrams display the differences in concentrations between the more evolved LKTs, CABs, BAs, HKCABs (Mg# < 60) as well as the primitive LKTs, CABs, BAs, and OIBs (Mg# > 60) (Figure 2-4). As SiO_2 increases, compatible major elements MgO, CaO, and FeO* tend to decrease in the bulk rock concentration (Figure 2-4). Concentrations of K_2O tend to increase as SiO_2 concentrations increase (Figure 2-4).

Concentrations of MgO decrease with increasing concentrations of SiO_2 for all FRVF BABB magma types (Figure 2-4A). Primitive samples tend to display higher MgO contents than the more evolved samples for each magma type. Primitive OIBs contain the highest values of MgO contents (9.01-9.23 wt %) found near Big Hole and the Devil's Garden vents. Primitive LKTs contain high MgO concentrations as well (up to 8.89 wt %), and not as low concentrations as primitive CABs, primitive OIBs, and high Mg# primitive BAs. Extremely low MgO concentrations (1.92 wt %) are found in BA sample FR-12-115 at the Black Hills. Evolved CAB samples do not reach as high MgO concentrations as the evolved LKT samples (Figure 2-4A).

Concentrations of FeO display an overall decrease with increasing SiO_2 contents (Figure 2-4B). LKTs, CABs and BAs tend to all contain high FeO values, where LKTs contain high FeO concentrations at relatively constant SiO_2 values (Figure 2-4B). CABs display an initial decrease in FeO contents with increasing SiO_2, then at approximately 51.27 wt % SiO_2 the FeO content increases with relatively constant SiO_2 values (Figure 2-4B).

Concentrations of Al_2O_3 tend to remain more or less constant with increasing SiO_2 values for primitive LKTs, CABs, BAs, and OIBs (Figure 12C). Evolved LKT samples display a slight increase in Al_2O_3 contents with increasing SiO_2 contents (Figure 2-4C). Evolved CABs and BAs tend to reach higher Al_2O_3 concentrations than LKTs and OIBs, the highest occurring in CAB sample FR-10-63 at a value of 20.87 wt % Al_2O_3 (Figure 2-4C). The lowest concentration is found in BA sample FR-13-192 at a value of 15.10 wt % Al_2O_3 (Figure 2-4C). High Al_2O_3 concentrations at high SiO_2 are displayed in

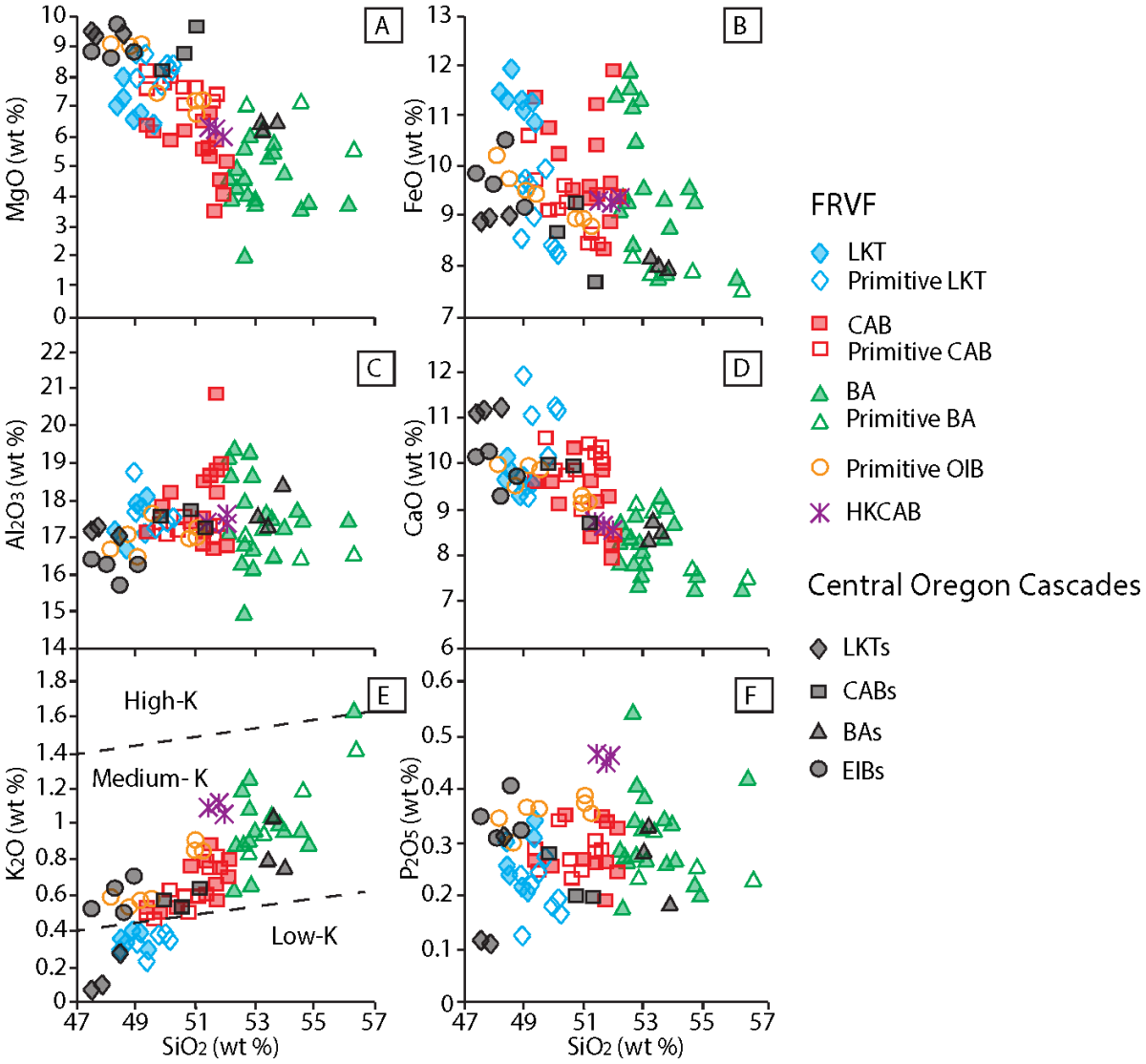

Figure 2-4: Whole rock variation diagrams of major elements vs. SiO_2 for each magma type and primitive magmas of FRVF BABBs. A) MgO vs. SiO_2; B) FeO* vs. SiO_2; C) Al_2O_3 vs. SiO_2; D) CaO vs. SiO_2; E) K_2O vs. SiO_2; Low-K, med-K, and high-K lines on the K_2O extracted from Miyashiro (1974); F) P_2O_5 vs. SiO_2. Values recorded as wt% oxides. Central Oregon Cascade LKTs extracted from Bacon (1990) Crater Lake samples 621, 894, and 1143 from lava flows; CABs extracted from Bacon (1990) Crater Lake sample 1530 from a lava/bomb from cone, and Rowe et al. (2009) lava samples TB-02-1 and SIC-02-1 323 and 329 km from the trench in the central Oregon Cascades respectively; BAs extracted from Bacon (1990) lava samples 854, 1141, and 1087; EIBs (enriched island basalts) extracted from Rowe et al. (2009) central Oregon Cascade lava samples HL-03-01, WF-02-01, NMB-03-01,and BLW-03-1 located 279, 292, 311, and 347 km from the trench respectively.

some CAB and BA sample (Figure 12C). One primitive LKT sample FR-10-30 from Big Hole displays a higher Al_2O_3 concentration (18.67 wt %) than the other primitive LKT samples (Figure 2-4C).

Concentrations of CaO tend to decrease with increasing SiO_2 contents for all magma types. LKTs contain higher CaO values (up to 11.87 wt %) than all other basalt types. The more evolved CAB and BA samples trend towards values as low as 7.37 wt % CaO (Figure 2-4D).

Concentrations of K_2O generally increase with increasing SiO_2 concentrations for all magma types (Figure 2-4E). LKT samples plot in the low-K area, containing a range of 0.22-0.44 wt % K_2O . All other basalt types plot within the medium-K area (0.45-1.69 wt % K_2O), with BA sample FR-13-191 reaching the highest K_2O value of 1.69 wt %. HKCABs display higher K_2O values than all other CABs. BAs display a higher range of K_2O concentrations (0.63-1.69 wt %) than all other magma types (Figure 2-4E).

Concentrations of P_2O_5 display decreasing concentrations with increasing SiO_2 concentrations for BA samples. BA sample FR-13-192 contains the highest P_2O_5 content of 0.54 wt %. Primitive LKTs tend to reach the lowest P_2O_5 values, where Reed Rock sample FR-13-152 contains 0.12 wt % P_2O_5 at a low SiO_2 concentration (48.92 wt %). HKCABs reach higher P_2O_5 concentrations than all CABs (0.44-0.46 wt %) (Figure 2-4E).

Central Oregon Cascade basaltic samples tend to plot onto similar major element concentrations as FRVF basalts for similar magma types (Figure 12). Some differences include central Oregon Cascade LKTs reaching higher MgO, lower K_2O and lower P_2O_5 concentrations at lower SiO_2 values than FRVF LKTs (Figure 2-4E).

According to the Miyashiro (1974) FeO*/MgO vs.SiO_2 tholeiitic and calc-alkaline dividing line, most samples plot into the tholeiitic high FeO*/MgO ratio area, even most CABs and BAs. A definitive distinct calc-alkaline trend towards lower FeO*/MgO ratios at higher SiO_2 values is visible for eastern primitive Green Mountain CAB samples (1.25 FeO*/MgO at 51.29 wt % SiO_2, to 1.13 FeO*/MgO at 51.61 wt %) (Figure 2-5).

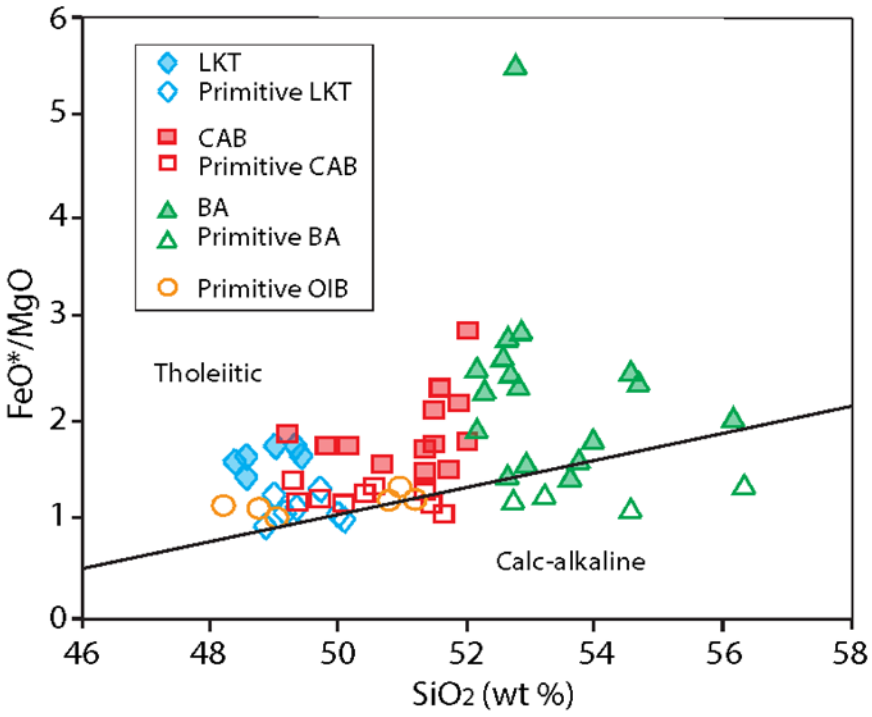

Figure 2-5. FeO* / MgO vs. SiO_2. Black line indicates division between tholeiitic and calc-alkaline compositions based on Miyashiro's (1974) tholeiitic vs. calc-alkaline line classification. Most basalts fall into the tholeiitic area. Note the decreasing FeO*/MgO contents with increasing SiO_2 calc-alkaline trend in primitive eastern CAB FRVF samples.

2.4.3 Ba/Nb Trace Element Concentrations

Ba and Nb trace element concentrations aid in distinguishing HFSE-enriched OIBs from subduction enriched CABs, HKCABs, and BAs, and incompatible element depleted LKTs (Figure 2-6). BAs reach higher Ba concentrations (up to 709 ppm) than all other magma types, and higher Nb concentrations (up to 13 ppm) than CABs and LKTs. OIBs are HFSE enriched and contain higher Nb concentrations (12-19) at lower Ba concentrations (153-302 ppm) than CABs, BAs and HKCABs. HKCABs display higher Ba concentrations (570-606 ppm) than CABs. FRVF BABBs contain similar trace element Ba and Nb concentrations as LKTs, CABs, BAs and enriched island basalts (EIBs) found in the central Oregon Cascades area. The FRVF OIBs contain similar HFSE-enrichment trends as found in the central Oregon Cascades EIBs (Figure 2-6).

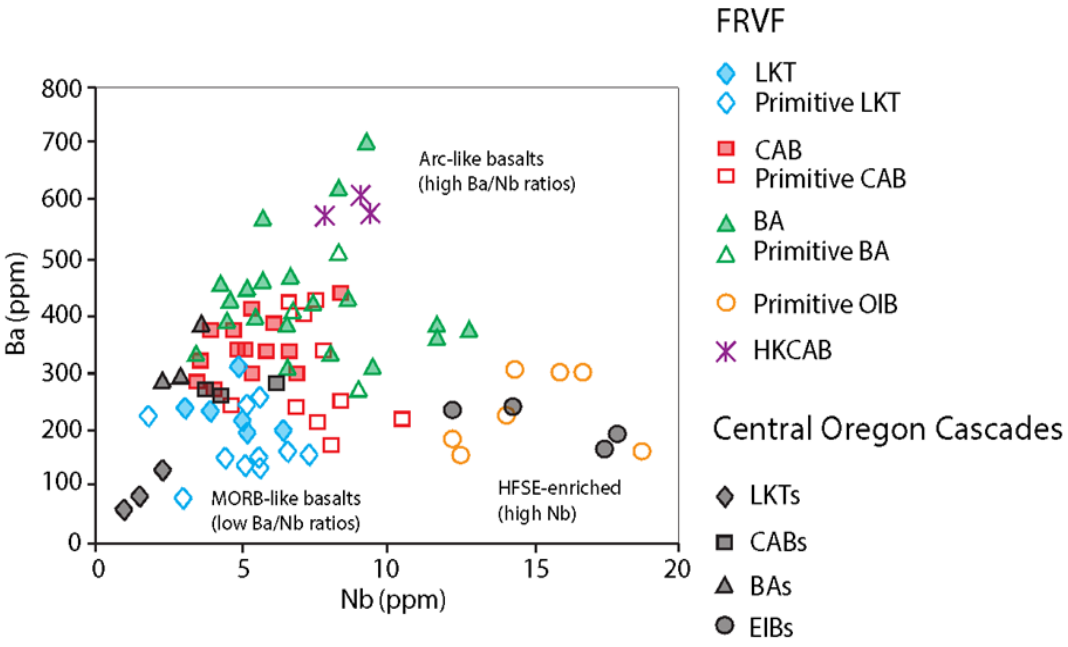

Figure 2-6. Incompatible element ratio diagram of LILE (Ba) vs. HFSE (Nb) to distinguish between MORB-like basalts (LKTs low Ba/Nb ratios), arc-like basalts (CABs high Ba/Nb ratios), and HFSE-rich intraplate basalts (OIB low Ba/Nb ratios with abnormally high Nb contents). Central Oregon Cascade LKTs extracted from Bacon (1990) Crater Lake samples 621, 894, and 1143 from lava flows; CABs extracted from Bacon (1990) Crater Lake sample 1530 from a lava/bomb from cone, and Rowe et al. (2009) lava samples TB-02-1 and SIC-02-1 323 and 329 km from the trench in the central Oregon Cascades respectively; BAs extracted from Bacon (1990) lava samples 854, 1141, and 1087; EIBs (enriched island basalts) extracted from Rowe et al. (2009) central Oregon Cascade lava samples HL-03-01, WF-02-01, NMB-03-01,and BLW-03-1 located 279, 292, 311, and 347 km from the trench respectively.

2.4.4 FRVF Western/Central vs. Eastern Primitive Geochemical Variations

Geochemical differences in major and trace element concentrations are evident within primitive magma types LKT, CAB, and OIBs across the arc from west to east. Primitive magma types are grouped into western/central and eastern sections based on their notable major and trace element compositional differences (refer to red FRVF division line in Figure 2-1). There were no notable compositional trends across the back-arc for the high Mg# BA primitive basalts and therefore were not grouped into western/central vs. eastern segments.

Western/central primitive LKTs contain lower CaO, and higher Na_2O, FeO*, TiO_2 and Ba concentrations than eastern primitive LKTs (Figure 2-7 & 2-8). Eastern primitive CABs contain lower FeO*, TiO_2, Na_2O, and higher CaO, K_2O, and Ba concentrations than western/central primitive CABs (Figure 2-7 & 2-8). Eastern primitive OIBs contain lower FeO*, MgO, CaO and higher SiO_2, Na_2O, K_2O, and Ba values than western/central primitive OIBs (Figure 2-7 & 2-8).

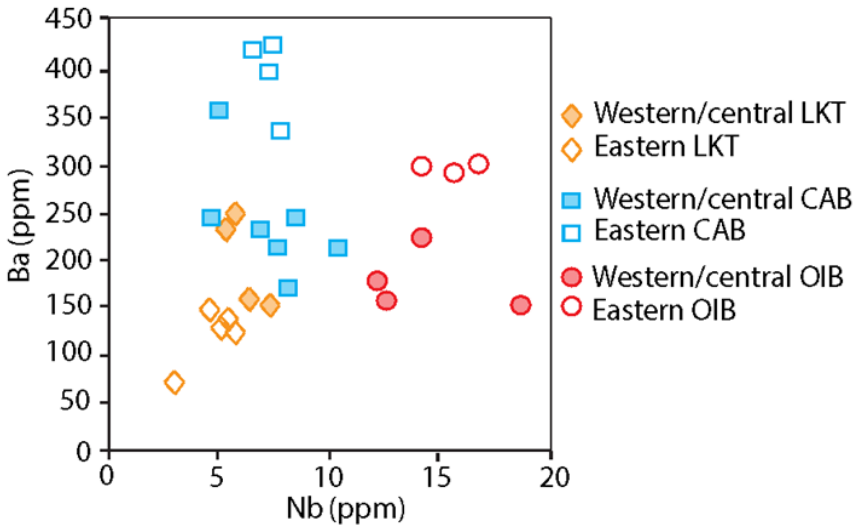

Figure 2-7. Primitive FRVF western/central vs. eastern basaltic whole rock trace element compositions of Ba vs. Nb. values recorded as ppm. Eastern OIBs display a greater enrichment in Ba than western/central OIBs. Eastern CABs display an overall greater enrichment in Ba than western/central CABs. Western/central LKTs display greater enrichment in both Ba and Nb than eastern LKTs.

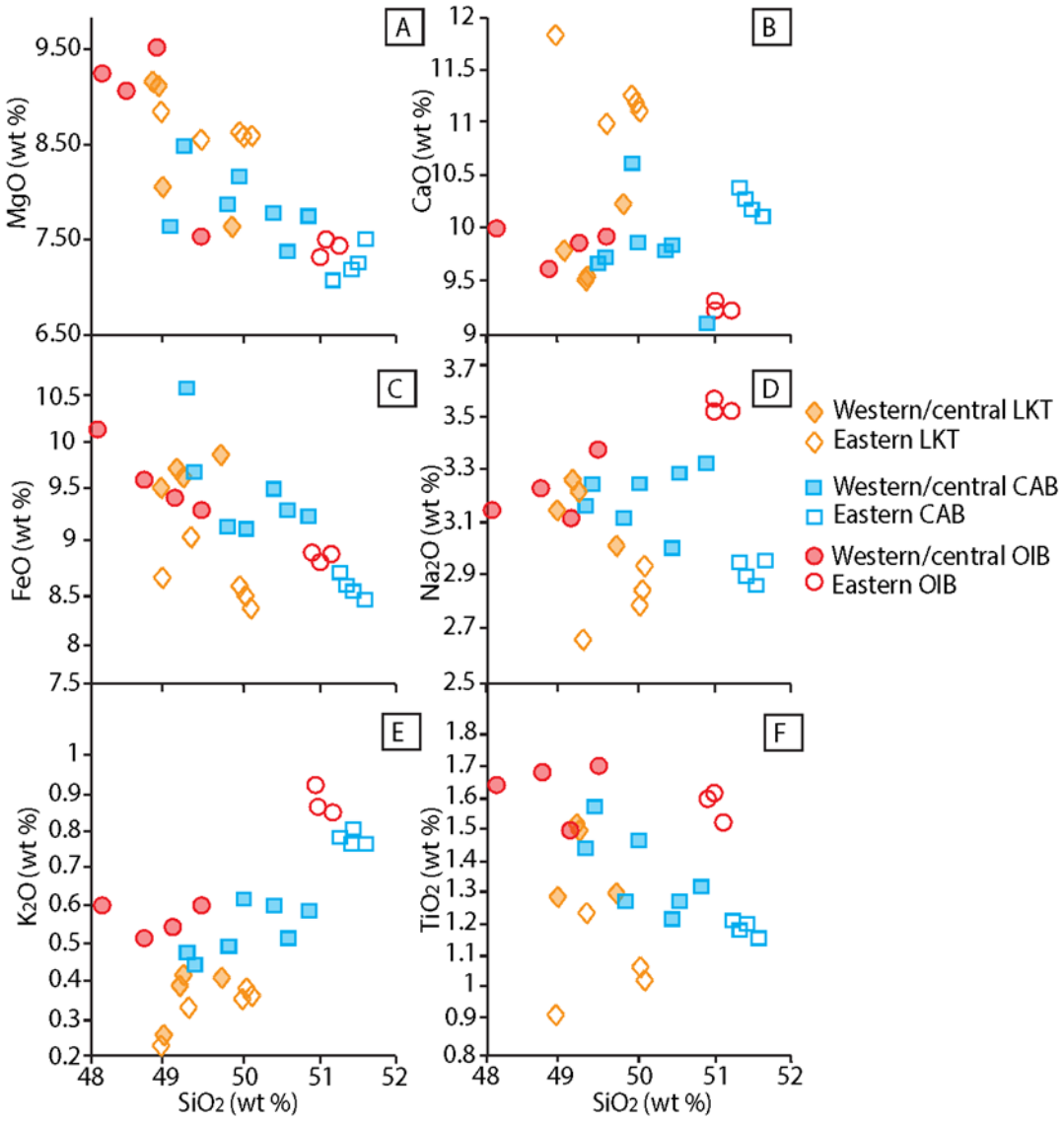

Figure 2-8: Primitive FRVF western/central and eastern basaltic whole rock compositions vs. SiO_2. A) MgO vs. SiO_2; B) CaO vs. SiO_2; C) FeO vs. SiO_2; D) Na_2O vs. SiO_2; E) K_2O vs. SiO_2; F) TiO_2 vs. SiO_2. Note the differences in major element concentrations within primitive magma types based on their distribution in the FRVF. All concentrations represented in wt %.

2.5 Discussion

2.5.1 Igneous Processes: Major Element Geochemistry

Whole rock variation diagrams of major element oxides against SiO_2 aids in the analysis of different magma types, and possible fractional crystallization trends of magmas erupted across the FRVF back-arc region. Primitive samples tend to display higher MgO contents than the more evolved samples for each rock type, suggesting an overall pattern of increasing olivine fractionation (Bacon, 1990; Bacon et al. 1997; Conrey et al. 1997) (Figure 2-4A).

CABs display an initial decrease in FeO contents with increasing SiO_2, then at approximately 51.27 wt % SiO_2 the FeO content increases with relatively constant SiO_2 values. This is possibly due to the onset of increasing oxide and Fe-rich olivine crystallization in the groundmass (Bacon, 1990; Bacon et al. 1997; Conrey et al. 1997) (Figure 2-4B). Green Mountain primitive CABs display an arc-like calc-alkaline trend of decreasing FeO content with increasing SiO_2 content, possibly due to the early crystallization of oxides (Bacon, 1990; Bacon et al. 1997; Conrey et al. 1997). The BA samples display a decrease in FeO content with increasing SiO_2 content, possibly a result of crystallization of more Fe-rich olivine phenocrysts in more evolved basaltic andesite samples (Bacon, 1990; Bacon et al. 1997; Conrey et al. 1997) (Figure 2-4B). This could also possibly be a result of more extensive oxide and pyroxene fractionation (Bacon, 1990).

High Al_2O_3 concentrations at high SiO_2 seen in some evolved CAB and BA samples can possibly be attributed to plagioclase crystal contamination, or plagioclase suppression with high H_2O contents (Bacon, 1990; Bacon et al. 1997; Conrey et al. 1997). Constant Al_2O_3 values as SiO_2 increases for primitive samples most likely indicate little to no plagioclase fractional crystallization (Bacon, 1990; Bacon et al. 1997; Conrey et al. 1997) (Figure 2-4C).

The concentration of CaO tends to decrease with increasing SiO_2 content for all magma types, possibly due to increased feldspar fractionation (Bacon, 1990; Bacon et al. 1997; Conrey et al. 1997) (Figure 2-4D).

Primitive western/central LKT sample FR-10-30 contains noticeably low SiO_2, CaO and higher Al_2O_3 concentrations, suggesting the magma was derived by dry, low degree partial melting at higher pressures where the presence of a hydrous phase, possibly amphibole, mediates major element concentrations (Conrey et al. 1997). Under these deep crustal conditions, the stability of plagioclase is reduced which can lead to either plagioclase-free fractionation, or preferential melting of plagioclase (Sekine & Wyllie, 1982; Sudo & Tatsumi 1990; Mclnnes & Cameron, 1994; Conrey, 1990; Conrey et al. 1997).

The concentration of K_2O generally increases with increasing SiO_2 concentrations due to its incompatibility in most crystal phases, and increased crustal contamination (Bacon, 1990; Bacon et al. 1997; Conrey et al. 1997) (Figure 2-4E).

More evolved BA samples tend to display decreasing P_2O_5 values with increasing SiO_2 values, most likely indicating apatite fractionation (Bacon, 1990; Bacon et al. 1997; Conrey et al. 1997) (Figure 2-4F).

2.5.2 Complex Primitive Magma Types: CAB Compositional Variability

A select few primitive western/central CAB samples display intermediate compositions between LKTs and OIBs (Figure 2-6 & 2-7). Samples FR-10-27, FR-10-77, FR-12-124, FR-13-172, FR-13-185 contain higher Nb concentrations (7-10 ppm) at low to intermediate Ba concentrations (170-246 ppm) (Figure 2-4E, Figure 2-7, Figure 2-8). Primitive CAB sample FR-10-46 appears to be plotted alongside the LKTs, but is still grouped as a CAB due to its higher K_2O contents of 0.61 wt %. LKT sample FR-10-24 appears to be plotted with the CABs, but its lower K_2O contents of 0.44 wt % classifies the magma as an LKT (Figure 2-4E, Figure 2-7, Figure 2-8). All samples were analyzed as western/central primitive CABs can also be described as transitional BABBs between MORBs, OIBs, and the true end-member CABs that are represented by the primitive Green Mountain samples.

Possible variations between primitive CABs and LKTs are the differences in the degree of partial melting, and the amount of LILE enrichment to the mantle wedges (Taylor & Martinez, 2003). A heterogeneous mixture of depleted and HFSE-rich intraplate mantle domains that have been enriched by a subduction component is possibly the source for magmas categorized as western/central primitive CABs (Taylor & Martinez, 2003).

According to the Miyashiro (1974) FeO*/MgO vs.SiO_2 variation diagram, most samples plot into the tholeiitic high FeO*/MgO ratio area, even most CABs and BAs (Figure 2-5). The addition of water to the mantle wedge leads to calc-alkaline differentiation trends where FeO*/MgO ratios are constant as SiO_2 increases. Tholeiitic differentiation trends result from dry, anhydrous mantle (Arculus, 2002). This could possibly mean the amount of hydrous subduction component added to the back-arc depleted mantle wedge is not efficient enough for magmas to follow the calc-alkaline fractionation trend for most evolved magma samples (Figure 2-5) (Borg et al. 1997; Arculus, 2002).

This possibly suggests that the FRVF does in fact promote anhydrous melting and fractional crystallization, or the LILE enrichment trend of CABs is really only producing

LKTs that are slightly more enriched than they should appear to be to represent a MORB-like composition. The classification of magma types still remains the same, as these seemingly BABB transitional magma types are difficult to categorize into a specific magma group based on major and trace element data. A definitive distinct calc-alkaline trend towards lower FeO*/MgO ratios at higher SiO_2 values is evident for eastern primitive Green Mountain CAB samples, and can easily be considered true CAB end-members (Figure 2-5) (Arculus, 2002).

2.5.3 Western/Central vs. Eastern Primitive Geochemical Interpretations

Primitive magma geochemistry aids in identifying variances in mantle source processes, such as the degree of partial melting, depth of melting, subduction enrichment, and the fertility of the mantle source.

Higher FeO* contents in western LKTs is a possible trend for melting of a deeper mantle source than eastern LKTs (Conrey et al. 1997) (Figure 2-8). Eastern LKT sample FR-13-152 found near Reed Rock contains the lowest SiO_2 and highest MgO content for primitive LKTs (Figure 2-8). This highly primitive sample (Mg# 68), contains the lowest TiO_2 , Na_2O , P_2O_5 , K_2O , Ba/Nb, and highest CaO contents out of all primitive LKT samples (Figure 2-8). This suggests the primary mantle source for Reed Rock eastern LKTs are derived from a shallow depleted lithospheric mantle reservoir (Bacon, 1990). Higher incompatible element concentrations in western LKTs suggest moderate enrichment by source contamination through a subduction modified mantle from mixing with a depleted back-arc mantle source (Bacon et al. 1997). Low Na_2O and TiO_2 values for the eastern dry end-members are due to the depletion of the mantle wedge, as reflected by lower Nb content (Taylor & Martinez, 2003; Wiens et al. 2006) (Figure 2-7 & 2-8). The higher Na_2O and TiO_2 contents of the more hydrous western/central LKT sources reflect additions of Na_2O and TiO_2 from a subduction component (Wiens et al. 2006) (Figure 2-8). The low Na_2O content in the eastern primitive LKT sources can result from depletion owing to previous melt extraction, whereas the western primitive LKT sources higher Na_2O contents can be a result of addition by a subduction component (Wiens et al. 2006) (Figure 2-8).

Eastern Primitive CABs contain low FeO* and TiO_2 contents, suggesting involvement of early Fe-Ti oxide fractionation under more oxidized conditions (Rowe et al. 2009) (Figure 2-8). Higher K_2O and Ba values are possibly due to a greater contribution of a subduction component to the mantle wedge, and/or crustal level assimilation (Bacon, 1990) (Figure 2-7 & 2-8). Higher CaO contents are possibly due to little to no plagioclase fractionation (Rowe et al. 2009) (Figure 2-8). Western primitive CAB sample FR-10-58 also shows high Ba values, but higher FeO* and TiO_2 values, suggesting LILE enrichment to a deeper magma source undergoing little to no Fe-Ti oxide fractionation (Bacon et al. 1990; Conrey et al. 1997) (Figure 2-7 & 2-8). High Al_2O_3, CaO, and low FeO* contents of eastern CABs is consistent with an origin by 20-30% partial melting of spinel peridotite at lower pressures of approximately 15 kbar (Hart, 1985; Bartels et al. 1991; Hirose & Kushiro, 1993; Conrey et al. 1997) (Figure 2-8).

Eastern primitive OIBs contain lower FeO*, MgO, CaO and higher SiO_2, Na_2O, K_2O, Ba, and generally higher Nb values than western/central primitive OIBs (Figure 2-7 & 2-8). These results point towards increased fractionation in the eastern primitive OIBs than the western/central primitive OIBs (Bacon, 1990). The higher concentrations of incompatible elements and lower concentrations of compatible elements in eastern primitive OIBs suggest higher degrees of partial melting of a more enriched mantle source than western/central primitive OIBs (Bacon et al. 1990; Conrey et al. 1997) (Appendix B, Figure 2-8). The lower CaO concentrations in eastern primitive OIBs are possibly due to more feldspar and possible pyroxene fractionation in the western/central primitive OIBs (Bacon et al. 1990; Conrey et al. 1997 (Figure 2-8). The lower FeO* contents in eastern primitive OIBs possibly suggest higher degrees of melting of a shallower mantle source to the east (Conrey et al. 1997) (Figure 2-8). The higher Ba contents in eastern primitive OIBs suggest a greater contribution of a subduction component to their mantle sources as opposed to primitive western/central OIB sources (Pearce et al. 2006) (Figure 2-7).

The lower FeO* and TiO_2 contents of eastern primitive LKTs and CABs can also be a result of suppressed plagioclase crystallization relative to olivine, which would

explain their high Al_2O_3 contents (Taylor & Martinez, 2003; Wiens et al. 2006) (Figure 2-8). This can also be a result their melts being a mixture between MORB and arc-like sources (Taylor & Martinez, 2003; Wiens et al. 2006).

2.6 Conclusions

The FRVF back-arc contains four distinct basalt types; LKTs, CABs including HKCABs, BAs, and OIBs. LKTs contain lower K_2O values (0.22-0.44 wt %) and reach lower Ba/Nb ratios. CABs tend to be enriched in LILEs relative to HFSEs (high Ba/Nb ratios) than other magmas. BAs contain >52 wt % SiO_2 and high Ba/Nb ratios, while OIBs contain high Nb concentrations ≥12.1 ppm, originating from HFSE-enriched intraplate mantle sources.

Western primitive LKTs contain lower CaO, higher Na_2O, FeO*, TiO_2 and Ba values than eastern primitive LKTs. Eastern primitive CABs contain lower FeO*, TiO_2, Na_2O, and higher CaO, K_2O, and Ba values than western/central primitive CABs. Eastern primitive OIBs contain lower FeO*, MgO, CaO and higher SiO_2, Na_2O, K_2O, Ba, and generally higher Nb values than western/central primitive OIBs.

Eastern primitive CABs contain a more defined calc-alkaline character than the western/central CABs, displaying decreasing FeO*/MgO contents with increasing SiO_2 contents. Western/central CABs represent geochemical data that are transitional between LKTs, OIBs, and true end-member CABs.

Major element and trace element differences between western/central and eastern basalts point towards shallower mantle origins in the east and deeper mantle origins in the west for each basalt type, especially the lower FeO* contents of the eastern primitive samples. These back-arc trends in major and trace element data for primitive basalts point towards lower degrees of partial melting of a more enriched deeper mantle source for western/central LKTs and higher degrees of partial melting of a more depleted shallower mantle source for eastern LKTs. Primitive eastern OIBs display higher degrees of partial melting of a shallow intraplate mantle source, while central and western OIBs represent deeper, lower degrees of partial melting of a similar intraplate source. Primitive

eastern CABs represent shallow, lower degrees of partial melting of a more subduction enriched mantle source than primitive western/central CABs.

CHAPTER 3: Eruptive Styles & Mineral Compositions

3.1 Introduction

The Fort Rock Volcanic Field (FRVF) erupted in a late Pliocene to late Pleistocene pluvial lake basin, containing a diverse array of hydrovolcanic landforms and basalt types. Eruptions of basaltic magma occurred along faults that trend NW-SE across the basin and adjacent highland, forming hydrovolcanoes within and on lake margins, and forming cinder cones beyond the lake margins (Brand & Heiken, 2009) (Chapter 2; Figure 2-1). The range of volcanic landforms reflects the various depths of the lake throughout the Pleistocene. The center of the basin contains basaltic features that are dominantly tuff cones and tuff rings, interpreted as the result of magma encountering shallow water (Heiken, 1971; Brand & Heiken, 2009). The boundaries of the pluvial lake basin contain features that are dominantly maars and cinder cones, where the magma either encountered groundwater or no water contact at all (Brand & Heiken, 2009). Lava fields are bordered by the pluvial lake shorelines near Fort Rock in the western/central area, and Christmas Valley in the eastern area (Chapter 2, Figure 2-1).

The majority of basalts collected around FRVF are lava and scoria/spatter samples derived through conventional eruptions. A total of three FRVF basaltic samples are juvenile bombs in tuff rings found in the Big Hole maar (basaltic andesite (BA) sample FR-10-32A), Fort Rock tuff ring (calc-alkaline (CAB) basalt sample FR-10-8A), and in the Black Hills tuff ring (low K-tholeiite (LKT) sample FR-13-157B), and erupted hydrovolcanically (Figure 2-1). Conventional eruptions are those in which there are not large quantities of water involved, and occur in part due to high gas contents in their magma sources (Heiken, 1971, Wohletz & Sheridan, 1983; Morrisey et al. 2000, Parfitt, 2004; Brand & Heiken, 2009; Clarke et al. 2005; Traglia et al. 2009). Hydrovolcanism results from the interaction between magma/lava and water, driven primarily by the volumetric expansion of external water heated through contact with magma, causing the magma to fragment explosively (Heiken, 1971, Wohletz & Sheridan, 1983; Morrisey et

al. 2000, Parfitt, 2004; Brand & Heiken, 2009; Clarke, 2005; Traglia et al. 2009). The availability of the water source from the ancient pluvial lake system in the Fort Rock area is thought to be the main controlling factor in these differences between eruptive styles.

The previous chapter determined that these basalts include low-K tholeiites (LKTs), calc-alkaline basalts (CABs), basaltic andesites (BAs), and ocean island basalts (OIBs) based on major and trace element data, and further examined geochemical variations between primitive western/central and eastern basalt types analyzed, and possible depth/degree of partial melting and mantle source compositional melting trends (Bacon et al. 1997; Conrey et al. 1997; Rowe et al. 2009).

This chapter focuses on the petrogenesis of these basalts, utilizing mineral compositions of major phenocryst phases plagioclase and olivine through microprobe analyses to determine if these crystal phases crystallized in equilibrium with their primary melt. Variations in groundmass crystallinity, grain sizes, and vesicle content between conventional lavas, cinder/spatter, and hydrovolcanic lava samples can determine possible rates of magma ascent, impacts of degassing, cooling and crystallization rates, and possible areas of increased water content around the FRVF study area.

3.2 Methods

A total of 75 thin sections were examined using an Olympus BX51 microscope. Petrographic reports included sample type, with phenocryst phases and modal percentages (Appendix C). Phenocryst phases were measured in (mm) through cellSens Standard (Appendix C). Modal percentages of phenocrysts were determined by approximation and point counting, analyzing approximately 300-500 points per slide (Appendix C). A total of 48 points were acquired per grid, each point 0.2 mm apart in a 1.2 mm by 1.6 mm grid space. Approximation of groundmass crystallinity percentages, average grain sizes, and vesicle content were recorded for each magma type (Appendix D). Juvenile bomb in the Black Hills tuff ring LKT sample FR-13-157B did not contain enough material for thin section.

Chemical analysis of olivine, plagioclase, and spinel inclusion grains were conducted at the University of Toronto (U of T) using an electron microprobe (Cameca SX-50/51) equipped with 3 tuneable wavelength dispersive spectrometers. Amongst the 12 samples chosen for analysis, 5 were primitive LKTs (FR-10-38, FR-10-39, FR-12-101, FR-12-130, FR-13-152) , one was a non-primitive LKT (FR-10-57), 4 primitive OIBs (FR-10-40, FR-10-85, FR-13-150, FR-13-171), a primitive CAB (FR-13-185), and a primitive BA (FR-13-168b). Microprobe beam current, beam size, beam energy, and standards used for each mineral are presented in Table 3-1. Microprobe analysis for olivine and plagioclase cores and rims were analyzed for all samples, with the exception of LKT samples FR-10-39, FR-10-57, and FR-10-85 for olivine analysis, and LKT samples FR-10-38 and FR-10-57 for plagioclase analysis (Appendix E-F). Spinel chemical compositions were analyzed for 6 LKT and OIB samples FR-10-38, FR-10-57, FR-12-101, FR-12-130, FR-10-40 and FR-10-85 found as inclusions in olivine phenocrysts (Appendix G). Calculated anorthite (An) ($xCaO/ (xCaO + xNa_2O)*100$), forsterite (Fo) ($xMgO/ (xMgO + xFeO)*100$), and Cr#'s ($xCr_2O_3/ (xCr_2O_3/xAl_2O_3)*100$) (molar) are included in these representative analyses (Appendix E-G). Total oxide contents containing 100 +/- 3% were omitted (Appendix E-G).

Detection limits display the lowest quantity of an element that can be distinguished by the microprobe. These were calculated by dividing the molecular weight percentages of the major and trace element oxides by the elements molecular weight, and multiplying it by the detection limit of analyzed for that same element (ex: xNa_2O / xNa * LOD (limit of detection)). Those analyses of phenocrysts and grains that contained a weight percent oxide value lower than the LOD recorded as not determined (n.d) (Appendix H).

Table 3-1. Conditions of electron microprobe analysis

Phase	Olivine	Plagioclase	Spinel (inclusions)
Beam current (kV)	35.0	15.0	35.0
Beam Size (kV)	1	10	1
Beam energy (keV)	15	15	15
Standards	haematsx1 albitesx1 anorthitesx1 sanidsx2 baritesx1 RbTiPO5/6	haematsx1 albitesx1 anorthitesx1 sanidsx2 baritesx1 RbTiPO5/6	haematsx1 albitesx1 anorthitesx1 sanidsx2 baritesx1 RbTiPO5/6
Elements analyzed	Mg, Fe^{2+}, Ni, Cr, K, Ca, Ni, Ti, Si, Al, Na	Ca, Na, Li, Fe^{2+}, Ba, K, Si, Mg, Al, Rb, Ti, Sr	Ti, Al, Cr, Fe^{2+}, Ni, Mg, V, Si, Zn, Ca

* Conducted at the University of Toronto (U of T) using an electron microprobe Cameca SX-50/51.

3.3 Results

3.3.1 Petrography of FRVF basalts

i. Phenocrysts

Basaltic samples include lava, scoria/spatter samples, and juvenile bombs in tuff rings (Appendix C-D). These basalts range from aphyric to porphyritic, containing phenocrysts of olivine, plagioclase, +/- amphiboles (Appendix C). The majority of the samples are crystal poor olivine basalts that contain phenocryst contents of approximately ≤ 1 – 10 % in abundance (Appendix C). These aphyric basalts are concentrated in all areas of the FRVF, and consist of both primitive and evolved samples (Figure 3-1B).

Phenocryst sizes range from approximately 0.3 - 6.5 mm for plagioclase, 0.3 – 3.6 mm for olivine, and 0.3- 0.8 mm for amphiboles (Appendix C). A total of 8 evolved samples (Mg# < 60) are porphyritic basalts, which generally contain phenocryst contents of approximately 13 – 35 % in abundance. These evolved (Mg # < 60) porphyritic basalts are lavas concentrated in BAs of the East Lava Field, as well as Big Hole, Wickiup Spring, McCarty Butte and Oatman Flat lava samples in the western/central areas (Figure 3-1A). This includes juvenile basaltic bomb sample FR-10-32A, containing a phenocryst content of approximately 15 % (Appendix C). There is no apparent correlation between phenocryst size and abundance based on their distribution in the FRVF, or magma/sample type (Appendix C).

Phenocrysts commonly display evidence of undercooling conditions of crystallization, including skeletal olivine (Figure 3-2B) and plagioclase. In some samples, skeletal olivines have an opaque alteration/ reaction rim (Figure 3-2B). There is consistent undercooling phenocryst textures such as skeletal olivine and plagioclase found in the majority of FRVF basalts. In most samples, sieve textures are visible in corroded, partially resorbed plagioclase cores (Figure 18A). Glomerocrysts of olivine and plagioclase is also a common feature in these basalts, indicating simultaneous crystallization (Figure 3-2C).

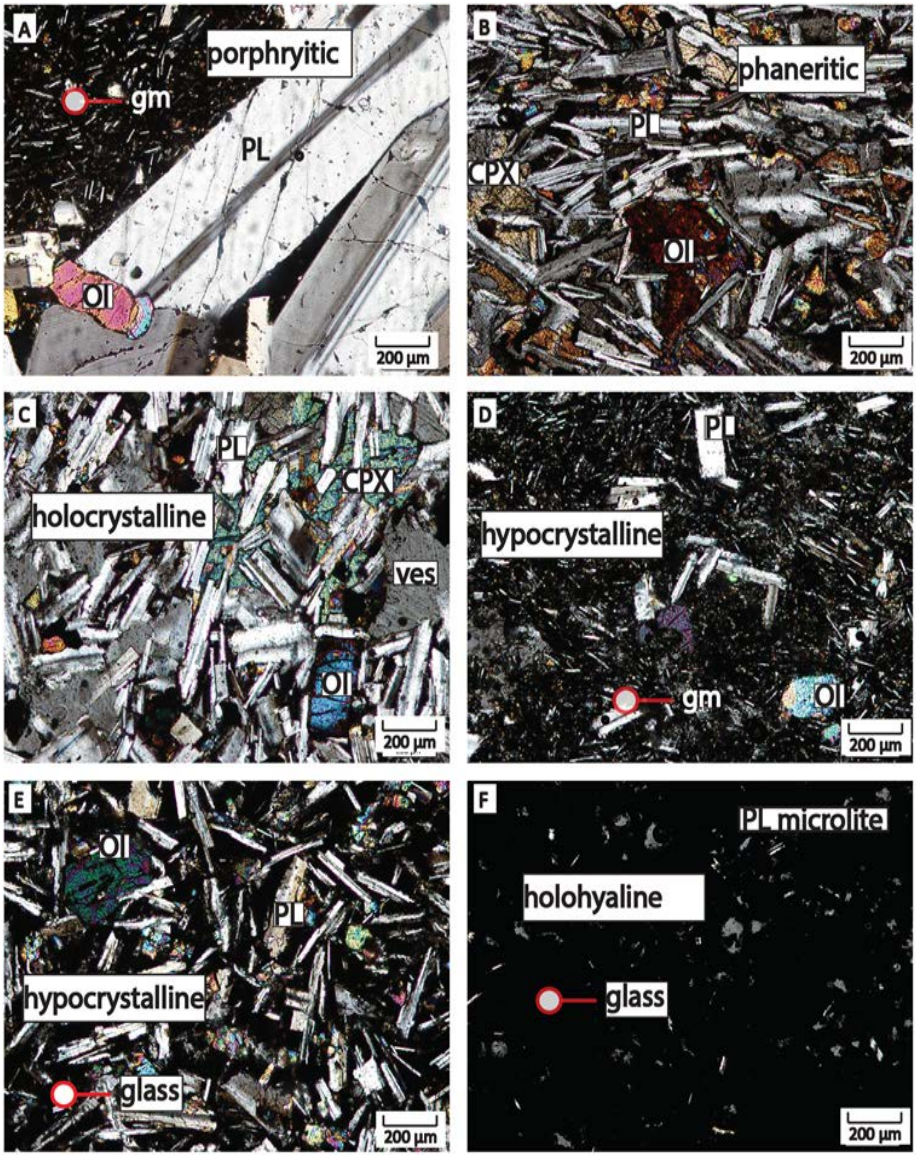

Figure 3-1. Micrographs of the different crystallinity contents of FRVF basalts. A) Porphyritic basalt with large plagioclase phenocrysts from the East Lava Field (FR-13-167) in eastern FRVF; B) aphyric basalt from the Oatman Flat (FR-10-58) in western/central FRVF ; C) holocrystalline coarse-grained basalt from Wickiup Spring north Wastina Butte (FR-10-74) in western/central FRVF; D) hypocrystalline fine - grained basalt from Four Craters Lava Field (FR-13-150) in eastern FRVF ; E) holo- to hypocrystalline, fine- to coarse grained basalt from Big Hole Katati Butte (FR-10-38) in western/central FRVF; F) cryptocrystalline / holohyaline scoria from Sixteen Butte Deadlog Butte (FR-13-184) in western/central FRVF, quenched basalt.

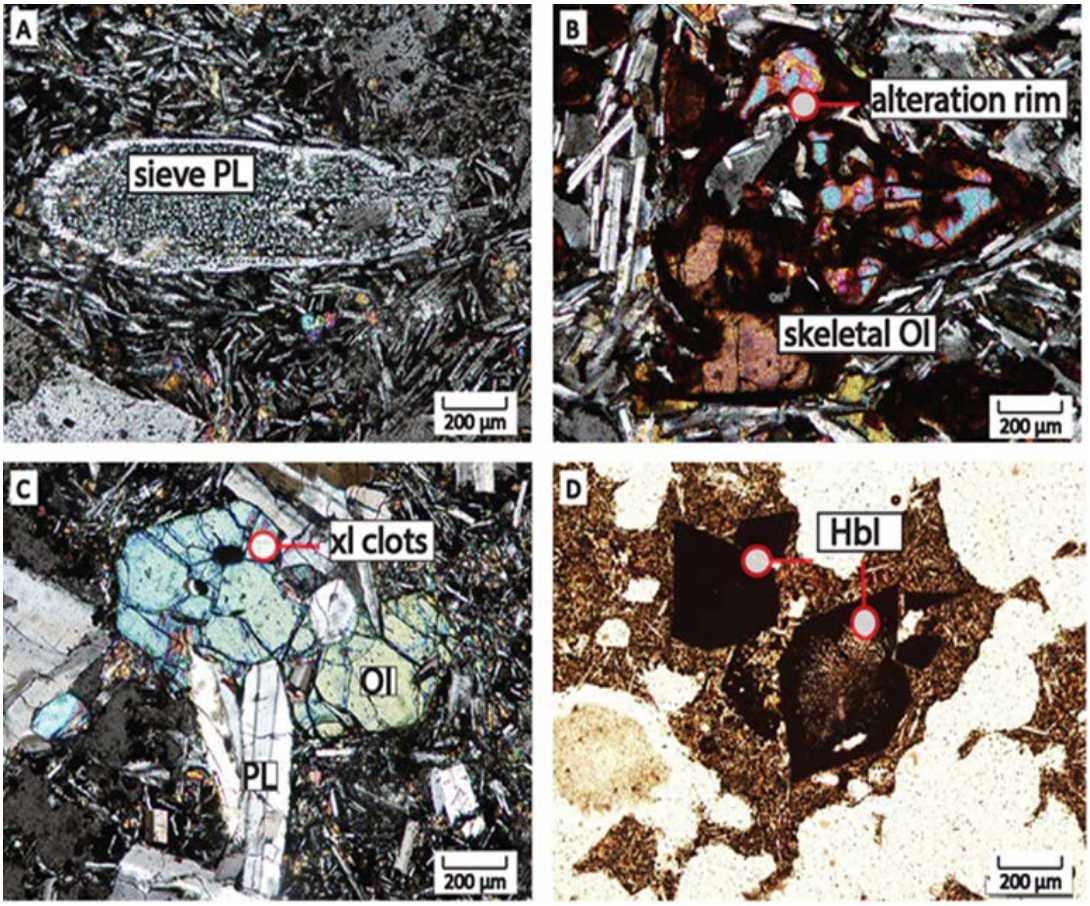

Figure 3-2. Micrographs of FRVF phenocryst textures in basalts. A) Sieve plagioclase phenocryst disequilibrium texture found in Big Hole Summit Butte lineament (FR-10-37) western/central FRVF ; B) skeletal olivine phenocryst undercooling texture from the McCarty Butte Lucky vent (FR-10-57) western/central FRVF. The mineral replacing the olivine grains (dark red oxidized color) can possibly be iddingsite ($MgFe_2Si_3O_{10}•4(H_2O)$), where reactions of gases and water in an oxidizing environment occur ; C) glomerocrysts of olivine and plagioclase phenocrysts from Reed Rock (FR-12-101) eastern FRVF ; D) dark, diamond - shaped amphibole phenocrysts in a spatter sample from the Blowouts (FR-10-85).

ii.Groundmass

In general, a fine-grained groundmass generally consists of approximately ≤ 0.1 mm to 0.2 mm plagioclase laths/microlites, oxides, +/- olivine, and +/- clinopyroxene in FRVF basalts. A coarse-grained groundmass generally consists of approximately 0.3 mm to 1 mm plagioclase laths, oxides, olivine, and +/- clinopyroxene. Purely holocrystalline samples display coarser-grained groundmass textures than the hypocrystalline samples. The overall range of FRVF basaltic lava textures display a holocrystalline to hypocrystalline groundmass, which contain fine- to coarser grained plagioclase laths, oxides, +/- olivine, +/- clinopyroxene, comprising approximately 25-85 % of the sample in a glassy matrix (Appendix C). All scoria/spatter samples display hypocrystalline to holohyaline groundmass of plagioclase microlites in a glass filled matrix (Figure 3-2F). All Juvenile bombs in tuff rings and maars display a hypocrystalline fine-grained groundmass (Appendix C).

Holocrystalline coarse-grained basaltic lavas are concentrated in the western/central sections, and are absent in the eastern sections (Figure 3-3C). Hypocrystalline fine-grained basaltic lavas are highly concentrated in the eastern FRVF areas (Figure 3-2D). Holocrystalline to hypocrystalline, fine to coarse-grained lava samples are found in western/central samples, and are absent in the eastern samples (Figure 3-2E).

A total of 17 basaltic lava samples and one spatter sample (CAB sample FR-10-185) contain clinopyroxene grains that tend to partially enclose plagioclase laths in a sub-ophitic/ ophiomottled texture (Appendix C). Larger grained clinopyroxenes (approximately 0.35 - 0.8 mm) occur in holocrystalline lava samples found near Big Hole, Wickiup Spring, McCarty, and Oatman Flat in the western/central area (Figure 3-3A). Smaller grained clinopyroxenes (approximately 0.1-0.2 mm) occur in holocrystalline to hypocrystalline Reed Rock lava samples in the eastern FRVF area (Figure 3-3B).

Basaltic lavas contain diktytaxitic textures where plagioclase laths bound, and/or protrude into the vesicles (Figure 3-3C).

Three spatter samples (FR-10-85 OIB, FR-10-30 LKT, and FR-13-185 CAB) contain remnants of diamond-shaped amphibole phenocrysts (Figure 18D). A total of 4 lava samples (FR-10-65, FR-10-71, FR-10-80, FR-13-192) display plagioclase laths that crystallized in a parallel to sub-parallel alignment in the groundmass (trachytic texture) due to the orientation within the lava flow (Figure 3-3D).

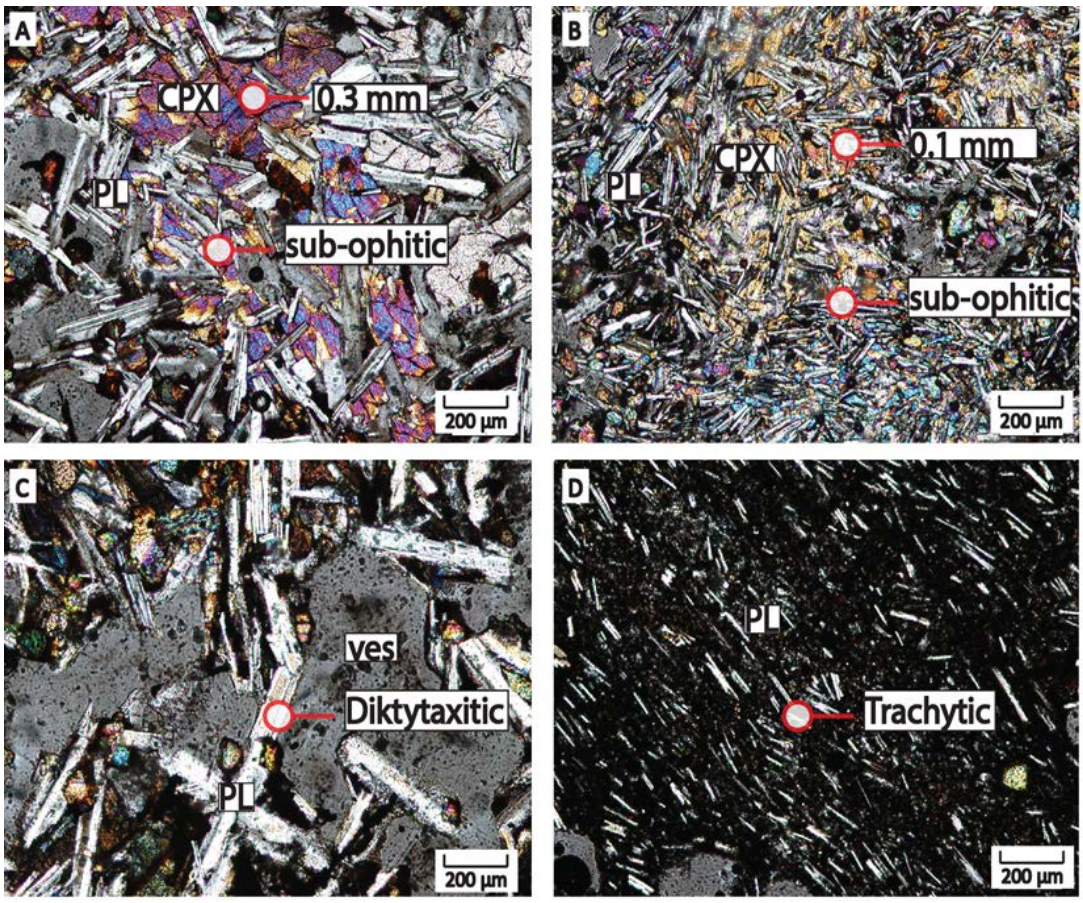

Figure 3-3. Micrographs of FRVF basaltic groundmass textures. A) Ophiomottled clinopyroxene partially enclosing plagioclase from McCarty Butte Lucky vent (FR-10-56) western/central FRVF; B) ophiomottled clinopyroxene from Reed Rock (FR-13-152) eastern FRVF. *Note the difference in crystallinity and size of sample FR-10-56 (coarse grained, holocrystalline) and sample FR-13-152 (fine-grained, hypocrystalline)*. C) Diktytaxitic plagioclase grains protrude into vesicles found in Big Hole (FR-10-40) western/central FRVF; D) Trachytic texture of parallel flow-banded plagioclase microlites in a cryptocrystalline groundmass found the South Ice Cave cinder pit (FR-10-80) western/central FRVF.

iii. Groundmass Crystallinity & Vesicle Content

FRVF lavas, scoria/spatter, and juvenile bombs display variations in groundmass crystallinity, average groundmass grain size, and vesicularity, characteristic of their eruptive styles and distribution across the back-arc basin. FRVF lavas contain higher groundmass crystallinity contents, grain sizes, and lower vesicle contents than scoria/spatter samples, and higher vesicle contents than juvenile basaltic bombs (Appendix D; Figure 3-4).

Western/central FRVF lava samples contain approximately 30-100 % groundmass crystallinity contents with 0.15-0.45 mm plagioclase, olivine, oxides, +/- clinopyroxene grains, and range from non-vesicular to approximately 30 % vesicles of variable shapes and sizes. Eastern FRVF lava samples do not reach as high groundmass crystallinity contents or as large average groundmass grain sizes as western/central FRVF lavas, containing approximately 15-80 % groundmass crystallinity contents, 0.1-0.2 mm plagioclase, olivine, oxides, +/- clinopyroxene grains (Figure 21). Vesicle content ranges from 2- 15 % of variable shapes and sizes. One lava sample from St. Patrick's Mountain (FR-13-191) displays higher groundmass crystallinity (~ 85 %) and higher average grain sizes (0.4 mm) than the other eastern lava samples, more characteristic of a western/central lava sample (Appendix D, Figure 3-4).

Western/central FRVF scoria and spatter samples contain approximately 2-55 % groundmass crystallinity contents with 0.1-0.35 mm plagioclase, olivine, oxides, +/- clinopyroxene grains, and contain approximately 15-50 % vesicles of variable shapes and sizes. Eastern FRVF spatter samples contain lower groundmass crystallinity contents (~ 2-5 %) and lower average grain sizes (~ 0.1-0.15 mm) of plagioclase microlites, +/- olivine, +/- oxides, and no clinopyroxene. Vesicle content ranges from 30-40 % of variable shapes and sizes, frequently containing some that are large (> 2 mm) and round (Appendix D, Figure 3-4).

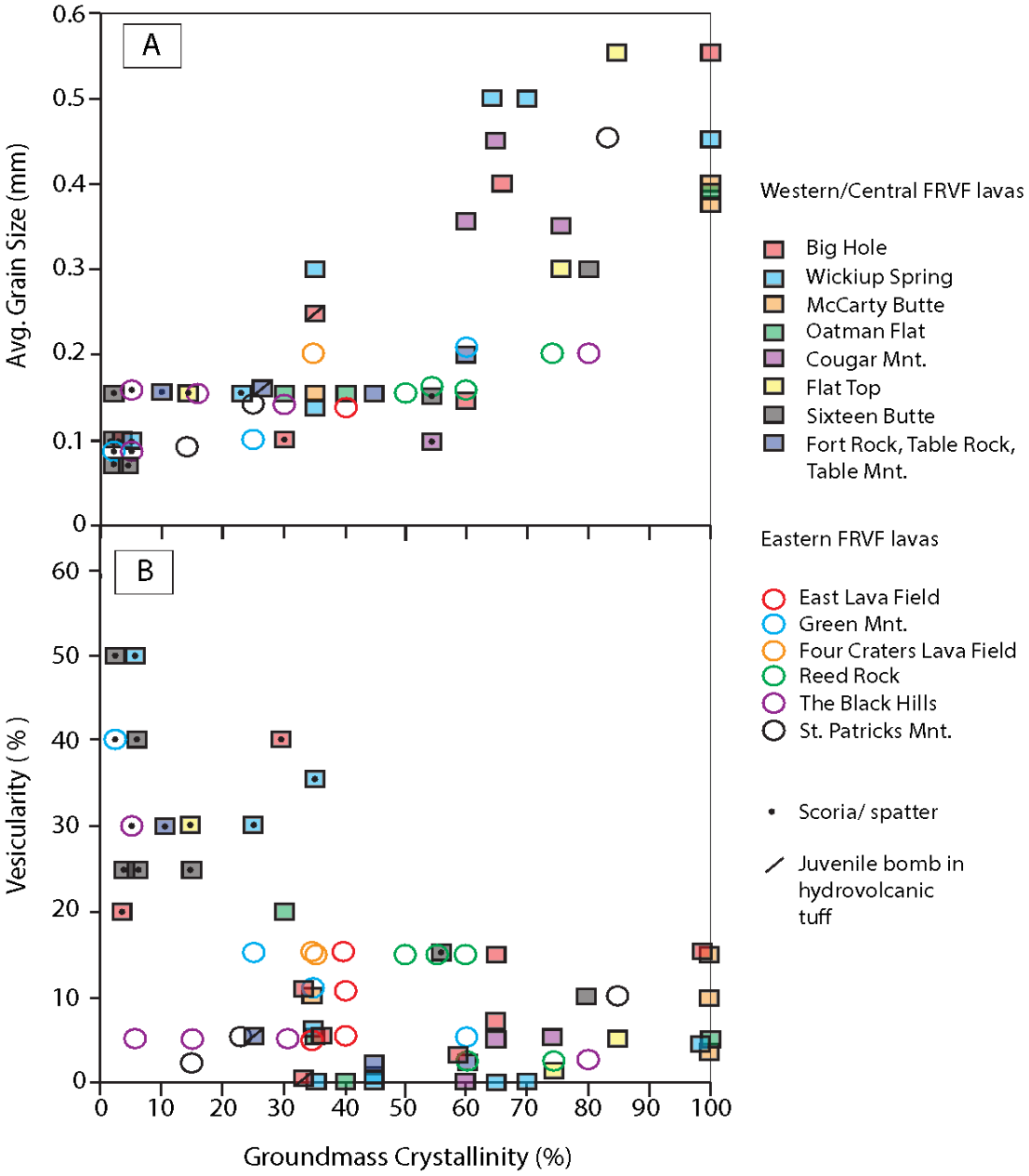

Figure 3-4. Changing eruptive styles across FRVF depicted by variations in groundmass crystallinity plotted against A) average groundmass grain size; and B) vesicle contents. Symbols with black dots represent scoria/spatter samples deposited by Strombolian eruptions. Filled squares and open circles represent lava samples from western/central FRVF and eastern FRVF respectively through conventional eruptions. Hydrovolcanic lava samples are represented by a black slanted line (FR-10-32A and FR-10-8A). Graphs constructed using data from Appendix D.

Figure 3-5. Micrographs depicting groundmass crystallinity and grain size differences in lavas from western/ central FRVF and eastern FRVF. High crystallinity contents and large grain sizes are displayed in each of the western/central FRVF lavas from Big Hole (FR-10-40), McCarty Butte (FR-10-46), Wickiup Spring (FR-10-74), Flat Top (FR-10-78), Oatman Flat (FR-10-58), and Cougar Mountain (FR-12-172). Note the phaneritic texture in each of the samples. Lower crystallinity contents and smaller grain sizes are displayed in each of the eastern FRVF lavas from Green Mountain (FR-12-89), Reed Rock (FR-12-101), Four Craters Lava Field (FR-13-150 & FR-13-151), and East Lava Field (FR-13-164 & FR-13-166). Note the porphyritic texture in sample FR-13-166.

Juvenile basaltic bomb sample FR-10-32A from the Big Hole maar contains approximately 35 % groundmass crystallinity contents with 0.25 mm grains of plagioclase laths and microlites, and is non-vesicular. Juvenile basaltic bomb from the Fort Rock tuff ring (FR-10-8A) contains lower groundmass crystallinity contents and grain sizes of plagioclase laths (~ 25 % and 0.1- 0.35 mm respectively), and also contains a vesicle content of approximately 5 % (Appendix D, Figure 3-4).

3.3.2 Microprobe Analysis

A total of 12 FRVF basaltic samples included primitive lava and spatter samples of different magma types, along with one evolved LKT sample. Plagioclase (An) and olivine (Fo) phenocryst analyses of core and rim contents were recorded to determine if these phases crystallized in equilibrium with its melt (bulk rock Mg#) (Appendix E-G; Table 3-2). Cr#'s and Mg#'s of spinel inclusions in olivine phenocrysts were also recorded to determine the diversity of chemical variability between magma types. These data are important for determining if there are any patterns or correlations between plagioclase, olivine, and spinel geochemistry, based on their magma types, eruptive styles, and distribution across the FRVF. Point counts recorded that phenocryst abundances in primitive samples were approximately 1- 5 %, while the evolved LKT sample FR-10-57 contained approximately 19 % phenocrysts (11 % plagioclase, 8 % olivine) (Appendix C, Table 3-2).

Table 3-2. Summary of modal and in situ analyses

Sample	Sample Type	Magma Type	Ol	Pl	Hbl	Fo**	An+	Sp. Type	Cr# (Sp.)	Mg# (Sp.)	Mg# (bulk)
FR-10-38	lava	LKT	x			76-86"	/	/			66
FR-10-39	lava	LKT	x	x		/	76-82	mc	31-36	49 -54	66
FR-10-57	lava	LKT	X	**X**		/	/	Tmt	11-45	12-16	56
FR-12-101	lava	LKT	x	x		85-86"	68-87	Tmt, 1 mag	1 -35	7-59	68
FR-12-130	lava	LKT	x	x		56-70"	71-89	Tmt	3-62	4 -8	66
FR-13-152	lava	LKT	x	x		54-77	82-89	/			68
FR-10-40	lava	OIB	x	x		61-82"	46-81	Tmt	44-97	2 -5	66
FR-10-85	spatter	OIB	x	x	x	/	68-86	mf, mag, mc	3-54	24-64	65
FR-13-150	lava	OIB	x	x		73-83	/	/			62
FR-13-171	lava	OIB	x	x		78-86	69-81	/			67
FR-13-168B	lava	BA	x	x		75-83	77-86	/			62
FR-13-185	spatter	CAB	x		x	53-92	/	/			64

x- 1-5 % crystal contents; X- 5-10 % crystal contents; **X**- 10-20 % crystal contents; Ol = olivine phenocrysts, Pl = plagioclase phenocrysts, Hbl = hornblende phenocrysts, Sp. = spinel inclusions in olivine phenocrysts. Fo** = range of Fo content of olivine phenocrysts. (")= only core analyses for Fo content. An+ = range of An content of plagioclase phenocrysts. Spinel types include; mc. = magnesiochromite; Tmt = titaniomagnetite; mag = magnetite; mf = magnesioferrite. Symbol (/) = no analysis. FR-10-57 contains Mg# < 60.

i. Plagioclase Phenocrysts

A total of 8 basaltic samples included primitive LKTs, OIBs, and BAs for plagioclase phenocryst analysis from both western/central and eastern areas. Five plagioclase phenocryst grains were chosen for each sample, for a total of 40 cores and 40 rims analyzed for An contents (Table 3-3) (Figure 3-6). Anorthite contents range from $An_{46\text{-}89.}$ Primitive OIB sample FR-10-40 has the widest range in An content, $An_{46\text{-}\ 81.}$ Plagioclase phenocrysts in all magma samples exhibit small range normal zonation patterns, containing more calcic (Ca-rich) cores crystallizing to more sodic (Na-rich) rims. An interesting find is that the primitive eastern FRVF samples (FR-12-101, FR-13-152, and FR-13-168B) contain some plagioclase phenocrysts that display reverse zonation patterns, a pattern that is absent in the primitive western/central FRVF samples (Table 3-3).

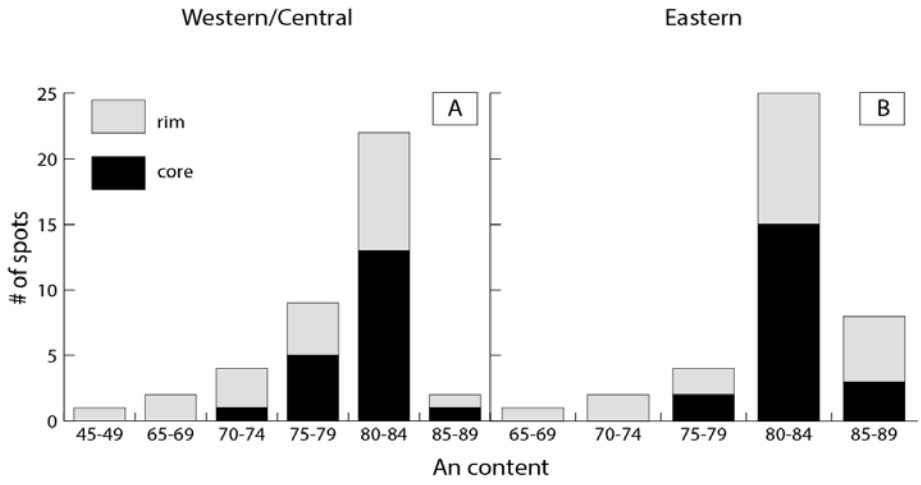

Figure 3-6. Stacked bar graph depicting plagioclase feldspar phenocryst core and rim An contents in primitive FRVF basalts between; A) western/central FRVF primitive basalts, and B) eastern FRVF primitive basalts. A) Consists of 10 phenocryst grain analyses from LKT and OIB lava samples FR-10-39 and FR-10-40 from Big Hole, 5 from OIB hornblende spatter sample FR-10-85 from the Blowouts, and 5 from OIB lava sample FR-13-171 from Cougar Mnt for a total of 20 cores and 20 rims analyzed. B) Consists of 15 phenocryst grain analyses from LKT Reed Rock lava samples FR-12-101, FR-12-130, and FR-13-152, 5 from East Lava Field high Mg# BA lava sample FR-13-168B for a total of 20 cores and 20 rims analyzed.

Table 3-3. Representative Analyses of Primitive Plagioclase Phenocryst Compositions

Location			An content	SiO_2	TiO_2	Al_2O_3	FeO*	MgO	CaO	Na_2O	K_2O	BaO	Rb_2O	SrO	Totals
Western/Central		**Sample #**													
Big Hole	**LKT**	**FR-10-39**													
	grain 1	core	82	48.11	0.10	32.24	0.36	0.14	13.91	3.37	0.09	0.00	0.00	0.00	98.32
		rim	77	50.66	0.16	30.95	0.50	0.18	12.45	4.06	0.13	0.00	0.00	0.00	99.09
	grain 5	core	82	49.54	0.09	32.97	0.41	0.18	14.24	3.41	0.10	0.05	0.02	0.00	101.03
		rim	80	49.68	0.08	32.25	0.51	0.16	13.21	3.70	0.08	0.00	0.00	0.00	99.67
Big Hole	**OIB**	**FR-10-40**													
	grain 2	core	81	49.66	0.09	32.86	0.31	0.12	13.73	3.61	0.12	0.00	0.00	0.00	100.50
		rim	80	49.82	0.12	32.57	0.51	0.05	13.50	3.78	0.20	0.01	0.00	0.01	100.55
	grain 4	core	73	51.66	0.28	29.33	1.40	0.24	11.80	4.75	0.41	0.00	0.00	0.00	99.86
		rim	46	58.89	0.19	25.78	0.54	0.07	5.82	7.63	0.92	0.06	0.00	0.00	99.91
Cougar Mountain	**OIB**	**FR-13-171**													
	grain 2	core	80	51.30	0.06	30.97	0.46	0.17	13.79	3.76	0.13	0.00	0.00	0.00	100.62
		rim	69	55.33	0.29	26.43	1.41	0.36	10.76	5.31	0.33	0.01	0.02	0.00	100.25
	grain 3	core	80	50.30	0.09	29.77	0.42	0.22	13.50	3.77	0.13	0.04	0.00	0.00	98.25
		rim	78	52.00	0.10	29.84	0.45	0.16	13.30	4.12	0.16	0.00	0.00	0.00	100.11
Eastern															
Reed Rock	**LKT**	**FR-12-101**													
	grain 1	core	84	48.73	0.03	33.53	0.33	0.24	14.47	3.09	0.08	0.00	0.00	0.00	100.48
		rim	87	47.40	0.05	34.44	0.39	0.22	15.29	2.55	0.05	0.05	0.01	0.00	100.44
	grain 3	core	82	49.63	0.04	32.65	0.54	0.24	13.82	3.44	0.10	0.13	0.00	0.00	100.58
		rim	68	53.97	0.35	25.40	2.20	1.52	10.29	5.41	0.30	0.00	0.00	0.00	99.45
East Lava Field	**BA**	**FR-13-168B**													
	grain 1	core	84	50.07	0.02	31.77	0.43	0.12	14.67	3.09	0.11	0.00	0.00	0.00	100.29
		rim	83	50.76	0.04	31.32	0.55	0.15	14.34	3.14	0.10	0.00	0.00	0.00	100.40
	grain 4	core	77	52.44	0.06	29.68	0.46	0.17	12.89	4.29	0.16	0.02	0.00	0.00	100.17
		rim	86	49.48	0.07	32.17	0.52	0.11	15.59	2.73	0.09	0.07	0.03	0.00	100.86

* Oxides are expressed as wt %. Analyses with < 98 % and > 102 % oxide totals were omitted.

ii. Olivine Phenocrysts

A total of 9 basaltic samples included analysis of primitive LKTs, CABs, OIBs, and BAs from both western/central and eastern FRVF areas. Five olivine phenocryst grains were chosen for each sample, for a total of 45 cores and 23 rims analyzed for Fo contents (Table 3-4) (Figure 3-7). Olivine Fo contents range from Fo_{53-92}. All eastern samples generally exhibit small range normal zonation patterns, containing Mg-rich cores and crystallizing to more Fe-rich rims (Table 3-4). Primitive eastern LKT sample FR-13-152 contains the lowest Fo contents of $Fo_{54-77,}$ and displays a larger range normal zonation pattern than the other eastern primitive samples analyzed (Table 3-4). The primitive western/central samples analyzed exhibit variable zonation patterns, containing Mg-rich cores and Fe-rich rims in one olivine phenocryst, then reversing to more Mg-rich rims and Fe-rich cores in another. Western/central spatter sample FR-13-185 exhibits reversely zoned olivine phenocryst grains in four out of the five grains analyzed (Table 3-4).

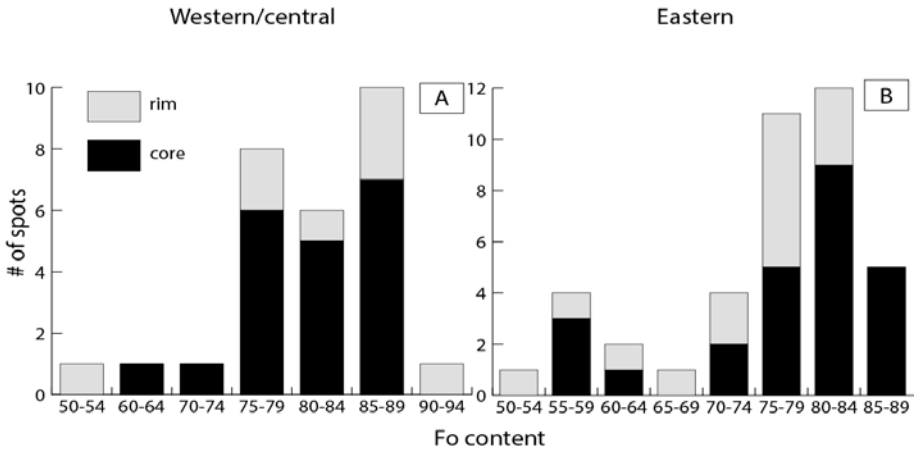

Figure 3-7. Stacked bar graph depicting olivine phenocryst core and rim Fo contents in primitive FRVF basalts between A; western/central FRVF primitive basalts and B; eastern FRVF primitive basalts. A; Consists of 10 core olivine grain analyses from LKT and OIB lava samples FR-10-38 and FR-10-40 from Big Hole, 4 core and rim and one core analysis from OIB lava sample FR-13-171 from Cougar Mnt, and 4 core and rim and one core analysis from hornblende basalt spatter sample FR-13-185 from Sixteen Butte. B; 25 phenocryst grain analyses from LKT Reed Rock lava samples FR-12-101, FR-12-130, and FR-13-152 (cores only in FR-12-101 and FR-12-130). 5 core and rim analyses from Four Craters Lava Field OIB sample FR-13-150, and 5 core and rim analyses from East Lava Field high Mg# BA lava sample FR-13-168B. A total of 45 cores and 23 rims were analyzed.

Table 3-4. Representative Analyses of Primitive Olivine Phenocryst Compositions

Location			Fo Content	SiO_2	TiO_2	Al_2O_3	FeO*	MnO	MgO	CaO	Na_2O	K_2O	NiO	Cr_2O_3	Totals
Western/Central		**Sample #**													
Cougar Mnt.	**OIB**	**FR-13-171**													
	grain 1	core	85	39.81	0.00	0.05	14.17	0.20	44.44	0.23	0.03	0.00	0.22	0.03	99.19
		rim	78	38.04	0.02	0.01	20.04	0.32	39.32	0.35	0.03	0.01	0.11	0.03	98.26
	grain 3	core	78	38.68	0.02	0.03	20.11	0.28	40.55	0.34	0.09	0.03	0.15	0.03	100.32
		rim	86	40.09	0.01	0.09	13.54	0.20	45.35	0.27	0.04	0.00	0.28	0.03	99.91
Sixteen Butte	**CAB**	**FR-13-185**													
	grain 2	core	88	40.57	0.01	0.03	11.53	0.23	47.08	0.21	0.04	0.02	0.24	0.02	100.00
		rim	92	40.95	0.02	0.02	7.84	0.39	48.77	0.10	0.08	0.01	0.17	0.01	98.37
	grain 3	core	86	40.75	0.00	0.04	13.15	0.28	43.72	0.22	0.07	0.04	0.22	0.03	98.52
		rim	53	37.97	0.08	0.13	37.60	0.16	24.13	0.14	0.10	0.07	0.08	0.03	100.49
Eastern															
Reed Rock	**LKT**	**FR-13-152**													
	grain 4	core	76	37.81	0.01	0.71	21.57	0.29	37.94	0.50	0.19	0.06	0.07	0.01	99.15
		rim	58	36.07	0.07	0.05	35.48	0.55	27.84	0.35	0.00	0.00	0.06	0.00	100.47
	grain 5	core	70	37.55	0.03	0.03	26.62	0.46	34.84	0.38	0.01	0.00	0.08	0.02	100.04
		rim	54	35.86	0.03	0.14	38.78	0.66	25.06	0.43	0.04	0.01	0.06	0.00	101.07
East Lava Field	**BA**	**FR-13-168B**													
	grain 1	core	81	39.37	0.03	0.03	17.60	0.23	42.39	0.23	0.02	0.00	0.17	0.01	100.09
		rim	75	37.53	0.03	0.01	22.48	0.35	37.49	0.27	0.04	0.02	0.09	0.05	98.36
	grain 5	core	82	39.52	0.00	0.05	17.25	0.19	43.08	0.18	0.02	0.00	0.16	0.03	100.48
		rim	75	37.98	0.00	0.01	22.43	0.39	37.96	0.30	0.05	0.02	0.11	0.02	99.26

* Oxides are expressed as wt %. Analyses with < 98 % and > 102 % oxide totals were omitted.

The MnO content in olivine phenocrysts tend to increase with decreasing Fo contents from core to rim displaying normal zonation patterns for eastern FRVF lava samples (Figure 3-8). Primitive western/central FRVF spatter sample FR-13-185 displays the opposite trend of decreasing MnO with slightly decreasing Fo contents, and in some grains MnO increasing at higher Fo contents displaying variable zonation patterns. Western/central FRVF lava sample FR-13-171 also display variable zonation patterns, as one olivine grain displays MnO decreasing at lowering Fo contents (Figure 3-8).

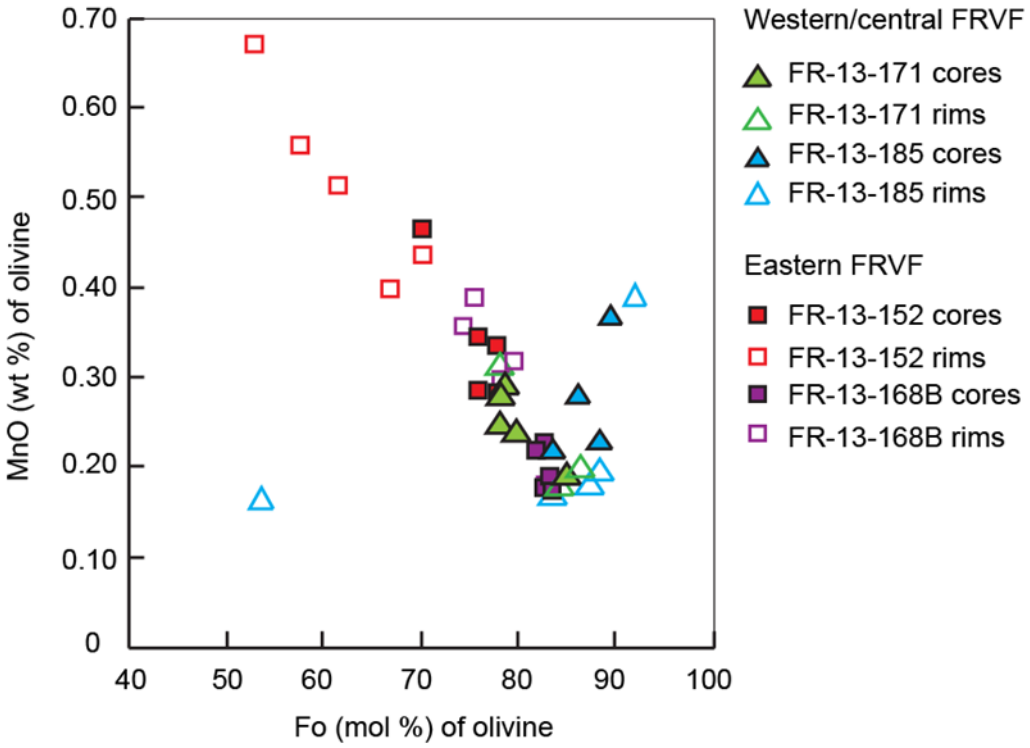

Figure 3-8. MnO (wt %) content vs. Fo (mol %) content of olivine phenocrysts for each sample. Note the oscillatory zonation patterns in western/central FRVF samples and normal zonation patterns in eastern FRVF samples.

iii. Spinel Inclusions

Spinels included in olivine phenocrysts vary in composition in FRVF LKTs and OIBs. Important major element oxides useful in determining different spinel end-members include weight percents of TiO_2, Al_2O_3, Cr_2O_3, FeO, and MgO (Table 3-5 & 3-6). These spinel groups may be subdivided into three series, according to whether the trivalent ion is Al, Fe, or Cr. Western/central primitive LKT samples contain magnesiochromites ($MgCr_2O_4$) for all five grains analyzed (Table 3-5 & 3-6). The more evolved western LKT sample contains titanomagnetites (Fe^{2+} (Fe^{3+}, Ti_2O_4)) for all 5 grains analyzed (Table 3-5 & 3-6). Western/central primitive hornblende basalt spatter sample FR-10-85 contain 3 different spinel groups; 3 grains analyzed for magnetite (Fe_3O_4), a single grain of magnesioferrite ($MgFe^{3+}{}_2O_4$), and a single grain of magnesiochromite ($MgCr_2O_4$) (Table 3-5 & 3-6). Eastern primitive LKT samples contain titanomagnetites for the 10 grains analyzed in Reed Rock LKT sample FR-12-101, and a single grain of magnetite (Fe_3O_4) analyzed in Reed Rock LKT sample FR-12-130 (Table 3-5 & 3-6). Eastern primitive OIB sample FR-10-40 contains titanomagnetites for all 5 grains analyzed. Eastern primitive samples contain less variable spinel compositions than the western/central primitive samples (Table 3-5 & 3-6).

Table 3-5. Sub-series of FRVF Spinels

Western/central	Location	Magma Type	Spinel Type	Oxide Range (wt %)
FR-10-39	Big Hole	LKT	Magnesiochromites ($MgCr_2O_4$)	MgO (13.3-14.6) Cr_2O_3 (24.0-28.0)
FR-10-57	McCarty Butte	LKT (non-primitive)	Titanomagnetites Fe^{2+} (Fe^{3+}, Ti_2O_4)	FeO (41.0-42.0) TiO_2 (50.1-52.3)
FR-10-40	Big Hole	OIB	Titanomagnetites Fe^{2+} (Fe^{3+}, Ti_2O_4)	FeO (57.7-68.1) TiO_2 (22.2-30.9)
FR-10-85	Blowouts	OIB	Magnetites (Fe_3O_4)	Fe_3O_4 (57.0-76.9)
			Magnesioferrites ($MgFe^{3+}{}_2O_4$)	Fe_2O_3 (60.4) MgO (16.7)
			Magnesiochromites ($MgCr_2O_4$)	Cr_2O_3 (25.6) MgO (20.6)
Eastern				
FR-12-101 FR-12-130	Reed Rock	LKT	Titanomagnetites Fe^{2+} (Fe^{3+}, Ti_2O_4)	FeO (45.6-77.5) TiO_2 (3.0-48.5)
			Magnetites (Fe_3O_4)	1 grain 100% Fe_3O_4

Table 3-6. Representative Analyses of Spinel Compositions in Olivine Phenocrysts

Location		Sp. Type	SiO_2	TiO_2	Al_2O_3	FeO*	Fe_2O_3	Fe_3O_4	MnO	MgO	CaO	Na2O	NiO	Cr_2O_3	V_2O_3	ZnO	Totals
Western/central																	
Big Hole	**FR-10-39**																
	grain 1	mc	0.17	1.18	34.14	24.37			0.27	13.28	0.07	0.06	0.17	24.58	0.30	0.10	98.66
	grain 2	mc	0.10	0.80	33.61	22.67			0.23	14.53	0.02	-0.12	0.23	27.05	0.17	0.10	99.39
McCarty Butte	**FR-10-57**																
	grain 1	Tmt	0.08	50.94	0.03	41.51			0.67	4.31	0.31	0.04	0.04	0.04	2.70	0.02	100.69
	grain 2	Tmt	0.09	51.64	0.05	41.70			0.51	3.31	0.24	-0.10	0.04	0.01	2.50	0.01	99.99
Eastern																	
Blowouts	**FR-10-85**																
	grain 2	mf	0.11	1.81	7.14		60.36		0.65	16.69	0.18	0.06	0.18	12.64	0.10	0.03	99.92
	grain 3	mc	2.82	0.78	29.74			20.26	0.40	20.60	0.53	0.05	0.11	25.57	0.14	0.15	101.42
	grain 6	mag	0.14	2.57	3.70			76.86	1.12	13.71	0.30	0.03	0.11	0.24	0.14	0.11	99.02
Reed Rock	**FR-12-130**																
	grain 1	mag	0.06	0.09	0.07			100.68	0.02	0.01	0.12	-0.09	0.00	0.01	0.02	-0.02	100.43
	grain 2	Tmt	0.23	21.62	1.01	72.96			0.52	2.66	0.28	-0.08	0.08	0.05	1.77	0.06	100.82

* Oxides are expressed as wt %. Sp. = Spinel; Tmt = titanomagnetite; mc= magnesiochromite, mag = magnetite, mf = magnesioferrite. Primitive western/central hornblende spatter sample FR-10-85 displays the most variable spinel compositions.

Spinels inclusions can also be distinguished based on their Mg#'s and Cr#'s (Figure 3-9). The high Mg#, low to moderate Cr# magnesiochromite spinels occur in all 5 grains of LKT primitive western sample FR-10-39, one spinel grain in LKT primitive eastern sample FR-12-101, and one spinel grain in primitive western/central basalt FR-10-85 . Moderate Mg# $\geq$ 24 contents, with low to moderate Cr# $\leq$ 54 contents contain magnesioferrites and magnetites in sample FR-10-85 (Figure 3-9). Low Mg# ($\leq$ 16), low to high Cr# titanomagnetites were analyzed in samples FR-10-57, FR-12-130 and FR-10-40 (Figure 3-9).

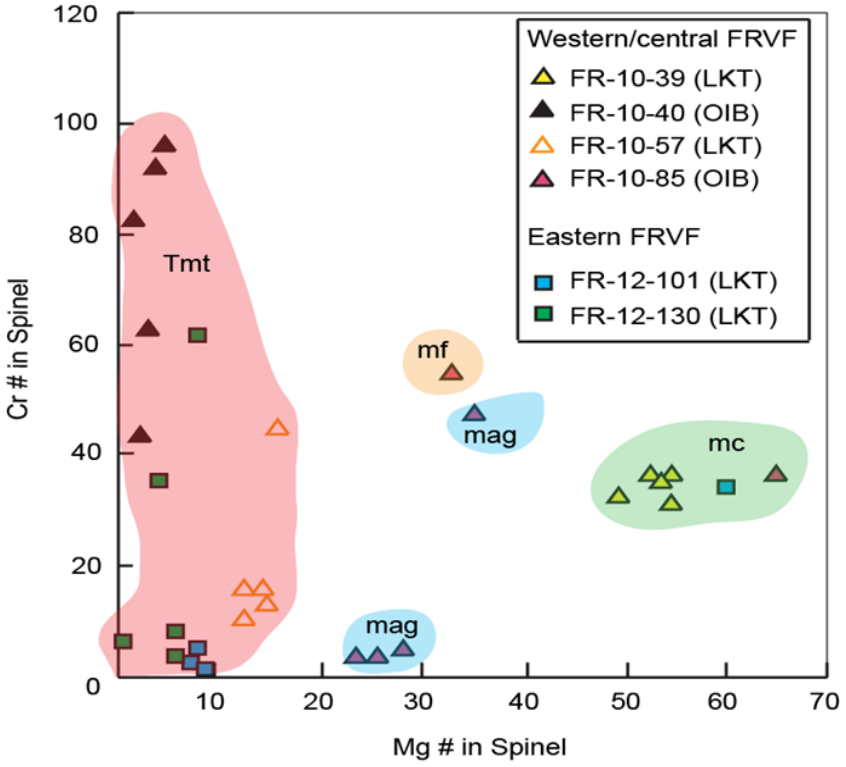

Figure 3-9. Cr# vs. Mg# in spinels to categorize different spinel groups as inclusions in olivine phenocrysts. The red field represents titanomagnetites (Tmt); blue fields are magnetite (mag); orange field is magnesioferrites (mf); and green field is magnesiochromites (mc).

3.4 Discussion

3.4.1 Changing Eruption Styles: Groundmass crystallinity

Eruptions of FRVF basalts are highly variable and complex, containing scoria/spatter and lava samples that have erupted conventionally, and also juvenile bombs in tuff rings and maars that have erupted hydrovolcanically. Many studies contribute eruption styles to variances in intrinsic factors such as; magma density, volatiles, viscosity, groundmass crystallinity, phenocrysts, and vesicle contents, as well as extrinsic factors that include conduit geometry (width, shape, and roughness) to the erupted magma. (Gonnermann & Manga, 2003; Houghton et al., 2004; Polacci et al. 2005; Mason et al. 2006; Pioli et al. 2009; Kent et al. 2010; Ruprecht & Bachmann; 2010, Maisonneuve et al. 2012). Evidence of FRVF eruption styles may be preserved in the groundmass crystallization and relative grain sizes, where finer-grained low crystallinity contents reflect scoria/spatter and juvenile bomb samples, and coarser-grained high crystallinity contents reflect conventional lava eruptions (Figure 3-4).

FRVF basalts display changing eruptive styles from hydrovolcanic to conventional evident from groundmass crystallinity and vesicle content variations (Figure 3-4). This suggests that the eruption style changed progressively from an initial hydrovolcanic phase, through a transitional stage, to one that was entirely Strombolian. The initial phase of activity was largely driven by magma-water (coolant) interaction causing intense fragmentation of the magma, and as a result, lower crystallinity and finer-grained groundmass textures of juvenile bomb samples found in the Big Hole maar, and Fort Rock and Black Hills tuff rings. Progressive increase in magma pressure within the conduit, with consequent progressive decline in magma–water interaction caused the decrease of fragmentation efficiency (Clarke et al. 2005). The occurrence of these processes is suggested by the increasing grain-size and groundmass crystallinity abundances of FRVF lava samples, as the water from the pluvial lake system became exhausted. The final eruptive stages gave rise to scoria/spatter samples through the dry Strombolian eruptions, depicted by their high vesicle content and low groundmass crystallinity content (Figure 3-4).

Vesicle development depends on depth of interaction and volatile content of the magma. Most vesicle growth occurs within 1 km of the surface (Heiken, 1971). The low vesicle contents of the juvenile bombs are indicative of hydrovolcanic eruptions, which inhibit vesiculation caused by rapid quenching of the magma (Clarke et al. 2005). This is caused by a rapid increase in viscosity due to a rapid decrease in temperature, preventing volatiles from exsolution (Fisher & Schmincke; 1984, Clarke et al. 2005). Pyroclastic deposits affected by added water to the system would reflect a reduction in vesicle size caused by increased vapour pressure and rapid quenching of the basaltic glass (Clarke et al. 2005). FRVF scoria/spatter samples exhibit larger, more rounded and more abundant intact vesicles. This implies a less volatile-rich eruption style such as a Strombolian eruption (Clarke et al. 2005).

i. Western/central vs. Eastern Lavas

FRVF western/central lavas display greater groundmass crystallinity contents, and larger average groundmass grains sizes than the eastern FRVF lavas (Figure 3-5). Western/central lava samples contain equigranular phaneritic basaltic textures. The high crystallinity groundmass content of western/central basaltic lava samples display an absence of substantial eruptive degassing and undercooling resulting in low rates of nucleation and high rates of crystal growth, creating these phaneritic textures of coarse-grained groundmass crystals (Conrey et al. 1997). Eastern lavas contain porphyritic basaltic textures with a fine-grained hypocrystalline groundmass. The finer-grained groundmass of eastern primitive basalts suggest substantial degassing and undercooling with a high rate of nucleation and a low rate of crystal growth, creating these porphyritic textures (Conrey et al. 1997) (Figure 3-5).

The variance in groundmass crystallinity and grain sizes between FRVF western/central and eastern lavas may be connected to different cooling rates, where slower cooling eruptions at a depth allows for increased groundmass crystallinity contents (Wall et al. 2014). Guilbaud et al. (2007) propose that groundmass crystallization is controlled by the timing of magma ascent and surface quenching, which these factors are additionally controlled by the rates of magma discharge and changing gas segregation. The high groundmass crystallinity and low vesicle contents of the western/central lavas

possibly implies an increased period of degassing and crystallization through slower magma ascent rates and effective gas separation from the magma (Guilbaud et al. 2007) (Figure 3-4). Higher groundmass crystallinity and larger grain sizes could also imply these were more water- rich magmas than the eastern lavas, possibly attributing to their closer distribution to the subduction zone than the eastern lavas. The low groundmass crystallinity and low vesicle contents of the eastern lavas suggest shallow fragmentation yielding a short crystallization period, but substantially efficient gas-melt separation of the rising magma (Guilbaud et al. 2007) (Figure 3-4).

3.4.2 Interpretation of Crystal Phases

i. Olivine Phenocrysts

Olivine phenocrysts display variable zonation patterns in primitive western/central basaltic samples. For example, primitive western/central CAB spatter sample FR-13-185 displayed reversely zoned olivine grains with respect to Fo and MnO contents (Figure 3-8). This suggests that magma mixing and/or recharge is occurring. This also suggests crystallization under more oxidizing conditions and increased H_2O contents, as is common in CABs (Conrey et al. 1997). The reverse zoning in Mn can be explained where an olivine xenocryst enters a hotter magma causing the partitioning of Mn into the crystal to be reduced (Conrey et al. 1997). The new equilibrium concentration of Mn in the olivine is lower than the actual concentration causing re-equilibration. The increasing concentrations of Mn in the rim are therefore due to the increasing partition coefficient of Mn, as the melt becomes more polymerized and crystallization occurs (Kohn et al. 1989; Clément et al. 2007) (Figure 3-8). This sample is interpreted to be a product of a dry Strombolian eruption.

ii. Plagioclase Phenocrysts

Plagioclase phenocrysts in a subset of eastern primitive basaltic samples displayed reverse zonation patterns (Table 3-3). The reverse zonation pattern suggests the interaction of the crystallizing magma with H_2O at a shallow depth (Housh & Luhr, 1991; Sisson & Grove, 1993; Couch et al., 2003). An increase in magma pressure or water contents while the phenocryst is crystallizing in the rising magma can promote

crystallization towards more An-rich rim compositions. This can also be a result of magma recharge through addition of more mafic magma to induce plagioclase disequilibrium (Tepley et al. 2010). Resorption sieve and skeletal textures of plagioclase grains found in most primitive samples suggest that the crystals experienced single to multiple changes in the crystallizing environmental setting (Nelson & Montana, 1992).

iii. Amphibole Phenocrysts

Amphibole phenocrysts were found in three spatter samples in western/central FRVF determined to have erupted conventionally. The texture and composition of these remnant hornblendes are interpreted to indicate dehydration and breakdown during their eruptions (Figure 3-2D). Natural hornblendes predictably form within the crust at temperatures between 960-1080ºC from liquids with less than about 6 wt % H_2O (Anderson, 2000). Rutherford (2003) discussed magmatic conditions and magma ascent as indicated by hornblende phase equilibria and reactions. Phase equilibria experiments on hornblendes in andesites indicate that the phenocryst assemblage of hornblende is stable in the range of 825 and 855ºC at a pressure of 130 MPa (Rutherford & Devine, 2003). The hornblendes are commonly rimmed or cored by crystals of pyroxene, plagioclase, and other minerals. FRVF basaltic hornblendes display extensive oxidization characterized by the appearance of increasing amounts of fine-grained magnetite that occur along the crystal margins of the hornblende by a reaction produced by decompression or oxidation (Rutherford, 2003) (Figure 3-2D). The origin of these FRVF hornblende basalts can possibly be attributed to water-rich hornblende crystallization during slow magma ascent from the storage zone at a depth, then dehydration and breakdown of these crystals as the dry Strombolian eruptions occur at the surface (Rutherford, 2003).

iv. Spinel Inclusions in Olivine Phenocrysts

Spinel inclusions in olivine phenocrysts analyzed for 4 different types of spinels in primitive basalts (Table 3-5; Figure 3-9). Fe-Ti rich titanomagnetites are the most common between western/central and eastern FRVF primitive LKTs and OIBs. Spatter OIB sample FR-10-85 contains the most diverse spinel groups out of all samples

analyzed. The chemistry of spinel inclusions and coexisting host olivine phenocrysts display a range of compositions that could have resulted from many factors that include crystallization temperature, pressure, oxygen fugacity, melt differentiation and/or magma mixing (Smith & Leeman, 2005). The spinel compositional variations between magma types can possibly be attributed to the geochemical diversity of FRVF LKTs and OIBs (Clynne & Borg, 1997).

3.5 Conclusions

The sample types of basalts in the FRVF include lavas, scoria/spatter, and juvenile bombs in tuff rings and maars. The eruption style changed progressively from an initial hydrovolcanic phase, through a transitional stage, to one that was entirely Strombolian. Eruptive styles are reflected through their variations in groundmass crystallinity, average groundmass grain size, and vesicularity. FRVF lavas contain higher groundmass crystallinity contents, grain sizes, and lower vesicle contents than scoria/spatter samples, and higher vesicle contents than juvenile basaltic bombs (Appendix D; Figure 3-4). FRVF scoria/spatter samples exhibit larger, more rounded and more abundant intact vesicles. This implies a less volatile-rich eruption style characteristic of a Strombolian eruption (Clarke et al. 2005). The low vesicle contents of the juvenile bombs are indicative of hydrovolcanic eruptions, which inhibit vesiculation caused by rapid quenching of the magma (Clarke et al. 2005).

Western/central FRVF lava samples display higher groundmass crystallinity contents, and larger groundmass grain sizes than the eastern lava samples (Figure 21). The high crystallinity groundmass content of western/central basaltic lava samples display an absence of substantial eruptive degassing and undercooling resulting in low rates of nucleation and high rates of crystal growth. These lavas are possibly more water-rich than the eastern lavas. The finer-grained groundmass of eastern primitive basalts suggests substantial degassing and undercooling with a high rate of nucleation and a low rate of crystal growth. These lavas possibly contain less H_2O contents, due to their distributions further east of the subduction zone.

Microprobe plagioclase and olivine core and rim analysis of primitive samples averaged a content of An80, and Fo81 content respectively. The reverse zonation patterns in primitive eastern FRVF lava plagioclase phenocrysts suggest the interaction of the crystallizing magma with H_2O at a shallow depth (Housh & Luhr, 1991; Sisson & Grove, 1993; Couch et al. 2003). Primitive western/central lava and spatter reverse zonation patterns in olivine phenocrysts suggest crystallization under more oxidizing conditions and possibly increased water contents. These patterns can also be attributed to magma recharge, where the addition of more mafic lava to their mantle source causes olivine and plagioclase disequilibrium (Tepley et al. 2010).

Spinel inclusions in olivine phenocrysts analyzed for 4 different types of spinels in primitive basalts. Fe-Ti rich titanomagnetites are the most common between western/central and eastern FRVF primitive LKTs and OIBs. Spatter OIB sample FR-10-85 contains the most diverse spinel groups out of all samples analyzed. The chemistry of spinel inclusions and coexisting host olivine phenocrysts display a range of compositions that could have resulted from many factors that include crystallization temperature, pressure, oxygen fugacity, melt differentiation and/or magma mixing (Smith & Leeman, 2005).

Hornblende basalts are found in western/central primitive spatter samples FR-10-30, FR-10-85, and FR-13-185. They appear as dark diamond shaped grains, containing a groundmass of microlitic plagioclase, olivines, opaques, and glass. The origin of these FRVF hornblende basalts can possibly be attributed to water-rich hornblende crystallization during slow magma ascent from the storage zone at a depth, then dehydration and breakdown of these crystals (Rutherford, 2003).

CHAPTER 4: Trace Element Concentrations in FRVF Primitive Magma Types: Proxies for Primary Mantle Source Processes

4.1 Introduction

Primitive FRVF magmas are extremely diverse, as four distinct primitive magma types analyzed for LKTs, CABs, high Mg# BAs, and OIBs based on their major and trace element data. Variations of Ba/Nb ratios distinguished primitive HFSE-enriched OIBs from subduction enriched CABs/BAs, and incompatible element depleted LKTs. These trace element concentrations illustrate end-member primitive liquids that reflect components of the mantle beneath the FRVF back-arc; a depleted back-arc mantle source, a subduction component, and an intraplate mantle source. (Nye & Reid, 1986; Bacon, 1990; Bacon et al. 1997; Conrey et.al, 1997; Reiners et al. 2000; Jordan et al. 2002; Leeman et al. 2005; Schmidt et al. 2008; Rowe et al. 2009; Schmidt & Grunder, 2011; du Bray & John, 2011).

Primitive FRVF magmas were further grouped into western/central and eastern sections based on their notable differences in major and trace element concentrations (Chapter 2, Figure 2-1). Western/central primitive LKTs contain lower CaO, higher Na_2O, FeO*, TiO_2 and Ba values than eastern primitive LKTs. Eastern primitive CABs contain lower FeO*, TiO_2, Na_2O, and higher CaO, K_2O, and Ba values than western/central primitive CABs. Eastern primitive OIBs contain lower FeO*, MgO, CaO and higher SiO_2, Na_2O, K_2O, Ba, and reach slightly higher Nb values than western/central primitive OIBs (Chapter 2, Figure 2-7 and 2-8).

Major element and Ba/Nb trace element variations point towards lower degrees of melting of a more enriched mantle source in primitive western/central LKTs than primitive eastern LKTs. Primitive eastern CABs represent lower degrees of melting of a more subduction enriched mantle source than primitive western/central CABs. Primitive eastern OIBs represent higher degrees of partial melting a similar HFSE-enriched mantle source to that of western/central primitive OIBs.

The main investigation arises as to whether these major and trace element interpretations are consistent with additional trace element ratio analyses of primitive

FRVF magma types. Trace element concentrations of these primitive FRVF magmas can aid in distinguishing between the depth/degree of partial melting, subduction enrichment, and mantle fertility trends of these mantle sources.

Previous geochemical studies of basalts suggest that HFSEs (such as Nb, Ta, Zr, Hf, and Ti) are not contributed by the subduction component, and therefore can be used independently to assess the fertility of the primary mantle source from which these primitive basalts are derived, as well as the extent of melting. Fluid mobile LILE trace element concentrations (such as Ba, Sr, Na, and K) are added to a primary mantle source of assumed constant HFSE composition, and can be used as a measure of subduction component addition (Hart et al. 1972; Pearce & Cann, 1973; Hawkins, 1976; Gill, 1976; Tarney et al. 1977; Saunders & Tarney, 1979; Hawkins & Melchior, 1985; Sinton & Fryer, 1987; Stopler & Newman, 1994; Bacon et al. 1997; Conrey et al. 1997; Hochstaedter et al. 2000; Hochstaedter et al. 2001; Taylor & Martinez, 2003; Pearce & Stern, 2005; Wiens et al. 2006; Bézos et al. 2009).

Comparison of LILE/LREE and HFSE/HREE ratios in primitive magmas aid in distinguishing differences in the degree of addition of a subduction component to the mantle source (higher LILE/LREE concentrations) and the fertility of the mantle source (higher HFSE/HREE concentrations) between the primitive magma types. Therefore, a ratio of a highly incompatible element to a less incompatible element gives a proxy for mantle enrichment and depletion. To evaluate the extent of subduction input in back-arc basins, previous studies use Ba/Nb, Ba/Zr, and La/Nb ratios as subduction input proxies, and plot it against Nb/Y and Nb/Zr ratios to project both subduction enrichment and mantle fertility trends on a single trace element ratio plot (Pearce et al. 2006).

The degree of partial melting of primitive FRVF magmas can be obtained through ratios of relatively immobile HFSE and HREE elements such as Y/Zr and Nb/Zr projected against a single trace element HFSE/HREE such as Y or Nb. Trace element ratios such as Nb/Y and Nb/Zr are relatively immobile during subduction, and can be relevant to primitive FRVF magmas that have been influenced by subduction. Fractionation melt models containing 1, 5, and 20 % aggregate melting points based on spinel lherzolite shallow depleted mantle and garnet lherzolite enriched mantle melting

models aid in determining possible depth and degree of partial melting of FRVF primitive magmas (Shaw, 1970; Sun & McDonough, 1989; Pearce & Parkinson, 1993; Bacon et al. 1997; Conrey et al. 1997).

According to major and trace element analyses in Chapter 2, primitive CABs are expected to display greater enrichment in LILEs and LREEs than primitive LKTs and OIBs. OIBs are expected to display a greater enrichment in HFSEs and HREEs than primitive LKTs and CABs. Primitive LKTs are expected to display depletions in incompatible trace elements compared to primitive CABs and OIBs.

Trace element variations between western/central and eastern FRVF primitive magmas is highly complex, as this chapter will analyze trace element concentrations and ratios through Inductively Coupled Plasma Mass Spectrometry (ICP-MS) and XRF analyses, and attempt to deduce the complexity of primary mantle sources beneath the FRVF back-arc.

4.2 Methods

A total of 75 fresh basaltic samples were crushed with an alumina jaw crusher into ~20-50 gram rock chips per sample and sent to the GeoAnalytical Laboratory at Washington State University (WSU) for X-ray fluorescence (XRF) analysis for 19 trace elements (Appendix B). The XRF technique uses a single low dilution fusion (2:1 ratio) of Li-tetraborate: sample for trace elements to provide maximum efficiency without loss of accuracy for data values (Johnson et al. 1999). Trace elements are analyzed in parts per million (ppm) with concentrations <0.1% that include; Ni, Cr, Sc, V, Ba, Rb, Sr, Zr, Y, Nb, Ga, Cu, Zn, Pb, La, Ce, Th, Nd, and U (Appendix B).

A total of 6 basaltic samples including primitive LKTs (FR-10-30, FR-10-38, and FR-12-101), non-primitive LKT (FR-10-87), and primitive OIBs (FR-10-40, FR-10-85) were chosen for Inductively Coupled Plasma Mass Spectrometry (ICP-MS) analysis of trace elements; (Cs, Rb, Ba, Th, U, Nb, Ta, La, Ce, Pb, Pr, Sr, Nd, Zr, Hf, Sm, Eu, Gd, Tb, Dy, Ho, Y, Er, Tm, Yb, and Lu) recorded in ppm (Appendix I) (Sun & McDonough , 1989).

4.3 Results

4.3.1 Primitive Trace Element Analyses

XRF analysis of 19 trace elements in 31 primitive FRVF basaltic samples display a variation of ranges based on their magma types (Table 4-1). Primitive LKTs generally contain a high range of compatible elements Ni and Cr, high Sc contents, and a low range of incompatible element contents V, Ba, Rb, Sr, Zr, Nb, La, Ce, Nd compared to CABs, BAs (Tables 4-1 & 4-2). Primitive CABs and BAs generally contain a lower range of compatible elements Ni and Cr, and reach higher incompatible element concentrations Ba, Rb, Sr, Zr, Nb, La, Ce, Nd than primitive LKTs. Primitive OIBs display a higher range of incompatible HFSE elements Nb and Zr than primitive LKTs, CABs, and BAs, and trace elements contents that are intermediate between primitive LKTs, CABs, and BAs concentrations (Table 4-1 & 4-2).

Table 4-1. Compositional Ranges of Primitive FRVF Magma Types

Primitive	Ni (ppm)	Cr (ppm)	Sc (ppm)	V (ppm)	Ba (ppm)	Rb (ppm)	Sr (ppm)	Zr (ppm)	Y (ppm)	Nb (ppm)	La (ppm)	Ce (ppm)	Nd (ppm)
<52% SiO_2													
LKT	123-187	208-315	28-41	65-217	71-250	3-7	190-383	73-129	24-30	3-7	1-14	12-25	8-18
CAB	69-171	165-337	27-38	195-231	170-426	4-16	284-485	105-141	25-34	5-10	7-18	19-36	12-20
OIB	110-191	178-362	27-32	184-220	153-302	7-14	305-440	131-172	27-30	12-19	10-17	24-36	18-21
>52% SiO_2													
High Mg# BA	93-155	129-272	23-27	157-194	268-501	17-33	315-429	123-162	25-29	7-12	9-17	25-31	16-18

* A total of 31 primitive FRVF basalts ; 9 primitive LKTs, 11 primitive CABs, 4 high Mg# BAs, and 7 primitive OIBs. Concentrations recorded in ppm.

Table 4-2. Representative Analyses of Primitive FRVF Magma Types

Sample	FR-10-30	FR-13-152	FR-10-77	FR-12-88	FR-10-85	FR-13-151	FR-13- 168B
Center/Quad	Big Hole	Reed Rock	Flat Top	G. Mnt.	Blowouts	F. Craters	Hogback
Type	LKT	LKT	CAB	CAB	OIB	OIB	BA
SiO_2	48.95	48.92	50.57	51.38	48.11	50.96	53.24
TiO_2	1.293	0.917	1.274	1.196	1.635	1.588	1.256
Al_2O_3	18.67	17.56	17.52	17.24	16.65	17.09	17.28
FeO*	9.64	8.66	9.37	8.60	10.21	8.94	7.91
MnO	0.17	0.16	0.16	0.16	0.17	0.16	0.14
MgO	7.90	8.89	7.19	7.17	9.11	7.25	6.26
CaO	9.78	11.87	9.87	10.28	10.02	9.20	9.06
Na_2O	3.13	2.67	3.28	2.91	3.13	3.52	3.56
K_2O	0.26	0.22	0.52	0.78	0.61	0.93	0.96
P_2O_5	0.23	0.12	0.24	0.29	0.35	0.37	0.33
Ni	157	145	109	77	180	121	93
Cr	211	253	187	182	296	207	158
Sc	31	41	31	36	32	28	26
V	65	209	213	226	207	205	194
Ba	250	71	212	400	153	302	368
Rb	3	3	7	16	9	14	17
Sr	383	190	379	485	305	439	429
Zr	105	73	109	117	155	172	149
Y	30	24	26	27	29	28	25
Nb	6	3	8	7	19	17	12
Ga	18	13	18	17	15	18	17
Cu	86	88	75	55	74	61	67
Zn	80	61	77	77	75	76	77
Pb	3	1	2	11	1	2	3
La	14	1	7	16	14	14	17
Ce	19	12	25	36	30	33	31
Th	0	0	0	3	0	2	2
Nd	18	8	15	19	19	21	18
U	0	0	0	0	0	0	2
Mg#	63	68	62	64	65	63	62

Total Fe represented as FeO*. Whole-rock powders analyzed at Washington State GeoAnalytical Lab.

4.3.2 Primitive LKT and OIB Trace Element Variations

Generation of an ICP-MS trace element abundance diagram plotted relative to Sun & McDonough's (1989) N-MORB normalized data displays differences in trace element concentrations between FRVF primitive LKTs (including one non-primitive sample) and primitive OIBs (Figure 4-1A) (Appendix I). The x-axis displays REEs (La to Lu) in order of degree of compatibility, where compatibility of the elements increase from left (LREEs) to right (HREEs) (Figure 4-1A). Additional spider diagrams were generated to display trace elements that incorporate LILEs (Cs, Ba, Rb, Sr, U, and Th) and HFSEs (Nb, Ta, Zr, and Hf) along with the REEs (Figure 4-1B).

FRVF N-MORB normalized magmas display approximately 1-6 times greater concentrations of LREEs than expected in an N-MORB mantle source (Figure 4-1A). All samples display a gently sloping pattern from higher LREE contents to lower HREE contents (Figure 4-1A). Primitive LKT sample FR-12-101 contains the lowest LREE values of any other sample (Figure 4-1A). Concentrations of HREEs contain similar (approximately ≤ 1 times) concentrations to that found in N-MORB normalized mantle sources for all LKTs and OIBs (Figure 4-1A). Primitive OIB sample FR-10-85, primitive LKT sample FR-10-30, and evolved LKT sample FR-10-87 contain slightly higher HREE concentrations than the other samples (Figure 4-1A). Primitive LKT samples FR-10-38 and FR-12-101 contain relatively lower LREE concentrations than the other samples, where primitive LKT sample FR-12-101 contains the lowest REE concentrations from La to Ho (Figure 4-1A). Primitive OIBs display higher concentrations of La and Ce than the LKT samples. Primitive LKT sample FR-10-30 displays lowered Ce concentrations, and also contains higher Sm, Eu, Gd, and Tb concentrations than all other samples. All samples display small positive Eu enrichments (Figure 4-1A).

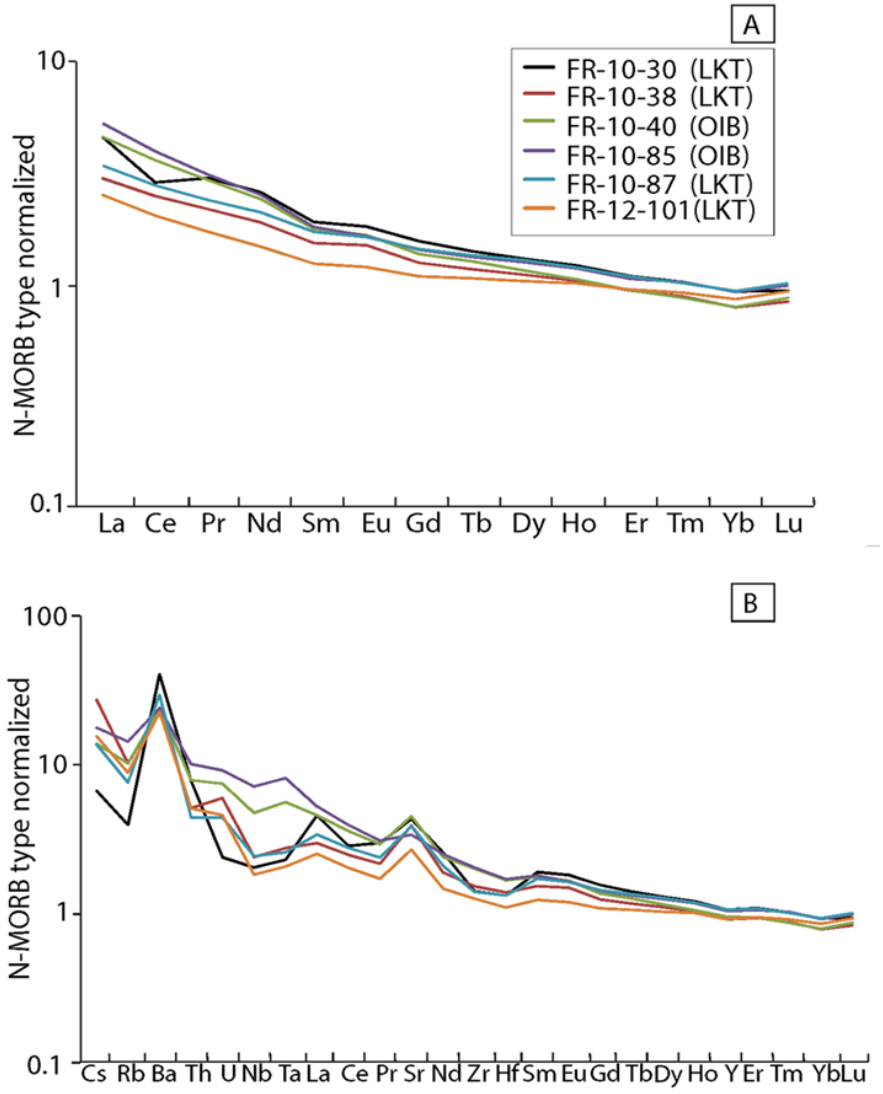

Figure 4-1. N-MORB element abundance diagrams displaying trace element data for FRVF primitive LKTs and OIBs (and one non-primitive LKT) on; A) an REE diagram, and B) a spider diagram including LILEs and HFSEs. Normalization N-MORB values from Sun & McDonough (1989). Primitive LKT samples FR-10-30 and FR-10-38, and primitive OIB sample FR-10-40 obtained from Big Hole. Primitive OIB sample FR-10-85 obtained from The Blowouts, evolved LKT sample FR-10-87 from Table Mountain, and primitive LKT sample FR-12-101 from Reed Rock. A) Gently sloping patterns from higher LREE concentrations to lower HREE concentrations in all samples. B) Higher concentrations of HFSE elements Nb, Ta, Zr and Hf in primitive OIB samples compared to the LKT samples.

Variations between LKTs and OIBs are displayed through incorporation of LILEs and HFSEs into the trace element N-MORB normalized variation diagram (Figure 26B). All samples display enrichment towards higher Cs, Ba and Sr concentrations, and lowered concentrations of Rb (Figure 4-1B). Primitive OIB samples display greater concentrations of U, Nb, Ta, Zr, and Hf than primitive LKTs and evolved primitive LKT sample FR-10-87. Primitive LKT sample FR-10-30 contains the lowest Cs, Rb, and U concentrations, but the highest Ba concentrations of any other sample (Figure 4-1B).

4.3.3 Primitive LKT, CAB and OIB Trace Element Variations

Whole rock variation diagrams of important trace elements plotted against MgO contents of FRVF primitive magmas displays variations between western/central and eastern samples of the same magma type (Figure 4-2).

Western/central primitive LKTs generally contain higher Ni, Ba, Sr, Zr and lower Sc concentrations than eastern primitive LKTs. Eastern primitive CABs generally contain lower Ni and Cr concentrations, and higher Sc, Ba, Rb, Sr, La, Ce and Nd concentrations at relatively lower MgO contents than western/central primitive CABs. Eastern primitive OIBs generally contain higher Ba, Sr, Zr, and Ce concentrations at lower MgO concentrations than western/central primitive OIB samples (Figure 4-2).

Primitive western/central OIB sample FR-10-78 from Flat Top displays similar Ni and Sr concentrations at similar MgO contents as primitive eastern OIBs (Figure 4-2D, Figure 4-3B). Primitive western/central CAB sample FR-10-58 from McCarty Butte displays similar Ba and Sr contents as primitive eastern CAB samples (Figure 4-2B & D, Figure 4-3C). Primitive western/central LKT samples FR-10-38 and FR-10-39 from Big Hole contains lower Ba, Sc, and higher Ni concentrations at higher MgO contents than the other primitive western/central LKT samples FR-10-30 from Big Hole, and FR-10-56 from McCarty Butte (Figure 4-2A, B, & E, Figure 4-3A).

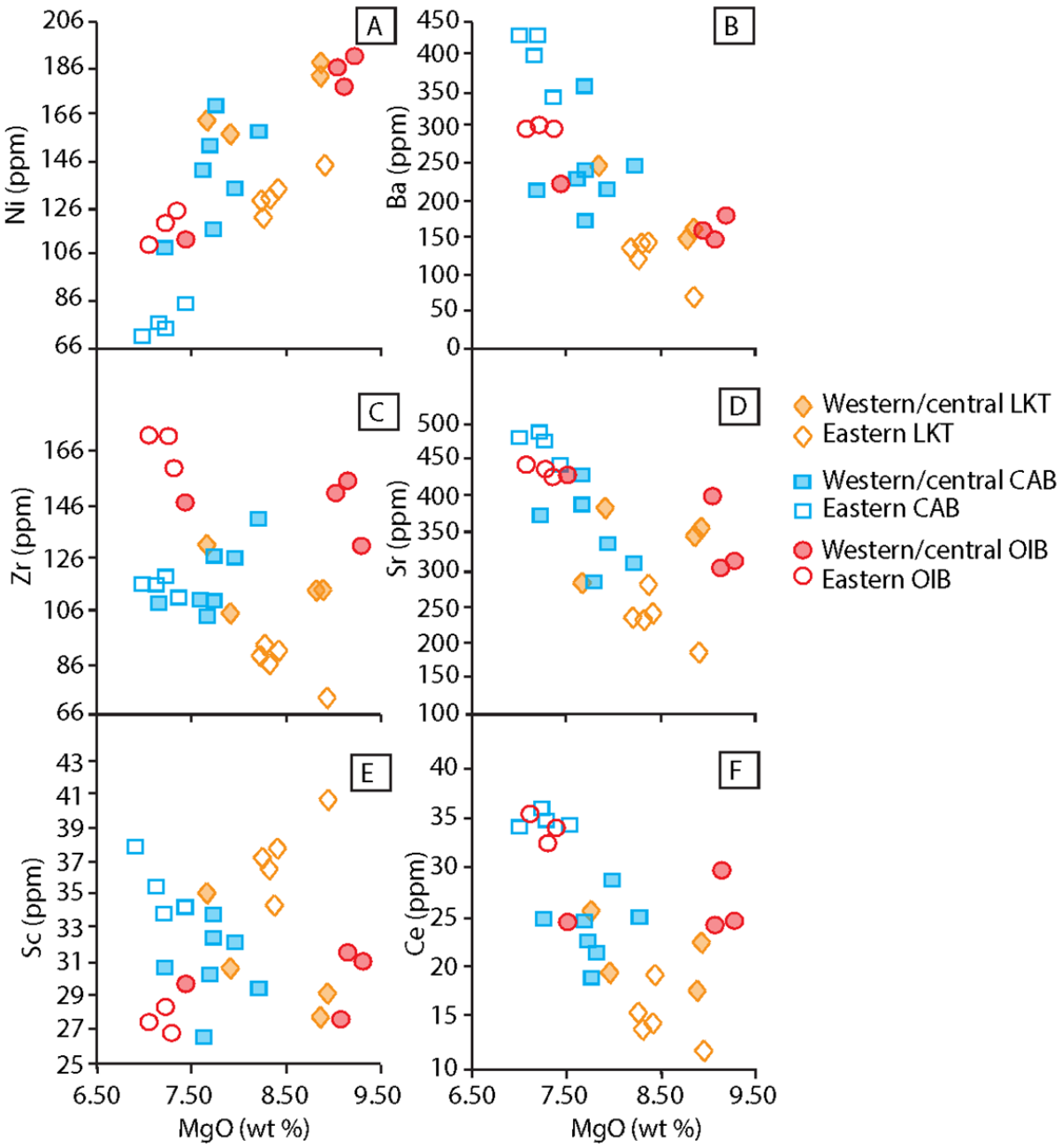

Figure 4-2. Whole-rock trace element variation diagrams of FRVF primitive magmas plotted against MgO. A) Ni vs. MgO ; B) Ba vs. MgO ; C) Zr vs. MgO; D) Sr vs. MgO; E) Sc vs. MgO; and F) Ce vs. MgO. Note the differences in trace element concentrations between western/central and eastern primitive samples within each magma type. MgO recorded in wt%, trace elements in ppm.

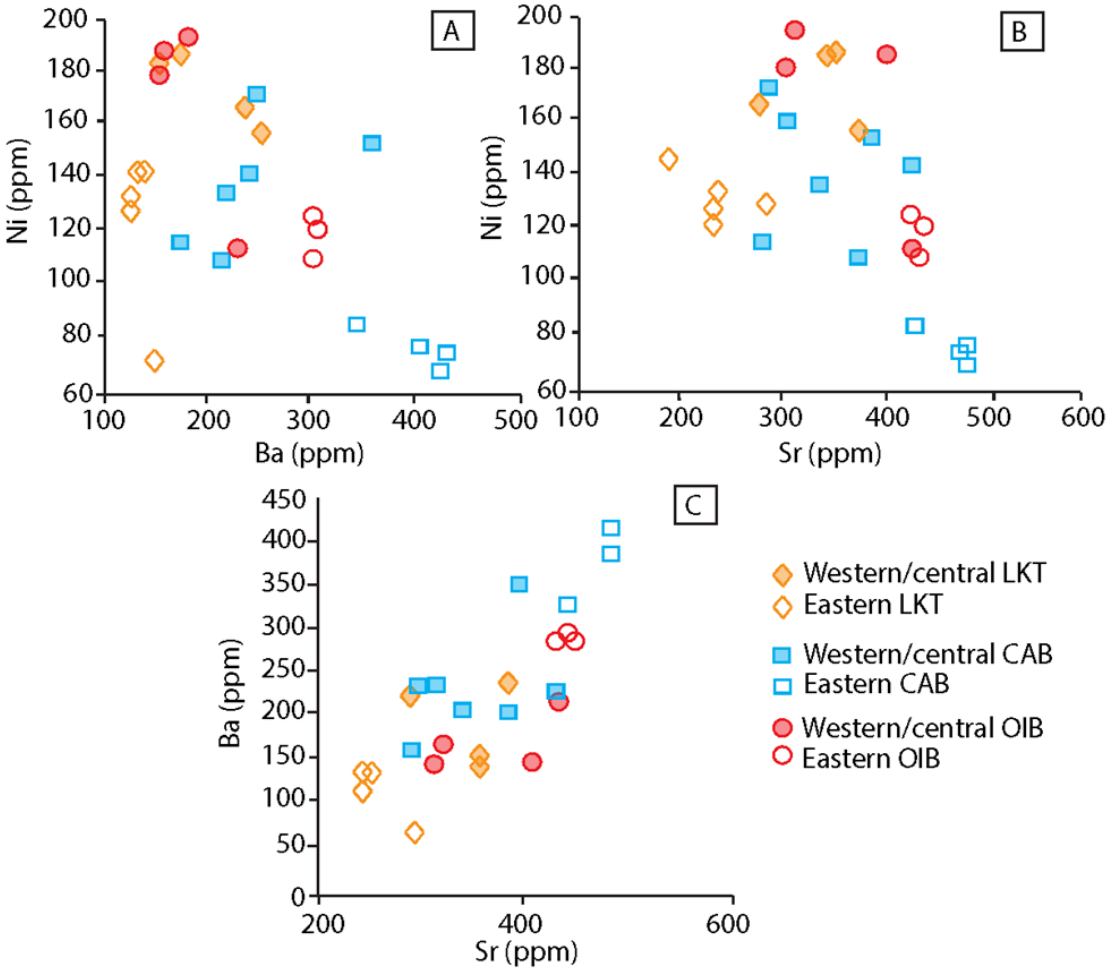

Figure 4-3. Whole-rock trace element variation diagrams for FRVF primitive magmas. A) Ni vs. Ba; B) Ni vs. Sr; and C) Ba vs. Sr. Trace elements recorded in ppm. Western/central LKTs display higher Ni concentrations, Ba, and Sr concentrations than eastern LKTs. Eastern primitive CABs display lower Ni, higher Ba and Sr concentrations than the majority of western/central primitive CABs. Eastern primitive OIBs display lower Ni, higher Ba and Sr concentrations than the majority of western/central primitive OIBs.

4.3.4 Primitive Trace Element Ratio Diagrams

Primitive LKTs display higher Y/Zr ratios (0.23-0.33) than primitive CABs and OIBs (Figure 4-4A). Primitive CABs display higher Y/Zr ratios (0.20-0.26) than primitive OIBs (0.16-0.23) (Figure 4-4A). Primitive LKTs display relatively low Nb/Zr ratios (0.04-0.06) at lower Nb concentrations (3-7 ppm) than primitive CABs and OIBs (Figure 4-4B). Primitive OIBs reach high Nb/Zr ratios (0.08-0.12) at higher Nb concentrations (12-19 ppm) than primitive CABs and OIBs (Figure 4-4B). Primitive LKTs contain lower Na_2O concentrations (2.67-2.94 wt %) at higher Sc contents (35-41 ppm) than primitive CABs and OIBs (Figure 4-4C). Primitive OIBs reach high Na_2O concentrations (3.12-3.55 wt %) at lower Sc contents (28-32 ppm) than primitive LKTs and CABs (Figure 4-4C).

Primitive eastern LKTs display higher Y/Zr ratios, lower Na_2O contents, and higher Sc contents than primitive western/central LKTs. Primitive western/central CABs contain higher Y/Zr ratios, higher Na_2O contents, and lower Sc contents than primitive eastern CABs. Primitive western/central OIBs display higher Y/Zr ratios, lower Na_2O contents, and higher Sc contents than primitive eastern OIBs (Figure 4-4).

Primitive eastern LKTs plot along the spinel lherzolite shallow depleted mantle melting line at higher degrees of melting than the western/central primitive LKTs on the Y/Zr and Y trace element ratio diagram (Figure 4-4A). Primitive OIBs plot closer to the garnet lherzolite enriched mantle melting line at lower degrees of melting than primitive CABs and LKTs (Figure 4-4A & B). Primitive western/central LKTs and CABs display variable concentrations of Y/Zr ratios and Y towards 5 % aggregate melting along the spinel lherzolite line, and also plots samples in between the two melting lines (Figure 4-4A).

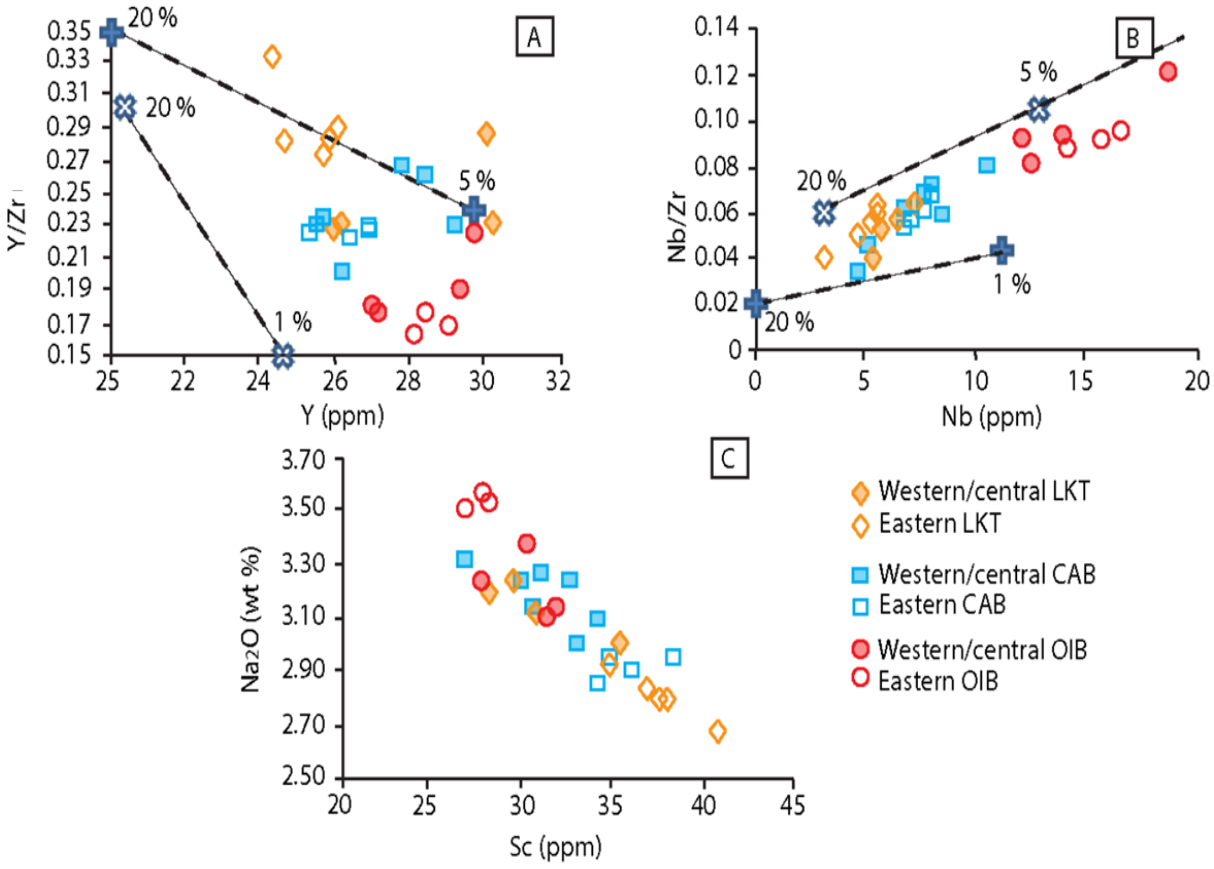

Figure 4-4. Trace element ratio diagrams illustrating the depth and degree of partial melting of primitive FRVF magmas. A) Y/Zr vs. Y and; B) Nb/Zr vs. Nb contains aggregated fractionation melt models (symbols at 1, 5, and 20% aggregate melting) extracted from Conrey et al. (1997). (+) symboled dashed line is spinel lherzolite shallow depleted mantle, (X) symboled dashed line is garnet lherzolite enriched mantle derived at greater depths. Lines derived using fertile MORB mantle data, and primitive undepleted mantle data from Pearce & Parkinson (1993). C) Na_2O (wt %) vs. Sc (ppm) Note the lower Y/Zr ratios and higher Nb/Zr ratios in primitive OIBs compared to primitive LKTs and CABs.

Primitive LKTs generally contain higher Ba/Nb at higher La/Nb concentrations than primitive OIBs, but do not reach as high concentrations as primitive CABs (Figure 4-5A). Primitive eastern LKT sample FR-13-151 from Reed Rock displays lower La/Nb values (0.43) than all primitive OIBs (Figure 4-5A). Eastern Primitive CABs from Green Mountain, western/central primitive CAB sample FR-10-46 and FR-10-58 from McCarty Butte, and primitive western/central LKT samples FR-10-30 from Big Hole and FR-10-56 from McCarty Butte display the highest Ba/Nb (43.4- 71.8) and La/Nb (1.63-2.57) ratios (Figure 4-5A). Higher Ba/Nb ratios than N-MORB at La/Nb >1 ppm occurs in all primitive samples except primitive OIB samples FR-10-85, FR-13-150, FR-13-151, FR-13-171, primitive LKT sample FR-13-152, and primitive CAB sample FR-10-77 (Figure 4-5A). Nb/Y ratios in primitive OIB samples display much higher values (0.41-0.64) than primitive LKTs and CABs (0.23- 0.36) (Figure 4-5B).

Primitive OIBs contain higher Nb/Zr (0.09- 0.12) ratios than primitive LKTs and CABs (0.04-0.08) (Figure 4-5C). Primitive LKTs and the majority of the western/central primitive CABs generally contain lower Nb/Zr at low to moderate Ba/Zr (1.77-2.38) ratios. Primitive eastern CABs and western/central primitive CAB sample FR-10-58 from McCarty Butte contain the highest Ba/Zr ratios (3.04-3.63) at lower Nb/Zr ratios than primitive OIBs (Figure 4-5C).

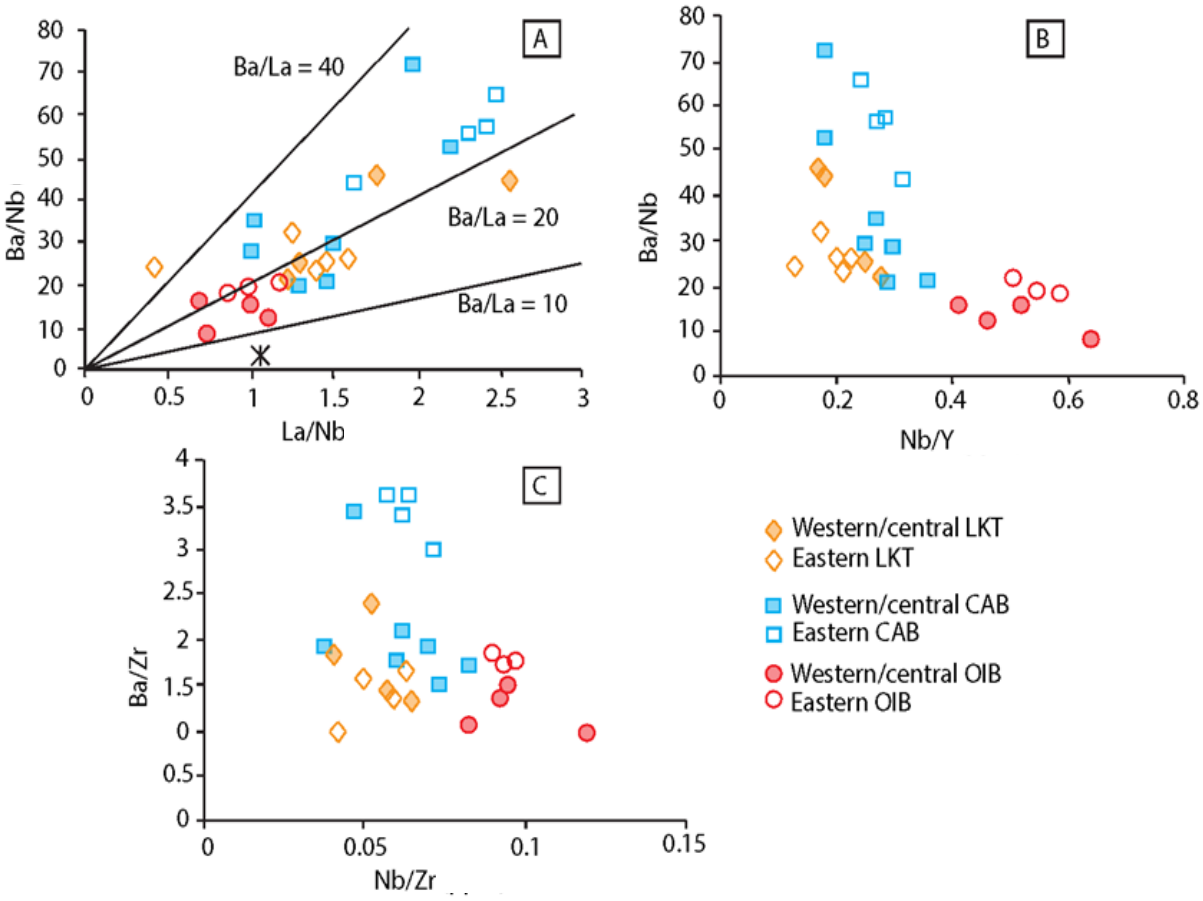

Figure 4-5. Trace element ratio diagrams illustrating subduction enrichment and mantle fertility trends of primitive FRVF magmas. A) Ba/Nb vs. La/Nb; N-MORB value point (black star) obtained from Sun & McDonough (1989). High Ba/Nb and La/Nb ratios= subduction enrichment, low Ba/Nb and La/Nb ratios= little to no addition of a subduction component. Ba/La lines extracted from Bacon et al. (1997). B) Ba/Nb vs. Nb/Y; high Nb/Y ratios = fertile mantle source. C) Ba/Zr vs. Nb/Zr ; high Ba/Zr ratios = subduction enrichment, high Nb/Zr ratios= fertile mantle source.

4.4 Discussion

4.4.1 Primitive LKT and OIB Trace Element Interpretations

The absence of well-developed LILE and LREE enrichment in primitive LKT and OIB samples chosen for ICP-MS analysis suggests lesser lithospheric mantle contributions in their genesis, crust is thin and compositionally primitive (Conrey et. al, 1997) (refer to Figure 4-1B). It can also imply that multiple batch melting and fractionation from the source occurred, and there were high degrees of melting of a relatively depleted non-fertile mantle source (Bacon et al. 1997)

Primitive OIBs have steep N-MORB patterns and comparatively smaller Nb/Ta wells than the primitive LKTs, suggestive of an intraplate component (Leeman et al. 2005) (Figure 4-1B). OIBs display a clear intraplate signature with high Nb and Ta concentrations. Negative Nb-Ta anomalies occur in all LKT samples, which are considered diagnostic of subduction-related arc magmatic rocks (Bacon, 1990). The absence of Nb-Ta negative anomalies in primitive OIB samples FR-10-40 and FR-10-85 suggests they have a MORB-like chemical affinity, or a less contaminated asthenospheric mantle source (du Bray & John, 2011). Primitive OIB sample FR-10-85 displays higher Cs, Rb, Th, U, Nb, and Ta, but lower Sr than primitive OIB sample FR-10-40, suggesting this is possibly due to minor source contamination or crustal contamination of sample FR-10-40 (du Bray & John, 2011) (Figure 4-1B).

La/Yb ratios for all FRVF LKT and OIB magmas display relatively shallow sloping patterns. Concentrations of La, Sm, and Th are relatively low in all samples, interpreted as a result of high degrees of melting (Rowe et al. 2009) (Appendix I). Low Nb/U ratios < 25, Ce/Yb ratios < 10, and Rb/Cs ratios < 50 that occur in primitive LKT sample FR-10-38 could be the result of regional contamination by subducted sediments or tectonically eroded crust (Saunders & Tarney, 1979; Rowe et al. 2009) (Appendix I).

High Sr/La ratios >35 in primitive LKT and OIB samples FR-10-38, FR-10-40, and FR-12-101 can possibly be attributed to subduction related components of slab melts, fluids, or arc magmas, that either were stored in the basal continental lithospheric mantle,

or had contaminated the supraslab asthenosphere (Saunders &Tarney, 1979; Gorring & Kay, 2001; du Bray & John, 2011) (Appendix I).

Primitive LKT sample FR-10-30 has the lowest Cs, Rb and Y concentrations, but the highest Ba, La, Pb, and Sr concentrations, suggestive of high degrees of melting of a depleted mantle source enriched by crustal contamination or source contamination (Bacon, 1990; Bacon et al. 1997; Conrey et al. 1997; Rowe et al. 2009; du Bray & John, 2011) (Figure 26B) (Appendix I). This sample is unique, containing a negative Ce anomaly. The presence of this anomaly can be attributed to subduction of pelagic sediment (Bacon et al. 1997). Pelagic sediment accumulates through settling of particles on the ocean floor. It may be that the negative anomaly results from ancient sediment subduction that locally affected the FRVF LKT source. (Neal & Taylor, 1989; Bacon et al. 1997) (Figure 4-1B).

4.4.2 Primitive Western/Central vs. Eastern Trace Element Interpretations

Higher Ni concentrations at lower MgO contents in primitive LKT samples FR-10-30 and FR-10-56 than primitive eastern LKTs can possibly be attributed to low degrees of melting of a more enriched mantle source, or olivine suppression during fractional crystallization (Bacon, 1990; Bacon et al. 1997; Conrey et al. 1997) (refer to Figure 4-2A).

Higher Zr concentrations in western/central primitive LKTs suggest a more enriched mantle source than eastern primitive LKTs, or more extensive fractional crystallization for the two western/central samples at lower MgO contents (Bacon, 1990; Bacon et al. 1997; Conrey et al. 1997) (refer to Figure 3C). Higher Zr concentrations in eastern primitive OIB samples are possibly due to more extensive fractional crystallization (Bacon, 1990) (Figure 4-2C).

Lower Ni and Cr concentrations at lower MgO contents in eastern primitive CAB samples suggest more extensive fractional crystallization than western/central primitive CAB samples (Figure 4-2A) (Table 4-2). Lower Sc concentrations in western primitive LKTs possibly due to lower degrees of melting than eastern primitive LKTs (Figure 4-2E). Higher concentrations of LILEs and LREEs, such as (Ba, Rb, Sr, La, Ce, Nd, Sc) in

eastern primitive samples suggest a greater influence of a subduction component to the eastern CAB mantle source than the western/central CAB source (Bacon, 1990; Bacon et al. 1997; Conrey et al. 1997) (Figure 4-2, Figure 4-3C).

Higher incompatible element concentrations of Ba and Sr in primitive eastern OIB samples possibly occur due to a greater influence of a subduction component to the intraplate mantle wedge than western OIB samples, or as a result of more extensive fractional crystallization (Bacon, 1990; Bacon et al. 1997; Conrey et al. 1997) (Figure 4-3C).

Primitive eastern CAB and OIB samples contain higher Ba and Sr concentrations than their western/central CAB and OIB counterparts (Figure 4-3C). The exception is for western CAB sample FR-10-58 which contains high Ba and Sr contents as well (Figure 28C). Eastern LKTs contain lower Ba and Sr concentrations than western/central primitive LKTs (Figure 4-3C). Overall, this suggests that primitive western LKTs, eastern CABs, and eastern OIBs mantle sources have been affected by a subduction component to a higher degree than their primitive eastern counterparts (Rowe et al. 2009) (Figure 4-3C).

Ni plotted against Ba and Sr concentrations display which primitive magmas have undergone more extensive fractionation and mantle source enrichment by subduction (Figure 4-3). Western/central LKTs show higher Ni concentrations, and higher Ba and Sr concentrations than eastern LKTs, suggestive of lower degrees of melting of a more subduction enriched mantle source than for eastern LKT mantle sources (Figure 4-3). Eastern primitive OIBs and western/central primitive OIB sample FR-10-78 display lower Ni concentrations, and slightly higher Ba and Sr concentrations than all the other primitive western/central OIBs (Figure 4-3). This suggests these samples have undergone more extensive fractionation, or are more affected by a subduction component than western/central OIBs (Figure 4-3). Eastern primitive CABs display lower Ni concentrations and higher Ba and Sr concentrations than the western CABs (Figure 4-3). Eastern primitive CABs have undergone higher degrees of melting of a more subduction enriched mantle source (Figure 4-3).

i. Depth and Degree of Partial Melting

High ratios of Y/Zr at moderate Y values represent high degrees of partial melting of a shallower, depleted mantle source (Figure 4-4A). Low Y/Zr ratios at moderate Y values represent lower degrees of partial melting of a deep enriched mantle source (Conrey, 1997) (Figure 4-4A). High Nb/Zr ratios at high Nb concentrations represent lower degrees of melting of a deep, enriched mantle source (Figure 4-4B). High Na_2O concentrations at low Sc concentrations represent a lower degree of partial melting at deeper asthenospheric levels (Figure 4-4C)(Bacon, 1990; Bacon et al. 1997; Conrey et al. 1997; Reiners et al. 2000; Jordan et al. 2002; Leeman et al. 2005; Schmidt et al. 2008; Rowe et al. 2009; Schmidt & Grunder, 2011; du Bray & John, 2011).

Primitive OIBs have low Y/Zr ratios, high Nb/Zr ratios at high Nb concentrations, and higher Na_2O concentrations at lower Sc contents than primitive LKTs and OIBs, consistent with a lower degree of partial melting of an enriched source at deeper asthenospheric levels (Figure 4-4). LKTs contain high Y/Zr ratios, low Nb/Zr ratios at low Nb concentrations, and lower Na_2O concentrations at higher Sc contents, consistent with high degrees of melting of a shallower, depleted mantle source (Figure 4-4). Primitive CABs contain trace element ratios that fall in between LKTs and OIBs, suggesting moderate degrees of melting of a moderately enriched mantle source at average depths (Figure 4-4).

Primitive eastern LKTs reach higher Y/Zr ratios, lower Na_2O contents, and higher Sc contents than primitive western/central LKTs (Figure 4-4). This suggests that primitive eastern LKTs represent higher degrees of melting of a more depleted mantle source than western/central LKTs. Primitive western/central CABs reach higher Y/Zr ratios, higher Na_2O contents, and lower Sc contents than primitive eastern CABs (Figure 4-4). This suggests that primitive eastern CABs represent lower degrees of melting of more enriched mantle source than western/central CABs. Primitive western/central OIBs reach higher Y/Zr ratios, lower Na_2O contents, and higher Sc contents than primitive eastern OIBs (Figure 4-4). This suggests that primitive eastern OIBs represent higher degrees of melting of shallower, less enriched mantle source than western/central OIBs.

These trace element diagrams are consistent with the assertion that primitive LKTs represent higher degrees of melting of shallow, depleted mantle, whereas primitive OIBs and CABs represent lower degrees of melting of a less depleted mantle.

ii. Subduction Enrichment & Mantle Fertility

Comparison of LILE/LREE ratios and HFSE/HREE ratios in primitive magmas aid in distinguishing differences in the degree of addition of a subduction component to the mantle source (higher LILE/LREE concentrations) and the fertility of the mantle source (higher HFSE/HREE concentrations) between the primitive magma types.

High Ba/Nb ratios at high La/Nb ratios of primitive CABs suggest that these magma sources are enriched by a subduction component (Figure 4-5A). Low Ba/Nb ratios at low La/Nb and Ba/La ratios of the primitive OIBs reflect a strong HFSE-enriched intraplate signature mantle source domain. (Sun & McDonough, 1989). Primitive LKTs contain higher Ba/Nb ratios at higher La/Nb ratios than primitive OIBs, but do not reach as high as primitive CAB values, suggesting that primitive LKTs contain a moderate to high subduction influence to the mantle source, and a moderate to low fertile mantle source (Bacon et al. 1997) (Figure 4-5A).

All eastern and western/central primitive LKTs contain lower Ba/Nb ratios at lower La/Nb ratios, with the exception of two primitive western/central LKT samples FR-10-30 and FR-10-56, where they have higher Ba/Nb and La/Nb ratios suggestive of enrichment of their magma sources by a subduction component to a higher degree than the other primitive LKT samples (Rowe et al. 2009) (Figure 4-5A). All eastern primitive CAB samples display high Ba/Nb ratios at high La/Nb ratios, along with two western primitive CAB samples (FR-10-46, FR-10-58) from McCarty Butte and Oatman Flat, suggesting these magma sources are enriched by a subduction component to a higher degree than the other primitive western CABs (Rowe et al. 2009) (Figure 4-5A).

Higher Ba/Nb ratios than N-MORB at La/Nb >1 occurs in most samples, and reflects that there is some degree of presence of a subduction derived component (Sun & McDonough, 1989) (Figure 4-5A). Primitive CAB and OIB samples FR-10-77, and FR-10-78 from the Flat Top vent in Cabin Lake all contain La/Nb ratios < 1 suggesting there

was little to no presence of a subduction component in this area (Sun & McDonough, 1989) (Figure 4-5A).

Studies from Sun & McDonough (1989) discuss differences in Ba/Nb and La/Nb ratios, and how they reflect differences in OIB and MORB mantle source characteristics. Low La/Nb ratios <1 observed in primitive OIB samples FR-10-78, FR-10-85, and FR-13-151 possibly reflects the mantle source character of the recycled oceanic crust, which has experienced dehydration partial melting in the subduction zone region (Sun & McDonough, 1989) (Figure 4-5A). Low La/Nb ratios in the mantle source could also be the result of mantle metasomatism and/or small degrees of partial melting, since Nb is more incompatible than La (Sun & McDonough, 1989). High La/Nb ratios greater than or equal to 0.9 found in primitive OIB samples FR-10-40, FR-13-150, FR-13-164 and FR-13-171, could be due to the introduction of subducted sediment into the OIB source, or it could be due to the presence of residual niobium-bearing titanite mineral during magma generation (Sun & McDonough, 1989) (Figure 4-5A) (Appendix I).

Ba/ Nb ratios > 15 in primitive OIB samples FR-10-78, FR-13-150 and FR-13-151, FR-13-164 are considered to be elevated to more arc-like compositions, where the addition of subducted slab components to magmas generated during slab dehydration and fluid –flux induced partial melting of the mantle wedge (Sun & McDonough, 1989) (Figure 4-5A). Ba/ Nb ratios < 15 in western/central primitive OIB samples FR-10-40, FR-10-85 and FR-13-171 resemble MORB-like compositions, possibly because these samples have undergone less fractionation than the other primitive OIB samples (Sun & McDonough, 1989) (Figure 4-5A) (Appendix I).

Ba/Zr ratios plotted against Nb/Zr ratios separates intraplate (high Nb/Zr ratio) magmas, from subduction related (high Ba/Zr ratio) magmas (Figure 6B). Primitive OIBs contain higher Nb/Zr ratios at lower Ba/Zr ratios, suggesting these magmas have a strong, intraplate HFSE-enriched mantle source (Bacon et al. 1997; Conrey et al. 1997) (Figure 4-5B). Primitive LKTs contain low to moderate Ba/Zr ratios at lower Nb/Zr ratios, suggesting these magmas contain a less fertile mantle source with a moderate subduction input (Bacon et al. 1997; Conrey et al. 1997; Rowe et al. 2009) (Figure 4-5B). Primitive CABs reach high Ba/Zr ratios at low to moderate Nb/Zr ratios suggesting these magmas

contain a moderately fertile mantle source with a greater contribution from a subduction component than in primitive LKT and OIB mantle sources (Figure 30B). Ba/Nb ratios plotted against Nb/Y ratios display similar trace element patterns for each primitive magma type.

Primitive LKTs contain lower Ba/Zr ratios, and also lower Nb/Zr ratios for all samples except for western/central LKT samples FR-10-30 and FR-10-56, which contain higher Ba/Zr ratios than all other primitive LKTs. The higher Ba/Zr ratios in these two samples suggest a stronger influence of a subduction component to their magma sources (Figure 4-5B). The most primitive (Mg# 68) eastern LKT sample FR-13-152 contains the lowest Ba/Zr ratio (0.97) at low Nb/Zr ratios (0.04) suggesting the primary magma source was depleted in both LILEs and HFSEs (Figure 4-5B). All primitive eastern CABs, and western/central primitive CAB sample FR-10-58 contain higher Ba/Zr ratios than the remaining western/central CABs. This suggests that these primitive CABs have been enriched in a subduction component to a greater degree than the western/central CABs (Bacon, 1990).

Ba/Nb ratios plotted against Nb/Y ratios represent similar trace element patterns for each magma type as the Ba/Zr and Nb/Zr ratio plot (Figure 4-5C). Primitive eastern CABs, two western CAB samples FR-10-58 and FR-10-46, and two primitive western LKT samples FR-10-30 and FR-10-56 contain higher Ba/Nb ratios (43-71.9) than their primitive counterparts, suggesting a stronger enrichment of a subduction component to their primary magma sources (Rowe et al. 2009) (Figure 4-5C).

FRVF primitive basalts are a product of partial melting of three different types of mantle sources; a LILE-enriched mantle source, a HFSE-enriched intraplate mantle source, and an incompatible element depleted mantle source (Figure 4-6). Partial melting of an HFSE-enriched mantle source occurs at greater depths for primitive OIBs, while the depleted mantle source for primitive LKTs occurs at shallower depths (Figure 4-6).

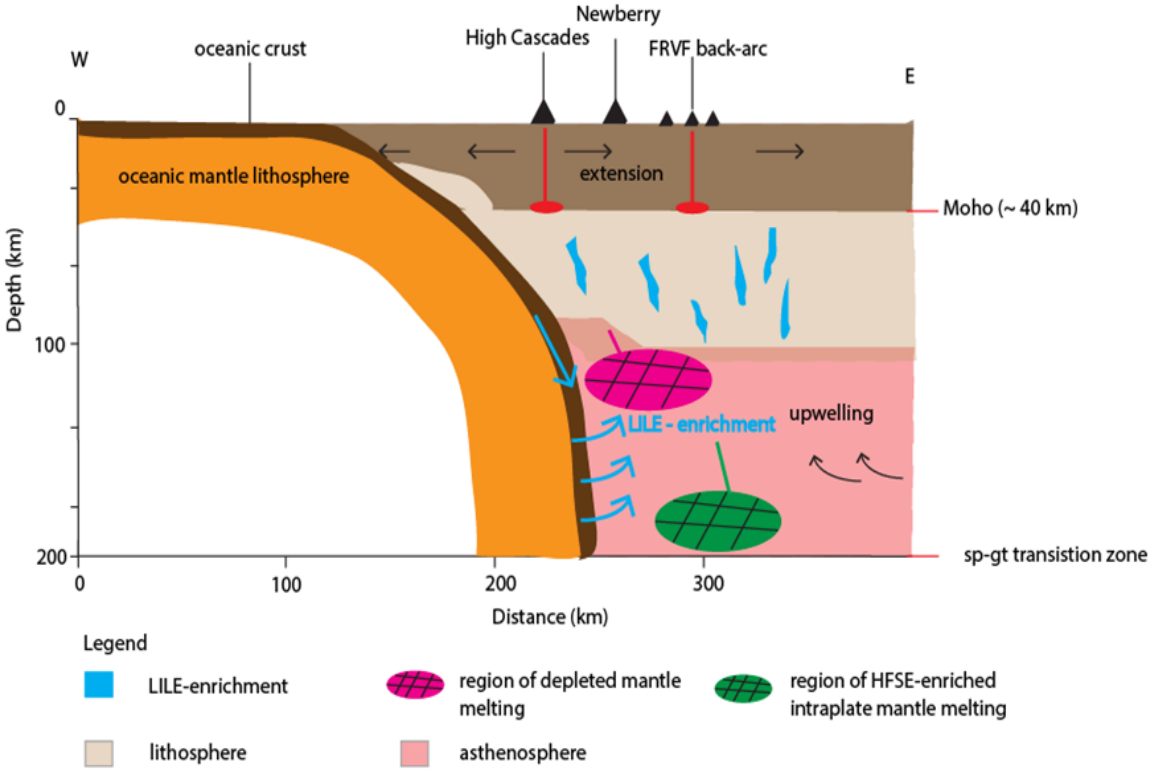

Figure 4-6. Cartoon of the Oregon Cascadia subduction zone and backarc magmatism. The Moho is approximately 40 km deep (Till et al. 2013). The subducting slab extends to a depth of approximately 90 km beneath the cascade arc (McCory et al. 2012). The thickness of the subducting slab is approximately 60 km thick (McCory et al. 2012). CABs result from the addition of LILEs from the oceanic crust to the mantle wedge, as well as induced melting of a variably LILE-enriched lithosphere. LKTs result from high degrees of shallow melting of a depleted mantle source. OIBs result from low degrees of deeper melting of a HFSE-enriched mantle source close to the spinel-garnet transition zone (sp-gt).

The subducting oceanic crust transfers LILE-enriched fluids to the overlying hot mantle wedge, which induces mantle melting. Additional processes that melt these mantle rock sources include increasing the temperature and/or decreasing the pressure. As these mantle sources melt, the partial melt that is extracted rises through upwelling from the

asthenosphere to eventually erupting at the surface of the FRVF. The continental crust is stretched through the extensional forces and faulting that occurs in the area. Decompression melting occurs, and these partial melts rise more efficiently through the thinned out crust erupting primitive magmas from these mantle sources (Figure 4-6).

4.5 Conclusions

The FRVF back-arc primitive basalt trace element concentrations are highly variable between and within magma types. Patterns of fluctuating depth and degree of partial melting, subduction enrichment, and mantle fertility trends of primary mantle sources are displayed through FRVF western/central and eastern primitive trace element concentrations and ratios. Trace element data display concentrations that were expected based on major element and Ba/Nb ratios derived from Chapter 2.

Primitive LKTs generally contain a higher range of compatible elements Ni and Cr, high Sc contents, and a low range of incompatible element contents V, Ba, Rb, Sr, Zr, Nb, La, Ce, Nd compared to CABs. Primitive CABs generally contain a lower range of compatible elements Ni and Cr, and reach higher incompatible element concentrations Ba, Rb, Sr, Zr, Nb, La, Ce, Nd than primitive LKTs. Primitive OIBs display a higher range of incompatible HFSE elements Nb and Zr than primitive LKTs, CABs, and trace elements contents that are intermediate between primitive LKTs, CABs, and BAs concentrations

Western/central primitive LKTs generally contain higher Ni, Ba, Sr, Zr and lower Sc concentrations than eastern primitive LKTs. Eastern primitive CABs generally contain lower Ni and Cr concentrations, and higher Sc, Ba, Rb, Sr, La, Ce and Nd concentrations than western/central primitive CABs. Eastern primitive OIBs generally contain higher Ba, Sr, Zr, and Ce concentrations than western/central primitive OIB samples.

Trace element data displayed gently sloping patterns of LREE enrichment and HREE depletion in all LKT and OIB samples. Eastern primitive LKT sample FR-12-101 contains lower LREE contents than western/central primitive LKT samples FR-10-30, FR-10-38. The absence of negative Nb-Ta anomalies for the OIB samples is consistent

with their MORB-like chemical affinity with a less contaminated asthenospheric mantle source than the LKTs.

Comparison of trace element concentrations and ratios display that primitive OIBs contain the highest concentrations of HFSEs, and are the most fertile mantle sources of any other primitive magma type. Eastern primitive CABs display greater LILE concentrations than western/central primitive CABs, with the exception of primitive western CAB samples FR-10-46 and FR-10-58. All primitive LKTs show relatively low LILE and HFSE ratios. The exception of western/central primitive samples FR-10-30 and FR-10-56 display higher LILE enrichment trends then the other primitive LKTs.

Overall, trace element concentrations point towards primitive LKTs displaying lower degrees of melting of a more depleted mantle source than primitive CABs and OIBs. Primitive CABs display lower degrees of melting of a greater subduction enriched mantle source than primitive LKTs. OIBs display lower degrees of melting of a more fertile mantle source than primitive LKTs.

Primitive eastern LKTs represent higher degrees of melting of a shallower, depleted mantle source than western/central LKTs. Primitive eastern CABs represent lower degrees of melting of deeper, more subduction enriched mantle source than western/central CABs. Primitive eastern OIBs represent higher degrees of melting of shallower, slightly less fertile mantle source than western/central OIBs, but greater contribution of a subduction component to their primary intraplate mantle source domain.

CHAPTER 5: Conclusions

The Fort Rock volcanic field (FRVF), an extensional back-arc basin, contains a diversity of primitive basaltic magma types associated with multiple hydrovolcanic eruptions of tuff rings/cones and maars, and conventional eruptions of cinder cones, spatter cones, and lava fields. The subduction of the Juan de Fuca Plate beneath the North American Plate, the bimodal volcanism of the High Lava Plains along the northwest trending faults of the Brothers Fault Zone, Newberry eruptions along the volcano's southeastern flanks, and the extension of the northwestern Basin & Range continental rift zone influenced the eruptions of these diverse primitive basalts.

Oregon includes an extensive history of subduction, volcanism, and formation of sediments and mountains from 400 Ma to present day. The subduction of the JDFP westward under the NAP triggered Neogene deformation, paleomagnetic rotations, and seismic activity that ultimately causes fore-arc migration of these blocks northward approximately 9 mm/yr. (Wells et al. 1998). Cascadia subduction in the Pacific Northwest dates back to approximately 35-40 Ma, comprised of the Western Cascade (~45-10 Ma) and the High Cascade (< 10 Ma) volcanism. The High Lava Plain bimodal volcanic eruptions aligned along the Brothers Fault Zone approximately 10 Ma. The rhyolites display a uniform decrease in age from east to west, where Newberry crater in the west lavas extruded less than 1 Ma. Newberry is a large shield volcano with a complex volcanic history that erupted a large amount of cinder, spatter, scoria and lava flows.

These areas contain four distinct primitive basaltic end-members based largely on major and trace element compositions, which includes; LKTs, CABs, BAs, and OIBs (Bacon, 1990; Hughes, 1990; Bacon et al. 1997; Conrey et al. 1997; Jordan et al. 2002; Schmidt et al. 2008; Rowe et al. 2009; Schmidt & Grunder, 2011; du Bray & John, 2011). Three mantle components created the primitive LKT, CAB/BA, and OIB magma types. A depleted mantle source similar to MORBs generates the LKTs; a mantle enriched by a modern, hydrous subduction component generates LILE enriched CABs; and a HFSE-enriched source like intraplate mantle domain generates OIBs. Primitive LKTs widely suggested a result of high degrees of melting of a shallower, depleted

mantle source, while primitive CABs, BAs, and OIBs result from low degrees of melting of a deeper, more enriched mantle source (Bacon, 1990; Hughes, 1990; Conrey et al. 1997; Rowe, 2009).

FRVF basaltic samples included lava, scoria/spatter and juvenile bombs in tuff rings and maars. Olivine and plagioclase are the main phenocryst phases in a finer-grained groundmass of oxides, olivine, plagioclase, +/- clinopyroxene, +/- glass. All basalts exhibit a range of phenocryst and groundmass textures that are not specific to just one magma type. The eruption style changed progressively from an initial hydrovolcanic phase, through a transitional stage, to one that was entirely Strombolian. Eruptive styles are reflected through their variations in groundmass crystallinity, average groundmass grain size, and vesicularity. FRVF lavas contain higher groundmass crystallinity contents, grain sizes, and lower vesicle contents than scoria/spatter samples, and higher vesicle contents than juvenile basaltic bombs. FRVF scoria/spatter samples exhibit larger, more rounded and more abundant intact vesicles. Western/central lavas contain higher groundmass crystallinity contents and larger groundmass grain sizes than the eastern lava samples. This suggests that western/central lavas underwent slower cooling rates from a depth with greater water contents than eastern lavas.

XRF and ICP-MS geochemical data determined that OIBs contain the highest concentrations of HFSEs, and are the most fertile mantle sources of any other primitive magma type. Eastern primitive CABs display greater LILE concentrations than LKTs and OIBs. All primitive LKTs display relatively lower LILE and HFSE concentrations than primitive CABs and OIBs.

Western/central primitive LKTs contain lower CaO and Sc concentrations, and higher Na_2O, FeO*, TiO_2, Ni, Ba, Sr, Zr values than eastern primitive LKTs, arguing for lower degrees of partial melting of a more fertile, subduction enriched deeper mantle source in the western/central FRVF sector. These basalts were likely influenced by the extensional forces of the Basin & Range and the northwest trending faults of the Brothers Fault Zone.

Eastern primitive CABs contain lower FeO*, TiO_2, Na_2O, Ni and Cr concentrations, and higher CaO, K_2O, Ba, Sc, Rb, Sr, La, Ce, and Nd concentrations than western/central primitive CABs, arguing for lower degrees of partial melting of a more subduction enriched mantle source than the western/central FRVF CABs. There is controversy as to whether primitive western/central CABs are actually true CAB end-members, as their higher FeO*/MgO ratios categorize them into tholeiitic magmas, but their higher K_2O values and enrichment in LILEs relative to primitive LKTs categorize them as CABs. These basalts can also be categorized as transitional between LKTs and OIBs. These basalts were likely influenced by the addition of a subduction component to their primary mantle sources through the subduction of the Juan de Fuca Plate beneath the North American Plate.

Eastern primitive OIBs contain lower FeO*, MgO, CaO, and higher SiO_2, Na_2O, K_2O, Ba, Sr, Zr, and Ce concentrations than western/central primitive OIBs, suggesting that eastern primitive OIBs represent lower degrees of partial melting of a more shallow, subduction enriched mantle source than the western/central primitive OIBs. These basalts were likely influenced by the occurrence of an intraplate mantle source beneath the back-arc region.

BIBLIOGRPAHY

Arculus, R. J. (2003). Use and Abuse of the Terms Calcalkaline and Calcalkalic. *Journal of Petrology*, 44(5), 929-935.

Anderson, A. (1980). Significance of hornblende in calc-alkaline andesites and basalts. *American Mineralogist*, 65, 837-851. *Journal of Petrology* 44.5 929-935.

Bacon, C. (1990). Calc-alkaline, Shoshonitic, and Primitive Tholeiitic Lavas from Monogenetic Volcanoes near Crater Lake, Oregon. *Journal of Petrology*, 31(1), 135-166.

Bacon, Charles, Robert Bruggman, and Michael Christiansen (1997). Primitive Magmas at Five Cascade Volcanic Fields: Melts from Hot, Heterogeneous Sub-Arc Mantle. *The Canadian Minerologist*, 35, 397-423.

Bartels, K., Kinzler, R., & Grove, T. (1991). High pressure phase relations of primitive high-alumina basalts from Medicine Lake volcano, northern California. *Contr. Mineral. And Petrol.*, 108(3), 253-270.

Bevis, K. (2013). (3) Field Guide to the Newberry Volcano and Christmas Valley-Fort Rock Area | In the Playground of Giants. Intheplaygroundofgiants.com. Retrieved 10 December 2015. http://intheplaygroundofgiants.com/field-guides-to-central-oregons-geology/field-guide-to-the-newberry-volcano-and-christmas-valley-fort-rock-area/

Bézos, A., Escrig, S., Langmuir, C., Michael, P., & Asimow, P. (2009). Origins of chemical diversity of back-arc basin basalts: A segment-scale study of the Eastern Lau Spreading Center. *J. Geophys. Res.*, 114(B6).

Borg, L., Clynne, M., & Bullen, T. (1997). The Variable Role of Slab-derived Fliuds in the Generation of a Suite of Primitive Calc-alkaline Lavas from the Southernmost Cascades, California. *The Canadian Minerologist*, 35, 425-452.

Brand, B. & Heiken, G (2009). Volcanoes to vineyards. Tuff Cones, Tuff Rings, and Maars of the Fort Rock--Christmas Valley Basin, Oregon: Exploring the Vast Array of Pyroclastic Features That Record Violent Hydrovolcanism at Fort Rock and the Table Rock Complex. Boulder, Colo.: *Geological Society of America.*

Camp, V. E., and M. E. Ross (2004), Mantle dynamics and genesis of mafic magmatism in the intermontane Pacific Northwest, *J. Geophys. Res.*, 109.

Christiansen, R. L., G. R. Foulger, and J. R. Evans (2002), Upper-mantle origin of the Yellowstone hotspot, *Geol. Soc. Am. Bull.*, 114, 1245 – 1256.

Clarke, H., Troll, V., Carrecedo, J., Byrne, K., & Gould, R. (2005). Changing Eruptive Styles and Texutral Features from Phreatomagmatic to Strombolian Activity of Basaltic Littoral Cones: Los Erales Cinder Cione, Tenerife, Canary Islands. *Estudios Geol*, 61, 121-134.

Clément, J., Caroff, M., Dudoignon, P., Launeau, P., Bohn, M., & Cotten, J. et al. (2007). A possible link between gabbros bearing High Temperature Iddingsite alteration and huge pegmatoid intrusions: The Society Islands, French Polynesia. *Lithos*, 96(3-4), 524-542.

Clynne, M.A., Borg, L.E. (1997). Olivine and chromian spinel in primitive calc-alkaline and tholeiitic lavas from the southern-most Cascade Range, California: a reflection of relative fertility of the source. *Canadian Mineralogist* 35, 453 – 472.

Conrey, R. (1990). Olivine analcimite in the Cascade Range of Oregon. *J. Geophys. Res*., 95(B12), 19639.

Conrey, R., Sherrod, D., Hooper, P., Swanson, D. (1997) Diverse Primitive Magmas in The Cascade Arc, Northern Oregon and Southern Washington. *The Canadian Minerologist* 35, 367-396.

Couch, S., Harford, C. L., Sparks, R. S. J. & Carroll, M. R. (2003). Experimental constraints on the conditions of formation of highly calcic plagioclase microlites at the Soufrie're Hills Volcano, Montserrat. *Journal of Petrology* 44, 1455-1475.

Draper, D. S. (1991), Late Cenozoic bimodal magmatism in the northern Basin and Range province of southeastern Oregon, J. Volcanol. Geotherm. Res., 47, 299–328.

du Bray, E.A., and John, D.A. (2011) Petrologic, tectonic, and metallogenic evolution of the Ancestral Cascades magmatic arc, Washington, Oregon, and northern California. *Geosphere,* 7, 1102–1133.

Eagar, K., Fouch, M., James, D., & Carlson, R. (2011). Crustal structure beneath the High Lava Plains of eastern Oregon and surrounding regions from receiver function analysis. *J. Geophys. Res*., 116(B2).

Fisher, R. V., Schmincke, H.-U. (1984). Pyroclastic rocks. Berlin: *Springer-Verlag, Berlin*, 69-85: 231-264.

Ford, M., Grunder, A., & Duncan, R. (2013). Bimodal volcanism of the High Lava Plains and Northwestern Basin and Range of Oregon: Distribution and tectonic implications of age-progressive rhyolites. *Geochemistry, Geophysics, Geosystems*, 14(8), 2836-2857.

Fort Rock tuff ring and Hole-in-the-ground photographs (Figure 5), extracted from the Bend Hiking Group [http://www.meetup.com/TheBendHikingGroup/] founded May 13, 2007.

Gill, J. B., (1976). Comparison and age of Lau Basin and Ridge volcanic rocks: implications for evolution of an interarc basin and remnant arc, *Geol. Soc. Amer. Bull*., 87, 1384–1395.

Glen, J. & Ponce, D. (2002). Large-scale fractures related to inception of the Yellowstone hotspot. *Geol*, 30(7), 647.

Gonnermann, H. M. & Manga, M. (2003). Explosive volcanism may not be an inevitable consequence of magma fragmentation. *Nature*, 426, 432-435.

Gorring, M. & Kay, S. (2001). Mantle Processes and Sources of Neogene Slab Window Magmas from Southern Patagonia, Argentina. *Journal of Petrology*, 42(6), 1067-1094.

Guilbaud, M., Blake, S., Thordarson, T., & Self, S. (2007). Role of Syn-eruptive Cooling and Degassing on Textures of Lavas from the AD 1783-1784 Laki Eruption, South Iceland. *Journal of Petrology*, 48(7), 1265-1294.

Hart, S. R., W.A. Glassley, and D. E. Karig (1972). Basalts and seafloor spreading behind the Mariana island arc. *Earth Planet. Sci. Lett.*, 15, 12–18.

Hart, W. (1985). Chemical and isotopic evidence for mixing between depleted and enriched mantle, northwestern U.S.A. *Geochimica Et Cosmochimica Acta*, 49(1), 131-144.

Hawkesworth, C., Turner, S., Gallagher, K., Hunter, A., Bradshaw, T., and Rogers, N., (1995). Calc-alkaline magmatism, lithospheric thinning and extension in the Basin and Range: *Journal of Geophysical Research*, v. 100, p. 10,271–10,286.

Hawkins, J. W., (1976). Petrology and geochemistry of basaltic rocks of the Lau Basin. *Earth Planet. Sci. Lett.*, 28, 283–297.

Hawkins, J. W., and J. T. Melchior, (1985). Petrology of Mariana Trough and Lau Basin basalts. *J. Geophys. Res*., 90, 11431–11468.

Heiken, G. (1971). Tuff rings: Examples from the Fort Rock-Christmas Lake Valley Basin, south-central Oregon. *J. Geophys. Res.*, 76(23), 5615-5626.

Higgins, M. (1973). Petrology of Newberry Volcano, Central Oregon. *Geol Soc America Bull*, 84(2), 455.

Hirose, K., & Kushiro, I. (1993). Partial melting of dry peridotites at high pressures: Determination of compositions of melts segregated from peridotite using aggregates of diamond. *Earth and Planetary Science Letters,* 114(4), 477-489.

Hochstaedter, A. G., Gill, J. B., Taylro, B., Ishizuka, O.,Yuasa, M. & Morita, S. (2000). Across-arc geochemical trends in the Izu-Bonin arc: constraints on source composition and mantle melting. *Journal of Geophysical Research*, 105, 495-512.

Hochstaedter, A., Gill, J., Peters, R., Broughton, P., Holden, P. & Taylor, B. (2001). Across-arc geochemical trends in the Izu-Bonin arc: Contributions from the subducting slab. *Geochemistry, Geophysics, Geosystems*, 2, 2000GC000105.

Hooper, P., Binger, G., & Lees, K. (2002). Ages of the Steens and Columbia River flood basalts and their relationship to extension-related calc-alkalic volcanism in eastern Oregon. *Geological Society of America Bulletin,* 114(1), 43-50.

Houghton, B. F.,Wilson, C. J. N., Del Carlo, P., Coltelli, M., Sable, J. E. & Carey, R. (2004). The influence of conduit processes on changes in style of basaltic Plinian eruptions: Tarawera 1886 and Etna 122 BC. *Journal of Volcanology and Geothermal Research*, 137, 1-14.

Housh, T. B. & Luhr, J. F. (1991). Plagioclase melt equilibria in hydrous systems. *American Mineralogist*, 76, 477-492.

Hughes, S. (1990). Mafic magmatism and associated tectonism of the Central High Cascade Range, Oregon. *J. Geophys. Res.*, 95(B12), 19623.

Jensen, R.A., Donnelly-Nolan, J.M., & Mckay, D.M. (2009). A field guide to Newberry Volcano, Oregon, in O'Connor, J.E., Dorsey, R.J., and Madin, I.P., eds., Volcanoes to Vineyards: Geologic Field Trips through the Dynamic Landscape of the Pacific Northwest: *Geological Society of America Field Guide,* 15.

Johnson, D., Hooper, P., & Conrey, R. (1999). XRF Analysis of Rocks and Minerals for Major and Trace Elements on a Single Low Dilution Li-tetraborate Fused Bead. JCPDS-International Centre for Diffraction Data, GeoAnalytical Laboratory, Washington State University. *Advances in X-ray Analysis,* v, 41, p. 843–867.

Jordan, B., Streck, M.J., Grunder, A.L., (2002). Bimodal volcanism and tectonism of the High Lava Plains, Oregon. Field guide to geologic processes in Cascadia: Oreg. *Dep. Geol. Min. Ind. Special Paper* 36:23-46.

Jordan, B. T., A. L. Grunder, R. A. Duncan, and A. L. Deino (2004), Geochronology of age-progressive volcanism of the Oregon High Lava Plains: Implications for the plume interpretation of Yellowstone. *J. Geophys. Res.*, 109, B10202.

Kent, A. J. R., Darr, C., Koleszar, A. M., Salisbury, M. J. & Cooper, K. M. (2010). Preferential eruption of andesitic magmas through recharge filtering. *Nature Geoscience*, 3, 631-636.

Kistler, R. W., and Z. E. Peterman (1978), Reconstruction of crustal blocks of California on the basis of initial strontium isotopic compositions of Mesozoic granitic rocks, U.S. *Geol. Surv. Prof. Pap*., 1071, 17 pp.

Kohn, S., Henderson, C., & Mason, R. (1989). Element zoning trends in olivine phenocrysts from a supposed primary high-magnesian andesite: an electron- and ion-microprobe study. *Contr. Mineral. And Petrol.*, 103(2), 242-252.

Leeman, W. P., Lewis, J. F., Evarts, R. C., Conrey, R. M. & Streck, M. J. (2005). Petrologic constraints on the thermal structure of the Cascades arc. *Journal ofVolcanology and Geothermal Research,* 140, 67-105.

Macdonald, G.A., & Katsura T. (1964). Chemical composition of Hawaiian lavas. *J Petrol.*, 5, 82-133.

Mackey, B., Castonguay, S., Wallace, P., & Weldon, R. (2014). Synchronous late Pleistocene extensional faulting and basaltic volcanism at Four Craters Lava Field, central Oregon, USA. *Geosphere*, 10(6), 1247-1254.

MacLeod, N. S., G. W. Walker, and E. H. McKee (1975). Geothermal significance of eastward increase in age of Upper Cenozoic rhyolitic domes in southeastern Oregon, U.S. *Geol. Surv.* Open File Rep., 75–348, 21 pp.

Madin, Ian P., 2009, Oregon: A Geologic History, Oregon Department of Geology and Mineral Industries Interpretive Series Map 28 [companion web page]. http://www.oregongeology.org/sub/publications/IMS/ims-028/index.htm

Maisonneuve, C., Dungan, M., Bachmann, O., & Burgisser, A. (2012). Petrological Insights into Shifts in Eruptive Styles at Volcan Llaima (Chile). *Journal Of Petrology*, 54(2), 393-420.

Mason, R. M., Starostin, A. B., Melnik, O. E. & Sparks, R. S. J. (2006). From Vulcanian explosions to sustained explosive eruptions: The role of diffusive mass transfer in conduit flow dynamics. *Journal of Volcanology and Geothermal Research*, 153, 148-165.

McBirney, A.R., and White, C.M. (1982). The Cascade province, in R.S. Thorpe, ed., Andesites: New York, *John Wiley and Sons*, p. 115-135.

McCrory, P., Blair, J., Waldhauser, F., & Oppenheimer, D. (2012). Juan de Fuca slab geometry and its relation to Wadati-Benioff zone seismicity. *Journal of Geophysical Research: Solid Earth*, 117(B9).

McKee, E. H., and G. W. Walker (1976), Potassium-argon ages of late Cenozoic silicic volcanic rocks, southeastern Oregon. *Isochron West*, 15, 37–4.

McInnes, B. & Cameron, E. (1994). Carbonated, alkaline hybridizing melts from a sub-arc environment: Mantle wedge samples from the Tabar-Lihir-Tanga-Feni arc, Papua New Guinea. *Earth and Planetary Science Letters*, 122(1-2), 125-141. http://dx.doi.org/10.1016/0012-821x(94)90055-8.

Meigs, A., Scarberry, K., Grunder, A., Carlson, R., Ford, M., Fouch, M., Grove, T., Hart, B., Iademarco, M., Jordan, B., Milliard, J., Streck, M., Trench, D., and Weldon, R. (2009). "Geological and geophysical perspectives on the magmatic and tectonic development of the High Lava Plains and northwest Basin and Range", From Volcanoes to Vineyards: *Geological Society of America Field Guide* "p. 435 -470".

Miyashiro, A., (1974) Volcanic rock series in island arcs and active continental margins: *American Journal of Science*, v. 274, p. 321–355.

Morrissey, M., Zimanowski, B., Wohletz, K. & Büttner, R. (2000). Phreatomagmatic Fragmentation. In: Sigurdsson, H. (ed.), Encyclopaedia of Volcanoes: *Academic Press*, 1417.

Neal, C. & Taylor, L. (1989). A negative Ce anomaly in a peridotite xenolith: Evidence for crustal recycling into the mantle or mantle metasomatism? *Geochimica Et Cosmochimica Acta*, 53(5), 1035-1040.

Nelson, S. T. & Montana, A. (1992). Sieve-textured plagioclase in volcanic rocks produced by rapid decompression. *American Mineralogist*, 77, 1242-1249.

Nye, C., & Reid, M. (1986). Geochemistry of primary and least fractionated lavas from Okmok Volcano, Central Aleutians: Implications for arc magmagenesis. *J. Geophys. Res.*, 91(B10), 10271.

"Overview of The High Lava Plains". Western Oregon Univeristy. N.p., 2003. Web. Accessed 9 July 2016. [www.wou.edu/las/physci/taylor/eisi/orr_orr1.PDF].

Parfitt, E. (2004). A discussion of the mechanisms of explosive basaltic eruptions. *Journal of Volcanology And Geothermal Research*, 134(1-2), 77-107.

Pearce, J. A., and J. R. Cann., (1973). Tectonic setting of basic volcanic rocks determined using trace element analyses. *Earth Planet. Sci. Lett.*, 19, 290–300.

Pearce, J., & Parkinson, I. (1993). Trace element models for mantle melting: application to volcanic arc petrogenesis. *Geological Society, London, Special Publications*, 76(1), 373-403.

Pearce, J. A., R. J. Stern, S. H. Bloomer, and P. Fryer, Geochemical Mapping of the Mariana Arc-Basin System. (2005): Implications for the Nature and Distribution of Subduction Components. *Geochem. Geophys. Geosyst.*, 6.

Pezzopane, S.K., and Weldon, R.J., II. (1993). Tectonic role of active faulting in central Oregon. *Tectonics*, v. 12, p. 1140–1169.

Pierce, K. L., and L. A. Morgan (1992). The track of the Yellowstone hotspot: Volcanism, faulting, and uplift, in Regional Geology of Eastern Idaho and Western Wyoming, edited by K. Link, M. A. Kuntz, and L. B. Platt, Mem. *Geol. Soc. Am.*, 179, 1–53.

Pioli, L., Azzopardi, B. J. & Cashman, K. V. (2009). Controls on the explosivity of scoria cone eruptions:Magma segregation at conduit junctions. *Journal of Volcanology and Geothermal Research*, 186,407-415.

Polacci, M., Rosi, M., Landi, P., Di Muro, A. & Papale, P. (2005). Novel interpretation for shift between eruptive styles in some volcanoes. *EOS Transactions American Geophysical Union*, 86, 333-336.

Reiners, P., Hammond, P., McKenna, J., & Duncan, R. (2000). Young basalts of the central Washington Cascades, flux melting of the mantle, and trace element signatures of primary arc magmas. *Contributions to Mineralogy and Petrology*, 138(3), 249-264.

Riddihough, R. (1984). Recent movements of the Juan de Fuca Plate System. *J. Geophys. Res.*, 89(B8), 6980.

Roth, J.B., Fouch, M.J., James, D.E., and Carlson, R.W. (2008). 3D seismic velocity structure of the northwestern United States: *Geophysical Research Letters*, v. 35, p. L15304.

Rowe, M., Kent, A., & Nielsen, R. (2009). Subduction Influence on Oxygen Fugacity and Trace and Volatile Elements in Basalts Across the Cascade Volcanic Arc. *Journal of Petrology*, 50(1), 61-91.

Ruprecht, P. & Bachmann, O. (2010). Pre-eruptive reheating during magma mixing at Quizapu volcano and the implications for the explosiveness of silicic arc volcanoes. *Geology* 38, 919-922.

Rutherford, M. (2003). Magmatic Conditions and Magma Ascent as Indicated by Hornblende Phase Equilibria and Reactions in the 1995-2002 Soufriere Hills Magma. *Journal of Petrology*, 44(8), 1433-1453

Saunders, A.D., and J. Tarney, (1979). The geochemistry of basalts from a back-arc spreading center in the East Scotia Sea. *Geochim. Cosmochim. Acta*, 43, 555–572.

Schmidt, M., Grunder, A., & Rowe, M. (2008). Segmentation of the Cascade Arc as indicated by Sr and Nd isotopic variation among diverse primitive basalts. *Earth and Planetary Science Letters*, 266(1-2), 166-181.

Schmidt, M. E., and A. L. Grunder. (2011): Deep Mafic Roots to Arc Volcanoes: Mafic Recharge and Differentiation of Basaltic Andesite at North Sister Volcano, Oregon Cascades. *Journal of Petrology*, 52.3 603-641. Web.

Sekine, T. & Wyllie, P. (1982). The system granite-peridotite-H2O at 30 kbar, with applications to hybridization in subduction zone magmatism. *Contr. Mineral. And Petrol*., 81(3), 190-202.

Shaw, D. M. (1970). Trace element fractionation during anataxis. *Geochim. Cosmochim. Acta*, 34, 237-243.

Sinton, J. M., and P. Fryer, (1987). Mariana Trough lavas from 18°N: implications for the origin of back arc basin basalts. *J. Geophys. Res.*, 92, 12782–12802.

Sisson, T., & Grove, T. (1993). Experimental investigations of the role of H_2O in calc-alkaline differentiation and subduction zone magmatism. *Contr. Mineral. And Petrol.*, *113*(2), 143-166.

Smith, D., & Leeman, W. (2005). Chromian spinel–olivine phase chemistry and the origin of primitive basalts of the southern Washington Cascades. *Journal of Volcanology and Geothermal Research*, 140(1-3), 49-66.

Stolper, E. & Newman, S. (1994). The role of water in the petrogenesis of Mariana trough magmas. *Earth and Planetary Science Letters*, 121, 293-325.

Streck, M. & Grunder, A. (2012). Temporal and crustal effects on differentiation of tholeiite to calcalkaline and ferro-trachytic suites, High Lava Plains, Oregon, USA. *Geochemistry, Geophysics, Geosystems*, 13(11).

Sudo, A. & Tatsumi, Y. (1990). Phlogopite and K-amphibole in the upper mantle: Implication for magma genesis in subduction zones. *Geophys. Res. Lett.*, 17(1), 29-32.

Sun, S., & McDonough, W. (1989). Chemical and isotopic systematics of oceanic basalts: implications for mantle composition and processes. *Geological Society, London, Special Publications*, 42(1), 313-345.

Tarney, J., A. D. Saunders, and S. D. Weaver, (1977). Geochemistry of volcanic rocks from the island arcs and marginal basins of the Scotia Sea region, in Island Arcs, Deep Sea Trenches and Back-arc Basins, edited by M. Talwani, and W. C. Pitman, pp 367–377, AGU, Washington D.C.

Taylor, B. & Martinez, F. (2003). Back-arc basin basalt systematics. *Earth and Planetary Science Letters*, 210(3-4), 481-497.

Tepley, F., Lundstrom, C., McDonough, W., & Thompson, A. (2010). Trace element partitioning between high-An plagioclase and basaltic to basaltic andesite melt at 1 atmosphere pressure. *Lithos*, 118(1-2), 82-94.

Till, C., Grove, T., Carlson, R., Donnelly-Nolan, J., Fouch, M., Wagner, L., & Hart, W. (2013). Depths and temperatures of <10.5 Ma mantle melting and the lithosphere-asthenosphere boundary below southern Oregon and northern California. *Geochemistry, Geophysics, Geosystems*, *14*(4), 864-879.

Traglia, F., Cimarelli, C., de Rita, D., & Gimeno Torrente, D. (2009). Changing eruptive styles in basaltic explosive volcanism: Examples from Croscat complex scoria cone, Garrotxa Volcanic Field (NE Iberian Peninsula). *Journal of Volcanology and Geothermal Research*, 180(2-4), 89-109.

Trehu, A., Asudeh, I., Brocher, T., Luetgert, J., Mooney, W., Nabelek, J., & Nakamura, Y. (1994). Crustal Architecture of the Cascadia Forearc. *Science*, 266(5183), 237-243.

Walker, G. W. (1974), Some implications of Late Cenozoic volcanism to geothermal potential in the High Lava Plains of south-central Oregon. *Ore Bin*, 36, 109–119.

Wall, K., Rowe, M., Ellis, B., Schmidt, M., & Eccles, J. (2014). Determining volcanic eruption styles on Earth and Mars from crystallinity measurements. *Nature Communications*, 5, 5090.

Wang, K., Wells, R., Mazzotti, S., Hyndman, R., & Sagiya, T. (2003). A revised dislocation model of interseismic deformation of the Cascadia subduction zone. *J. Geophys. Res*., 108(B1).

Wells, R., Weaver, C., & Blakely, R. (1998). Fore-arc migration in Cascadia and its neotectonic significance. *Geol*, 26(8), 759.

Wells, R.E., Weaver, C.S., Blakely, R.J., (1999). Microplate motions and neotectonics of the Cascadia forearc. *Seismological Research Letters*, 70, 209.

Wiens, D., Kelley, K., & Plank, T. (2006). Mantle temperature variations beneath back-arc spreading centers inferred from seismology, petrology, and bathymetry. *Earth and Planetary Science Letters*, 248(1-2), 30-42.

Winter, J. (2001). An introduction to igneous and metamorphic petrology. Upper Saddle River, NJ: Prentice Hall.

Wohletz, K. & Sheridan, M. (1983). Hydrovolcanic explosions; II, Evolution of basaltic tuff rings and tuff cones. *American Journal of Science*, 283(5), 385-413.

APPENDICES

Appendix A: Hand sample descriptions and locations of 75 mafic basalts from FRVF

Sample	Location		Quad	Vent	Hand Sample Description
FR-10-8A	N43˚22.545'	W121˚04.249'	Cabin Lake	Fort Rock	juvenile basalt bomb, ~3 % pl>ol. CAB
FR-10-24	N43˚09.888'	W120˚52.823'	Tuff Butte	Table Rock (TRC1)	ol basalt agglutinate from the summit of Table Rock. LKT
FR-10-26	N43˚09.867'	W120˚52.959'	Tuff Butte	Table Rock (TRC1)	xl-poor olivine basalt, ~5% pl>ol, glomerocrysts. Table Rock capping lava. CAB.
FR-10-27	N43˚27.84'	W121˚21.107'	Big Hole	Summit Butte Lineament, cone 5014	xl poor ol basalt, ~ 2 % pl phenocrysts.CAB
FR-10-30	N43˚27.354'	W121˚20.427'	Big Hole	Summit Butte Lineament, cone 4844	hbl spatter basalt, ~ 7 % hbl > pl. LKT
FR-10-32A	N43˚26.816'	W121˚20.618'	Big Hole	Summit Butte Lineament, unknown vent	juvenille porphyritic basalt bomb in hydrovolcanic tuff, ~ 15 % pl > ol. BA.
FR-10-37	N43˚26.735'	W121˚19.971'	Big Hole	Summit Butte Lineament?	xl-poor olivine basalt, ~ 1 % pl>ol. BA.
FR-10-38	N43˚27.367'	W121˚17.753'	Big Hole	Katati Butte spatter cone	xl-poor olivine basalt, 1% pl>ol, diktytaxitic. LKT.
FR-10-39	N43˚26.964'	W121˚17.905'	Big Hole	Beehive spatter cone E of Katati Butte	xl-poor olivine basalt, ~1% pl>ol. LKT.
FR-10-40	N43˚26.869'	W121˚16.902'	Big Hole	Newberry	xl-poor basalt, 2% pl=ol, diktytaxitic. OIB.
FR-10-42	N43˚24.644'	W121˚17.977'	Big Hole	Big Hole	plag star basalt, ~ 5 % pl>ol. LKT.
FR-10-44	N43˚25.135'	W121˚18.024'	Big Hole	Big Hole	juvenile scoria clasts, xl-poor, 3 % pl>ol. BA.
FR-10-46	N43˚20.519'	W121˚11.091'	McCarty Butte	Big Hole	xl-poor olivine basalt, ~5% pl>ol ~ 1mm xls, glomerocrysts, thick flow. CAB.
FR-10-48	N43˚19.724'	W121˚11.665'	McCarty Butte	McCarty	porphyritic ol basalt, ~35% pl>ol, ~2.5 mm pl xls, ~2mm ol xls.CAB.
FR-10-56	N43˚20.8486'	W121˚09.529'	McCarty Butte	Lucky	xl-poor olivine basalt, ~5% xl ol>plag, diktytaxitic. LKT.
FR-10-57	N43˚20.614'	W.121˚09.218'	McCarty Butte	Lucky	capping olivine basalt, ~10 % xls, diktytaxitic. LKT.
FR-10-58	N43˚13.657'	W121˚11.606'	Oatman Flat	Oat Butte	~2% xls up to ~ 0.3 mm, no plag phenocrysts.CAB.
FR-10-59	N43˚13.925'	W121˚12.163'	Oatman Flat	Oat Butte	xl-poor ol basalt, ~5% xls, glomerocrysts ol+pl. HKCAB.
FR-10-60	N43˚14.051'	W121˚13.360'	Oatman Flat	Oat Butte	ol basalt agglutinate, ~3% xls. HKCAB.
FR-10-62	N43˚13.983'	W121˚13.450'	Oatman Flat	Oat Butte	xl-poor ol basalt , ol>pl. HKCAB.
FR-10-63	N43˚13.667'	W121˚13.720'	Oatman Flat	middle cone of Oat-Wing lineament	purple ol basalt, ~20% pl>ol.CAB.
FR-10-65	N43˚20.255'	W121˚22.462'	Wickiup Spr.	Lookout Point	xl-poor ol basalt aggluntinate vent, ~1% xls pl>ol. CAB.
FR-10-66	N43˚19.154'	W121˚20.170'	Wickiup Spr.	cone east of Wickiup Spring	xl-poor ol basalt, ~3% plag>>ol. CAB.
FR-10-67	N43˚19.927'	W121˚19.240'	Wickiup Spr.	Wickiup Butte	highly vesicular red scoria, ~< 1 % xls, pl>ol. BA.
FR-10-68	N43˚19.748'	W121˚18.756'	Wickiup Spr.	Wickiup Butte	xl-poor ol basalt < 1 % xls, BA.
FR-10-69	N43˚19.814'	W121˚17.977'	Wickiup Spr.	cone east of Wickiup Butte	xl-poor ol basalt, < 1 % xls.BA.
FR-10-70A	N43˚19.352'	W121˚16.533'	Wickiup Spr.	conte 5798, Wastina lineament	highly vesicular scoria, <1% xls. BA.
FR-10-71	N43˚19.691'	W121˚16.349'	Wickiup Spr.	cone northeast of cone 5798, Wastina lineament	xl-poor basalt, 1% pl>ol. CAB.
FR-10-72A	N43˚20.308'	W121˚16.513'	Wickiup Spr.	bump west of Wastina Butte	xl-poor ol basalt, ~2% pl>ol. BA.

Appendix A: continued

Sample	Location		Quad	Vent	Hand Sample Description
FR-10-73	N43˚20.324'	W121˚16.275'	Wickiup Spr.	south Wastina Butte	xl-poor scoria , < 1 % xls. BA.
FR-10-74	N43˚20.692'	W121˚15.834'	Wickiup Spr.	north Watina Butte	ol basalt agglutinate, ~15% pl>ol, large pl. BA.
FR-10-77	N43˚29.345'	W121˚06.753'	Cabin Lake	Flat Top	capping ol basalt, ~5% pl>ol, ~2%, glomerocrysts, pl ~0.9 mm, ol ~0.8 mm xls. CAB.
FR-10-78	N43˚29.016'	W121˚07.016'	Cabin Lake	Newberry	ol basalt, ~5 % xls pl>ol, ol-only glomerocrysts, vesicular, diktytaxitic. OIB.
FR-10-79	N43˚29.892'	W121˚06.471'	Cabin Lake	scoria cone NW of Flat Top	glassy aphanitic basalt scoria, ~35% round vesicles. BA.
FR-10-80	N43˚34.469'	W121˚05.695'	South Ice Cave	South Ice Cave Cinder Pit	highly vesicular scoria , ~1% pl ~ 0.2 mm.CAB.
FR-10-82	N43˚35.786'	W120˚53.042'	Sixteen Butte	unnamed flat-topped butte	ol basalt, ~5 % pl>ol, diktytaxitic, vesicular. BA.
FR-10-84	N43˚32.288'	W120˚51.552'	Fox Butte	cone 5272	scoria, ~ 4 % pl>ol.BA.
FR-10-85	N43˚30.649'	W120˚51.770'	Fox Butte	Blowouts	glassy xl-poor spatter sample, ~1% pl=ol, highly vesicular ~40 %.OIB.
FR-10-86	N43˚27.619'	W120˚50.328'	Hogback Butte	north cone in cone 4774 lineament	xl-poor basalt, ~5 % pl>ol. CAB.
FR-10-87	N43˚23.440	W120˚51.820'	Hogback Butte	Table Mountain	capping pl basalt, ~5% xls, plag>ol. LKT.
FR-12-87B	N43˚23.124'	W120˚43.253'	Jack's Place	Green Mountain	xl-poor ol.-basalt w/ xl clots, pl>ol ~0.5 mm xls, . CAB.
FR-12-88	N43˚22.989'	W120˚43.322'	Jack's Place	East Green Mountain	glassy xl-poor ol-basalt w/ ~3% pl>ol ~0.6 mm xls, glomerocrysts. CAB.
FR-12-89	N43˚23.189'	W120˚43.609'	Jack's Place	Green Mountain	medium xl ol-basalt 10-15% plag>ol, abundant angular vesicles, glomerocrysts. CAB.
FR-12-95	N43˚22.584'	W120˚43.557'	Jack's Place	South of Green Mountain	xl-poor ol-basalt lava, 3-4% pl=ol xls, glomerocrysts, 15% angular vesicles. CAB.
FR-12-99	N43˚20.628'	W120˚44.453'	Crack-in-the-Ground	Reed Rock	xl-poor (~5%) ol-basalt, pl > ol , angular vesicles~20%, diktytaxitic. LKT.
FR-12-100	N43˚20.636'	W120˚44.541'	Crack-in-the-Ground	Reed Rock	xl-poor ol-basalt intrusive, pl > ol ~0.6mm, N-S trend dike, NW side, tuff contact. LKT.
FR-12-101	N43˚20.317'	W120˚44.425'	Crack-in-the-Ground	Reed Rock	xl-poor ol-basalt lava, 2-3% xls, pl> ol, , holocrystalline groundmass w/ 20% rounded vesicles. LKT.
FR-12-108B	N43˚10.119'	W120˚41.014'	Christmas Valley	The Black Hills (NW Ring)	aphyric vesicular ~20%, ol-basalt, ~2% pl>ol, dark grey glassy groundmass.CAB.
FR-12-114	N43˚10.653'	W120˚39.800'	Christmas Valley	Eastern Lineament	aphyric agglutinate basalt lava, diktytaxitic , plag> ol.CAB.
FR-12-115	N43˚10.332'	W120˚39.878'	Christmas Valley	Eastern Lineament	streaked red-purple-grey aphyric basalt agglutinate. BA.
FR-12-124	N43˚25.090'	W120˚53.190'	Cougar Mountain	The Devil's Garden	xl-poor ol-basalt lava, ~5% xls, pl ~ 2 mm > ol ~ 1 mm, 3-4 mm xl clots. CAB.
FR-12-130	N43˚21.002'	W120˚42.302'	Crack-in-the-Ground	South Green Mountain 2	xl-poor ol-basaltic agglutinate, variable vesicularity, ~5 % ~1 mm xls, ol =plag. LKT.
FR-13-150	N43° 20.910'	W120°40.951'	Crack-in-the-Ground	SE Four Craters Lava Field.	xl-poor ol basalt, pl phenocrysts 2% > olivine.OIB.
FR-13-151	N43° 21.263'	W 120°41.028'	Crack-in-the-Ground	SE Four Craters Lava Field.	xl-poor ol basalt, 3% pl>ol, ~ 1 mm xls. OIB.
FR-13-152	N43° 18.296'	W120°43.712'	Crack-in-the-Ground	South Reed Rock.	glomerocrysts of olivine + pl grains ~3 % pl> ol, LKT.
FR-13-153B	N43° 07.088'	W120° 35.322'	St.Patricks	St.Patricks	5% phenocrysts with plag>olivine, BA.
FR-13-157B	N43° 09.694'	W120° 41.367'	Black Hills	SE of vent 4827 T	Juvenille bomb, 3% plag phenocrysts > olivine. LKT.
FR-13-164	N43° 25.854	W120° 41.982'	Jack's Place	SW of Twin Buttes	~15% vesicles, glomerocrysts of plag + ol, 3-5% phenocrysts of pl> ol. OIB.
FR-13-165	N43° 28.173'	W120° 43.451'	Jack's Place	Twin Buttes	~15% vesicles, porphyritic ol basalt ~ 15 % xls. MOBL. BA.

Appendix A: continued

Sample	Location		Quad	Vent	Hand Sample Description
FR-13-166	N43° 28.024'	W120° 43.789'	Jack's Place	Twin Buttes	vesicles ~ 1-2 mm, glomerocrysts of plag +ol, 15% plag phenocrysts > ol. MOBL. BA.
FR-13-167	N43° 27.859	W120° 43.266'	Jack's Place	S of Twin Buttes	glomerocrysts of plag+ ol , phenocrysts 10% plag > ol. MOBL. BA.
FR-13-168B	N43° 26.234'	W120° 47.560'	Hogback Butte	Twin Buttes	crystalline groundmass, glomerocrysts of plag + ol. 5% plag phenocrysts w/ minor ol . BA.
FR-13-171	N43°24.832'	W120° 58.548'	Cougar Mountain	E of cone 4819	xl- rich groundmass, ~ 5 % phenocrysts plag> ol, vesicles present. Diktytaxitic. OIB.
FR-13-172	N43° 28.078'	W121° 56.985'	Cougar Mountain	S of cone 4819	xl- rich groundmass, large glomerocrysts, diktytaxitic , phenocrysts of plag > ol ~ 0.6 mm xls.LKT.
FR-13-178A	N43° 09.877'	W120° 40.740'	Christmas Valley	cone 4078 T	dike, aphanitic , dark gray xl poor. 2% plag > ol phenocrysts. LKT.
FR-13-178B	N43° 09.873'	W120° 40.740'	Christmas Valley	cone 4078 T	dike.Lighter gray groundmass, glomerocrysts of ol + plag, equigranular. Minor alteration ol products. LKT.
FR-13-181	N43° 32.700'	W120° 57.707'	Sixteen Butte	SW of cone 4859	scoria ~3% pl phenocrysts, no ol. CAB.
FR-13-182	N43° 33.078'	W120° 57.235'	Sixteen Butte	cone 4859	scoria, glomerocrysts of plag phenocrysts ~3 %, vesicles ~30 %. BA.
FR-13-183	N43° 33.931'	W120° 57.732'	Sixteen Butte	Horseshoe Butte	scoria, larger phenocrysts + vesicles than 181,182. Poikolitic pl clusters, diktytaxitic. BA.
FR-13-184	N43° 35.296'	W120° 58.197'	Sixteen Butte	Deadlog Butte	scoria~15% vesicles , ~10% pl xls. Cluster of pl grains. BA
FR-13-185	N43° 36.342'	W120° 58.937'	Sixteen Butte	Polytop Butte	hbl spatter sample, 3 % hbl/ol phenocrysts, fine grained dark gray groundmass, little to no olivine. CAB.
FR-13-188	N43°35.271'	W120° 53.318'	Sixteen Butte	No Name Buttes	scoria cryptocrystalline. BA.
FR-13-191	N43° 08.514'	W120° 34.628'	Fandango	NW of cone 5313 T	non-vesicular- ~5% olivine + plag phenocrysts, ~1 % plag > ol glomerocrysts. Diabase dike. BA.
FR-13-192	N43° 08.514'	W120° 34.628'	Fandango	NW of cone 5313 T	Dark gray groundmass, non- vesicular w/ alteration products along perlitic cracks, <3% pl phenocrysts. BA.
FR-13-194C	N43 08.360'	W120 34.693'	Fandango	E of cone 5313 T	phenocryst poor with ~2% plag >ol xls. CAB.

Appendix B: Major and trace element chemical compositions for FRVF basalts. Evolved basalts (Mg# < 60); primitive basalts (Mg# > 60). Analyses obtained through X-ray fluorescence (XRF). Major oxides recorded in (wt%), trace elements in (ppm).

Sample	FR-10-24	FR-10-42	FR-10-57	FR-10-87	FR-13-157B	FR-13-178A	FR-13-178B	FR-10-8A	FR-10-26
Center/Quad	Table Rock	Big Hole	McCarty	Hogback	Black Hills	Christmas Valley	Christmas Valley	Fort Rock	Table Rock
Type	LKT	LKT	LKT	LKT	LKT	LKT	LKT	CAB	CAB
SiO2	49.29	48.49	48.60	48.40	49.33	49.03	48.99	50.71	49.24
TiO2	1.54	1.56	1.68	1.64	1.47	1.48	1.48	1.26	1.53
Al2O3	17.30	17.00	16.64	17.05	18.01	17.81	17.74	17.43	17.25
FeO*	11.28	11.29	11.85	11.44	10.82	11.10	11.30	9.50	11.37
MnO	0.19	0.19	0.20	0.19	0.17	0.18	0.18	0.16	0.19
MgO	6.52	7.94	7.34	7.27	6.53	6.64	6.70	6.29	6.51
CaO	9.72	9.76	9.82	10.04	9.70	9.56	9.51	10.33	9.65
Na2O	3.42	3.19	3.29	3.27	3.34	3.56	3.44	3.26	3.46
K2O	0.44	0.33	0.35	0.40	0.28	0.43	0.43	0.78	0.52
P2O5	0.31	0.26	0.24	0.30	0.35	0.21	0.22	0.28	0.27
Total	100.0	100.0	100.0	100.0	100.0	100.0	100.0	100.0	100.0
Na2O+K2O	3.85	3.52	3.64	3.66	3.62	3.99	3.88	4.04	3.98
Ni	81	136	114	110	108	104	110	91	83
Cr	103	212	97	121	69	70	73	68	102
Sc	32	33	36	32	31	29	30	27	32
V	288	236	287	267	305	281	300	241	302
Ba	309	213	194	190	229	232	233	338	268
Rb	4	4	3	5	2	3	3	11	6
Sr	437	286	314	348	465	459	458	548	431
Zr	90	114	103	105	69	77	77	97	88
Y	28	33	33	31	28	26	26	23	28
Nb	5	5	5	6	4	4	3	5	4
Ga	20	19	20	18	21	20	20	20	20
Cu	97	74	60	77	63	117	104	80	109
Zn	98	90	105	96	101	98	99	83	98
Pb	2	0	2	1	2	2	3	1	3
La	8	6	5	9	9	4	7	11	9
Ce	24	21	19	24	13	17	16	23	22
Th	0	0	0	0	1	1	1	1	0
Nd	16	16	16	16	13	15	13	17	16
U	0	1	1	1	0	2	0	1	1
Mg#	55	60	56	57	56	56	55	58	55

Appendix B: continued

Sample	FR-10-48	FR-10-63	FR-10-65	FR-10-66	FR-10-71	FR-10-80	FR-10-82	FR-10-86	FR-12-108B	FR-12-114
Center/Quad	McCarty	Oatman Flat	Oatman Flat	Oatman Flat	Wickiup	South Ice Cave	Sixteen	Fox	Black Hills	Black Hills
Type	CAB	CAB	CAB	CAB	CAB	CAB	CAB	CAB	CAB	CAB
SiO2	51.27	51.59	51.97	51.92	51.45	51.71	51.21	51.47	49.76	50.18
TiO2	1.38	1.15	1.18	1.25	1.20	1.21	1.20	1.63	1.54	1.33
Al2O3	18.45	20.87	18.97	19.03	18.58	18.17	17.54	16.82	17.77	18.27
FeO*	9.41	8.43	9.38	9.68	9.54	8.87	9.62	11.24	10.84	10.25
MnO	0.16	0.14	0.16	0.16	0.16	0.15	0.17	0.19	0.18	0.17
MgO	5.65	3.60	5.16	4.48	5.60	6.00	6.53	5.49	6.20	5.98
CaO	9.19	9.96	8.29	8.40	8.66	9.27	9.63	8.61	9.63	9.19
Na2O	3.42	3.49	3.94	4.02	3.79	3.59	3.21	3.67	3.33	3.73
K2O	0.81	0.59	0.70	0.81	0.66	0.77	0.62	0.63	0.51	0.55
P2O5	0.27	0.20	0.25	0.25	0.35	0.27	0.27	0.27	0.26	0.36
Total	100.0	100.0	100.0	100.0	100.0	100.0	100.0	100.0	100.0	100.0
Na2O+K2O	4.23	4.08	4.63	4.84	4.45	4.37	3.83	4.30	3.83	4.27
Ni	78	34	69	72	71	85	62	56	96	91
Cr	122	50	45	19	66	56	34	25	61	53
Sc	27	22	24	24	24	26	32	29	30	26
V	230	186	225	234	189	224	231	258	356	182
Ba	335	320	367	379	415	299	295	333	280	339
Rb	10	7	9	6	7	11	9	8	6	4
Sr	555	655	705	681	701	548	297	398	461	563
Zr	100	62	67	91	85	110	109	120	80	85
Y	24	21	20	22	21	24	29	31	27	23
Nb	6	4	4	5	5	7	5	7	3	5
Ga	20	19	20	20	20	19	18	21	20	19
Cu	70	65	102	114	86	71	61	53	95	100
Zn	83	76	93	91	88	78	92	104	103	88
Pb	3	2	4	2	4	3	3	3	2	3
La	9	8	9	12	13	9	7	12	5	9
Ce	20	18	27	21	27	27	23	27	20	27
Th	1	0	1	1	0	0	0	0	1	1
Nd	14	12	15	15	18	17	12	17	14	18
U	0	1	1	1	1	1	1	2	0	1
Mg#	56	47	54	49	55	59	59	51	55	55

Appendix B: continued

Sample	FR-13-181	FR-13-194C	FR-10-32A	FR-10-67	FR-10-68	FR-10-69	FR-10-70A	FR-10-72A	FR-10-73	FR-10-74
Center/Quad	Sixteen	Black Hills	Big Hole	Wickiup	Wickiup	Wickiup	Wickiup	Wickiup	Wickiup	Wickiup
Type	CAB	CAB	BA	BA	BA	BA	BA	BA	BA	BA
SiO2	51.96	51.34	53.93	52.26	52.18	52.85	52.88	54.67	54.59	52.13
TiO2	1.90	1.43	1.36	1.23	1.24	1.31	1.85	1.22	1.24	1.09
Al2O3	16.79	16.83	17.24	19.30	18.72	18.87	16.29	17.56	17.62	19.23
FeO*	11.97	10.42	8.71	9.32	9.35	9.61	11.36	9.31	9.53	9.07
MnO	0.20	0.18	0.16	0.16	0.16	0.16	0.19	0.16	0.16	0.15
MgO	4.16	6.81	4.92	3.98	4.99	4.09	3.93	3.91	3.86	4.85
CaO	7.91	8.47	8.74	8.57	8.31	7.66	7.93	7.64	7.39	8.71
Na2O	3.99	3.26	3.72	4.00	3.91	4.22	4.19	4.42	4.44	3.95
K2O	0.80	0.90	0.95	0.89	0.87	0.96	0.98	0.90	0.95	0.63
P2O5	0.33	0.35	0.27	0.28	0.27	0.27	0.40	0.21	0.23	0.18
Total	100.0	100.0	100.0	100.0	100.0	100.0	100.0	100.0	100.0	100.0
Na2O+K2O	4.79	4.16	4.67	4.90	4.78	5.18	5.18	5.32	5.39	4.58
Ni	24	112	38	60	78	55	11	15	15	40
Cr	8	145	101	32	24	7	0	21	18	54
Sc	29	27	29	25	24	22	36	25	25	26
V	241	225	205	201	240	234	215	242	183	223
Ba	431	388	308	397	388	446	454	440	428	334
Rb	9	15	17	10	10	8	16	15	18	9
Sr	402	402	349	676	656	689	555	672	654	730
Zr	148	119	144	99	92	91	112	74	75	58
Y	37	28	33	23	23	28	36	21	22	19
Nb	9	6	9	6	5	4	6	5	5	3
Ga	22	18	19	21	21	20	22	21	20	20
Cu	43	88	50	102	111	121	114	126	99	124
Zn	122	90	86	92	89	99	117	95	89	87
Pb	1	4	3	4	4	3	3	5	4	2
La	13	13	13	12	11	20	13	9	8	7
Ce	33	31	31	30	24	25	26	22	27	15
Th	1	3	1	2	1	0	0	0	1	0
Nd	20	19	18	15	17	23	19	16	16	11
U	2	0	3	1	0	0	0	0	0	0
Mg#	42	58	54	47	53	47	42	47	46	53

Appendix B: continued

Sample	FR-10-84	FR-12-115	FR-13-153B	FR-13-165	FR-13-166	FR-13-167	FR-13-182	FR-13-183	FR-13-184	FR-13-188
Center/Quad	Fox	Black Hills	St.Patricks	Jack's Place	Jack's Place	Jack's Place	Sixteen	Sixteen	Sixteen	Sixteen
Type	BA	BA	BA	BA	BA	BA	BA	BA	BA	BA
SiO2	52.65	52.73	52.88	53.53	53.52	53.61	52.60	53.64	52.13	52.63
TiO2	1.63	1.66	1.32	1.24	1.24	1.26	1.86	1.41	1.69	1.22
Al2O3	16.83	19.29	16.71	17.54	17.53	17.48	16.54	16.48	17.11	18.04
FeO*	11.28	10.56	9.60	7.88	7.88	7.89	11.59	9.33	11.39	8.44
MnO	0.19	0.17	0.17	0.14	0.14	0.14	0.20	0.17	0.19	0.15
MgO	4.58	1.92	6.13	5.53	5.49	5.57	4.15	5.98	4.64	5.77
CaO	8.29	7.44	8.05	9.18	9.21	9.14	7.82	8.41	7.87	8.92
Na2O	3.61	4.58	3.73	3.61	3.66	3.60	4.02	3.33	3.83	3.69
K2O	0.66	1.25	1.09	1.02	1.00	0.99	0.90	1.00	0.86	0.87
P2O5	0.29	0.41	0.32	0.33	0.34	0.33	0.34	0.26	0.29	0.28
Total	100.0	100.0	100.0	100.0	100.0	100.0	100.0	100.0	100.0	100.0
Na2O+K2O	4.27	5.83	4.81	4.64	4.66	4.59	4.92	4.33	4.69	4.56
Ni	47	57	104	60	59	63	22	79	43	77
Cr	22	19	129	124	124	128	7	117	20	52
Sc	28	24	25	28	27	28	28	28	29	25
V	205	257	213	198	193	196	270	185	224	216
Ba	384	568	463	376	368	379	433	301	423	330
Rb	12	12	19	17	17	17	15	23	15	17
Sr	401	620	401	447	443	439	399	248	397	547
Zr	126	112	131	154	151	151	147	139	135	118
Y	33	30	30	27	26	27	36	36	37	24
Nb	7	6	7	13	12	12	9	7	7	8
Ga	22	21	18	18	19	17	22	19	21	20
Cu	42	112	69	71	71	74	36	67	34	58
Zn	115	97	91	77	76	75	120	84	105	81
Pb	3	6	5	5	4	4	3	5	3	4
La	10	14	14	14	20	17	14	10	10	13
Ce	26	31	29	33	33	36	36	27	28	24
Th	0	3	3	3	2	2	2	2	2	2
Nd	19	21	18	20	20	19	21	18	20	14
U	0	0	0	0	1	0	1	1	2	1
Mg#	46	28	57	60	59	60	43	57	46	59

Appendix B: continued

Sample	FR-13-191	FR-13-192	FR-10-59	FR-10-60	FR-10-62	FR-10-30	FR-10-38	FR-10-39	FR-10-56	FR-12-99	FR-12-100
Center/Quad	Fandango	Fandango	Oatman Flat	Oatman Flat	Oatman Flat	Big Hole	Big Hole	Big Hole	McCarty	Reed Rock	Reed Rock
Type	BA	BA	HKCAB	HKCAB	HKCAB	LKT	LKT	LKT	LKT	LKT	LKT
SiO2	56.26	52.57	51.41	51.89	51.77	48.95	49.20	49.18	49.71	50.05	50.02
TiO2	1.12	1.94	1.33	1.31	1.32	1.29	1.50	1.49	1.29	1.02	1.05
Al2O3	17.42	15.10	17.50	17.54	17.59	18.67	17.22	17.19	17.33	17.55	17.43
FeO*	7.77	11.86	9.48	9.42	9.38	9.64	9.71	9.75	9.94	8.43	8.47
MnO	0.14	0.21	0.17	0.16	0.11	0.17	0.17	0.16	0.18	0.16	0.16
MgO	3.85	4.48	6.24	5.96	6.21	7.90	8.84	8.89	7.67	8.22	8.27
CaO	7.37	8.38	8.82	8.71	8.71	9.78	9.49	9.48	10.18	11.17	11.21
Na2O	3.95	3.72	3.53	3.52	3.30	3.13	3.20	3.24	3.01	2.80	2.84
K2O	1.69	1.20	1.05	1.05	1.11	0.26	0.44	0.41	0.42	0.39	0.37
P2O5	0.43	0.54	0.46	0.45	0.44	0.23	0.24	0.22	0.28	0.21	0.18
Total	100.0	100.0	100.0	100.0	100.0	100.0	100.0	100.0	100.0	100.0	100.0
Na2O+K2O	5.64	4.92	4.58	4.57	4.41	3.39	3.64	3.64	3.42	3.18	3.21
Ni	33	14	100	108	101	157	183	187	166	129	123
Cr	23	12	123	123	123	211	296	298	315	244	246
Sc	23	35	26	26	25	31	28	29	35	37	37
V	202	328	214	209	211	65	213	217	206	209	210
Ba	709	620	606	580	570	250	153	161	238	132	129
Rb	25	16	14	15	16	3	7	6	6	5	5
Sr	560	441	655	643	643	383	351	355	284	237	237
Zr	177	148	151	148	146	105	113	113	129	91	94
Y	27	38	35	27	29	30	26	26	30	26	26
Nb	9	8	9	9	8	6	7	6	5	5	6
Ga	20	22	18	19	18	18	16	17	17	16	16
Cu	95	74	69	101	93	86	62	74	83	93	81
Zn	88	112	93	95	89	80	83	80	79	65	65
Pb	8	5	4	4	6	3	2	1	2	2	2
La	22	17	26	18	18	14	9	8	9	7	8
Ce	45	37	41	46	47	19	17	23	25	15	14
Th	3	2	1	1	2	0	1	0	1	1	1
Nd	22	24	29	26	26	18	13	15	16	10	11
U	3	2	0	1	1	0	0	1	2	0	1
Mg#	51	44	58	57	58	63	66	66	62	67	67

Appendix B: continued

Sample	FR-12-101	FR-12-130	FR-13-152	FR-10-27	FR-10-46	FR-10-58	FR-10-77	FR-12-87B	FR-12-88	FR-12-89	FR-12-95
Center/Quad	Reed Rock	Reed Rock	Reed Rock	Big Hole	McCarty	Oatman Flat	Cabin Lake	Green Mnt.	Green Mnt.	Green Mnt.	Green Mnt.
Type	LKT	LKT	LKT	CAB	CAB	CAB	CAB	CAB	CAB	CAB	CAB
SiO2	50.08	49.30	48.92	50.85	50.42	49.28	50.57	51.61	51.38	51.29	51.45
TiO2	1.03	1.23	0.92	1.32	1.21	1.44	1.27	1.16	1.20	1.21	1.20
Al2O3	17.56	17.39	17.56	17.48	17.19	17.22	17.52	17.09	17.24	17.23	17.26
FeO*	8.36	9.06	8.66	9.33	9.58	10.65	9.37	8.43	8.60	8.72	8.56
MnO	0.16	0.16	0.16	0.16	0.17	0.18	0.16	0.16	0.16	0.16	0.16
MgO	8.37	8.33	8.89	7.62	7.72	7.69	7.19	7.41	7.17	6.95	7.20
CaO	11.13	11.00	11.87	9.08	9.82	9.61	9.87	10.12	10.28	10.38	10.18
Na2O	2.79	2.94	2.67	3.31	3.00	3.15	3.28	2.96	2.91	2.95	2.87
K2O	0.36	0.34	0.22	0.60	0.61	0.49	0.52	0.78	0.78	0.80	0.82
P2O5	0.17	0.25	0.12	0.26	0.27	0.30	0.24	0.27	0.29	0.30	0.30
Total	100.0	100.0	100.0	100.0	100.0	100.0	100.0	100.0	100.0	100.0	100.0
Na2O+K2O	3.15	3.28	2.89	3.91	3.62	3.64	3.80	3.75	3.69	3.76	3.69
Ni	133	129	145	143	171	153	109	85	77	69	74
Cr	251	208	253	165	337	300	187	198	182	171	181
Sc	38	35	41	27	33	30	31	35	36	38	34
V	207	207	209	208	195	231	213	212	226	226	219
Ba	143	142	71	235	242	356	212	338	400	424	426
Rb	6	3	3	8	12	5	7	15	16	16	16
Sr	241	287	190	431	287	394	379	438	485	482	480
Zr	92	88	73	110	127	105	109	111	117	117	118
Y	26	25	24	25	26	28	26	25	27	27	26
Nb	5	6	3	7	5	5	8	8	7	7	7
Ga	16	14	13	18	17	19	18	17	17	17	17
Cu	72	76	88	67	50	75	75	58	55	59	49
Zn	63	67	61	79	76	90	77	77	77	74	76
Pb	1	2	1	2	2	2	2	3	11	3	2
La	6	9	1	7	10	10	7	13	16	16	18
Ce	20	15	12	25	22	22	25	35	36	35	35
Th	1	1	0	1	1	0	0	2	3	3	3
Nd	13	14	8	16	13	17	15	17	19	20	20
U	1	0	0	1	0	1		2	0	1	2
Mg#	68	66	68	63	63	60	62	65	64	63	64

Appendix B: continued

Sample	FR-12-124	FR-13-172	FR-13-185	FR-10-37	FR-10-44	FR-13-168B	FR-10-79	FR-10-40	FR-10-78	FR-10-85
Center/Quad	Cougar Mnt.	Cougar Mnt.	Sixteen	Big Hole	Big Hole	Hogback	Cabin Lake	Big Hole	Cabin Lake	Blowouts
Type	CAB	CAB	CAB	BA	BA	BA	BA	OIB	OIB	OIB
SiO2	50.01	49.79	49.35	56.34	54.56	53.24	52.70	48.72	49.46	48.11
TiO2	1.46	1.27	1.55	1.11	1.08	1.26	1.21	1.66	1.68	1.64
Al2O3	17.17	17.38	17.35	16.53	16.45	17.28	17.13	17.07	17.62	16.65
FeO*	9.18	9.17	9.76	7.45	7.91	7.91	8.21	9.71	9.39	10.21
MnO	0.17	0.17	0.18	0.14	0.14	0.14	0.14	0.16	0.16	0.17
MgO	7.93	7.73	8.21	5.62	7.15	6.26	7.13	9.01	7.44	9.11
CaO	9.87	10.61	9.66	7.56	7.70	9.06	9.13	9.63	9.92	10.02
Na2O	3.24	3.11	3.24	3.61	3.56	3.56	3.26	3.23	3.36	3.13
K2O	0.63	0.50	0.45	1.41	1.19	0.96	0.85	0.52	0.61	0.61
P2O5	0.35	0.27	0.25	0.24	0.26	0.33	0.24	0.30	0.36	0.35
Total	100.00	100.00	100.00	100.0	100.0	100.00	100.0	100.0	100.0	100.0
Na2O+K2O	3.87	3.61	3.69	5.02	4.75	4.52	4.11	3.75	3.98	3.73
Ni	135	116	158	94	155	93	122	186	113	180
Cr	231	202	218	129	272	158	216	362	178	296
Sc	32	34	30	23	24	26	27	28	30	32
V	215	219	200	160	157	194	189	184	220	207
Ba	216	170	246	501	408	368	268	157	225	153
Rb	11	9	4	33	28	17	19	7	9	9
Sr	338	284	308	315	345	429	378	403	435	305
Zr	127	110	141	162	158	149	125	152	148	155
Y	29	28	34	29	26	25	25	27	27	29
Nb	10	8	8	8	7	12	9	12	14	19
Ga	17	16	17	18	17	17	17	17	18	15
Cu	68	87	61	48	54	67	68	60	68	74
Zn	76	74	81	74	74	77	72	75	77	75
Pb	2	2	3	6	5	3	4	2	3	1
La	13	11	13	13	9	17	9	14	10	14
Ce	29	19	25	25	28	31	30	24	25	30
Th	1	2	2	2	2	2	0	1	0	0
Nd	19	12	19	18	17	18	16	18	19	19
U		0	2	0	1	2		1		
Mg#	64	64	64	61	65	62	65	66	62	65

Appendix B: continued

Sample	FR-13-150	FR-13-151	FR-13-164	FR-13-171
Center/Quad	Four Craters	Four Craters	Jack's Place	Devil's Garden
Type	OIB	OIB	OIB	OIB
SiO2	50.99	50.96	51.15	49.08
TiO2	1.607	1.588	1.506	1.502
Al2O3	17.19	17.09	17.06	16.56
FeO*	8.89	8.94	8.86	9.53
MnO	0.158	0.157	0.156	0.172
MgO	7.05	7.25	7.33	9.23
CaO	9.31	9.20	9.21	9.89
Na2O	3.55	3.52	3.51	3.12
K2O	0.88	0.93	0.86	0.56
P2O5	0.375	0.373	0.357	0.365
Total	100.00	100.00	100.00	100.00
Na2O+K2O	4.43	4.44	4.37	3.67
Ni	110	121	125	191
Cr	189	207	215	358
Sc	28	28	27	31
V	205	205	204	209
Ba	297	302	297	179
Rb	13	14	13	9
Sr	440	439	429	314
Zr	171	172	160	131
Y	29	28	28	30
Nb	16	17	14	12
Ga	16	18	17	15
Cu	65	61	66	77
Zn	77	76	76	79
Pb	2	2	2	2
La	16	14	17	12
Ce	36	33	35	25
Th	1	2	3	2
Nd	20	21	21	18
U	0	0	1	0
Mg#	62	63	63	67

APPENDIX C: Petrographic Reports of FRVF Basalts

Big Hole

FR-10-27: Crystal poor olivine basalt. Olivine is the only phenocryst phase (~ 1.5 -2 mm) with an abundance of ~ 2 %. Groundmass is fine- grained, hypocrystalline containing plagioclase laths and microlites (≤0.1-0.4 mm), olivine (0.1-0.5 mm), oxides (0.1 mm) in a glassy matrix with an abundance of ~35 %.

Matrix (glass) ~63%, Groundmass (plagioclase >olivine >oxides) ~ 35 %

Phenocrysts (olivine) ~ 2 %

FR-10-30: Primitive hornblende basalt from a spatter cone, highly vesicular sample. Phenocrysts are amphibole (~ 0.5 mm) and plagioclase (~ 0.7 mm), with an abundance of ~ 7 %. Groundmass is fine- grained, hypocrystalline containing plagioclase microlites (~ ≤ 0.1 mm), olivine (~ 0.1 mm) and oxides (~ 0.1 mm) in a glassy matrix with an abundance of ~ 30 %.

Point Count- 328 points

Matrix (glass) - 207 points (63 %), Groundmass (plagioclase> oxides > olivine) - 98 points (30 %)

Phenocrysts (amphiboles > plagioclase) - 23 points (7 %)

- amphiboles- 16 points (5 %)

- plagioclase- 7 points (2 %)

FR-10-32A: Juvenile porphyritic basalt bomb in hydrovolcanic tuff. Phenocrysts are plagioclase (~ 0.8 mm – 2.7 mm) and olivine (one grain 2.3 mm). Plagioclase phenocrysts are much more abundant than olivine phenocrysts ~ 15 %. Groundmass is fine- grained, hypocrystalline containing olivine (~0.1-0.4 mm), plagioclase microlites and laths (≤ 0.1-0.4 mm) in a glassy matrix with an abundance of ~ 35 %.

Matrix (glass) ~ 50 %, Groundmass (plagioclase > olivine > oxides) ~ 35 %

Phenocrysts (plagioclase> olivine) ~ 15 %

Appendix C: continued

FR-10-37: Crystal poor primitive olivine basalt. Phenocrysts are plagioclase (~ 0.6 - 1 mm) and olivine (~ 0.7 mm). Plagioclase phenocrysts are more abundant than olivine phenocrysts ~ 2% (plagioclase ~ 1.5 % and olivine ~ 0.5 %). Groundmass is fine- grained, holocrystalline containing olivine (~0.1-0.2 mm), plagioclase laths (~0.1-0.2 mm), clinopyroxene (0.1-0.2 mm) and oxides (≤ 0.1 mm), with an abundance of ~ 60 %. Groundmass contains sub-ophitic textures of partially enclosed plagioclase laths in clinopyroxene grains.

Matrix (glass) ~ 38 %, Groundmass (plagioclase > clinopyroxene > olivine≥ oxides) ~ 60 %

Phenocrysts (plagioclase> olivine) ~ 2 %

FR-10-38: Crystal poor primitive olivine basalt. Olivine is the only phenocryst phase (~ 0.9 mm) with an abundance of ~ 1 %. Groundmass is coarse- grained holo- to hypocrystalline, and contains plagioclase laths (~ 0.2-0.5 mm), olivine (~ 0.3-0.6 mm), and oxides (~ 0.3 -0.5 mm) in a glassy matrix. Diktytaxitic textures are common in the groundmass.

Point Count- 365 points

Matrix (glass) - 124 points (34 %)

Groundmass (plagioclase >olivine ≥ oxides) - 238 points (65 %)

- oxides – 44 points (12%)
- plagioclase -124 points (34%)
- olivine- 70 points (19 %)

Phenocrysts (olivine) - 3 points (1 %)

Appendix C: continued

FR-10-39: Crystal poor primitive olivine basalt. Phenocrysts are olivine (~ 0.8 mm) and plagioclase (~ 1.4 mm) with an abundance of ~ 1 %. Groundmass is coarse- grained holo- to hypocrystalline, and contains plagioclase laths (~ 0.3-0.5 mm), olivine (~ 0.3-0.5 mm), and oxides (~ 0.3 -0.5 mm) in a glassy matrix. Diktytaxitic textures are common in the groundmass.

Point Count- 408 points

Matrix (glass) - 139 points (34 %)

Groundmass (plagioclase >olivine > oxides) - 265 points (65 %)

-oxides – 41 points (10 %)

- plagioclase -151 points (37 %)

- olivine- 73 points (18 %)

Phenocrysts (plagioclase = olivine) - 4 points (~ 1 %)

- plagioclase- 2 points (0.5 %)

- olivine- 2 points (0.5 %)

FR-10-40: Crystal poor primitive olivine basalt. Phenocryst phases are olivine (~ 0.9-1.7 mm) and plagioclase (~ 1.5-1.7 mm) with an abundance of ~ 2 %. Groundmass is coarse- grained, holocrystalline and contains plagioclase laths (~ 0.3-0.9 mm), olivine (~ 0.2-0.5 mm), clinopyroxene (0.3-0.7 mm), and oxides (~ 0.25 mm) with an abundance of ~ 98 %. Groundmass contains sub-ophitic and diktytaxitic textures.

Point Count- 436 points

Groundmass (plagioclase > clinopyroxene > olivine > oxides) - 427 points (98 %)

- plagioclase- 181 points (42 %)

- clinopyroxene- 112 points (24 %)

- olivine- 78 points (18 %)

- oxides- 56 points (14 %)

Phenocrysts (olivine = plagioclase) - - 9 points (2 %)

- plagioclase – 5 points (1 %)

- olivine- 4 points (1 %)

Appendix C: continued

FR-10-42: Crystal poor olivine basalt. Phenocrysts are plagioclase (~0.8 – 2.5 mm) and olivine (~ 0.6 – 1.1 mm) with an abundance of ~ 5 %. Phenocrysts of olivine are more abundant than plagioclase phenocrysts (~ 4 % olivine and ~ 1 % plagioclase). Phenocrysts of olivine contain alteration rims. Groundmass is fine -grained, hypocrystalline and consists of plagioclase microlites and laths (≤ 0.1 – 0.2 mm), olivine (~ 0.1 mm), oxides (≤ 0.1 mm) in a glassy matrix with an abundance of ~ 35 %.

Matrix (glass) ~ 60 %, Groundmass (plagioclase > olivine> oxides) ~ 35 %

Phenocrysts (olivine > plagioclase) ~ 5 %

FR-10-44: Primitive juvenile scoria clast, a highly vesicular sample. Phenocryst phases are plagioclase (~ 0.5-0.9 mm) and olivine (~ 0.5 -1.6 mm) with an abundance of ~ 3 %. Phenocrysts of plagioclase are more abundant than olivine phenocrysts (plagioclase ~ 2 % and olivine ~ 1 %). Groundmass is hypocrystalline to holohyaline consisting mostly of a glassy matrix.

Wickiup Spring Quadrant

FR-10-65: Crystal poor basalt. Microphenocryst phases are plagioclase (~ 0.3-0.47 mm) and olivine (~ 0.4 mm) with an abundance of ~ 1 %. Plagioclase microphenocrysts have a greater abundance than olivine microphenocrysts. Groundmass is fine grained hypocrystalline, containing plagioclase microlites and laths (~≤ 0.1-0.3 mm), olivine (~≤ 0.1- 0.2 mm), oxides (~≤ 0.1 mm) in a glassy matrix with an abundance of ~ 99 %. Groundmass contains sub-trachytic plagioclase laths.

Matrix (glass) ~ 64%, Groundmass (plagioclase > olivine > oxides) ~ 35 %

Microphenocrysts (plagioclase > olivine) ~ 1 %

FR-10-66: Crystal poor olivine basalt. Phenocryst phases are plagioclase (~ 0.9– 1.2 mm) and olivine (~ 0.6-0.9 mm) with an abundance of ~ 3 %. Plagioclase phenocrysts are greater than olivine microphenocrysts in abundance (plagioclase ~ 2.5% and olivine ~ 0.5 %). Groundmass is fine to coarse- grained hypocrystalline, containing plagioclase microlites and laths (~≤ 0.1 – 0.6 mm), olivine (~≤ 0.1- 0.3 mm), oxides (~ 0.1 mm) in a glassy matrix with an abundance of ~ 35 %.

Matrix (glass) ~ 62 %, Groundmass (plagioclase > olivine > oxides) ~ 35 %

Microphenocrysts (plagioclase> olivine) ~ 3 %

Appendix C: continued

FR-10-67: Highly vesicular red scoria sample. One phenocryst grain of plagioclase is visible (~ 1.2 mm) Groundmass is hypocrystalline to holohyaline, containing fine to coarse grained plagioclase laths and microlites (≤ 0.1 – 0.2 mm) with an abundance of ~ 25 % in a glassy matrix ~ 74 %.

Groundmass (plagioclase > olivine > oxides) ~ 25 %

FR-10-68: Crystal poor basalt. There are no phenocryst phases in this sample. Groundmass is fine to coarse grained, holo- to hypocrystalline, containing plagioclase laths (~ 0.5-0.9 mm), olivine (~ 0.35- 0.65 mm), and oxides (~ 0.15 mm) in a glassy matrix.

Matrix (glass) ~ 30 %, Groundmass (plagioclase > olivine > oxides) ~ 70 %

FR-10-69: Crystal poor basalt. There are no phenocryst phases in this sample. Groundmass is fine to coarse grained, holo-to hypocrystalline, containing plagioclase laths (~ 0.3- 1 mm), olivine (~ 0.1-0.5 mm), and oxides (~0.1 mm) in a glassy matrix.

Matrix (glass) ~ 35 %, Groundmass (plagioclase > olivine> oxides) ~ 65 %

FR-10-70A: Highly vesicular scoria sample. There are no phenocryst phases present. Groundmass is hypocrystalline to holohyaline, containing plagioclase microlites (~ 0.1 mm) ~ 5 % in a glassy matrix ~ 95 %.

FR-10-71: Crystal poor olivine basalt. Microphenocryst phases are plagioclase (~0.4-0.8 mm) and oxidized olivine (~ 0.3-0.4 mm), with an abundance of ~ 1%. Plagioclase microphenocrysts are more abundant than olivine microphenocrysts. Olivine microphenocrysts contain alteration rims. Groundmass is fine-grained hypocrystalline and contains plagioclase microlites and laths (≤ 0.1- 0.2 mm), olivine (≤ 0.1 mm), and oxides (≤ 0.1 mm) in a glassy matrix with an abundance of 99%. Groundmass contains sub-trachytic texture of plagioclase laths.

Matrix (glass) -54 %, Groundmass (plagioclase > olivine > oxides) ~ 45 %

Microphenocrysts (plagioclase > olivine) ~ 1 %

FR-10-72A: Crystal poor olivine basalt. Phenocryst phases are plagioclase (~ 0.55- 2.1 mm) and olivine (~ 0.55 mm) with an abundance of ~ 2 %. Plagioclase phenocrysts are more abundant than olivine phenocrysts (~ 1.5 % plagioclase and ~ 0.5 % olivine). Groundmass is fine- grained hypocrystalline, containing plagioclase microlites and laths (≤ 0.1-0.3 mm), olivine (≤ 0.1-0.3 mm), and oxides (≤ 0.1 mm) ~ 45 % in a glassy matrix ~ 55 %.

FR-10-73: Highly vesicular red scoria sample. Microphenocryst phase is plagioclase (~ 0.4- 0.8 mm) (no olivine) with an abundance of ~ 1%. Groundmass is fine-grained hypocrystalline containing plagioclase microlites and laths (≤ 0.1- mm – 0.3 mm) ~ 35 % in a glassy matrix with an abundance of ~ 64 %.

Appendix C: continued

FR-10-74: Sub-porphyritic olivine basalt agglutinate. Phenocryst phases are plagioclase (~ 1.1 to 2.5 mm) (A single very large plagioclase grain visible ~ 6.5 mm) and olivine (~0.7 to 1.3 mm) with an abundance of ~ 15 %. Plagioclase phenocrysts are more abundant than olivine phenocrysts (plagioclase ~ 10 % and olivine ~ 5 %). Groundmass is coarse-grained holocrystalline, and contains plagioclase laths (~ 0.5 mm), olivine (~ 0.3 mm), clinopyroxene (~ 0.4 – 0.7 mm), and oxides (~ 0.2- 0.4 mm) with an abundance of ~ 85 %. Sub-ophitic and diktytaxitic textures are common in the groundmass.

Groundmass (plagioclase > clinopyroxene >olivine ≥ oxides) ~ 85 %

Phenocrysts (plagioclase > olivine) ~ 15 %

McCarty Butte

FR-10-46: Primitive crystal poor olivine basalt. Phenocryst phases are plagioclase (~ 1.6 – 4.2 mm) and olivine (~ 1.3 - 2.8 mm) with an abundance of ~ 5%. Plagioclase phenocrysts are more abundant than olivine phenocrysts (plagioclase ~ 4% and olivine ~ 1%). Groundmass is coarse-grained holocrystalline, and contains plagioclase laths (~ 0.3-0.6 mm), olivine (~ 0.25 mm), clinopyroxene (~ 0.25 – 0.45 mm), and oxides (~ 0.15 – 0.2 mm) with an abundance of ~ 95 %. Diktytaxitic and sub-ophitic textures in the groundmass are common.

Groundmass (plagioclase > clinopyroxene > olivine ≥ oxides) ~ 95 %

Phenocrysts (plagioclase> olivine) ~ 5 %

FR-10-48: Porphyritic olivine basalt. Phenocryst phases are plagioclase (~ 1.1 mm - 5.8 mm) and olivine (~ 0.8 mm – 2.5 mm) with an abundance of ~ 35 %. Plagioclase phenocrysts are more abundant than olivine phenocrysts (~ 25 % plagioclase and ~ 10 % olivine). Groundmass is coarse-grained holocrystalline, and contains plagioclase laths (~ 0.3-0.7 mm), olivine (~ 0.2-0.5 mm), clinopyroxene (~ 0.1 – 0.2 mm), and oxides (~0.1-0.4 mm) with an abundance of ~ 80 %. Diktytaxitic textures are common.

Groundmass (plagioclase> olivine ≥ clinopyroxene ≥ oxides) ~ 80 %

Phenocrysts (plagioclase > olivine) ~ 35 %

Appendix C: continued

FR-10-56: Primitive crystal poor olivine basalt. Phenocryst phases are plagioclase (~ 2.3 mm) and olivine (~ 1.2 – 3.4 mm) with an abundance of ~ 5 %. Multiple phenocrysts of plagioclase are skeletal features. Plagioclase and olivine phenocrysts contain similar modes. Groundmass is coarse-grained holocrystalline, and contains plagioclase (~ 0.3-0.7 mm), olivine (~ 0.2-0.4 mm), clinopyroxene (~ 0.4- 0.8 mm), and oxides (~ ≤ 0.1 mm) with an abundance of ~ 95 %. Diktytaxitic and sub-ophitic textures are common.

Groundmass (plagioclase > clinopyroxene > olivine > oxides) ~ 95 %

Phenocrysts (plagioclase > olivine) ~ 5 %

FR-10-57: Porphyritic olivine basalt. Microphenocryst phases are plagioclase (~ 0.5- 0.9 mm) and olivine (~ 0.3- 0.9 mm) with an abundance of ~ 15 %. Glomerocrysts of plagioclase and olivine are a common feature. Plagioclase phenocrysts are more abundant than olivine phenocrysts (plagioclase ~ 8 % and olivine ~ 7 %). Groundmass is fine-grained hypocrystalline, and contains plagioclase laths and microlites (0.1- 0.2 mm), olivine (~ 0.1- 0.2 mm), clinopyroxene (~ 0.3- 0.5 mm), and oxides (≤ 0.1 mm)in a glassy matrix with an abundance of ~ 35 %. Diktytaxitic and ophiomottled textures are common in the groundmass.

Point Count- 457 points

Matrix (glass) – 210 points (46 %)

Groundmass (plagioclase > clinopyroxene ≥ olivine > oxides) – 160 points - (35 %)

- plagioclase- 59 points- (13 %)
- clinopyroxene - 46 points (10 %)
- olivine- 37 points -(8 %)
- oxides- 18 points- (4 %)

Phenocrysts (plagioclase > olivine) - 87 points- (19 %)

- plagioclase -50 points- (11 %)
- olivine -37 points- (8 %)

Appendix C: continued

Oatman Flat

FR-10-58: Primitive crystal poor olivine basalt. Microphenocryst phase is olivine (~ 0.7 mm) (no plagioclase phenocrysts) with an abundance of ~ 2 %. Olivine microphenocrysts contain red oxidized alteration rims to possibly iddingsite. Groundmass is coarse-grained holocrystalline, and contains plagioclase laths (~ 0.4-0.7 mm), olivine (~ 0.2-0.4 mm), clinopyroxene (~ 0.3- 0.5 mm) and oxides (~ 0.1-0.2 mm) with an abundance of ~ 98 %. Sub-ophitic and diktytaxitic textures are common in the groundmass.

Groundmass (plagioclase > clinopyroxene > olivine > oxides) ~ 98 %

Phenocrysts (olivine) ~ 2 %

FR-10-59: Crystal poor olivine basalt. Phenocryst phases are plagioclase (~ 0.7 - 1.1 mm) and olivine (~ 0.6 to 1 mm) with an abundance of ~ 5 %. Glomerocrysts of plagioclase and olivine is a common texture. Olivine phenocrysts are more abundant than plagioclase phenocrysts (~ 3.5 % olivine and ~ 1.5 % plagioclase). Groundmass is fine-grained hypocrystalline contains plagioclase laths and microlites (~ 0.1-0.2 mm), olivine (~0.1-0.2 mm), and oxides (≤ 0.1 mm) in a glassy matrix with an abundance of ~ 35 %.

Matrix (glass) ~ 60 %, Groundmass (plagioclase > olivine > oxides) ~ 35 %

Phenocrysts (olivine > plagioclase) ~ 5 %

FR-10-60: Crystal poor olivine basalt. Phenocryst phases are plagioclase (~ 0.75 mm – 2 mm) and olivine (~ 0.7 mm) with an abundance of ~ 5 %. Glomerocrysts of plagioclase and olivine are a common feature. Olivine alteration products are visible. Olivine phenocrysts are greater than plagioclase phenocrysts in abundance (~ 3.5 % olivine and ~ 1.5 % plagioclase). Groundmass is fine-grained hypocrystalline, and contains plagioclase laths and microlites (~ ≤ 0.1-0.2 mm), olivine (~0.1-0.2 mm) and oxides (≤ 0.1 mm) in a glassy matrix with an abundance of ~ 35 %.

Matrix (glass) ~ 60 %, Groundmass (plagioclase > olivine > oxides) ~ 35 %

Phenocrysts (olivine > plagioclase) ~ 5 %

Appendix C: continued

FR-10-62: Crystal poor olivine basalt. Phenocryst phases are plagioclase (~ 0.85 mm), and olivine (~ 0.8- 1 mm) with an abundance of ~ 3 %. Glomerocrysts of plagioclase and olivine is a common feature. Phenocrysts of olivine are greater in abundance than phenocrysts of plagioclase (olivine ~ 2.5 % and plagioclase ~ 0.5 %). Groundmass is fine-grained hypocrystalline, and contains plagioclase microlites and laths (≤ 0.1 – 0.2 mm), olivine (~ 0.1-0.2 mm), and oxides (≤ 0.1 mm) in a glassy matrix with an abundance of ~ 30 %.

Matrix (glass) ~ 67 %, Groundmass (plagioclase > olivine > oxides) ~ 30 %

Phenocrysts (olivine > plagioclase) ~ 3 %

FR-10-63: Porphyritic olivine basalt. Phenocryst phases are plagioclase (~ 0.85 – 5.2 mm) and olivine (~ 0.74 – 1.8 mm) with an abundance of ~ 20 %. Olivine phenocrysts are altered to iddingsite. Phenocrysts of plagioclase are much more abundant than olivine phenocrysts (plagioclase ~ 18 % and olivine ~ 3 %). Groundmass is fine-grained holocrystalline and contains plagioclase microlites and laths (~≤ 0.1- 0.2 mm), olivine (~ 0.1-0.2 mm), and oxides (~ ≤ 0.1 – 0.2 mm) in a glassy matrix with an abundance of ~ 40 %.

Matrix (glass) ~ 20 %, Groundmass (plagioclase > oxides > olivine) ~ 40 %

Phenocrysts (plagioclase >> olivine) ~ 20 %

Fort Rock tuff ring

FR-10-8A: Juvenile basalt bomb. Microphenocryst phases are plagioclase (~ 0.6 – 1 mm) and olivine (0.5 mm) with an abundance of ~ 3 %. Plagioclase phenocrysts are more abundant than olivine phenocrysts (plagioclase ~ 2.5 % and olivine ~ 0.5 %). Groundmass is fine-grained hypocrystalline and contains plagioclase microlites and laths (≤ 0.1 – 0.2 mm), olivine (≤ 0.1- 0.2 mm), and oxides (≤ 0.1 mm) in a glassy matrix with an abundance of ~ 25 %.

Cabin Lake- Flat Top maar

FR-10-77: Primitive crystal poor olivine basalt. Phenocrysts phases are plagioclase (~ 0.8 – 1.8 mm) and olivine (~ 0.8 mm) with an abundance of ~ 5 %. Glomerocrysts of plagioclase and olivine phenocrysts is a common feature. Olivine phenocrysts display alteration rims. Olivine phenocrysts are more abundant than plagioclase phenocrysts (olivine ~ 3 % and plagioclase ~ 2 %). Groundmass is coarse to fine-grained holo- to hypocrystalline, and contains plagioclase microlites and laths (≤0.1-0.5 mm), olivine (0.1-0.4 mm) and oxides (≤ 0.1 mm) in a glassy matrix with an abundance of ~ 75 %.

Matrix (glass) ~ 20 %, Groundmass (plagioclase > olivine > oxides) ~ 75 %

Phenocrysts (olivine > plagioclase) ~ 5 %

Appendix C: continued

FR-10-78: Primitive crystal poor olivine basalt. Olivine is the only phenocryst phase (~ 0.6-0.8 mm) (plagioclase laths are large (up to ~ 1.1 mm) but is part of the groundmass) with an abundance of ~ 3 %. Groundmass is coarse-grained holo- to hypocrystalline, and contains plagioclase laths (~ 0.2 – 1 mm), olivine (~0.1-0.4 mm), and oxides (0.1 mm) in a glassy matrix with an abundance of ~ 85 %.

Matrix (glass) ~ 11 %, Groundmass (plagioclase> oxides> olivine) ~ 85 %

Phenocrysts (olivine) ~ 4%

FR-10-79: Highly vesicular olivine spatter sample. Phenocryst phases are plagioclase (~ 0.6 mm) and olivine (~ 0.8 mm) with an abundance of ~ 2 %. Olivine Phenocrysts are more abundant than plagioclase phenocrysts (olivine ~ 1.5 % and plagioclase ~ 0.5 %). Olivine and plagioclase phenocrysts are skeletal. Groundmass is fine-grained hypocrystalline to holohyaline, and contains plagioclase microlites (≤ 0.1-0.2 mm), olivine (≤ 0.1-0.2 mm), and oxides (≤ 0.1 mm) in a glassy matrix with an abundance of 15 %.

Matrix (glass) ~ 83 %, Groundmass (plagioclase >olivine> oxides) ~ 15 %

Phenocrysts (olivine > plagioclase) ~ 2 %

South Ice Cave Cinder Pit

FR-10-80: Highly vesicular olivine scoria. Olivine is the only phenocryst phase (2 grains at ~ 0.6 mm) with an abundance of ~ < 1 %. Groundmass is fine grained hypocrystalline to holohyaline, and contains plagioclase microlites, olivine, and oxides (≤0. 1 mm) in a glassy matrix with an abundance of ~ 15 %. Trachytic texture where the plagioclase microlites are moving in the direction of the magma flow is visible.

Matrix (glass) ~ 84 %, Groundmass (plagioclase > oxides > olivine) ~ 15 %

Phenocrysts (olivine) ~ 1 %

Appendix C: continued

Sixteen Butte

FR-10-82: Porphyritic olivine basalt. Phenocryst phases are plagioclase (~0.6 – 2.3 mm) and olivine (~0.4 – 0.8 mm) with an abundance of ~ 5 %. Plagioclase phenocrysts are more abundant than olivine phenocrysts (~ 3.5 % plagioclase and ~ 1.5 % olivine). Glomerocrysts of olivine and plagioclase phenocrysts is a common feature. Olivine phenocrysts are altered to iddingsite. Groundmass is medium- grained holocrystalline to hypocrystalline, and contains plagioclase (~ 0.25-0.4 mm), olivine (~0.2 mm), clinopyroxene (~ 0.2 mm), and oxides (0.1 mm) with an abundance of ~ 80 % in a glassy matrix. Diktytaxitic textures are a common feature in the groundmass

Matrix (glass) ~ 15 %, Groundmass (plagioclase > clinopyroxene >olivine> oxides) ~ 80 %

Phenocrysts (plagioclase > olivine) ~ 5 %

FR-13-181: Highly vesicular olivine scoria. Phenocryst phases are plagioclase (~0.6 – 1.5 mm) and olivine (~0.6 – 0.7 mm) with an abundance of ~ 3 %. Plagioclase phenocrysts are more abundant than olivine phenocrysts (~2 % plagioclase and ~ 1 % olivine). Groundmass is fine-grained hypocrystalline to holohyaline and contains plagioclase microlites (≤ 0.1- 0.2 mm) in a glassy matrix with an abundance of ~ 5 %.

FR-13-182: Olivine scoria. Phenocryst phases are plagioclase (~ 0.6 – 1.2 mm) and olivine (~ 0.4 – 0.6 mm) with an abundance of ~ 3 %. Plagioclase phenocrysts are more abundant than olivine phenocrysts (~ 2.5 % plagioclase and ~ 0.5 % olivine). Groundmass is fine-grained hypocrystalline to holohyaline, and contains plagioclase microlites (≤ 0.1- 0.2 mm) in a glassy matrix with an abundance of ~ 3 %.

FR-13-183: Extremely vesicular scoria. Plagioclase is the only phenocryst phase (~ 0.5- 0.9 mm) with an abundance of ~ 1 %. Groundmass is hypocrystalline to holohyaline, and makes up ~2 % of the sample.

FR-13-184: Scoria sample. Plagioclase is the only phenocryst phase (~ 0.4 – 1.2 mm) with an abundance of ~ 2 %. Groundmass is hypocrystalline to holohyaline, containing plagioclase microlites (≤ 0.1 mm) in a glassy matrix with an abundance of ~ 5 %.

Appendix C: continued

FR-13-185: Primitive hornblende basalt (spatter). Microphenocryst phases are amphiboles (~ 0.5 mm) and olivine (~ 0.5 mm) with an abundance of ~ 3 %. Amphibole microphenocrysts are more abundant than olivine microphenocrysts (amphibole ~ 2 % and olivine ~ 1 %). Groundmass is fine-grained hypocrystalline, containing plagioclase (~0.1-0.2 mm), clinopyroxene (~ 0.2 mm), olivine (~ ≤ 0.1 mm), oxides (≤ 0.1 mm), and glass with an abundance of ~ 25 %.

Point Count- 389 points

Matrix (glass) – 164 points (42 %)

Groundmass (plagioclase > clinopyroxene > oxides > olivine) - 213 points (55 %)

Phenocrysts (amphibole > olivine) - 12 points (3 %)

- amphibole- 8 points (2 %)

- olivine- 4 points (1 %)

FR-13-188: Scoria sample. Plagioclase is the only phenocryst phase (1 grain at ~ 0.8 mm) with an abundance of < 1 %. Groundmass is fine-grained hypocrystalline to holohyaline, and contains plagioclase microlites (0.1 mm) in a glassy matrix with an abundance of ~ 3 %.

Fox Butte

FR-10-84: Scoria sample. Plagioclase is the only phenocryst phase (~ 0.7 - 2 mm) with an abundance of ~ 4 %. Groundmass is hypocrystalline to holohyaline, and contains plagioclase laths (~ 0.1- 0.35 mm) in a glassy matrix with an abundance of ~ 10 %.

Appendix C: continued

FR-10-85: Hornblende basalt (spatter). Microphenocryst phases are plagioclase (~ 0.3 – 0.75 mm), amphiboles (~ 0.3 – 0.8 mm), and olivine (~ 0.4 mm) with an abundance of ~ 5 %. Amphibole microphenocrysts are more abundant than plagioclase microphenocrysts, which are more abundant than olivine microphenocrysts (~ amphibole ~ 3.5 %, plagioclase ~ 1 %, and olivine ~ 0.5 %). Groundmass is fine-grained hypocrystalline and contains plagioclase microlites (≤ 0.1 mm), olivine (≤ 0.1 mm), and oxides (≤ 0.1 mm) in a glassy matrix with an abundance of ~ 55 %.

Point Count- 367 points

Matrix (glass) - 147 points (40 %)

Groundmass (plagioclase > olivine > oxides) - 202 points (55 %)

Microphenocrysts (amphibole > plagioclase > olivine) - 18 points (5 %)

- amphibole- 13 points (3.5 %)

- plagioclase- 4 points (1 %)

- olivine- 1 point (0.5 %)

Cougar Mountain- Devils Garden

FR-12-124: Primitive crystal poor olivine basalt. Phenocryst phases are plagioclase (~ 1.1 – 1.8 mm) and olivine (~ 0.7 – 3.6 mm) with an abundance of ~ 7 %. Olivine phenocrysts are more abundant than plagioclase phenocrysts (olivine ~ 4.5 % and plagioclase ~ 2.5 %). Glomerocrysts of plagioclase and olivine phenocrysts is a common feature. Groundmass is coarse-grained holo- to hypocrystalline, and contains plagioclase laths (~ 0.3 – 0.5 mm), olivine (~ 0.3-0.5 mm), clinopyroxene (~ 0.3 -0.4 mm), and oxides (~0.2 mm) in a glassy matrix with an abundance of ~ 93 %. Diktytaxitic textures are common in this sample. There are minor glass products.

Matrix (glass) ~ 18, Groundmass (plagioclase > clinopyroxene > olivine > oxides) ~ 75 %

Phenocrysts (olivine > plagioclase) ~ 7 %

Appendix C: continued

FR-13-171: Primitive crystal poor olivine basalt. Phenocryst phases are olivine (~ 0.5 – 1.4 mm) and plagioclase (~ 1 -1.3 mm) with an abundance of ~ 6 %. Groundmass is coarse-grained holo- to hypocrystalline, and contains plagioclase laths (~ 0.2 - 0.8 mm), olivine (~ 0.2-0.4 mm), and oxides (0.3 mm) in a glassy matrix with an abundance of ~ 94 %. Diktytaxitic textures are common in this sample. There are minor glass products.

Point Count- 390 points

Matrix (glass) - 132 points (34 %)

Groundmass (plagioclase > oxides > olivine) - 234 points (60 %)

Phenocrysts (olivine= plagioclase) - 24 points (6 %)

- 12 points (3 %)

- 12 points (3 %)

FR-13-172: Primitive crystal poor olivine basalt. Phenocryst phases are plagioclase (~ 0.7 – 1.5 mm) and olivine (~ 0.6 – 1.1 mm) with an abundance of ~ 5 %. Plagioclase and olivine phenocrysts contain similar abundances. Groundmass is fine- to coarse-grained holo to hypocrystalline, and contains plagioclase laths and microlites (~ 0.1- 0.8 mm), olivine (~ 0.2- 0.4 mm), and oxides (~0.1- 0.3 mm) in a glassy matrix. Groundmass is ~ 65 % of the sample.

Matrix (glass) ~ 30 %, Groundmass (plagioclase > olivine > oxides) ~ 65 %

Phenocrysts (plagioclase ≥ olivine) ~ 5 %

Hogback Butte

FR-10-86: Crystal poor olivine basalt. Phenocryst phases are plagioclase (~ 0.7 – 1 mm) and olivine (1 grain at 1.8 mm) with an abundance of ~ 6 %. Plagioclase phenocrysts are much more abundant than olivine phenocrysts (plagioclase ~ 5 % and olivine ~ 1 %). Groundmass is fine-grained hypocrystalline, containing plagioclase laths and microlites (~ ≤ 0.1 – 0.3 mm), olivine (~ 0.1 -0.2 mm), oxides (≤ 0.1 mm) in a glassy matrix. Plagioclase laths and microlites are more abundant than olivine and oxides in the groundmass.

Appendix C: continued

FR-10-87: Crystal poor olivine basalt. Phenocryst phases are plagioclase (~ 0.5 – 1.2 mm) and olivine (0.5 – 1.1 mm) with an abundance of ~ 4 %. Plagioclase phenocrysts are more abundant than olivine phenocrysts (plagioclase ~ 2.5 % and olivine ~ 1.5 %). Olivine phenocrysts are oxidized and altered. Groundmass is fine-grained hypocrystalline, and contains plagioclase microlites and laths (~ ≤ 0.1- 0.2 mm), olivine (~0.1-0.2 mm), clinopyroxene (~ 0.1-0.2 mm) and oxides (~ 0.1 - 0.2 mm) in a glassy matrix with an abundance of ~ 96 %. Groundmass contains ophiomottled textures.

Matrix (glass) ~ 51 %, Groundmass (plagioclase > clinopyroxene > oxides> olivine) ~ 45 %

Phenocrysts (plagioclase > olivine) ~ 4 %

Tuff Butte- Table Mountain maar complex

FR-10-24: Crystal poor olivine basalt (spatter sample). Phenocryst phases are plagioclase (~ 0.7 – 1.3 mm) and olivine (~ 0.6 – 1 mm) with an abundance of ~ 5 %. Plagioclase phenocrysts are more abundant than olivine phenocrysts (plagioclase ~ 3 % and olivine ~ 2 %). Groundmass is fine-grained hypocrystalline to holohyaline, and contains plagioclase microlites and laths (≤ 0.1 – 0.2 mm) and olivine (~ ≤ 0.1 mm) in a glassy matrix with an abundance of ~ 10 %.

FR-10-26: Crystal poor olivine basalt. Phenocryst phases are plagioclase (~ 0.6 – 1.6 mm) and olivine (~ 0.4- 1.2 mm) with an abundance of ~ 8 %. Plagioclase phenocrysts are more abundant than olivine phenocrysts (plagioclase ~ 5.5 % and olivine ~ 2.5 %). Groundmass is fine-grained holocrystalline to hypocrystalline, and contains plagioclase laths (~ 0.1 – 0.3 mm), olivine (~ 0.1-0.2 mm), clinopyroxene (~ 0.2-0.3 mm) and oxides (~ 0.1 mm) with an abundance of in a glassy groundmass with an abundance of ~ 60 %. Groundmass contains an ophiomottled texture.

Matrix (glass) ~ 32 %, Groundmass (plagioclase > clinopyroxene > olivine > oxides) ~ 60 %

Phenocrysts (plagioclase > olivine) ~ 8 %

Jack's Place- East Lava Field

FR-13-164: Primitive crystal poor olivine basalt. Phenocryst phases are plagioclase (~ 0.7 mm) and olivine (~ 0.5 – 1.6 mm) with an abundance of ~ 5 %. Olivine phenocrysts are much more abundant than plagioclase phenocrysts (olivine ~ 4.5 % and plagioclase ~ 0.5 %). Clusters of olivine phenocrysts are present in this sample. Groundmass is fine-grained hypocrystalline, and contains plagioclase laths and microlites (~ ≤ 0.1 – 0.2 mm), olivine (~ ≤ 0.1 – 0.2 mm), and oxides (≤ 0.1 – 0.2 mm) in a glassy matrix with and abundance of ~ 40 %.

Matrix (glass) ~ 55 %, Groundmass (plagioclase > olivine ≥ oxides) ~ 40 %

Phenocrysts (olivine >> plagioclase) ~ 5 %

FR-13-165: Porphyritic olivine basalt. Phenocryst phases are plagioclase (~ 0.7- 2.9 mm) and olivine (~ 0.5 – 1.5 mm) with an abundance of ~ 13 %. Plagioclase phenocrysts are more abundant than olivine phenocrysts (plagioclase ~ 8 % and olivine ~ 5 %). Glomerocrysts of plagioclase and olivine phenocrysts are present in this sample. Groundmass is fine-grained hypocrystalline, and contains plagioclase laths and microlites (~≤ 0.1 – 0.2 mm), olivine (~ 0.1-0.2 mm), and oxides (~ ≤ 0.1 mm) in a glassy matrix with an abundance of ~ 40 %.

Matrix (glass) ~ 47 %, Groundmass (plagioclase > olivine > oxides) ~ 40 %

Phenocrysts (plagioclase > olivine) ~ 13 %

FR-13-166: Porphyritic olivine basalt. Phenocryst phases are plagioclase (~ 0.7 – 3.3 mm) and olivine (~ 0.5 – 1.1 mm) with an abundance of ~ 16 %. Plagioclase phenocrysts are more abundant than olivine phenocrysts (plagioclase ~ 10 % and olivine ~ 6 %). Glomerocrysts of plagioclase and olivine phenocrysts are present in this sample. Groundmass is fine-grained hypocrystalline, and contains plagioclase laths and microlites (~ ≤ 0.1 – 0.2 mm), olivine (~≤ 0.1-0.2 mm), and oxides (~ 0.1 -0.2 mm) in a glassy matrix with an abundance of ~ 40 %.

Matrix (glass) ~44 %, Groundmass (plagioclase > olivine > oxides) ~ 40 %

Phenocrysts (plagioclase > olivine) ~ 16 %

FR-13-167: Porphyritic olivine basalt. Phenocryst phases are plagioclase (~ 0.7 – 3.2 mm) and olivine (~ 0.5 – 0.9 mm) with an abundance of ~ 18 %. Plagioclase phenocrysts are more abundant than olivine phenocrysts (plagioclase ~ 12 % and olivine ~ 6 %). Glomerocrysts of plagioclase and olivine phenocrysts are present in this sample. Groundmass is fine-grained, hypocrystalline and contains plagioclase laths and microlites (~ ≤ 0.1 – 0.2 mm), olivine (~≤ 0.1-0.2 mm), and oxides (~ 0.1 -0.2 mm) in a glassy matrix with an abundance of ~ 40 %.

Groundmass (plagioclase > olivine > oxides) ~ 40 %

Phenocrysts (plagioclase > olivine) ~ 18 %

Appendix C: continued

FR-13-168B: Primitive crystal poor olivine basalt. Phenocryst phases are plagioclase (~ 0.5 – 2 mm) and olivine (~ 0.5 – 2 mm) with an abundance of ~ 6 %. Plagioclase phenocrysts are slightly more abundant than olivine phenocrysts (plagioclase ~ 3.6 % and olivine ~ 2.4 %). Glomerocrysts of plagioclase and olivine phenocrysts are present in this sample. Groundmass is fine-grained, hypocrystalline and contains plagioclase laths and microlites (~ ≤ 0.1 – 0.3 mm), olivine (~≤ 0.1- 0.2 mm), and oxides (~ 0.1 -0.2 mm) in a glassy matrix with an abundance of ~ 40 %.

Point Count- 452 points

Matrix (glass)- 244 points (54 %)

Groundmass (plagioclase > olivine > oxides) - 181 points (40 %)

Phenocrysts (plagioclase > olivine) - 27 points (6 %)

- plagioclase- 16 points- (3.6 %)

- olivine- 11 points – (2.4 %)

Jack's Place- Green Mountain

FR-12-87B: Crystal poor primitive olivine basalt. Microphenocryst phases are plagioclase (~ 0.45 – 0.8 mm) and olivine (~ 0.45 mm) with an abundance of ~ 6 %. Plagioclase microphenocrysts are more abundant than olivine microphenocrysts (plagioclase ~ 4 % and olivine ~ 2%). Crystal clots of plagioclase and olivine are present in this sample. Groundmass is fine to coarse-grained holocrystalline to hypocrystalline, and contains plagioclase laths and microlites (~ ≤ 0.1 – 0.3 mm), olivine (~≤ 0.1- 0.2 mm), and oxides (~ 0.1 -0.2 mm) in a glassy matrix with an abundance of ~ 60 %.

Matrix (glass) ~ 34 %, Groundmass (plagioclase > olivine > oxides) ~ 60 %

Microphenocrysts (plagioclase > olivine) ~ 6 %

FR-12-88: Highly vesicular crystal poor primitive olivine basalt (spatter). Microphenocryst phases are plagioclase (~ 0.4 – 0.8 mm) and olivine (~ 0.4- 0.6 mm) with an abundance of ~ 8 %. Plagioclase microphenocrysts are more abundant than olivine phenocrysts (plagioclase ~ 5 % and olivine ~ 3 %). Crystal clots of plagioclase and olivine are present in this sample. Groundmass is fine-grained hypocrystalline to holohyaline, and contains plagioclase microlites (~ ≤ 0.1 mm) and olivine (~≤ 0.1 mm) in a glassy matrix with an abundance of ~ 2 %.

Matrix (glass) ~ 90 %, Groundmass (plagioclase > olivine) ~ 2 %

Microphenocrysts (plagioclase > olivine) ~ 8 %

Appendix C: continued

FR-12-89: Primitive crystal poor olivine basalt. Phenocryst phases are plagioclase (~ 0.6- 3.3 mm) and olivine (~ 0.6- 1.3 mm) with an abundance of ~ 8 %. Plagioclase phenocrysts are more abundant than olivine phenocrysts (plagioclase ~ 5 % and olivine ~ 3 %). Glomerocrysts of plagioclase and olivine are present in this sample. Groundmass is fine-grained hypocrystalline, and contains plagioclase laths and microlites (~ ≤ 0.1 mm), olivine (~≤ 0.1 mm), and oxides (~ ≤ 0.1 mm) in a glassy matrix with an abundance of ~ 25 %.

Matrix (glass)~ 67 %, Groundmass (plagioclase > olivine> oxides) ~ 25 %

Microphenocrysts (plagioclase > olivine) ~ 8 %

FR-12-95: Primitive olivine basalt. Phenocryst phases are plagioclase (~ 0.6- 0.9 mm) and olivine (~ 0.6- 1.1 mm) with an abundance of ~ 10 %. Plagioclase phenocrysts are more abundant than olivine phenocrysts (plagioclase ~ 6 % and olivine ~ 4 %). Glomerocrysts of plagioclase and olivine are present in this sample. Groundmass is fine-grained hypocrystalline, and contains plagioclase laths and microlites (~ ≤ 0.1 -0.2 mm), olivine (~≤ 0.1- 0.2 mm), and oxides (~ ≤ 0.1 mm) in a glassy matrix with an abundance of ~ 35 %.

Matrix (glass) ~ 55 %, Groundmass (plagioclase > olivine> oxides) ~ 35 %

Microphenocrysts (plagioclase > olivine) ~ 10 %

Four Craters Lava Field

FR-13-150: Primitive crystal poor olivine basalt. Phenocryst phases are plagioclase (~ 0.8 mm) and olivine (~ 0.7- 1.6 mm) with an abundance of ~ 8 %. Plagioclase and olivine phenocrysts contain similar abundances. Glomerocrysts of plagioclase and olivine are present in this sample. Groundmass is fine-grained hypocrystalline, and contains plagioclase laths and microlites (~ ≤ 0.1 -0.3 mm), olivine (~≤ 0.1- 0.3 mm), and oxides (~ ≤ 0.1 mm) in a glassy matrix with an abundance of ~ 35 %.

Point Count- 479 points

Matrix (glass) – 273 points (57 %)

Groundmass (plagioclase > olivine> oxides) - 168 points (35 %)

Phenocrysts (plagioclase ≥ olivine) - 38 points (8 %)

- plagioclase- 20 points (4 %)
- olivine - 18 points (4 %)

Appendix C: continued

FR-13-151: Primitive crystal poor olivine basalt. Phenocryst phases are plagioclase (~ 0.8-2.7 mm) and olivine (~ 0.8- 1.3 mm) with an abundance of ~ 6 %. Plagioclase phenocrysts are more abundant than olivine phenocrysts (plagioclase ~ 4 % and olivine ~ 2 %). Glomerocrysts of plagioclase and olivine are present in this sample. Groundmass is fine-grained hypocrystalline, and contains plagioclase laths and microlites (~ ≤ 0.1 -0.3 mm), olivine (~≤ 0.1- 0.3 mm), and oxides (~ ≤ 0.1 mm) in a glassy matrix with an abundance of ~ 35 %.

Matrix (glass) ~ 59 %, Groundmass (plagioclase > olivine > oxides) ~ 35 %

Phenocrysts (plagioclase > olivine) ~ 6 %

Reed Rock

FR-12-99: Primitive crystal poor olivine basalt. Phenocryst phases are plagioclase (~ 1.6 -2.4 mm) and olivine (~ 0.8- 1 mm) with an abundance of ~ 3 %. Plagioclase phenocrysts are more abundant than olivine phenocrysts (plagioclase ~ 2 % and olivine ~ 1 %). Glomerocrysts of plagioclase and olivine are present in this sample. Groundmass is fine-grained holo- to hypocrystalline, and contains plagioclase laths and microlites (~ ≤ 0.1 -0.2 mm), olivine (~≤ 0.1-0.2 mm), clinopyroxene (~0.1-0.2 mm) and oxides (~ ≤ 0.1-0.2 mm) in a glassy matrix with an abundance of ~ 55 %. Sub-ophitic textures are common in the groundmass.

Matrix (glass) ~ 42 %, Groundmass (plagioclase > clinopyroxene > olivine > oxides) ~ 55 %

Phenocrysts (plagioclase > olivine) ~ 3 %

FR-12-100: Primitive crystal poor olivine basalt. Phenocryst phases are plagioclase (~ 0.8 -1.4 mm) and olivine (~ 0.8- 1.6 mm) with an abundance of ~ 3 %. Plagioclase phenocrysts are more abundant than olivine phenocrysts (plagioclase ~ 2 % and olivine ~ 1 %). Crystal clots plagioclase and olivine grains are present in this sample. Groundmass is fine-grained holo-to hypocrystalline, and contains plagioclase laths and microlites (~ ≤ 0.1 -0.2 mm), olivine (~≤ 0.1-0.2 mm), clinopyroxene (~0.2 mm) and oxides (~ ≤ 0.1-mm) in a glassy matrix with an abundance of ~ 97 %. Sub-ophitic textures are common in the groundmass.

Matrix (glass) ~ 47 %, Groundmass (plagioclase > olivine > clinopyroxene > oxides) ~ 50 %

Phenocrysts (plagioclase > olivine) ~ 3 %

Appendix C: continued

FR-12-101: Primitive crystal poor olivine basalt. Phenocryst phases are plagioclase (~ 0.8- 1.6 mm) and olivine (~ 0.6- 1.1 mm) with an abundance of ~ 5 %. Plagioclase phenocrysts are more abundant than olivine phenocrysts (plagioclase ~ 3 % and olivine ~ 2 %). Glomerocrysts of plagioclase and olivine phenocrysts are present in this sample. Groundmass is fine –grained holocrystalline to hypocrystalline, and contains plagioclase laths and microlites (~ ≤ 0.1 -0.4 mm), olivine (~≤ 0.1- 0.2 mm), clinopyroxene (~0.2 mm) and oxides (~ ≤ 0.1-mm) in a glassy matrix with an abundance of ~ 60 %. The groundmass contains an ophiomottled texture.

Point Count- 422 points

Matrix (glass) - 274 points (35 %)

Groundmass (plagioclase > clinopyroxene > olivine ≥ oxides) - 253 points (60 %)

Phenocrysts (plagioclase > olivine) - 21 points (5 %)

- plagioclase- 13 points (3 %)

- olivine- 8 points (2 %)

FR-12-130: Primitive crystal poor olivine basalt. Phenocryst phases are plagioclase (~ 0.9- 1.1 mm) and olivine (~ 0.8- 1.1 mm) with an abundance of ~ 4 %. Olivine phenocrysts are more abundant than plagioclase phenocrysts (olivine ~ 2.5 % and plagioclase ~ 1.5 %). Glomerocrysts of plagioclase and olivine phenocrysts are present in this sample. Groundmass is fine-grained holocrystalline, and contains plagioclase laths (~0.2 mm), olivine (~0.2 mm), clinopyroxene (~0.2 mm) and oxides (~ ≤ 0.1-mm) with an abundance of ~ 60 %. The groundmass contains ophiomottled and sub-ophitic textures.

Point Count- 407 points

Matrix (glass) - 260 points (64 %)

Groundmass (plagioclase > clinopyroxene > olivine ≥ oxides) - 244 points (60 %)

Phenocrysts (olivine > plagioclase) - 16 points (4 %)

- plagioclase- 6 points (1.5 %)

- olivine- 10 points (2.5 %)

Appendix C: continued

FR-13-152: Primitive crystal poor olivine basalt. Phenocryst phases are plagioclase (~ 0.7- 1.2 mm) and olivine (~ 0.7-0.8 mm) with an abundance of ~ 2 %. Olivine phenocrysts and plagioclase phenocrysts contain similar abundances (olivine ~ 1 % and plagioclase ~ 1 %). Glomerocrysts of plagioclase and olivine phenocrysts are present in this sample. Groundmass is fine-grained holocrystalline, and contains plagioclase laths (~0.1 -0.3 mm), olivine (~0.1- 0.3 mm), clinopyroxene (~0.2 -0.3 mm) and oxides (~ ≤ 0.1-mm) with an abundance of ~ 75 %. The groundmass contains ophiomottled and sub-ophitic textures.

Point Count- 498 points

Matrix (glass) - 359 points (21 %)

Groundmass (plagioclase > clinopyroxene > olivine ≥ oxides) - 349 points (75 %)

Phenocrysts (plagioclase ≥ olivine) - 10 points (2 %)

- plagioclase- 6 points (1 %)

- olivine- 4 points (1 %)

The Black Hills

FR-12-108B: Highly vesicular basalt spatter. Phenocryst phases are plagioclase (~ 0.6- 1.1 mm) and olivine (~ 0.6-0.8 mm) with an abundance of ~ 2 %. Plagioclase phenocrysts are more abundant than olivine phenocrysts (olivine ~ 0.5 % and plagioclase ~ 1.5 %). Glomerocrysts of plagioclase and olivine phenocrysts are present in this sample. Groundmass is fine-grained hypocrystalline to holohyaline, and contains plagioclase laths and microlites (~≤0.1 -0.3 mm), olivine (~0.1- 0.2 mm), and oxides (~ ≤ 0.1-mm) in a glassy matrix with an abundance of ~ 5 %.

FR-12-114: Crystal poor basalt. Plagioclase is the only phenocryst phase (~ 1.1 mm) with an abundance of ~ < 1 %. Groundmass is fine-grained hypocrystalline to holohyaline containing plagioclase microlites (≤ 0.1 mm) and oxides (≤ 0.1 mm) in a glassy matrix with an abundance of ~ 5 %.

FR-12-115: Crystal poor basalt. Plagioclase is the only phenocryst phase (~ 1.1 mm) with an abundance of ~ < 1 %. Groundmass is hypocrystalline to holohyaline, containing plagioclase laths and microlites (≤ 0.1 mm) and oxides (≤ 0.1 mm) in a glassy matrix with an abundance of ~ 5 %.

Appendix C: continued

FR-13-153B: Crystal poor basalt. Plagioclase is the only phenocryst phase (~ 1.1 mm) with an abundance of ~ < 1 %. All plagioclase phenocrysts display sieve textures, crystallization out of equilibrium with the magma. Groundmass is fine-grained hypocrystalline to holohyaline, containing plagioclase laths and microlites (≤ 0.1 – 0.2 mm), olivine (~0.1-0.2 mm) and oxides (≤ 0.1- 0.2 mm) in a glassy matrix with an abundance of ~ 15 %.

FR-13-178A: Crystal poor basalt from a dike. No phenocrysts phases present. Groundmass is fine-grained hypocrystalline to holohyaline, containing plagioclase laths and microlites (≤ 0.1 mm), olivine (~0.1 mm) and oxides (≤ 0.1) in a glassy matrix with an abundance of ~ 15 %.

FR-13-178B: Crystal poor olivine basalt from a dike. Phenocryst phases are plagioclase (~ 0.7-0.9 mm) and olivine (~ 0.6-0.8 mm) with an abundance of ~ 3 %. Plagioclase phenocrysts are more abundant than olivine phenocrysts (plagioclase ~ 2 % and olivine ~ 1%). Olivine phenocrysts display alteration rims. Groundmass is fine-grained holocrystalline to hypocrystalline, and contains plagioclase laths (~ 0.1-0.5 mm), olivine (~0.1-0.4 mm), clinopyroxene (0.2-0.4 mm) and oxides (~ ≤ 0.1 mm) with an abundance of ~ 80 %. Groundmass contains sub-ophitic textures.

Matrix (glass) ~ 17 %, Groundmass (plagioclase > clinopyroxene > olivine > oxides) ~ 80 %

Phenocrysts (plagioclase > olivine) ~ 3 %

St. Patrick's Mountain

FR-13-191: Crystal poor olivine basalt from a diabase dike. Phenocryst phases are plagioclase (~ 0.9 mm) and olivine (~ 0.7-0.9 mm) with an abundance of ~ 2 %. Plagioclase phenocrysts are more abundant than olivine phenocrysts (plagioclase ~ 1.5 % and olivine ~ 0.5%). Groundmass is coarse-grained holocrystalline to hypocrystalline, and contains plagioclase laths (~ 0.5-0.7 mm), olivine (~0.2-0.6 mm), and oxides (~ 0.5 mm) in a glassy matrix with an abundance of ~ 85 %.

Matrix (glass) ~ 13 %, Groundmass (plagioclase > olivine ≥ oxides) ~ 85 %

Phenocrysts (plagioclase > olivine) ~ 2 %

FR-13-192: Crystal poor olivine basalt from a diabase dike. Phenocryst phases are plagioclase (~ 0.7 mm) and olivine (~ 0.7 mm) with an abundance of ~ 1 %. Groundmass is fine-grained hypocrystalline, and contains plagioclase microlites and laths (~ ≤ 0.1 – 0.2 mm), olivine (~ 0.1-0.2 mm), and oxides (≤ 0.1 mm) in a glassy matrix. Plagioclase microlites in the groundmass display a trachytic texture.

Matrix (glass) ~ 76 %, Groundmass (plagioclase > olivine ≥ oxides) ~ 25 %

Phenocrysts (plagioclase ≥ olivine) ~ 1 %

Appendix C: continued

FR-13-194C: Crystal poor basalt. Plagioclase is the phenocryst phase (~ 1- 1.4 mm) with an abundance of ~ < 1 %. All plagioclase phenocrysts display sieve textures, crystallization out of equilibrium with the magma. Groundmass is fine-grained hypocrystalline to holohyaline, containing plagioclase microlites and laths (≤ 0.1 -0.3 mm), olivine (~ 0.1-0.2 mm), and oxides (≤ 0.1 mm) ~ 15 % in a glassy matrix.

Appendix D: Approximations of groundmass crystallinity, average groundmass grain sizes, and vesicularity.

Western/Central	Sample Type	Crystallinity (%)	Grain sizes (avg. mm)	Vesicle content (%)
Big Hole				
FR-10-27 (CAB)	lava	35	0.3	5
FR-10-30 (LKT)	spatter	30	0.1	40
FR-10-32A (BA)	juvenile bomb in maar	35	0.25	0
FR-10-37 (BA)	lava	60	0.15	2
FR-10-38 (LKT)	lava	65	0.4	7
FR-10-39 (LKT)	lava	65	0.4	15
FR-10-40 (OIB)	lava	100	0.55	15
FR-10-42 (LKT)	lava	35	0.15	10
FR-10-44 (BA)	scoria	3	0.1	20
Wickiup				
FR-10-65 (CAB)	lava	35	0.15	0
FR-10-66 (CAB)	lava	35	0.3	5
FR-10-67 (BA)	scoria	25	0.35	30
FR-10-68 (BA)	lava	70	0.5	0
FR-10-69 (BA)	lava	65	0.5	0
FR-10-70A (BA)	scoria	5	0.1	50
FR-10-71 (CAB)	lava	45	0.15	0
FR-10-72A (BA)	lava	45	0.15	1
FR-10-73 (BA)	scoria	35	0.15	35
FR-10-74 (BA)	lava	100	0.45	5
McCarty				
FR-10-46 (CAB)	lava	100	0.4	5
FR-10-48 (CAB)	lava	100	0.35	10
FR-10-56 (LKT)	lava	100	0.4	15
FR-10-57 (LKT)	lava	35	0.15	10
Oatman				
FR-10-58 (CAB)	lava	100	0.4	5
FR-10-59 (HKCAB)	lava	35	0.15	5
FR-10-60 (HKCAB)	lava	35	0.15	5
FR-10-62 (HKCAB)	lava	30	0.15	30
FR-10-63 (CAB)	lava	40	0.15	0
Fort Rock				
FR-10-8A (CAB)	juvenile bomb in tuff ring	25	0.15	5

Appendix D: continued

Western/Central	Sample Type	Crystallinity (%)	Grain sizes (avg. mm)	Vesicle content (%)
Cabin Lake-Flat Top				
FR-10-77 (CAB)	lava	75	0.3	1
FR-10-78 (OIB)	lava	85	0.55	5
FR-10-79 (BA)	scoria	15	0.15	30
South Ice Cave				
FR-10-80 (CAB)	scoria	15	0.1	25
Sixteen Butte				
FR-10-82 (BA)	lava	80	0.3	10
FR-13-181 (CAB)	scoria	5	0.15	40
FR-13-182 (BA)	scoria	3	0.15	25
FR-13-183 (BA)	scoria	2	0.1	50
FR-13-184 (BA)	scoria	5	0.1	25
FR-13-185 (CAB)	scoria	55	0.15	15
Devils Garden				
FR-12-124 (CAB)	lava	75	0.35	5
FR-13-171 (OIB)	lava	60	0.35	0
FR-13-172 (CAB)	lava	65	0.45	5
Blowouts				
FR-10-85 (OIB)	spatter	55	0.1	35
Table Mnt.				
FR-10-87 (LKT)	lava	45	0.15	2
Table Rock				
FR-10-24 (LKT)	spatter	10	0.15	30
FR-10-26 (CAB)	lava	60	0.2	2

Appendix D: continued

Eastern	Sample Type	Crystallinity (%)	Grain sizes (avg. mm)	Vesicle content (%)
East Lava Field				
FR-13-164 (OIB)	lava	40	0.15	10
FR-13-165 (BA)	lava	40	0.15	15
FR-13-166 (BA)	lava	40	0.15	15
FR-13-167 (BA)	lava	40	0.15	15
FR-13-168B (BA)	lava	40	0.15	5
Green Mnt.				
FR-12-87B (CAB)	lava	60	0.2	5
FR-12-88 (CAB)	spatter	2	0.1	40
FR-12-89 (CAB)	lava	25	0.1	15
FR-12-95 (CAB)	lava	35	0.15	10
Four Craters Lava Field				
FR-13-150 (OIB)	lava	35	0.2	15
FR-13-151 (OIB)	lava	35	0.2	15
Reed Rock				
FR-12-99 (LKT)	lava	55	0.15	15
FR-12-100 (LKT)	lava	50	0.15	15
FR-12-101 (LKT)	lava	60	0.15	15
FR-12-130 (LKT)	lava	60	0.15	2
FR-12-152 (LKT)	lava	75	0.2	2
Black Hills				
FR-12-108B (CAB)	spatter	5	0.15	30
FR-12-114 (CAB)	lava	5	0.1	5
FR-12-115 (BA)	lava	5	0.1	5
FR-13-153B (BA)	lava	30	0.15	5
FR-13-178A (LKT)	lava	15	0.1	5
FR-13-178B (LKT)	lava	80	0.2	2
St. Patricks Mnt				
FR-13-191 (BA)	lava	85	0.4	10
FR-13-192 (BA)	lava	25	0.15	5
FR-13-194C (CAB)	lava	15	0.1	2

Appendix E: Plagioclase phenocryst core and rim chemical compositions through microprobe analyses. Major oxides recorded in (wt%). Analyses with < 98 % and > 102 % oxide totals were omitted; n.d= no detection.

	Oxide (wt%)	**SiO_2**	**TiO_2**	**Al_2O_3**	**FeO***	**MgO**	**CaO**	**Na_2O**	**K_2O**	**BaO**	**Rb_2O**	**SrO**	**Total**	**An Content**
Western/Central	**Sample #**													
LKT	**FR-10-39**													
grain 1	core	48.11	0.10	32.24	0.36	0.14	13.91	3.37	0.09	n.d	n.d	n.d	98.32	82
	rim	50.66	0.16	30.95	0.50	0.18	12.45	4.06	0.13	n.d	n.d	n.d	99.09	77
grain 2	core	51.20	0.10	30.88	0.66	0.22	12.44	4.28	0.13	n.d	n.d	n.d	99.91	76
	rim	50.69	0.14	31.19	0.61	0.19	12.59	4.22	0.13	n.d	n.d	n.d	99.75	77
grain 3	core	48.72	0.12	32.91	0.49	0.19	13.36	3.58	0.09	n.d	n.d	n.d	99.46	80
	rim	49.25	0.07	32.70	0.54	0.14	13.88	3.51	0.06	n.d	n.d	n.d	100.14	81
grain 4	core	49.05	n.d	32.80	0.47	0.12	14.03	3.58	0.09	n.d	n.d	n.d	100.14	81
	rim	50.00	0.11	32.40	0.51	0.16	13.60	3.66	0.09	n.d	n.d	n.d	100.55	80
grain 5	core	49.54	0.09	32.97	0.41	0.18	14.24	3.41	0.10	n.d	n.d	n.d	100.96	82
	rim	49.68	0.08	32.25	0.51	0.16	13.21	3.70	0.08	n.d	n.d	n.d	99.67	80
OIB	**FR-10-40**													
grain 1	core	50.13	0.02	32.09	0.43	0.17	13.22	3.84	0.15	n.d	n.d	n.d	100.05	79
	rim	52.42	0.17	30.33	0.54	0.13	11.41	5.10	0.24	n.d	n.d	n.d	100.35	71
grain 2	core	49.66	0.09	32.86	0.31	0.12	13.73	3.61	0.12	n.d	n.d	n.d	100.50	81
	rim	49.82	0.12	32.57	0.51	0.05	13.50	3.78	0.20	n.d	n.d	n.d	100.54	80
grain 3	core	50.10	0.12	32.44	0.43	0.12	13.20	3.96	0.16	n.d	n.d	n.d	100.53	79
	rim	52.33	0.13	29.84	0.75	0.12	10.85	5.22	0.28	n.d	n.d	n.d	99.52	70
grain 4	core	51.66	0.28	29.33	1.40	0.24	11.80	4.75	0.41	n.d	n.d	n.d	99.86	73
	rim	58.89	0.19	25.78	0.54	0.07	5.82	7.63	0.92	n.d	n.d	n.d	99.85	46
grain 5	core	49.74	0.06	32.43	0.44	0.09	13.39	3.85	0.16	n.d	n.d	n.d	100.15	79
	rim	51.30	0.08	30.92	0.53	0.15	12.06	4.48	0.23	n.d	n.d	n.d	99.75	75

Appendix E: continued

Western/Central	Oxide (wt%) / Sample #	SiO_2	TiO_2	Al_2O_3	FeO*	MgO	CaO	Na_2O	K_2O	BaO	Rb_2O	SrO	Total	An Content
OIB	**FR-10-85**													
grain 1	core	47.03	0.65	28.70	3.15	2.50	13.90	2.92	0.25	n.d	n.d	n.d	99.10	84
	rim	48.07	0.06	32.83	0.54	0.14	14.62	3.05	0.08	n.d	n.d	n.d	99.38	84
grain 2	core	48.24	0.07	33.33	0.44	0.19	14.81	2.96	0.11	n.d	n.d	n.d	100.15	85
	rim	47.38	0.07	33.78	0.44	0.16	15.06	2.78	0.06	n.d	n.d	n.d	99.74	86
grain 3	core	48.36	0.49	30.38	2.46	1.86	13.80	2.90	0.15	n.d	n.d	n.d	100.39	84
	rim	49.14	0.10	33.53	0.55	0.21	14.66	3.10	0.11	n.d	n.d	n.d	101.39	84
grain 4	core	49.87	0.08	32.59	0.54	0.15	13.62	3.68	0.12	n.d	n.d	n.d	100.64	80
	rim	53.25	0.25	28.85	1.76	0.22	10.36	5.32	0.36	0.12	n.d	n.d	100.47	68
grain 5	core	48.86	0.06	33.58	0.47	0.25	14.53	3.11	0.11	n.d	n.d	n.d	100.98	84
	rim	48.63	n.d	33.30	0.47	0.17	14.41	3.27	0.12	n.d	n.d	n.d	100.36	83
Eastern	**Sample #**													
LKT	**FR-12-101**													
grain 1	core	48.73	n.d	33.53	0.33	0.24	14.47	3.09	0.08	n.d	n.d	n.d	100.45	84
	rim	47.40	n.d	34.44	0.39	0.22	15.29	2.55	0.05	n.d	n.d	n.d	100.33	87
grain 2	core	49.80	0.12	31.70	0.72	0.25	13.51	3.71	0.14	n.d	n.d	n.d	99.95	80
	rim	48.79	0.19	31.49	1.37	0.56	13.94	3.44	0.13	n.d	n.d	n.d	99.91	82
grain 3	core	49.63	n.d	32.65	0.54	0.24	13.82	3.44	0.10	0.13	n.d	n.d	100.54	82
	rim	53.97	0.35	25.40	2.20	1.52	10.29	5.41	0.30	n.d	n.d	n.d	99.45	68
grain 4	core	48.51	n.d	33.56	0.47	0.16	14.79	2.87	0.07	n.d	n.d	n.d	100.44	85
	rim	47.89	n.d	33.91	0.52	0.18	15.33	2.74	0.09	n.d	n.d	n.d	100.66	86
grain 5	core	46.35	0.05	34.00	0.40	0.18	15.24	2.67	0.10	n.d	n.d	n.d	98.98	86
	rim	47.21	n.d	33.53	0.49	0.21	14.79	2.62	0.10	n.d	n.d	n.d	98.95	86

Appendix E: Continued

Eastern	Oxide (wt%) Sample #	SiO_2	TiO_2	Al_2O_3	FeO*	MgO	CaO	Na_2O	K_2O	BaO	Rb_2O	SrO	Total	An Content
LKT	**FR-12-130**													
grain 1	core	50.00	n.d	32.56	0.65	0.12	13.66	3.70	0.12	n.d	n.d	n.d	100.82	80
	rim	50.67	0.08	31.02	0.78	0.08	11.99	4.37	0.24	n.d	n.d	n.d	99.24	75
grain 2	core	50.03	n.d	32.37	0.93	0.05	13.39	3.65	0.14	n.d	n.d	n.d	100.56	80
	rim	50.41	n.d	31.38	1.51	0.28	12.99	3.98	0.17	n.d	n.d	n.d	100.73	78
grain 3	core	49.37	0.06	32.66	0.80	0.05	13.81	3.66	0.15	n.d	n.d	n.d	100.55	81
	rim	51.99	0.15	30.63	0.87	0.15	11.86	4.77	0.19	n.d	n.d	n.d	100.61	73
grain 4	core	46.27	n.d	34.99	0.61	0.05	16.24	2.15	0.05	n.d	n.d	n.d	100.36	89
	rim	49.39	n.d	32.38	0.70	0.10	13.71	3.62	0.13	n.d	n.d	n.d	100.04	81
grain 5	core	49.52	n.d	32.85	0.64	0.08	13.79	3.53	0.13	n.d	n.d	n.d	100.55	81
	rim	52.97	0.10	30.31	0.71	0.20	11.11	5.13	0.26	n.d	n.d	n.d	100.79	71
LKT	**FR-13-152**													
grain 1	core	51.06	n.d	31.26	0.35	0.14	14.17	3.56	0.11	n.d	n.d	n.d	100.66	81
	rim	51.47	0.07	30.71	0.40	0.15	13.86	3.67	0.12	n.d	n.d	n.d	100.45	81
grain 2	core	50.80	n.d	31.21	0.40	0.17	14.78	3.15	0.12	n.d	n.d	n.d	100.63	84
	rim	50.31	0.07	31.33	0.49	0.11	14.64	3.39	0.09	n.d	n.d	n.d	100.43	83
grain 3	core	51.13	n.d	31.44	0.44	0.17	14.41	3.36	0.13	n.d	n.d	n.d	101.08	83
	rim	50.80	n.d	31.00	0.50	0.16	14.15	3.50	0.13	n.d	n.d	n.d	100.23	82
grain 4	core	51.26	n.d	30.93	0.34	0.13	14.27	3.43	0.15	n.d	n.d	n.d	100.50	82
	rim	51.34	0.06	30.86	0.60	0.14	14.01	3.53	0.13	n.d	n.d	n.d	100.66	81
grain 5	core	52.10	0.13	30.41	0.39	0.16	13.34	3.86	0.16	n.d	n.d	n.d	100.56	79
	rim	49.98	n.d	31.89	0.47	0.14	15.26	2.91	0.08	n.d	n.d	n.d	100.73	85

Appendix E: continued

	Oxide (wt%)	SiO_2	TiO_2	Al_2O_3	FeO*	MgO	CaO	Na_2O	K_2O	BaO	Rb_2O	SrO	Total	An Content
Eastern	**Sample #**													
BA	**FR-13-168b**													
grain 1	core	50.07	n.d	31.77	0.43	0.12	14.67	3.09	0.11	n.d	n.d	n.d	100.27	84
	rim	50.76	n.d	31.32	0.55	0.15	14.34	3.14	0.10	n.d	n.d	n.d	100.35	83
grain 2	core	50.33	n.d	31.30	0.45	0.15	14.92	3.12	0.13	n.d	n.d	n.d	100.39	84
	rim	51.24	0.13	30.45	0.50	0.17	14.25	3.44	0.13	n.d	n.d	n.d	100.31	82
grain 3	core	50.92	n.d	30.71	0.42	0.16	13.95	3.72	0.11	n.d	n.d	n.d	100.00	81
	rim	52.16	0.07	29.81	0.58	0.19	13.54	3.82	0.13	n.d	n.d	n.d	100.31	80
grain 4	core	52.44	0.06	29.68	0.46	0.17	12.89	4.29	0.16	n.d	n.d	n.d	100.15	77
	rim	49.48	0.07	32.17	0.52	0.11	15.59	2.73	0.09	n.d	n.d	n.d	100.76	86
grain 5	core	50.22	0.06	31.33	0.36	0.13	14.71	3.15	0.08	n.d	n.d	n.d	100.04	84
	rim	51.18	n.d	31.53	0.45	0.17	14.43	3.34	0.11	n.d	n.d	n.d	101.22	83

Appendix F: Olivine phenocryst core and rim chemical compositions through microprobe analyses. Major oxides recorded in (wt%). Analyses with < 98 % and > 102 % oxide totals were omitted; n.d= no detection.

Western/Central	Oxides (wt%) Sample #	SiO_2	TiO_2	Al_2O_3	FeO*	Na_2O	MnO	MgO	CaO	K_2O	NiO	Cr_2O_3	Totals	Fo Content
LKT	**FR-10-38**													
grain 1	core	39.79	0.02	0.08	14.45	n.d	0.20	45.20	0.22	n.d	0.29	0.05	100.31	85
grain 2	core	39.07	n.d	0.06	16.99	n.d	0.23	43.03	0.28	n.d	0.19	0.07	99.92	82
grain 3	core	39.00	0.06	0.08	14.31	0.07	0.18	44.11	0.23	0.03	0.27	n.d	98.32	85
grain 4	core	38.24	0.05	n.d	21.71	n.d	0.39	39.43	0.29	n.d	0.10	0.06	100.27	76
grain 5	core	39.78	0.02	0.07	13.68	n.d	0.20	45.74	0.25	0.02	0.31	n.d	100.07	86
OIB	**FR-10-40**													
grain 1	core	37.77	0.03	n.d	23.97	n.d	0.39	37.22	0.34	n.d	0.11	n.d	99.83	73
grain 2	core	39.05	0.02	0.07	16.66	n.d	0.23	43.33	0.24	n.d	0.21	n.d	99.81	82
grain 3	core	38.76	0.03	n.d	20.15	n.d	0.30	40.83	0.29	n.d	0.18	n.d	100.53	78
grain 4	core	38.47	0.03	0.06	21.34	n.d	0.33	39.97	0.35	0.02	0.10	n.d	100.67	77
grain 5	core	36.25	0.22	n.d	33.91	n.d	0.50	29.99	0.36	n.d	0.08	n.d	101.31	61
OIB	**FR-13-171**													
grain 1	core	39.81	n.d	n.d	14.17	n.d	0.20	44.44	0.23	n.d	0.22	n.d	99.07	85
	rim	38.04	0.02	n.d	20.04	n.d	0.32	39.32	0.35	n.d	0.11	n.d	98.19	78
grain 2	core	38.42	n.d	0.08	17.87	0.12	0.24	40.94	0.28	0.04	0.19	0.05	98.24	80
	rim	39.65	n.d	0.11	15.09	0.11	0.18	44.50	0.20	0.05	0.27	0.05	100.21	84
grain 3	core	38.68	0.02	n.d	20.11	0.09	0.28	40.55	0.34	0.03	0.15	n.d	100.26	78
	rim	40.09	n.d	0.09	13.54	n.d	0.20	45.35	0.27	n.d	0.28	n.d	99.83	86
grain 4	core	39.27	0.04	n.d	20.30	0.06	0.29	40.97	0.39	n.d	0.11	0.08	101.51	78
	rim	38.07	0.02	n.d	20.04	n.d	0.27	39.78	0.29	n.d	0.10	0.05	98.61	78
grain 5	core	38.26	0.06	0.27	20.12	0.07	0.25	39.16	0.35	0.05	0.09	0.05	98.72	78

Appendix F: continued

	Oxides (wt%)	SiO_2	TiO_2	Al_2O_3	FeO*	Na_2O	MnO	MgO	CaO	K_2O	NiO	Cr_2O_3	Totals	Fo Content
Western/Central	**Sample #**													
CAB	**FR-13-185**													
grain 1	core	40.21	n.d	0.08	15.45	n.d	0.18	43.32	0.30	n.d	0.24	0.06	99.84	83
	rim	39.95	0.02	n.d	11.87	n.d	0.20	46.05	0.04	n.d	0.17	n.d	98.30	87
grain 2	core	40.57	n.d	n.d	11.53	n.d	0.23	47.08	0.21	0.02	0.24	n.d	99.90	88
	rim	40.95	0.02	n.d	7.84	0.08	0.39	48.77	0.10	n.d	0.17	n.d	98.33	92
grain 3	core	40.75	n.d	n.d	13.15	0.07	0.28	43.72	0.22	0.04	0.22	n.d	98.45	86
	rim	37.97	0.08	0.13	37.60	0.10	0.16	24.13	0.14	0.07	0.08	n.d	100.46	53
grain 4	core	39.23	n.d	0.06	15.44	n.d	0.22	43.39	0.16	n.d	0.22	n.d	98.71	83
	rim	40.21	n.d	n.d	11.94	0.17	0.18	46.48	0.21	0.02	0.24	n.d	99.43	87
grain 5	core	41.72	0.08	n.d	10.12	0.09	0.38	48.33	0.09	n.d	0.16	n.d	100.96	89
Eastern														
LKT	**FR-12-101**													
grain 1	core	40.00	n.d	0.06	13.06	n.d	0.20	46.21	0.25	n.d	0.25	n.d	100.03	86
grain 2	core	40.09	n.d	n.d	12.94	n.d	0.15	46.43	0.27	n.d	0.21	n.d	100.09	86
grain 3	core	39.99	n.d	0.07	13.96	n.d	0.26	45.49	0.26	n.d	0.20	n.d	100.21	85
grain 4	core	40.10	n.d	0.08	13.03	n.d	0.20	46.49	0.27	n.d	0.20	n.d	100.37	86
grain 5	core	40.03	n.d	n.d	13.29	n.d	0.21	45.90	0.26	0.02	0.21	n.d	99.92	86
LKT	**FR-12-130**													
grain 1	core	37.56	0.04	n.d	26.66	0.05	0.46	35.04	0.34	n.d	0.08	n.d	100.23	70
grain 2	core	35.61	0.08	n.d	36.95	n.d	0.69	26.73	0.36	n.d	0.05	n.d	100.47	56
grain 3	core	36.15	0.04	n.d	34.62	n.d	0.56	29.00	0.37	n.d	0.04	n.d	100.78	60
grain 4	core	35.97	0.03	n.d	34.97	0.05	0.64	28.55	0.35	0.02	0.05	n.d	100.63	59
grain 5	core	36.52	0.06	0.16	34.23	0.18	0.55	27.77	0.25	0.09	0.09	n.d	99.90	59

Appendix F: continued

Eastern	Oxides (wt%) / Sample #	SiO_2	TiO_2	Al_2O_3	FeO*	Na_2O	MnO	MgO	CaO	K_2O	NiO	Cr_2O_3	Totals	Fo Content
LKT	**FR-13-152**													
grain 1	core	38.30	0.03	n.d	22.45	n.d	0.35	38.29	0.34	0.03	0.09	n.d	99.87	75
	rim	37.24	0.02	n.d	26.74	n.d	0.44	34.66	0.39	0.02	0.12	n.d	99.62	70
grain 2	core	38.63	n.d	0.06	20.92	0.14	0.34	39.71	0.37	0.02	0.10	0.06	100.35	77
	rim	36.95	n.d	n.d	29.18	n.d	0.40	32.87	0.36	n.d	0.09	n.d	99.85	67
grain 3	core	38.57	0.02	n.d	21.05	n.d	0.29	39.42	0.36	n.d	0.11	0.05	99.88	77
	rim	36.48	0.03	n.d	32.97	n.d	0.51	29.73	0.39	n.d	0.06	n.d	100.21	62
grain 4	core	37.81	n.d	0.71	21.57	0.19	0.29	37.94	0.50	0.06	0.07	n.d	99.13	76
	rim	36.07	0.07	n.d	35.48	n.d	0.55	27.84	0.35	n.d	0.06	n.d	100.43	58
grain 5	core	37.55	0.03	n.d	26.62	n.d	0.46	34.84	0.38	n.d	0.08	n.d	99.98	70
	rim	35.86	0.03	0.14	38.78	n.d	0.66	25.06	0.43	n.d	0.06	n.d	101.02	54
OIB	**FR-13-150**													
grain 1	core	39.21	n.d	0.07	16.45	n.d	0.25	43.05	0.18	n.d	0.19	n.d	99.39	82
	rim	39.33	n.d	n.d	16.39	n.d	0.24	42.90	0.22	n.d	0.14	n.d	99.23	82
grain 2	core	39.40	n.d	n.d	16.94	n.d	0.23	43.20	0.20	n.d	0.16	n.d	100.13	82
	rim	38.57	n.d	0.06	21.55	n.d	0.34	39.10	0.28	n.d	0.09	n.d	100.00	76
grain 3	core	38.72	0.04	n.d	22.08	n.d	0.36	38.73	0.28	n.d	0.09	n.d	100.30	76
	rim	38.00	0.08	n.d	23.76	n.d	0.42	36.88	0.41	0.02	0.05	n.d	99.61	73
grain 4	core	39.25	n.d	n.d	16.02	n.d	0.23	43.17	0.20	n.d	0.21	n.d	99.07	83
	rim	39.25	n.d	n.d	16.31	n.d	0.21	42.72	0.24	n.d	0.17	n.d	98.90	82
grain 5	core	39.46	0.02	n.d	16.70	n.d	0.22	42.91	0.20	n.d	0.19	n.d	99.69	82
	rim	38.63	0.04	n.d	22.44	n.d	0.31	38.94	0.29	n.d	0.08	n.d	100.74	76

Appendix F: continued

Eastern	Oxides (wt%) / Sample #	SiO_2	TiO_2	Al_2O_3	FeO*	Na_2O	MnO	MgO	CaO	K_2O	NiO	Cr_2O_3	Totals	Fo Content
BA	**FR-13-168b**													
grain 1	core	39.37	0.03	n.d	17.60	n.d	0.23	42.39	0.23	n.d	0.17	n.d	100.03	81
	rim	37.53	0.03	n.d	22.48	n.d	0.35	37.49	0.27	0.02	0.09	0.05	98.30	75
grain 2	core	39.24	n.d	0.06	15.49	0.10	0.17	43.72	0.19	n.d	0.24	n.d	99.21	83
	rim	39.33	n.d	n.d	16.41	n.d	0.18	43.25	0.16	n.d	0.19	n.d	99.51	82
grain 3	core	39.14	n.d	n.d	15.98	0.07	0.21	42.75	0.33	n.d	0.17	n.d	98.65	82
	rim	38.50	0.02	n.d	20.05	n.d	0.30	40.09	0.24	n.d	0.11	n.d	99.31	78
grain 4	core	38.97	n.d	n.d	16.61	0.15	0.24	42.80	0.16	0.02	0.18	n.d	99.31	82
	rim	38.62	n.d	n.d	19.76	n.d	0.32	40.35	0.24	n.d	0.12	n.d	99.42	78
grain 5	core	39.52	n.d	n.d	17.25	n.d	0.19	43.08	0.18	n.d	0.16	n.d	100.38	82
	rim	37.98	n.d	n.d	22.43	n.d	0.39	37.96	0.30	0.02	0.11	n.d	99.19	75

Appendix G: Chemical compositions of spinel inclusions in olivine phenocrysts. Major oxides recorded in (wt %). Analyses with < 98 % and > 102 % oxide totals were omitted; n.d = no detection.

	Oxides (wt%)	SiO_2	TiO_2	Al_2O_3	FeO*	MnO	MgO	CaO	Na_2O	NiO	Cr_2O_3	V_2O_3	ZnO	Total	Cr#	Mg#
Western/central	**Sample #**															
LKT	**FR-10-39**															
	grain 1	0.17	1.18	34.14	24.37	0.27	13.28	0.07	0.06	0.17	24.58	0.30	0.10	98.66	33	49
	grain 2	0.10	0.80	33.61	22.67	0.23	14.53	0.02	n.d	0.23	27.05	0.17	0.10	99.51	35	53
	grain 3	0.13	0.82	32.85	22.10	0.18	14.65	n.d	0.05	0.23	27.98	0.19	0.10	99.29	36	54
	grain 4	0.43	0.85	32.85	22.89	0.22	14.19	0.07	0.05	0.20	27.96	0.18	0.12	100.01	36	52
	grain 5	0.14	0.92	36.18	22.43	0.23	14.60	0.03	0.06	0.19	24.01	0.21	0.11	99.13	31	54
OIB	**FR-10-40**															
	grain 1	0.27	27.65	0.28	68.07	0.49	1.03	0.07	n.d	n.d	0.33	2.17	0.07	100.43	44	3
	grain 2	0.12	26.98	0.50	67.83	0.64	1.30	0.04	n.d	0.03	1.29	2.08	0.10	100.91	64	3
	grain 3	0.05	22.22	0.34	57.74	0.66	1.64	n.d	0.05	0.04	14.35	2.43	0.25	99.76	97	5
	grain 4	0.08	26.37	0.50	65.89	0.69	0.71	n.d	0.16	n.d	3.74	2.09	0.23	100.46	83	2
	grain 5	0.07	30.88	0.29	59.07	0.53	1.32	n.d	n.d	n.d	4.93	2.13	0.17	99.38	92	4
LKT	**FR-10-57**															
	grain 1	0.08	50.94	n.d	41.51	0.67	4.31	0.31	0.04	0.04	n.d	2.70	n.d	100.59	45	16
	grain 2	0.09	51.64	0.05	41.70	0.51	3.31	0.24	n.d	0.04	n.d	2.50	n.d	100.08	11	12
	grain 3	0.05	52.26	0.08	40.97	0.60	3.37	0.19	n.d	0.02	n.d	2.61	n.d	100.15	16	13
	grain 4	0.49	50.11	0.10	41.26	0.63	4.03	0.70	n.d	n.d	n.d	2.54	0.05	99.93	14	15
	grain 5	n.d	51.24	n.d	42.01	0.64	3.88	0.15	n.d	0.03	n.d	2.60	0.05	100.61	16	14

Appendix G: continued

	Oxides (wt%)	SiO_2	TiO_2	Al_2O_3	FeO*	Fe_2O_3	Fe_3O_4	MnO	MgO	CaO	Na_2O	NiO	Cr_2O_3	V_2O_3	ZnO	Total	Cr#	Mg#
Western/Central	**Sample #**																	
OIB	**FR-10-85**																	
	grain 1	0.63	1.36	6.25		72.78		1.33	15.25	0.14	0.32	0.16	0.34	0.12	0.15	98.57	3	27
	grain 2	0.11	1.81	7.14		60.36		0.65	16.69	0.18	0.06	0.18	12.64	0.10	n.d	99.91	54	33
	grain 3	2.82	0.78	29.74			20.26	0.40	20.60	0.53	0.05	0.11	25.57	0.14	0.15	101.42	37	64
	grain 4	0.13	1.98	8.75			56.97	0.60	17.18	0.17	n.d	0.19	12.05	0.11	0.08	98.22	48	35
	grain 5	0.14	3.05	3.97			75.20	0.91	14.65	0.36	n.d	0.16	0.24	0.17	0.06	98.90	4	26
	grain 6	0.14	2.57	3.70			76.86	1.12	13.71	0.30	0.03	0.11	0.24	0.14	0.11	99.02	4	24
Eastern																		
LKT	**FR-12-130**																	
	grain 1	0.06	0.09	0.07			100.68	n.d	n.d	0.12	n.d	n.d	n.d	n.d	n.d	101.01	6	0
	grain 2	0.23	21.62	1.01	72.96			0.52	2.66	0.28	n.d	0.08	0.05	1.77	0.06	101.25	3	6
	grain 3	0.24	16.80	0.26	77.45			0.55	2.01	0.39	n.d	0.05	0.22	1.99	0.12	100.09	36	4
	grain 4	0.05	48.48	0.04	45.60			0.39	2.19	0.09	n.d	0.03	0.09	2.71	0.06	99.74	62	8
	grain 5	0.23	20.38	0.77	73.97			0.58	2.67	0.16	n.d	0.04	0.10	1.86	0.08	100.82	8	6
LKT	**FR-12-101**																	
	grain 1	7.75	34.62	1.79	46.35			0.53	2.34	2.14	1.78	n.d	n.d	1.46	0.04	98.80	1	8
	grain 2	1.61	23.71	1.35	67.13			0.46	3.14	0.70	n.d	0.04	n.d	1.30	0.05	99.47	3	8
	grain 3	35.57	0.17	0.37	33.39			0.96	21.31	3.30	3.09	0.03	n.d	n.d	0.04	98.23		
	grain 4	2.73	41.90	0.44	48.30			0.61	2.16	0.41	n.d	0.02	n.d	2.19	0.04	98.81	4	7
	grain 5	0.14	0.49	34.47	19.93			0.18	16.08	n.d	n.d	0.19	27.71	0.20	0.07	99.45	35	59

Appendix H: Detection limits of major oxides analyzed in plagioclase, olivine, and spinel grains.

Plagioclase		**Oxide (wt%)**	**SiO_2**	**TiO_2**	**Al_2O_3**	**FeO***	**MgO**	**CaO**	**Na_2O**	**K_2O**	**BaO**	**Rb_2O**	**SrO**
Western/Central		**Sample #**											
LKT		**FR-10-39**											
	grain 1	core	0.04	0.05	0.07	0.03	0.03	0.02	0.08	0.03	0.16	0.13	0.16
		rim	0.03	0.06	0.06	0.03	0.03	0.03	0.10	0.02	0.16	0.13	0.17
	grain 2	core	0.03	0.06	0.07	0.03	0.03	0.02	0.08	0.03	0.16	0.13	0.18
		rim	0.03	0.07	0.07	0.03	0.03	0.03	0.09	0.02	0.16	0.13	0.19
	grain 3	core	0.03	0.06	0.07	0.03	0.03	0.03	0.09	0.02	0.13	0.13	0.18
		rim	0.03	0.06	0.07	0.03	0.03	0.03	0.09	0.03	0.12	0.13	0.17
	grain 4	core	0.03	0.05	0.07	0.03	0.03	0.02	0.09	0.02	0.16	0.12	0.17
		rim	0.03	0.06	0.07	0.03	0.03	0.03	0.09	0.02	0.16	0.13	0.16
	grain 5	core	0.03	0.06	0.07	0.03	0.03	0.02	0.09	0.02	0.15	0.12	0.17
		rim	0.03	0.05	0.06	0.03	0.03	0.03	0.09	0.02	0.16	0.13	0.18
OIB		**FR-10-40**											
	grain 1	core	0.03	0.07	0.07	0.03	0.03	0.02	0.07	0.03	0.14	0.13	0.17
		rim	0.03	0.05	0.06	0.03	0.03	0.03	0.09	0.02	0.13	0.13	0.16
	grain 2	core	0.03	0.06	0.07	0.03	0.03	0.03	0.07	0.02	0.16	0.13	0.17
		rim	0.04	0.06	0.06	0.03	0.03	0.03	0.09	0.02	0.17	0.13	0.16
	grain 3	core	0.03	0.05	0.06	0.03	0.03	0.03	0.09	0.02	0.14	0.13	0.16
		rim	0.03	0.06	0.06	0.03	0.03	0.02	0.08	0.02	0.14	0.13	0.14
	grain 4	core	0.03	0.06	0.06	0.03	0.03	0.02	0.08	0.03	0.16	0.13	0.17
		rim	0.03	0.05	0.07	0.03	0.03	0.02	0.08	0.02	0.15	0.13	0.16
	grain 5	core	0.03	0.07	0.06	0.03	0.03	0.02	0.08	0.02	0.15	0.13	0.17
		rim	0.03	0.06	0.06	0.03	0.03	0.02	0.08	0.02	0.15	0.13	0.15

Appendix H: continued

Plagioclase		**Oxide (wt%)**	**SiO_2**	**TiO_2**	**Al_2O_3**	**FeO***	**MgO**	**CaO**	**Na_2O**	**K_2O**	**BaO**	**Rb_2O**	**SrO**
Western/Central		**Sample #**											
OIB		**FR-10-85**											
	grain 1	core	0.04	0.05	0.07	0.03	0.03	0.03	0.07	0.02	0.18	0.13	0.19
		rim	0.03	0.06	0.07	0.03	0.03	0.02	0.08	0.02	0.14	0.13	0.15
	grain 2	core	0.03	0.06	0.06	0.03	0.03	0.03	0.09	0.02	0.16	0.13	0.16
		rim	0.03	0.06	0.07	0.03	0.03	0.02	0.06	0.03	0.14	0.13	0.17
	grain 3	core	0.03	0.06	0.06	0.03	0.03	0.02	0.09	0.03	0.17	0.13	0.16
		rim	0.03	0.06	0.06	0.03	0.03	0.02	0.09	0.02	0.14	0.13	0.16
	grain 4	core	0.04	0.06	0.07	0.03	0.03	0.03	0.08	0.03	0.17	0.12	0.17
		rim	0.03	0.05	0.07	0.03	0.03	0.02	0.08	0.02	0.11	0.13	0.18
	grain 5	core	0.03	0.05	0.07	0.03	0.03	0.03	0.07	0.03	0.14	0.13	0.16
		rim	0.04	0.06	0.07	0.03	0.03	0.03	0.08	0.03	0.15	0.13	0.15
Eastern		**Sample #**											
LKT		**FR-12-101**											
	grain 1	core	0.03	0.07	0.06	0.03	0.03	0.02	0.09	0.03	0.16	0.13	0.16
		rim	0.04	0.06	0.06	0.03	0.03	0.03	0.07	0.02	0.14	0.13	0.16
	grain 2	core	0.03	0.06	0.07	0.03	0.03	0.02	0.07	0.03	0.15	0.13	0.17
		rim	0.03	0.06	0.07	0.03	0.03	0.03	0.08	0.03	0.19	0.13	0.17
	grain 3	core	0.03	0.06	0.07	0.03	0.03	0.03	0.07	0.02	0.13	0.13	0.17
		rim	0.03	0.06	0.06	0.03	0.03	0.02	0.08	0.03	0.16	0.13	0.16
	grain 4	core	0.03	0.06	0.07	0.03	0.03	0.03	0.06	0.02	0.15	0.13	0.16
		rim	0.03	0.06	0.07	0.03	0.03	0.03	0.08	0.02	0.13	0.13	0.18
	grain 5	core	0.03	0.05	0.07	0.03	0.03	0.03	0.00	0.03	0.14	0.13	0.20
		rim	0.03	0.06	0.07	0.03	0.03	0.02	0.08	0.02	0.17	0.13	0.16

Appendix H: continued

Plagioclase		**Oxide (wt%)**	**SiO_2**	**TiO_2**	**Al_2O_3**	**FeO***	**MgO**	**CaO**	**Na_2O**	**K_2O**	**BaO**	**Rb_2O**	**SrO**
Eastern		**Sample #**											
LKT		**FR-12-130**											
	grain 1	core	0.03	0.06	0.06	0.03	0.03	0.02	0.08	0.02	0.13	0.13	0.16
		rim	0.03	0.06	0.07	0.03	0.03	0.03	0.09	0.02	0.12	0.13	0.15
	grain 2	core	0.03	0.06	0.07	0.03	0.03	0.03	0.08	0.02	0.17	0.13	0.17
		rim	0.03	0.06	0.07	0.03	0.03	0.02	0.07	0.02	0.14	0.13	0.20
	grain 3	core	0.03	0.06	0.07	0.03	0.03	0.02	0.08	0.03	0.13	0.12	0.14
		rim	0.03	0.06	0.07	0.03	0.03	0.02	0.08	0.02	0.15	0.12	0.16
	grain 4	core	0.03	0.06	0.06	0.03	0.03	0.03	0.09	0.03	0.14	0.13	0.18
		rim	0.03	0.06	0.06	0.03	0.03	0.02	0.08	0.03	0.17	0.13	0.17
	grain 5	core	0.03	0.06	0.06	0.03	0.03	0.02	0.00	0.03	0.15	0.13	0.16
		rim	0.03	0.06	0.07	0.03	0.03	0.03	0.09	0.02	0.14	0.13	0.14
LKT		**FR-13-152**											
	grain 1	core	0.04	0.04	0.06	0.03	0.03	0.03	0.08	0.02	0.13	0.14	0.17
		rim	0.04	0.06	0.07	0.03	0.03	0.03	0.08	0.02	0.12	0.13	0.16
	grain 2	core	0.04	0.06	0.07	0.03	0.03	0.03	0.10	0.03	0.19	0.12	0.16
		rim	0.04	0.06	0.07	0.03	0.03	0.03	0.09	0.02	0.15	0.13	0.16
	grain 3	core	0.04	0.05	0.06	0.03	0.03	0.03	0.07	0.02	0.13	0.13	0.17
		rim	0.04	0.06	0.07	0.03	0.03	0.03	0.08	0.02	0.14	0.12	0.16
	grain 4	core	0.03	0.06	0.07	0.03	0.03	0.03	0.07	0.02	0.17	0.13	0.16
		rim	0.04	0.06	0.06	0.03	0.03	0.03	0.08	0.02	0.18	0.13	0.16
	grain 5	core	0.04	0.06	0.07	0.03	0.03	0.03	0.08	0.02	0.16	0.13	0.17
		rim	0.04	0.05	0.06	0.03	0.03	0.03	0.09	0.02	0.13	0.13	0.16

Appendix H: continued

Plagioclase		**Oxide (wt%)**	**SiO_2**	**TiO_2**	**Al_2O_3**	**FeO***	**MgO**	**CaO**	**Na_2O**	**K_2O**	**BaO**	**Rb_2O**	**SrO**
Eastern		**Sample #**											
BA		**FR-13-168b**											
	grain 1	core	0.04	0.06	0.07	0.03	0.03	0.02	0.08	0.02	0.17	0.13	0.16
		rim	0.04	0.05	0.07	0.03	0.03	0.03	0.09	0.03	0.15	0.13	0.17
	grain 2	core	0.04	0.06	0.06	0.03	0.03	0.03	0.07	0.02	0.12	0.13	0.16
		rim	0.04	0.06	0.07	0.03	0.03	0.03	0.09	0.02	0.15	0.13	0.18
	grain 3	core	0.04	0.06	0.06	0.03	0.03	0.03	0.09	0.03	0.17	0.13	0.15
		rim	0.04	0.05	0.07	0.03	0.03	0.03	0.08	0.02	0.14	0.14	0.15
	grain 4	core	0.04	0.06	0.07	0.03	0.03	0.02	0.08	0.02	0.15	0.13	0.17
		rim	0.04	0.06	0.07	0.03	0.03	0.02	0.09	0.03	0.13	0.13	0.16
	grain 5	core	0.05	0.06	0.06	0.03	0.03	0.02	0.08	0.03	0.15	0.14	0.17
		rim	0.04	0.06	0.07	0.03	0.03	0.03	0.08	0.03	0.13	0.13	0.14

Appendix H: continued

Olivine		**Oxides (wt%)**	**SiO_2**	**TiO_2**	**Al_2O_3**	**FeO***	**Na_2O**	**MnO**	**MgO**	**CaO**	**K_2O**	**NiO**	**Cr_2O_3**
		Sample #											
Western/Central													
LKT		**FR-10-38**											
	grain 1	core	0.03	0.02	0.06	0.04	0.06	0.04	0.03	0.02	0.02	0.03	0.05
	grain 2	core	0.03	0.02	0.06	0.04	0.06	0.03	0.03	0.02	0.02	0.03	0.05
	grain 3	core	0.03	0.02	0.06	0.04	0.06	0.03	0.03	0.02	0.02	0.03	0.05
	grain 4	core	0.03	0.02	0.06	0.04	0.06	0.03	0.03	0.02	0.02	0.03	0.05
	grain 5	core	0.03	0.02	0.06	0.04	0.05	0.03	0.03	0.02	0.02	0.03	0.05
OIB		**FR-10-40**											
	grain 1	core	0.03	0.02	0.06	0.04	0.06	0.03	0.03	0.02	0.03	0.03	0.05
	grain 2	core	0.03	0.02	0.06	0.04	0.06	0.03	0.03	0.02	0.02	0.03	0.05
	grain 3	core	0.03	0.02	0.06	0.04	0.06	0.03	0.03	0.02	0.02	0.03	0.05
	grain 4	core	0.03	0.02	0.06	0.04	0.06	0.03	0.03	0.02	0.02	0.03	0.05
	grain 5	core	0.03	0.02	0.07	0.04	0.07	0.04	0.03	0.02	0.02	0.03	0.05
OIB		**FR-13-171**											
	grain 1	core	0.03	0.02	0.07	0.04	0.06	0.03	0.03	0.02	0.02	0.03	0.05
		rim	0.03	0.02	0.07	0.04	0.07	0.03	0.03	0.02	0.02	0.03	0.05
	grain 2	core	0.03	0.02	0.06	0.03	0.06	0.03	0.03	0.02	0.02	0.03	0.05
		rim	0.03	0.02	0.07	0.04	0.06	0.03	0.03	0.02	0.02	0.03	0.05
	grain 3	core	0.04	0.02	0.06	0.04	0.06	0.03	0.03	0.02	0.02	0.03	0.05
		rim	0.03	0.02	0.07	0.04	0.07	0.03	0.03	0.02	0.02	0.03	0.05
	grain 4	core	0.03	0.02	0.06	0.04	0.06	0.03	0.03	0.02	0.02	0.03	0.05
		rim	0.03	0.02	0.07	0.04	0.07	0.04	0.03	0.02	0.03	0.03	0.05
	grain 5	core	0.03	0.02	0.07	0.04	0.07	0.03	0.03	0.02	0.02	0.03	0.05

Appendix H: continued

Olivine		**Oxides (wt%)**	SiO_2	TiO_2	Al_2O_3	**FeO***	Na_2O	**MnO**	**MgO**	**CaO**	K_2O	**NiO**	Cr_2O_3
Western/Central		**Sample #**											
CAB		**FR-13-185**											
	grain 1	core	0.03	0.02	0.07	0.04	0.07	0.03	0.03	0.02	0.02	0.03	0.05
		rim	0.03	0.02	0.07	0.04	0.06	0.04	0.03	0.02	0.02	0.03	0.05
	grain 2	core	0.03	0.02	0.06	0.04	0.06	0.03	0.03	0.02	0.02	0.03	0.05
		rim	0.03	0.02	0.06	0.04	0.06	0.03	0.03	0.02	0.02	0.03	0.05
	grain 3	core	0.03	0.02	0.06	0.04	0.06	0.03	0.03	0.02	0.02	0.03	0.05
		rim	0.04	0.02	0.07	0.04	0.08	0.03	0.03	0.02	0.02	0.04	0.05
	grain 4	core	0.03	0.02	0.06	0.04	0.06	0.03	0.03	0.02	0.02	0.03	0.05
		rim	0.03	0.02	0.06	0.04	0.07	0.03	0.03	0.02	0.02	0.03	0.05
	grain 5	core	0.03	0.02	0.06	0.04	0.06	0.03	0.03	0.02	0.02	0.03	0.05
Eastern													
LKT		**FR-12-101**											
	grain 1	core	0.03	0.02	0.06	0.04	0.06	0.03	0.03	0.02	0.02	0.03	0.05
	grain 2	core	0.03	0.02	0.06	0.04	0.05	0.03	0.03	0.02	0.02	0.03	0.05
	grain 3	core	0.03	0.02	0.06	0.04	0.05	0.03	0.03	0.02	0.02	0.03	0.05
	grain 4	core	0.03	0.02	0.06	0.04	0.06	0.03	0.03	0.02	0.02	0.03	0.05
	grain 5	core	0.03	0.02	0.06	0.04	0.06	0.03	0.03	0.02	0.02	0.03	0.05
LKT		**FR-12-130**											
	grain 1	core	0.03	0.02	0.06	0.04	0.06	0.03	0.03	0.02	0.02	0.03	0.05
	grain 2	core	0.03	0.02	0.06	0.04	0.07	0.03	0.03	0.02	0.03	0.03	0.05
	grain 3	core	0.03	0.02	0.06	0.04	0.07	0.03	0.03	0.02	0.02	0.03	0.05
	grain 4	core	0.03	0.02	0.06	0.04	0.07	0.03	0.03	0.02	0.02	0.03	0.05
	grain 5	core	0.03	0.02	0.06	0.04	0.07	0.04	0.03	0.02	0.02	0.03	0.05

Appendix H: continued

Olivine		**Oxides (wt%)**	**SiO_2**	**TiO_2**	**Al_2O_3**	**FeO***	**Na_2O**	**MnO**	**MgO**	**CaO**	**K_2O**	**NiO**	**Cr_2O_3**
		Sample #											
Eastern													
LKT		**FR-13-152**											
	grain 1	core	0.03	0.02	0.07	0.04	0.07	0.03	0.03	0.02	0.02	0.03	0.05
		rim	0.03	0.02	0.07	0.04	0.08	0.03	0.03	0.02	0.02	0.03	0.05
	grain 2	core	0.03	0.02	0.06	0.04	0.07	0.03	0.03	0.02	0.02	0.03	0.05
		rim	0.03	0.02	0.07	0.04	0.08	0.04	0.03	0.02	0.03	0.04	0.05
	grain 3	core	0.03	0.02	0.07	0.04	0.07	0.03	0.03	0.02	0.02	0.03	0.05
		rim	0.03	0.02	0.07	0.04	0.07	0.04	0.03	0.02	0.02	0.03	0.05
	grain 4	core	0.03	0.02	0.07	0.04	0.07	0.04	0.03	0.02	0.02	0.04	0.05
		rim	0.03	0.02	0.07	0.05	0.08	0.04	0.03	0.02	0.03	0.04	0.05
	grain 5	core	0.03	0.02	0.07	0.04	0.08	0.03	0.03	0.02	0.02	0.04	0.05
		rim	0.04	0.02	0.07	0.04	0.08	0.04	0.03	0.02	0.03	0.03	0.05
OIB		**FR-13-150**											
	grain 1	core	0.03	0.02	0.06	0.04	0.06	0.03	0.03	0.02	0.02	0.03	0.05
		rim	0.03	0.02	0.06	0.04	0.07	0.03	0.03	0.02	0.02	0.03	0.05
	grain 2	core	0.03	0.02	0.06	0.04	0.07	0.03	0.03	0.02	0.02	0.03	0.05
		rim	0.03	0.02	0.06	0.04	0.07	0.03	0.03	0.02	0.02	0.03	0.05
	grain 3	core	0.03	0.02	0.07	0.04	0.07	0.03	0.03	0.02	0.02	0.03	0.05
		rim	0.03	0.02	0.07	0.04	0.07	0.03	0.03	0.02	0.02	0.03	0.05
	grain 4	core	0.03	0.02	0.06	0.04	0.07	0.03	0.03	0.02	0.02	0.03	0.05
		rim	0.03	0.02	0.07	0.04	0.07	0.03	0.03	0.02	0.02	0.03	0.05
	grain 5	core	0.03	0.02	0.06	0.04	0.07	0.03	0.03	0.02	0.02	0.03	0.05
		rim	0.03	0.02	0.07	0.04	0.07	0.03	0.03	0.02	0.02	0.03	0.05

Appendix H: continued

Olivine		**Oxides (wt%)**	**SiO_2**	**TiO_2**	**Al_2O_3**	**FeO**	**Na_2O**	**MnO**	**MgO**	**CaO**	**K_2O**	**NiO**	**Cr_2O_3**
		Sample #											
Eastern													
BA		**FR-13-168b**											
	grain 1	core	0.03	0.02	0.06	0.04	0.07	0.03	0.03	0.02	0.02	0.03	0.05
		rim	0.04	0.02	0.07	0.04	0.07	0.03	0.03	0.02	0.02	0.03	0.05
	grain 2	core	0.03	0.02	0.06	0.04	0.06	0.04	0.03	0.02	0.03	0.03	0.05
		rim	0.03	0.02	0.06	0.04	0.07	0.04	0.03	0.02	0.02	0.03	0.05
	grain 3	core	0.03	0.02	0.06	0.04	0.06	0.03	0.03	0.02	0.02	0.03	0.05
		rim	0.03	0.02	0.07	0.04	0.07	0.03	0.03	0.02	0.02	0.04	0.05
	grain 4	core	0.03	0.02	0.07	0.04	0.07	0.03	0.03	0.02	0.02	0.03	0.05
		rim	0.03	0.02	0.07	0.04	0.07	0.03	0.03	0.02	0.02	0.03	0.05
	grain 5	core	0.03	0.02	0.06	0.04	0.07	0.03	0.03	0.02	0.02	0.03	0.05
		rim	0.03	0.02	0.07	0.04	0.07	0.03	0.03	0.02	0.02	0.03	0.05

Appendix H: continued

Spinel	**Oxides (wt%)**	**SiO_2**	**TiO_2**	**Al_2O_3**	**FeO***	**MnO**	**MgO**	**CaO**	**Na_2O**	**NiO**	**Cr_2O_3**	**V_2O_3**	**ZnO**
	Sample #												
Western/central													
LKT	**FR-10-39**												
	grain 1	0.03	0.02	0.06	0.03	0.07	0.03	0.02	0.03	0.02	0.06	0.04	0.04
	grain 2	0.03	0.02	0.06	0.03	0.07	0.03	0.02	0.03	0.02	0.06	0.04	0.03
	grain 3	0.03	0.02	0.06	0.03	0.06	0.03	0.02	0.03	0.02	0.06	0.04	0.03
	grain 4	0.03	0.02	0.06	0.03	0.06	0.03	0.02	0.03	0.02	0.06	0.04	0.03
	grain 5	0.03	0.02	0.06	0.03	0.07	0.03	0.02	0.03	0.02	0.06	0.04	0.03
OIB	**FR-10-40**												
	grain 1	0.03	0.02	0.06	0.03	0.11	0.03	0.03	0.03	0.03	0.06	0.04	0.04
	grain 2	0.03	0.02	0.06	0.03	0.12	0.03	0.03	0.03	0.03	0.06	0.04	0.04
	grain 3	0.03	0.02	0.06	0.03	0.10	0.04	0.03	0.03	0.03	0.06	0.04	0.04
	grain 4	0.03	0.02	0.06	0.03	0.11	0.03	0.03	0.03	0.03	0.06	0.04	0.04
	grain 5	0.03	0.02	0.06	0.03	0.11	0.03	0.03	0.03	0.03	0.06	0.04	0.04
LKT	**FR-10-57**												
	grain 1	0.03	0.02	0.06	0.03	0.09	0.03	0.03	0.03	0.02	0.06	0.04	0.04
	grain 2	0.03	0.02	0.05	0.03	0.09	0.03	0.03	0.03	0.02	0.06	0.04	0.04
	grain 3	0.03	0.03	0.05	0.03	0.09	0.03	0.03	0.03	0.02	0.06	0.04	0.04
	grain 4	0.03	0.03	0.05	0.03	0.09	0.03	0.03	0.03	0.03	0.06	0.04	0.04
	grain 5	0.03	0.02	0.06	0.03	0.09	0.03	0.03	0.03	0.02	0.06	0.05	0.04

Appendix H: continued

Spinel	**Oxides (wt%)**	**SiO_2**	**TiO_2**	**Al_2O_3**	**FeO***	**MnO**	**MgO**	**CaO**	**Na_2O**	**NiO**	**Cr_2O_3**	**V_2O_3**	**ZnO**
	Sample #												
Western/central													
OIB	**FR-10-85**												
	grain 1	0.03	0.02	0.06	0.03	0.09	0.03	0.03	0.03	0.02	0.05	0.04	0.04
	grain 2	0.03	0.02	0.06	0.03	0.09	0.03	0.03	0.03	0.02	0.06	0.04	0.04
	grain 3	0.03	0.02	0.06	0.03	0.06	0.03	0.02	0.03	0.02	0.06	0.04	0.03
	grain 4	0.03	0.02	0.06	0.03	0.08	0.03	0.03	0.03	0.02	0.06	0.04	0.04
	grain 5	0.03	0.02	0.06	0.03	0.10	0.03	0.03	0.03	0.03	0.05	0.04	0.04
	grain 6	0.03	0.02	0.06	0.03	0.10	0.03	0.03	0.03	0.02	0.05	0.04	0.04
Eastern													
LKT	**FR-12-130**												
	grain 1	0.03	0.02	0.06	0.04	0.12	0.03	0.03	0.03	0.03	0.05	0.04	0.04
	grain 2	0.03	0.02	0.06	0.03	0.11	0.03	0.03	0.03	0.03	0.06	0.04	0.04
	grain 3	0.03	0.02	0.06	0.03	0.11	0.03	0.03	0.03	0.03	0.05	0.04	0.04
	grain 4	0.03	0.03	0.06	0.03	0.08	0.03	0.03	0.03	0.02	0.06	0.05	0.04
	grain 5	0.03	0.02	0.06	0.04	0.11	0.03	0.03	0.03	0.03	0.06	0.04	0.04
LKT	**FR-12-101**												
	grain 1	0.03	0.02	0.05	0.03	0.09	0.03	0.03	0.03	0.02	0.06	0.04	0.04
	grain 2	0.03	0.02	0.06	0.03	0.10	0.03	0.03	0.03	0.02	0.06	0.04	0.04
	grain 3	0.03	0.02	0.04	0.03	0.06	0.03	0.02	0.03	0.02	0.05	0.04	0.03
	grain 4	0.03	0.02	0.05	0.03	0.09	0.03	0.03	0.03	0.02	0.06	0.04	0.04
	grain 5	0.03	0.02	0.06	0.03	0.06	0.03	0.02	0.03	0.02	0.06	0.04	0.03

Appendix I: Trace element analyses of LKTs and OIBs through Inductively Coupled Plasma Mass Spectrometry (ICP-MS) (recorded in ppm). Normalized mid-ocean ridge basalt (N-MORB) values obtained from Sun & McDonough (1989).

Sample # ICP-MS	Cs ppm	Rb ppm	Ba ppm	Th ppm	U ppm	Nb ppm	Ta ppm	La ppm	Ce ppm	Pb ppm	Pr ppm	Sr ppm
FR-10-30 (LKT)	0.05	2.20	254.33	0.93	0.11	4.72	0.30	11.32	21.23	3.12	3.91	386.52
FR-10-38 (LKT)	0.19	5.67	146.40	0.61	0.28	5.53	0.36	7.38	18.45	1.64	2.83	347.99
FR-10-40 (OIB)	0.10	5.68	151.37	0.94	0.35	11.00	0.74	11.35	26.69	1.54	3.83	402.23
FR-10-85 (OIB)	0.12	7.96	150.91	1.21	0.43	16.54	1.07	13.03	29.31	1.38	4.05	302.50
FR-10-87 (LKT)	0.10	4.23	185.44	0.53	0.21	5.60	0.34	8.42	20.59	1.45	3.11	346.69
FR-12-101(LKT)	0.11	4.91	141.46	0.61	0.21	4.21	0.27	6.23	15.07	1.30	2.24	240.50

N-MORB normalized	Cs ppm	Rb ppm	Ba ppm	Th ppm	U ppm	Nb ppm	Ta ppm	La ppm	Ce ppm	Pb ppm	Pr ppm	Sr ppm
FR-10-30 (LKT)	6.63	3.93	40.37	7.75	2.36	2.02	2.28	4.53	2.83	10.40	2.96	4.29
FR-10-38 (LKT)	27.10	10.12	23.24	5.09	5.92	2.38	2.73	2.95	2.46	5.45	2.15	3.87
FR-10-40 (OIB)	13.79	10.14	24.03	7.81	7.41	4.72	5.57	4.54	3.56	5.12	2.90	4.47
FR-10-85 (OIB)	17.62	14.22	23.95	10.06	9.12	7.10	8.08	5.21	3.91	4.60	3.07	3.36
FR-10-87 (LKT)	13.63	7.55	29.44	4.39	4.38	2.41	2.56	3.37	2.75	4.84	2.36	3.85
FR-12-101(LKT)	15.48	8.78	22.45	5.04	4.55	1.81	2.05	2.49	2.01	4.32	1.70	2.67

Appendix I: continued

Sample # ICP-MS	Nd ppm	Zr ppm	Hf ppm	Sm ppm	Eu ppm	Gd ppm	Tb ppm	Dy ppm	Ho ppm	Y ppm	Er ppm	Tm ppm
FR-10-30 (LKT)	18.67	103.40	2.68	4.95	1.83	5.68	0.93	5.85	1.21	29.48	3.19	0.46
FR-10-38 (LKT)	13.67	111.62	2.82	3.98	1.51	4.54	0.77	4.96	1.03	25.41	2.75	0.40
FR-10-40 (OIB)	17.39	146.87	3.40	4.62	1.68	4.97	0.84	5.18	1.05	26.51	2.76	0.39
FR-10-85 (OIB)	18.19	149.56	3.46	4.71	1.66	5.20	0.88	5.65	1.18	28.92	3.11	0.46
FR-10-87 (LKT)	15.16	102.66	2.69	4.47	1.64	5.24	0.89	5.76	1.19	29.52	3.17	0.46
FR-12-101(LKT)	10.64	92.35	2.23	3.22	1.20	3.94	0.70	4.65	1.01	25.35	2.78	0.41

N-MORB normalized	Nd ppm	Zr ppm	Hf ppm	Sm ppm	Eu ppm	Gd ppm	Tb ppm	Dy ppm	Ho ppm	Y ppm	Er ppm	Tm ppm
FR-10-30 (LKT)	2.56	1.40	1.31	1.88	1.80	1.54	1.39	1.28	1.20	1.05	1.08	1.01
FR-10-38 (LKT)	1.87	1.51	1.37	1.51	1.48	1.23	1.15	1.09	1.02	0.91	0.93	0.87
FR-10-40 (OIB)	2.38	1.98	1.66	1.76	1.64	1.35	1.25	1.14	1.04	0.95	0.93	0.86
FR-10-85 (OIB)	2.49	2.02	1.69	1.79	1.63	1.41	1.31	1.24	1.16	1.03	1.05	1.01
FR-10-87 (LKT)	2.08	1.39	1.31	1.70	1.61	1.42	1.34	1.27	1.18	1.05	1.07	1.00
FR-12-101(LKT)	1.46	1.25	1.09	1.22	1.18	1.07	1.05	1.02	1.00	0.91	0.94	0.91

Appendix I: continued

Sample # ICP-MS	Yb ppm	Lu ppm
FR-10-30 (LKT)	2.80	0.42
FR-10-38 (LKT)	2.37	0.38
FR-10-40 (OIB)	2.38	0.39
FR-10-85 (OIB)	2.78	0.44
FR-10-87 (LKT)	2.81	0.45
FR-12-101(LKT)	2.58	0.42

N-MORB normalized	Yb ppm	Lu ppm
FR-10-30 (LKT)	0.92	0.93
FR-10-38 (LKT)	0.78	0.83
FR-10-40 (OIB)	0.78	0.86
FR-10-85 (OIB)	0.91	0.98
FR-10-87 (LKT)	0.92	1.00
FR-12-101(LKT)	0.85	0.92